

University of Massachusetts Medical School

eScholarship@UMMS

---

GSBS Dissertations and Theses

Graduate School of Biomedical Sciences

---

2015-01-23

## Advancements in the Synthesis and Application of Near-Infrared Imaging Reagents: A Dissertation

Steven M. Pauff

*University of Massachusetts Medical School*

Let us know how access to this document benefits you.

Follow this and additional works at: [https://escholarship.umassmed.edu/gsbs\\_diss](https://escholarship.umassmed.edu/gsbs_diss)



Part of the [Biochemistry Commons](#), [Chemistry Commons](#), and the [Molecular Biology Commons](#)

---

### Repository Citation

Pauff SM. (2015). Advancements in the Synthesis and Application of Near-Infrared Imaging Reagents: A Dissertation. GSBS Dissertations and Theses. <https://doi.org/10.13028/M2BG6B>. Retrieved from [https://escholarship.umassmed.edu/gsbs\\_diss/751](https://escholarship.umassmed.edu/gsbs_diss/751)

This material is brought to you by eScholarship@UMMS. It has been accepted for inclusion in GSBS Dissertations and Theses by an authorized administrator of eScholarship@UMMS. For more information, please contact [Lisa.Palmer@umassmed.edu](mailto:Lisa.Palmer@umassmed.edu).

**ADVANCEMENTS IN THE SYNTHESIS AND APPLICATION OF NEAR-  
INFRARED IMAGING REAGENTS**

A Dissertation Presented

By

Steven Michael Pauff

Submitted to the Faculty of the  
University of Massachusetts Graduate School of Biomedical Sciences, Worcester  
in partial fulfillment of the requirements for the degree of

DOCTOR OF PHILOSOPHY

January 23, 2015

Biochemistry and Molecular Pharmacology


ADVANCEMENTS IN THE SYNTHESIS AND APPLICATION OF NEAR-INFRARED  
IMAGING REAGENTS

A Dissertation Presented

By

Steven Michael Pauff

The signatures of the Dissertation Defense Committee signify  
completion and approval as to style and content of the Dissertation

  
\_\_\_\_\_  
Stephen C. Miller, Ph.D., Thesis Advisor

  
\_\_\_\_\_  
Osman Bilsel, Ph.D., Member of Committee

  
\_\_\_\_\_  
Anthony Carruthers, Ph.D., Member of Committee

  
\_\_\_\_\_  
Gang Han, Ph.D., Member of Committee

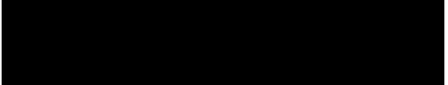
  
\_\_\_\_\_  
Jie Song, Ph.D., Member of Committee

  
\_\_\_\_\_  
Maolin Guo, Ph.D., Member of Committee

The signature of the Chair of the Committee signifies that the written dissertation meets the  
requirements of the Dissertation Committee

  
\_\_\_\_\_  
William Kobertz, Ph.D., Chair of Committee

The signature of the Dean of the Graduate School of the Biomedical Sciences signifies that the  
student has met all graduation requirements of the school

  
\_\_\_\_\_  
Anthony Carruthers, Ph.D.,  
Dean of the Graduate School of Biomedical Sciences

Program in Biochemistry and Molecular Pharmacology  
September 21, 2015

## DEDICATION

I dedicate this thesis to the two most important ladies in my life. Amanda, without you, I wouldn't be here today, you make life worth living. Candy, thanks for always being there, I never could have gotten through college without you.

## ACKNOWLEDGEMENTS

First, I would like to acknowledge my thesis advisor, Stephen Miller. He gave me the opportunity to become both a chemist and a biologist, a skill set that I hope to cultivate over the years to come. I also have to thank him for allowing me the chance to run free with my work. Knowing how much my molecules meant to me, he never tried to make me let go, even when some of them were not panning out. You helped me become the chemist I am today.

I am very grateful to my committee members, both present and past: Bill Kobertz, Tony Carruthers, Osman Bilsel, Jie Song, Gang Han, and Kirsten Hagstrom. Their support and guidance over the years has been invaluable. I also truly appreciate Maolin Guo for offering his time to serve as my outside committee member. Thank you all for helping to make my defense enjoyable.

A special thanks is owed to Poshen (Benson) Chen, Brendan Hilbert, Yvonne Chan, and Spencer Adams Jr. for their contributions to my project. I could not have completed this work without their help. I would like to thank Paul Furcinnitti from the Digital Light Microscopy Core and Karin Green at the Proteomics and Mass Spectrometry Facility for all their help in cell imaging and small molecule HRMS. I would also like to acknowledge the American Heart Association for helping to fund my work on the development of NIR nitric oxide sensors.

Thanks also goes out to my people in the Miller lab, you helped make grad school fun, and that's something. Katryn Harwood, your help with cell culture and imaging when I first started in the lab made the rest of my time there possible. Finally, I thank my beautiful wife, Amanda Hughes; you just make everyday better.

## ABSTRACT

Fluorescence-based imaging techniques provide a simple, highly sensitive method of studying live cells and whole organisms in real time. Without question, fluorophores such as GFP, fluorescein, and rhodamines have contributed vastly to our understanding of both cell biology and biochemistry. However, most of the fluorescent molecules currently utilized suffer from one major drawback, the use of visible light. Due to cellular autofluorescence and the absorbance of incident light by cellular components, fluorescence imaging with visible wavelength fluorophores often results in high background noise and thus a low signal-to-noise ratio. Fortunately, this situation can be ameliorated by altering the wavelength of light used during imaging. Near-infrared (NIR) light (650-900 nm) is poorly absorbed by cells; therefore, fluorophores excited by this light provide a high signal-to-noise ratio and low background in cellular systems. While these properties make NIR fluorophores ideal for cellular imaging, most currently available NIR molecules cannot be used in live cells.

The first half of this thesis addresses the synthetic difficulties associated with preparing NIR fluorophores that can be used within living systems. Small molecule NIR fluorophores are inherently hydrophobic which makes them unsuitable for use in the aqueous environment of the cell. Water-solubility is imparted to these dyes through highly polar sulfonates, which subsequently prevents the dyes from entering the cell. The novel work presented here details

synthetic routes to aid in the development of sulfonated NIR fluorophores, which can be delivered into live cells through the inclusion of an esterase-labile sulfonate protecting group. Application of these synthetic techniques should allow for the development of novel NIR fluorophores with intracellular applications.

The second half of this thesis addresses the need for novel NIR imaging reagents. Although several classes of NIR scaffolds do exist, most NIR probes are derivatives of a single class, heptamethine indocyanines. The work described here increases this palette by displaying the ability of NIR oxazines to function as an imaging reagent in live cells and *in vivo* and as a molecular sensor of biologically-relevant environmental conditions. Combined, the work contained herein has the capacity to not only advance the current NIR toolkit, but to expand it so that fluorescence imaging can move out of the dark and into the NIR light.



## TABLE OF CONTENTS

Dedication .....	iii
Acknowledgements .....	iv
Abstract .....	vi
Table of Contents .....	viii
List of Tables .....	x
List of Schemes .....	xi
List of Figures .....	xii
List of Third Party Copyrighted Material .....	xvi
List of Symbols and Abbreviations.....	xvii
List of Multimedia Objects .....	xx
Preface .....	xxi
<b>CHAPTER I: Introduction .....</b>	<b>1</b>
Fluorescence.....	1
Fluorescence and Biology .....	5
Flaws in Fluorescence Imaging Techniques .....	7
Near-Infrared Light .....	11
NIR Fluorophores .....	14
Flaws of NIR Fluorophores .....	22
Summary.....	23
<b>CHAPTER II: A trifluoroacetic acid-labile sulfonate protecting group and its     use in the synthesis of a near-IR fluorophore .....</b>	<b>24</b>
Summary.....	24
Introduction .....	25
Results and Discussion .....	28
Conclusions.....	42
Materials and Methods .....	42
<b>CHAPTER III: Synthesis of near-IR fluorescent oxazine dyes with esterase-     labile sulfonate esters .....</b>	<b>61</b>
Summary .....	61
Introduction .....	62

Results and Discussion .....	64
Conclusions .....	75
Materials and Methods .....	75
<b>CHAPTER IV: Delivery of sulfonated near-IR oxazines into the cytoplasm of living cells .....</b>	<b>114</b>
Summary .....	114
Introduction .....	115
Results and Discussion .....	118
Conclusions .....	166
Materials and Methods .....	172
<b>CHAPTER V: Synthesis and characterization of near-IR oxazine sensors of pH and nitric oxide .....</b>	<b>184</b>
Summary .....	184
Introduction .....	184
Results and Discussion .....	191
Conclusions .....	228
Materials and Methods .....	231
<b>CHAPTER VI: Discussion .....</b>	<b>262</b>
<b>Bibliography.....</b>	<b>272</b>
<b>APPENDIX 1 .....</b>	<b>283</b>
Multimedia Legend.....	283

## LIST OF TABLES

Table 2.1	Stability of TFMT sulfonate esters
Table 2.2	TFA cleavage of sulfonate esters <b>6</b> and <b>7</b>
Table 2.3	TFA cleavage of compound <b>6</b> employing different percentages of water as a cation scavenger
Table 4.1	ESI-HRMS m/z values for NIR oxazine fluorophores collected from U2-OS cells
Table 5.1	Photophysical properties of <b>16</b> and <b>17</b> in PBS, pH 7.4
Table 5.2	Values for curve fitting of TCSPC data
Table 5.3	Non-linear regression parameters for the one-phase association model employed in Figure 5.15
Table 5.4	Values for curve fitting of pH Sensor <b>22</b> TCSPC data
Table 5.5	Preparation of buffered solutions for pH sensitivity experiments

## LIST OF SCHEMES

- Scheme 2.1 Ruppert-Prakash synthesis of potential reagents for the development of sulfonate protecting groups
- Scheme 2.2 Synthesis of TFMT sulfonate esters
- Scheme 2.3 Synthesis of bis-sulfonated oxazine dye (**1**) using the TFA-labile TFMT sulfonate protecting group
- Scheme 2.4 Synthesis of bis-sulfonate oxazine dye (**1**) using 1,3-propanesultone
- Scheme 3.1 Synthesis of a sulfonated oxazine dye
- Scheme 3.2 Incorporation of TFMB and AcOTFMB sulfonate esters into an oxazine dye
- Scheme 3.3 Synthesis of iodopropyl sulfonates
- Scheme 3.4 Synthesis of sulfonate ester derivatives of MR121
- Scheme 3.5 Synthesis of a sulfonated MR121 derivative
- Scheme 3.6 Intramolecular nucleophiles can cause self-immolation of AcOTFMB sulfonates
- Scheme 3.7 Bypassing phenols: formation of bis-sulfonated oxazine dyes from silyl ether and anisole starting materials
- Scheme 5.1 Synthesis of PET donor for oxazine-based nitric oxide sensor
- Scheme 5.2 Synthesis of oxazine-based nitric oxide sensor
- Scheme 5.3 Synthesis of unquenched (fluorescent) form of nitric oxide sensor
- Scheme 5.4 Synthesis of oxazine-based pH sensor

## LIST OF FIGURES

- Figure 1.1 Jablonski diagram illustrating electronic processes occurring after photon absorption
- Figure 1.2  $\pi$ -orbital system of conjugated molecules
- Figure 1.3 Methods of molecular luminescence
- Figure 1.4 Indocyanine Green (ICG)
- Figure 1.5 Commonly employed fluorophores for biological imaging
- Figure 1.6 Autofluorescence of live 3T3B cells
- Figure 1.7 Absorbance spectra of melanin, oxyhemoglobin (HbO<sub>2</sub>), and water
- Figure 1.8 Near-infrared light produces little to no autofluorescence background in whole organisms
- Figure 1.9 Examples of visible light absorbing/emitting organic fluorophores
- Figure 1.10 Examples of NIR organic fluorophores
- Figure 1.11 Ring pucker from the terminal azacyclohexane rings of the pentacyclic oxazine scaffold
- Figure 2.1 Bis-sulfonate oxazine (**1**) and bis-sulfonate ester (**2**)
- Figure 2.2 Analytical HPLC traces of Compound **6** and the purified material from cleavage and stability analyses of TFMT-sulfonate ester protecting group
- Figure 2.3 Analytical HPLC of bis-sulfonated oxazine dye (**1**)
- Figure 3.1 Esterase-labile protecting group for sulfonates
- Figure 3.2 NIR oxazines functionalized with AcOTFMB-sulfonate esters are cleaved to the free sulfonate dye *in vitro* by pig liver esterase
- Figure 3.3 Only the NIR oxazine dye functionalized with AcOTFMB-sulfonate esters (**34**) is cleaved to the free sulfonate dye upon treatment with pig liver esterase *in vitro*
- Figure 4.1 Structure of AcOTFMB

- Figure 4.2 NIR oxazines functionalized with AcOTFMB-sulfonate esters are converted to sulfonated NIR oxazines upon *in vitro* treatment with pig liver esterase
- Figure 4.3 Pentacyclic NIR oxazines functionalized with sulfonates and sulfonate esters
- Figure 4.4 The lipophilic NIR oxazines **AcOTFMB-Ox** and **TFMB-Ox** diffuse into live U2-OS cells while the hydrophilic **Sulf-Ox** NIR oxazines are excluded from the cytoplasm
- Figure 4.5 Sulfonate ester NIR oxazines localize to mitochondria upon entry into the cytoplasm
- Figure 4.6 NIR oxazines functionalized with esterase-stable TFMB sulfonate esters (**TFMB-Ox**) display persistent mitochondrial localization over 3 hours
- Figure 4.7 U2-OS cells treated with NIR oxazines functionalized with esterase-labile AcOTFMB sulfonate esters (**AcOTFMB-Ox**) display diffuse fluorescence within 20 minutes of dye treatment but lose intracellular NIR fluorescence within 90 minutes of dye treatment
- Figure 4.8 Esterase-labile **AcOTFMB-Ox** dyes are converted to **Sulf-Ox** within living cells while esterase-stable **TFMB-Ox** dyes are unaffected by the cellular environment
- Figure 4.9 Inhibition of the efflux transporters MRP1 and Pgp results in increased retention of bis-sulfonated NIR oxazines
- Figure 4.10 shRNA knockdown of MRP1 and Pgp results in the increased retention of bis-sulfonated NIR oxazines
- Figure 4.11 *in vivo* imaging in mice with NIR bis-sulfonated oxazines
- Figure 4.12 *in vivo* imaging with Indocyanine Green
- Figure 4.13 RT-qPCR results of ABCB1 and ABCC1 expression in U2-OS cells expressing shRNA against the transporter
- Figure 5.1 IR780/783-derived fluorescent sensors
- Figure 5.2 NIR BODIPY and Aza-BODIPY fluorescent sensors
- Figure 5.3 NIR oxazine scaffold

- Figure 5.4 Quenching of fluorescence via photoinduced electron transfer (PET)
- Figure 5.5 The electron rich *o*-diaminobenzene reacts with nitric oxide to produce the electron poor benzotriazole
- Figure 5.6 General architecture for design of fluorescent sensor
- Figure 5.7 Molecular modeling reveals that a 3-carbon spacer between the NIR oxazine scaffold and *o*-diaminobenzene allows the closest approach between PET donor and acceptor
- Figure 5.8 Reaction of **16** with nitric oxide produces the benzotriazole functionalized NIR oxazine **17**
- Figure 5.9 Absorbance spectra of **16** and **17** in PBS, pH 7.4
- Figure 5.10 Emission spectra of **16** and **17** in PBS, pH 7.4
- Figure 5.11 Integrated fluorescence intensity of 10  $\mu$ M **16** and **17** in PBS, pH 7.4
- Figure 5.12 Time correlated single photon counting (TCSPC) suggests a complex mechanism for quenching of NIR oxazine-derived NO sensor **16**
- Figure 5.13 Changes in the fluorescence intensity of **16** upon treatment with ROS and RNS
- Figure 5.14 Increase in the fluorescence intensity of ROS/RNS treated NO sensor upon treatment with nitric oxide
- Figure 5.15 NO sensor **16** can detect changes in nitric oxide concentration
- Figure 5.16 Oxazine-derived NO sensor **16** is relatively insensitive to pH
- Figure 5.17 The electron-rich phenylamine can be reversibly protonated to produce the electron poor phenyl ammonium cation
- Figure 5.18 Absorption and emission spectra for pH sensor **22** in pH 4 and pH 7 solutions
- Figure 5.19 Integrated fluorescence intensity of **22** in pH 4 and pH 7 solutions
- Figure 5.20 Fluorescence intensity of **22** in pH 2-8 solutions
- Figure 5.21 Integrated fluorescence intensity of pH sensor **22** in solutions of pH 2-8

Figure 5.22 The apparent pKa of pH sensor **22** is 4.8

Figure 5.23 Time correlated single photon counting (TCSPC) suggests that the pH-related PET-quenching of NIR oxazine-derived pH sensor **22** is complex



**LIST OF THIRD PARTY COPYRIGHTED MATERIAL**

Figure 1.1	Dr. Kendric C. Smith	Permitted without license number
Figure 1.6	Dr. Jane E. Aubin	Permitted without license number
Figure 1.7	Dr. Karsten König	3543561141056
Figure 1.8	Dr. John V. Frangioni	3543570035802

## LIST OF SYMBOLS AND ABBREVIATIONS

A	pre-exponential amplitude
$\alpha$	alpha
ABC	ATP-binding cassette
AcOH	acetic acid
AcOTFMB	<i>p</i> -Acetoxytrifluoromethylbenzyl
AU	absorbance unit
AU	arbitrary unit
BCRP	breast cancer resistance protein
BF	Bright Field
Boc	<i>t</i> -Butoxycarbonyl
BODIPY	Boron-dipyrromethene
$\chi$	chi
CPS	counts per second
Cy	Cyanine
DAPI	4',6-Diamidino-2-phenylindole
DEA-NONOate	Diethylammonium (Z)-1-(N,N-diethylamino)diazen-1-ium-1,2-diolate
DIC	Differential interference contrast
DMEM	Dulbecco's Modified Eagle's Medium
DMF	N,N'-Dimethylformamide
DMSO	Dimethyl sulfoxide
DNA	deoxyribonucleic acid
DsRed	<i>Discosoma</i> Red Fluorescent Protein
EGFP	Enhanced Green Fluorescent Protein
Em	emission
eq	equivalent(s)
ESI-HRMS	Electrospray Ionization-High Resolution Mass Spectrometry
EtOH	ethanol
Ex	excitation
f	final
$\Phi$	quantum yield
$\Phi_{FI}$	fluorescence quantum yield
FBS	fetal bovine serum
FDA	Food and Drug Administration
FITC	Fluorescein isothiocyanate
GFP	Green Fluorescent Protein
h	hour
H <sup>+</sup>	proton
HbO <sub>2</sub>	oxyhemoglobin
HBSS	Hank's balanced salt solution
h $\nu$	light

HOMO	highest occupied molecular orbital
HPLC	High Pressure Liquid Chromatography
i	initial
$I_0$	initial intensity
iBu	isobutyl
ICG	Indocyanine Green
IP	intraperitoneal
iPr	isopropyl
IR	infrared
IV	intravenous
k	rate constant
$\lambda$	wavelength
LUMO	highest occupied molecular orbital
<i>m</i>	<i>meta</i>
MDR	multidrug resistance protein
MeOH	methanol
min	minute(s)
mol	mole
MRP	multidrug resistance associated protein
NADPH	reduced Nicotinamide adenine dinucleotide phosphate
Neo	Neopentyl
NIR	near-infrared
NMR	Nuclear Magnetic Resonance
NO	nitric oxide
Ox	Oxazine
<i>p</i>	<i>para</i>
$\pi$	pi
PBS	phosphate buffered saline
PET	photoinduced electron transfer
Pgp	permeability glycoprotein
pKa	acid dissociation constant
PLE	pig liver esterase
RFP	Red Fluorescent Protein
RFU	relative fluorescence units
RNS	reactive nitrogen species
ROI	region of interest
ROS	reactive oxygen species
RP	Reversed-phase
rt	room temperature
RT-qPCR	Reverse transcription-quantitative polymerase chain reaction
$S_0$	ground singlet state
$S_{n>0}$	excited singlet state
shRNA	short hairpin ribonucleic acid
Sulf	Sulfonate

<i>t</i>	<i>tert</i>
$\tau$	time constant
$\tau_{12}$	half-time
$\tau_{\text{Fl}}$	fluorescence lifetime
$T_{n \neq 0}$	excited triplet state
TBS	<i>tert</i> -Butyldimethylsilyl
TCE	Trichloroethyl
TCSPC	Time-correlated Single Photon Counting
TFA	Trifluoroacetic acid
TFE	Trifluoroethyl
TFMB	$\alpha$ -Trifluoromethylbenzyl
TFMT	Trifluoromethyltolyl
THF	Tetrahydrofuran
TLC	Thin layer chromatography
TMS	Trimethylsilyl
UV	ultraviolet
<i>v</i>	volume
YFP	Yellow Fluorescent Protein

## LIST OF MULTIMEDIA OBJECTS

- Movie 4.1 Real-time monitoring of **AcOTFMB-Ox1** diffusion into U2-OS cells: DIC
- Movie 4.2 Real-time monitoring of **AcOTFMB-Ox1** diffusion into U2-OS cells: NIR
- Movie 4.3 Real-time monitoring of **TFMB-Ox1** diffusion into U2-OS cells: DIC
- Movie 4.4 Real-time monitoring of **TFMB-Ox1** diffusion into U2-OS cells: NIR
- Movie 4.5 Real-time monitoring of **AcOTFMB-Ox2** diffusion into U2-OS cells: DIC
- Movie 4.6 Real-time monitoring of **AcOTFMB-Ox2** diffusion into U2-OS cells: NIR
- Movie 4.7 Real-time monitoring of **TFMB-Ox2** diffusion into U2-OS cells: DIC
- Movie 4.8 Real-time monitoring of **TFMB-Ox2** diffusion into U2-OS cells: NIR

## PREFACE

Publications derived from work contained within this thesis:

In CHAPTER II: Pauff, S. M. and Miller, S. C. "A Trifluoroacetic Acid-labile Sulfonate Protecting Group and Its Use in the Synthesis of a Near-IR Fluorophore." *Journal of Organic Chemistry* **2013**, *78* (2), 711-716.

In CHAPTER III: Pauff, S. M. and Miller, S. C. "Synthesis of Near-IR Fluorescent Oxazine Dyes with Esterase-Labile Sulfonate Esters." *Organic Letters* **2011**, *13* (23), 6196-6199.

I thank Po Shen Chen of the Fazzio Lab for preparing the MRP1 and Pgp knockdown U2-OS cells employed in Chapter IV and for preparing the RT-qPCR data used in Figure 4.13. I thank Dr. Brenden Hilbert of the Kelch Lab for performing the molecular modeling used in Chapter V and preparing the structures used for Figure 5.7. I thank Spencer Adams Jr. of the Miller Lab for performing the mouse imaging in Chapter IV and for preparing the images used in Figures 4.11 and 4.12.

Work described in Chapter V was funded partly through a predoctoral fellowship awarded by the American Heart Association (13PRE13970011).

## CHAPTER I: Introduction

### *Fluorescence*

Fluorescence is formally defined as a type of luminescence, the emitting of light by any substance not resulting from temperature increases, which results from photon absorption and occurs from an excited singlet state (Lakowicz, 2006). This definition is best visualized using a Jablonski diagram, which describes molecular processes that can occur after electron excitation (Figure 1.1). The vast majority of molecules exist in a singlet ground state ( $S_0$ ), which is simply an electronic state having all electron spins paired. Upon absorbing a photon (upward solid arrows), an electron will be promoted to a higher singlet energy level ( $S_{n>0}$ ). Once excited, the electron can return to the ground state by a variety of methods, both non-radiative (wavy arrows) and radiative (downward solid arrows). When the electron returns from  $S_{n>0}$  back to  $S_0$  via photon emission, the radiative relaxation is referred to as fluorescence.

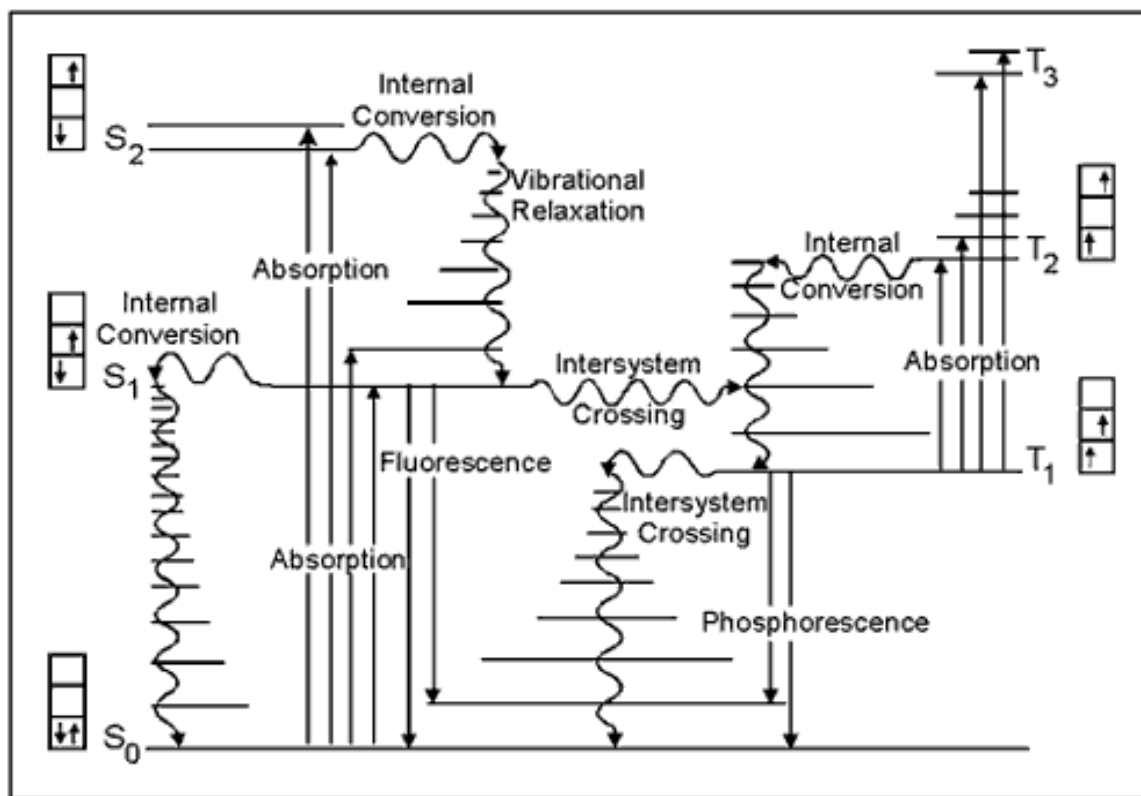


**Figure 1.1: Jablonski diagram illustrating electronic processes occurring after photon absorption.** Solid arrows: photon absorption/emission. Wavy arrows: non-radiative energy pathways. Adapted with permission from Dr. Kendrick C. Smith of Stanford University School of Medicine from <http://www.photobiology.info/Photochem.html>.

From the Jablonski diagram, it might appear that fluorescence could occur from any molecule that can absorb light (Figure 1.1). However, fluorescence is highly dependent on molecular structure and, in practice, is generally limited to structurally constrained molecules possessing a high degree of conjugation; e.g., aromatic compounds (Lakowicz, 2006; Nijegorodov and Downey, 1994; Nijegorodov et al., 2006; Sauer et al., 2011). The key feature of highly conjugated and aromatic molecules is the extended  $\pi$ -orbital system, which



results in an energy decrease between electronic energy levels. This energy decrease allows these molecules to absorb lower energy, non-ionizing radiation (Sauer et al., 2011). Another structural characteristic of fluorescent molecules results from the geometric constraints brought about by higher bond orders. Highly conjugated molecules in general, and fluorescent molecules in particular, tend to be planar. This structural feature favors fluorescence as the planarity of the molecule also applies to the  $\pi$ -orbital system; i.e., the  $\pi$  orbitals will tend to lie within the same plane (Figure 1.2) (Sauer et al., 2011). This trait is generally associated with electron delocalization, as observed for molecules like benzene. As delocalization results in resonance stabilization, the planarity produced by conjugation further contributes to energy decreases between electronic orbitals. While these features favor the production of fluorescence, they have a detrimental effect on the use of these molecules in biological systems, as will be highlighted later.

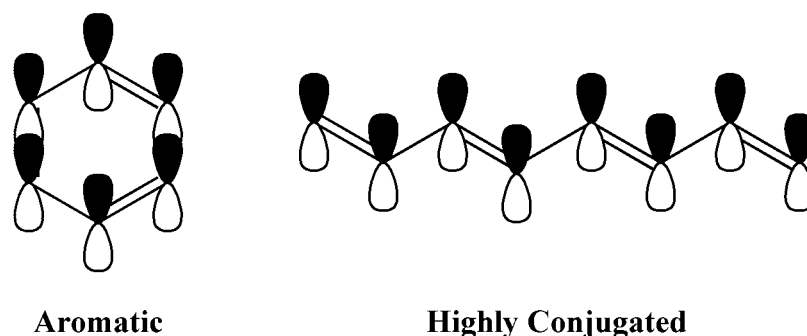


**Figure 1.2:  $\pi$ -orbital system of conjugated molecules.** Organic molecules showing the extended pi-orbital system resulting from conjugation. Left side: Benzene. Right side: Octa-1,3,5,7-tetraene.

Fluorescence has unique characteristics that distinguish it from other forms of luminescence. Since fluorescence is a singlet to singlet transition, photon emission is extremely rapid, occurring on the order of nanoseconds (Lakowicz, 2006). This is compared with phosphorescence, shown in Figure 1.1 as relaxation from an excited triplet state ( $T_{n \neq 0}$ ), which usually occurs on the order of milliseconds to seconds (Lakowicz, 2006). Furthermore, since fluorescence only involves electron excitation and relaxation, the fluorescent molecule, or fluorophore, is not limited to a single fluorescent event. This is contrasted with chemiluminescence and bioluminescence in which light emission occurs as a result of a chemical reaction and thus the light-emitter is of single use (Figure 1.3). The rapid response time and extended reagent life has made fluorescence a useful tool for biology, a feature which will be discussed in greater detail below.

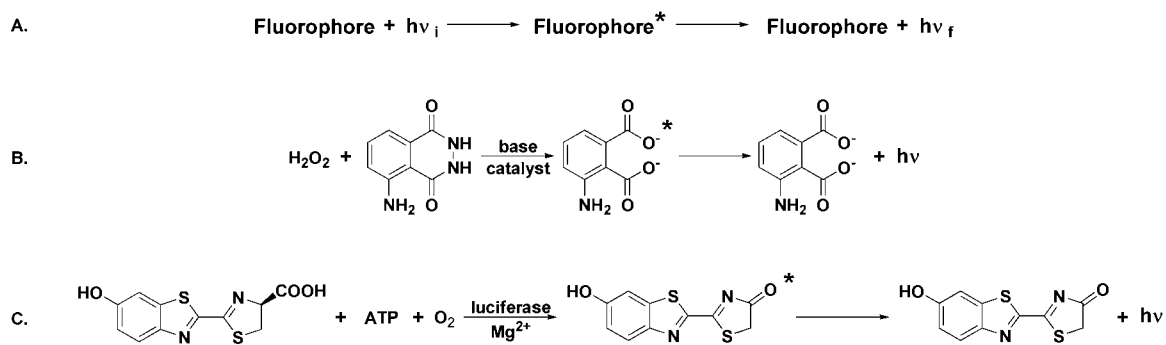


**Figure 1.3: Methods of molecular luminescence.** A. Fluorescence or phosphorescence. B. Chemiluminescence: reaction of hydrogen peroxide with luminal. C. Bioluminescence: luciferase/D-luciferin reaction. \* indicates excited state molecule/ion,  $h\nu$ : light,  $i$ : initial wavelength/energy,  $f$ : final wavelength/energy.

## Fluorescence and Biology

Fluorescence is, without doubt, one of the most indispensable tools employed in biology. The use of fluorescence has allowed us to sequence genomes, monitor protein folding, examine DNA and protein binding interactions, study protein localization and kinetics, quantitate gene expression, and peer into whole cells and organisms (Fei and Gu, 2009; Fernández-Suárez and Ting, 2008; Franca et al., 2002; Ntziachristos, 2006; Prendergast, 1991; Rao et al., 2007; Zimmer, 2002). In addition to basic research, fluorescence has made direct contributions to human health. For example, the near-infrared fluorescent Indocyanine Green is an FDA approved contrast reagent and has been employed during diagnostic and surgical procedures (Figure 1.4) (Marshall et al., 2010; Ohba et al., 2012; Zehri et al., 2014). Of all these roles, it is in the arena of cellular imaging that fluorescence has made its greatest impact.

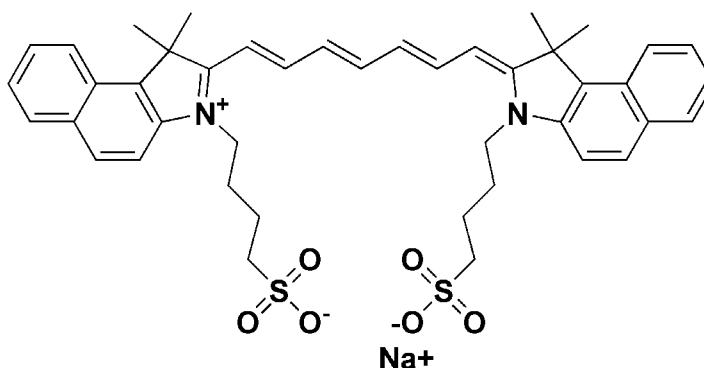


Figure 1.4: Indocyanine Green (ICG).

Fluorescence has provided biologists with the opportunity to image cells with detail unattainable by more classical techniques, such as bright and dark field microscopy (Perlasamy, 2001). This is because fluorescence imaging employs light emitting contrast agents, fluorophores, which can be designed to label proteins and DNA, a feature that has allowed the imaging of individual molecules within their native environments (Ntziachristos, 2006; Perlasamy, 2001). In fact, due to the advancements in instrumentation associated with fluorescence microscopy, we are now even able to image single molecules within cells (Ntziachristos, 2006; Perlasamy, 2001). With the advent of fluorescent proteins, cell biologists have even been able to monitor the intracellular environment, in real time, without the need of additional interrogating agents (Ntziachristos, 2006; Zimmer, 2002).

The contributions of fluorescence imaging are not limited to cells. Non-fluorescent microscopy techniques are of little use when imaging whole organisms (Hilderbrand and Weissleder, 2010; Ntziachristos, 2006). However, as certain wavelengths of light have the ability to penetrate through tissue, fluorescence has allowed us to non-invasively peer into the inner workings of whole organisms (Frangioni, 2003; Hilderbrand and Weissleder, 2010; Ntziachristos, 2006). For example, Indocyanine Green is used both for imaging liver function and as a general contrast agent for angiograms (Marshall et al., 2010). Likewise, current work on long wavelength fluorescent proteins will soon

allow us to non-invasively image deeper into a living organism than has ever been performed in a laboratory setting.

There are primarily two imaging techniques employed in biological research: fluorescence and bioluminescence. Fluorescence has several aspects that make its use preferable over bioluminescence. Fluorescence is rapid, with light emission occurring within  $10^{-8}$  to  $10^{-9}$  seconds (Lakowicz, 2006). This is faster than most enzyme-catalyzed reactions; therefore, compared to the enzyme-catalyzed bioluminescence, fluorescence imaging occurs in real time. Fluorescence is also much brighter than bioluminescence, which means for the same image, less fluorophore and less time is required when employing fluorescence as the imaging method (Sullivan, 2007). Most importantly, fluorescence is inherent to the molecule. Unlike bioluminescence, which requires the reaction of luciferase with luciferin to generate light, a fluorescent protein is itself fluorescent. This means that getting signal via fluorescence imaging will not be dependent on a cofactor diffusing through a cell membrane and locating an enzyme (Lee, 2008). All these features favor the use of fluorescence for live cell and *in vivo* imaging because they all offer the promise of visualizing the subject with the least amount of perturbation.

### **Flaws in Fluorescence Imaging Techniques**

Despite all the benefits of fluorescence-based imaging techniques, using fluorescence to investigate cells and whole organisms has several drawbacks.

Fluorescence imaging generally employs visible (400-650 nm) light. Visible wavelength radiation, particularly wavelengths between 400-500 nm, has been found to produce genotoxic effects similar to those caused by UV radiation (Botta et al., 2009; Pflaum et al., 1994; Pflaum et al., 1998). This is significant, as the frequently employed enhanced Green Fluorescent Protein (EGFP) is excited by light with these toxic wavelengths (excitation: 488 nm) (Figure 1.5). Other well-known fluorophores including 4',6-diamino-3-phenylindole (DAPI) (excitation: 358 nm), Fluorescein (excitation: 494 nm), and Cy2 (excitation: 492 nm) also require the input of light that is inherently dangerous to biological systems (Figure 1.5). Employing an input that damages the very system under interrogation undoubtedly calls into question the utility of the technique as well as the results obtained from severely disrupted cells.

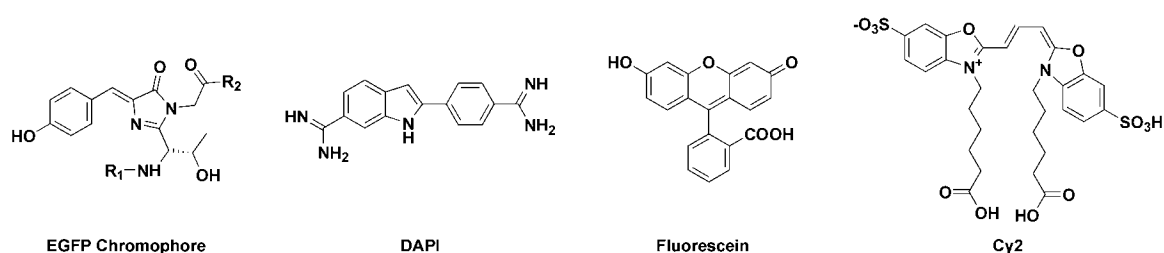


**Figure 1.5: Commonly employed fluorophores for biological imaging.**

The issue of phototoxicity is easily addressed by using fluorophores excited by less phototoxic, longer wavelength radiation (500-650 nm). However, phototoxicity is not the only problem encountered when imaging with visible wavelength fluorophores. Cells and organisms contain many molecules that emit

visible light (Monici, 2005). These endogenous compounds include, but are not limited to, reduced nicotinamide adenine dinucleotide phosphate (NADPH), pteridine derivatives such as flavins, porphyrins, and proteins containing high quantities of aromatic amino acids (Andersson-Engels et al., 1997; Monici, 2005). The fluorescence of endogenous compounds, termed autofluorescence, is highly problematic for both the technique and results obtained from fluorescence imaging as it profoundly decreases the signal to noise ratio of exogenous fluorophores and thus lowers image resolution (Frangioni, 2003) (Figure 1.6).



**Figure 1.6: Autofluorescence of live 3T3B cells.** Image obtained with Zeiss fluorescence microscope using a UG1 excitation filter (360 nm), a 420 nm dichroic filter, and a long pass emission filter (418 nm). Image adapted from (Aubin, 1979).

While the use of visible light for imaging live cells has some limitations, its utility in living organisms is almost completely hindered due to light scattering,

autofluorescence, and the absorbance of excitational light by molecules such as hemoglobin (Dobrucki, 2007; Escobedo et al., 2010; Frangioni, 2003; Ghoroghchian et al., 2009; König, 2000; Rao et al., 2007; Tromberg et al., 2000). In live cells and organisms, visible light undergoes extensive scattering due to interactions with non-homogenous particles, such as organelles and tissue components (Cheong et al., 1990; Dobrucki, 2007; Ghoroghchian et al., 2009). Due to photon spreading produced by light scattering, imaging with visible light is associated with low spatial resolution and plagued by high autofluorescence (Dobrucki, 2007; Genina et al., 2008; Jansen et al., 2006; Tromberg et al., 2000). Light scattering however is not the only cause of autofluorescence. As with live cells, organisms are composed of molecules that can emit visible light upon direct excitation. In fact, autofluorescence in whole organisms occurs to such a high extent that deconvoluting light from exogenous versus endogenous fluorophores becomes almost impossible (Frangioni, 2003). On top of these obstacles, the high absorbance of visible light by biological components, such as oxyhemoglobin, minimizes the availability of photons for the excitation of exogenous fluorophores (Figure 1.7) (Frangioni, 2003; König, 2000; Tsai et al., 2001). Due to these complications, imaging organisms with visible light is inefficient beyond the most peripheral locations.

However, fluorescence imaging of organisms is possible. We have already noted that diagnostic and surgical procedures have been performed using Indocyanine Green as a contrast agent (Marshall et al., 2010; Ohba et al., 2012;



Zehri et al., 2014). The feature of this dye that makes *in vivo* fluorescence imaging possible is that it is not a visible wavelength fluorophore. Indocyanine Green can be used for imaging because it absorbs and emits NIR light.

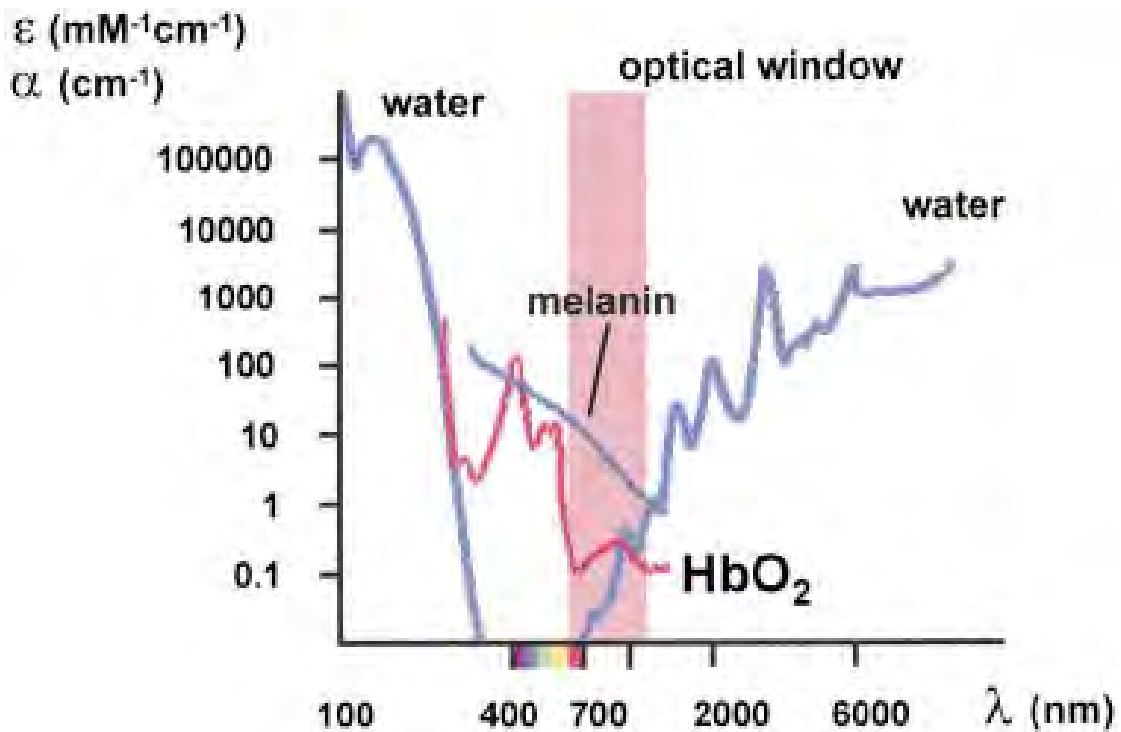


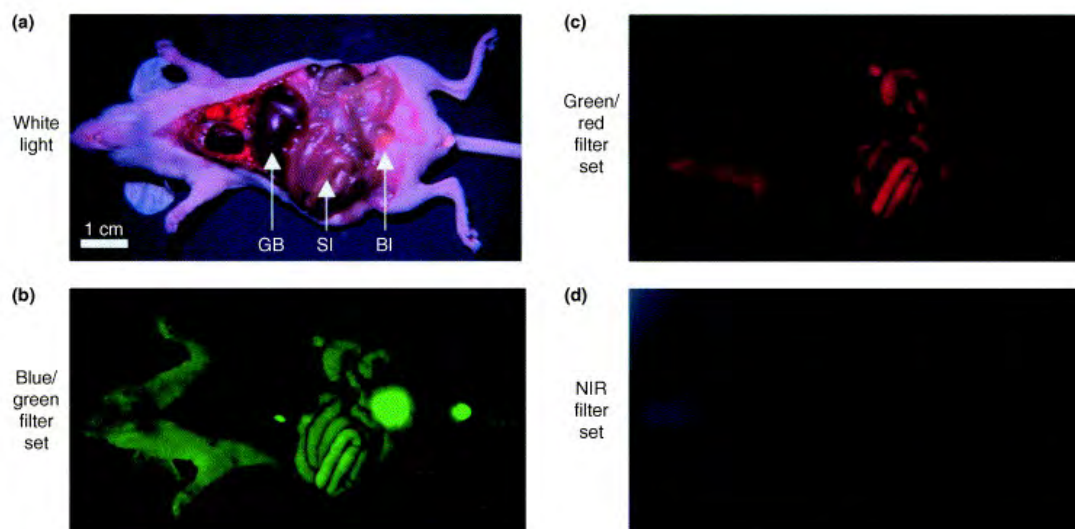
**Figure 1.7: Absorbance spectra of melanin, oxyhemoglobin (HbO<sub>2</sub>), and water.** Figure adapted from (König, 2000).

### Near-infrared Light

Over the last two decades, fluorescence imaging with near-infrared (NIR) light (650-900 nm) has risen to the forefront of biology as a superior alternative to visible light (Escobedo et al., 2010; Frangioni, 2003; Guo et al., 2014; Rao et al., 2007; Weissleder, 2001). NIR radiation has several extremely important features

that support the use of fluorophores capable of absorbing and emitting these wavelengths. Very few biological molecules absorb NIR light (König, 2000; Zhang et al., 2012). As phototoxicity results from the excitation of biological molecules, the limited absorption of NIR radiation means a drastic decrease in cell damage and death (Guo et al., 2014). This increase in cell viability easily translates to a higher degree of experimental reliability and clearly explains why NIR should be favored for imaging.

However, the poor absorbance of NIR light by biological components does not simply affect cell viability; it directly enhances the results obtained through imaging. Background autofluorescence is minimized when using NIR light for imaging because NIR light does not excite endogenous compounds to any great extent (Escobedo et al., 2010; Frangioni, 2003; Guo et al., 2014; Rao et al., 2007; Zhang et al., 2012). This feature was best exemplified by Frangioni imaging a mouse containing no exogenous fluorophores with visible and NIR light (Figure 1.8) (Frangioni, 2003). Only the NIR filter set provided an image without interfering autofluorescence. This result clearly presents the advantages of imaging with NIR light.



Current Opinion in Chemical Biology

**Figure 1.8: Near-infrared light produces little to no autofluorescence background in whole organisms.** Mouse was not treated with any exogenous fluorophores. After sacrificing, the mouse was immediately imaged using the following filter sets (b) Excitation: 460-500 nm/Emission: 505-560 nm, (c) Excitation: 525-555 nm/Emission: 590-650 nm, (d) Excitation: 725-775 nm/Emission: 790-830 nm. Image adapted from (Frangioni, 2003).

Poor absorbance of NIR light by biological components has yet another advantage. As mentioned above, hemoglobin is one of the primary deterrents to using visible wavelength fluorophores in living organisms (Frangioni, 2003; König, 2000; Pansare et al., 2012; Tsai et al., 2001). However, Figure 1.7 shows that hemoglobin only poorly absorbs NIR light (König, 2000). This means that fluorophores that absorb and emit NIR radiation can be employed in live animals (Frangioni, 2003; König, 2000; Pansare et al., 2012). Indeed, this is the primary reason that Indocyanine Green can be used as a biomedical contrast agent (Marshall et al., 2010).

The poor absorption of NIR light by hemoglobin and other tissue components means that NIR light can penetrate further into tissue than visible light (Frangioni, 2003; Guo et al., 2014; König, 2000; Pansare et al., 2012; Peng and Draney, 2004; Zhang et al., 2012). This feature is further enhanced due to a decrease in light scattering associated with NIR wavelengths (Escobedo et al., 2010; Ghoroghchian et al., 2009; Peng and Draney, 2004). As described in Equation 1.1,

$$1.1) \quad I \propto 1/\lambda^4$$

scattering intensity from an excitation source is inversely proportional to the fourth power of wavelength (Ghoroghchian et al., 2009). Thus, compared to visible light, the longer wavelength NIR excitational light will experience a much smaller decrease in photon intensity when employed in biological media (Peng and Draney, 2004). With decreased autofluorescence, decreased excitational light absorption and scattering, and decreased phototoxicity, the case for using NIR light for cellular and whole organism imaging is not a difficult one to present. Strangely, compared to visible wavelength fluorophores, the NIR toolkit is relatively bare.

### **NIR Fluorophores**

Whereas multiple visible wavelength absorbing/emitting fluorophores can be found dispersed among a wide variety of classes including: acridines, alizarins, boron-dipyrromethenes (BODIPYs), cyanines, fluoresceins, oxazines,

rhodamines, and a large variety of fluorescent proteins (DsRed, GFP, RFP, YFP, etc.), the list of NIR absorbing/emitting fluorophores is much smaller (Figure 1.9). There are primarily four classes of NIR fluorophores: BODIPYs, cyanines, phthalocyanines, or squaraines, and of this group, only indocyanine derivatives are employed in fluorescence imaging to a great extent (Figure 1.10) (Guo et al., 2014; Escobedo et al., 2010; Pansare et al., 2012; Peng and Draney, 2004; Rao et al., 2007; Zhang et al., 2012). Encouragingly, there has been work in increasing the NIR scaffold toolkit and there are now a handful of NIR fluorescent proteins, oxazines, and most recently, silicon-rhodamines (Si-rhodamines) (Figure 1.10) (Escobedo et al., 2010; Koide et al., 2011; Koide et al., 2012; Luo et al., 2011; Pansare et al., 2012; Peng and Draney, 2004; Piatkevich et al., 2013; Rao et al., 2007; Shcherbakova and Verkhusha, 2013; Zhang et al., 2012). Each of these classes has features that favor and deter their use in biological imaging.

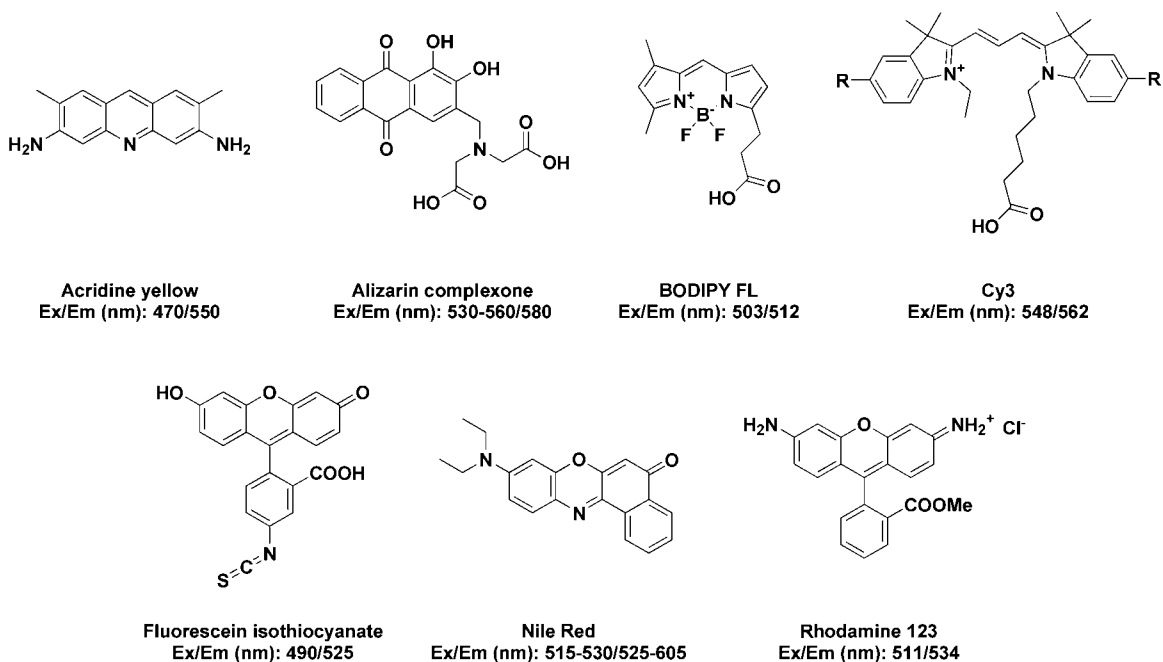


**Figure 1.9: Examples of visible light absorbing/emitting organic fluorophores.** Wavelengths obtained from <http://www.olympusfluoview.com/theory/fluorochromedata.html>

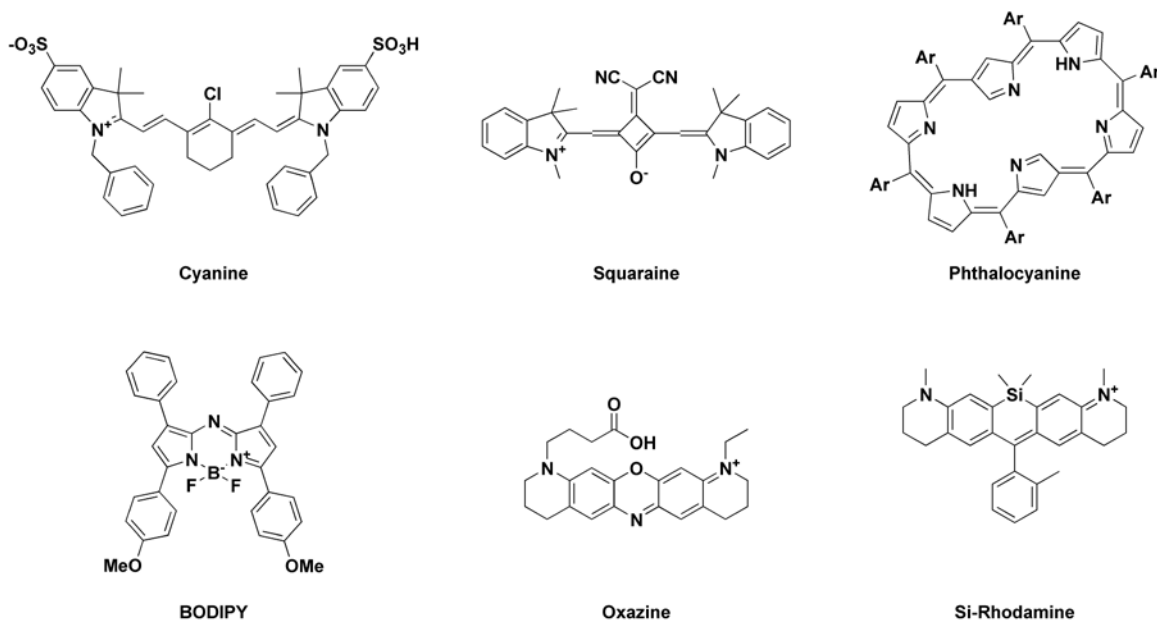


**Figure 1.10: Examples of NIR organic fluorophores.** Structures from (Koide et al., 2012; Luo et al., 2011; Marmé et al., 2003).

Squaraines dyes, recognizable by their characteristic oxocyclobutenolate core, have chemical and photophysical characteristics that should make them ideal imaging reagents (Luo et al., 2011; Pansare et al., 2012; Zhang et al; 2012). These fluorophores generally have high extinction coefficients and quantum yields, which gives them desirably bright fluorescence (Luo et al., 2011; Pansare et al., 2012; Zhang et al; 2012). They also tend to be very photostable, which makes them well suited for biological applications requiring extended imaging times (Pansare et al., 2012). Both the central cyclobutene ring, as well as the terminal aryl groups can be functionalized, making these compounds prime targets for use as probes (Luo et al., 2011; Zhang et al., 2012). Unfortunately, due to their structural planarity and high degree of conjugation,

these compounds are notoriously insoluble in water, limiting their usefulness within cells and organisms (Luo et al., 2011; Pansare et al., 2012). Work has been done to increase their water-solubility through the addition of negatively charged groups, such as sulfonates, but this appears to have a detrimental effect on their fluorescence intensity (Pansare et al., 2012).

Phthalocyanines are porphyrin derivatives which have found use in both research and medicine (Allen et al., 2001; Escobedo et al., 2010; Whitacre et al., 2000). These compounds are renowned for their high photostability and large extinction coefficients (Luo et al., 2011; Peng and Draney, 2004). Unfortunately, these molecules are hydrophobic and often aggregate in aqueous environments (Peng and Draney, 2004). Functionalization of these dyes with polar groups have led to increased solubility in water; however, due to their ability to function as photosensitizers, their use as imaging reagents can result in phototoxic side effects (Allen et al., 2001; Escobedo et al., 2010; Luo et al., 2011; Whitacre et al., 2000).

Cyanines, particularly heptamethines, are without question the most commonly employed NIR dyes in biology (Luo et al., 2011; Peng and Draney, 2004). This class contains the well known imaging reagents IR-780 and IR-783 that have been employed as scaffolds for developing fluorescent sensors of metal ions, nitric oxide, and hydrogen peroxide (Karton-Lifshin et al., 2011; Li et al., 2011; Sasaki et al., 2005). This class also contains Indocyanine Green, the



only NIR dye approved for use in humans (Marshall et al., 2010; Ohba et al., 2012; Zehri et al., 2014). Cyanine dyes are celebrated for their high extinction coefficients and long wavelength fluorescence (Luo et al., 2011; Pansare et al., 2012). However, they tend to have low photostability, poor water solubility, and low quantum yields in aqueous environments (Luo et al., 2011; Pansare et al., 2012; Peng and Draney, 2004). Some of these problems have been addressed through sulfonation of the dye scaffold, which has led to the development of multiple water-soluble cyanine derivatives, including the commercially available Alexa Fluor<sup>®</sup> dyes (Molecular Probes) (Mujumdar et al., 1993). However, sulfonated molecules are generally unable to diffuse through cellular membranes, which prevents these dyes from being employed in live cell imaging (Stolz, 2001; Wuhmann et al., 1980).

There are a growing number of NIR BODIPY scaffolds available for fluorescence imaging (Ni and Wu, 2014). BODIPYS are famous for their bright fluorescence, high quantum yield, and high photostability (Luo et al., 2011; Ni and Wu, 2014; Pansare et al., 2012). Even in water, these dyes are reported to have a quantum yield approaching unity (Luo et al., 2011). However, the BODIPY scaffold is among the least water-soluble of all the dyes listed above and increasing conjugation to obtain NIR absorbance and emission only enhances this negative feature (Luo et al., 2011; Ni and Wu, 2014; Pansare et al., 2012).

The pentacyclic oxazine scaffold is a NIR fluorophore with great potential for live cell and *in vivo* imaging (Hintersteiner et al., 2005, Stöhr et al., 2010; van de Linde et al., 2012). This dye has several properties that favor its use as a cellular imaging reagent. It has a compact structure which minimizes the hydrophobic surface area available for dye aggregation (Peng and Draney, 2004). Ring pucker from the terminal azacyclohexane rings further helps to alleviate aggregation in aqueous environments (Figure 1.11). Oxazines also exhibit high photostability and bright NIR fluorescence (Anzalone et al., 2013; Escobedo et al., 2010; Vogelsang et al., 2009). Despite these features, this dye is rarely employed for NIR imaging.

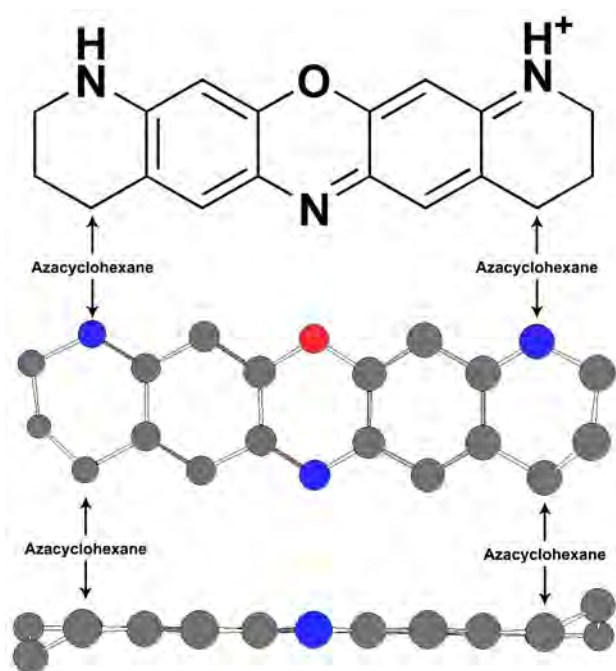


**Figure 1.11: Ring pucker from the terminal azacyclohexane rings of the pentacyclic oxazine scaffold.**

One of the newest classes of NIR dyes are silicon analogs of rhodamines (Si-rhodamines) (Koide et al., 2011; Koide et al., 2011; Koide et al., 2012). These dyes owe their NIR absorption and emission to hyperconjugation induced by a central silicon, which results in an extensive decrease in the energy difference between the ground and excited states (Guo et al., 2014; Koide et al., 2011; Koide et al., 2011; Koide et al., 2012). As the increased conjugation does not require addition of polymethine chains or aromatic rings, the hydrophobicity of these compounds compared to their visible wavelength conjugates would not be expected to differ to any great extent. These new fluorophores have already been used in the preparation of ion sensors (mercury and calcium) and have even shown promise for imaging in live cells (Egawa et al., 2011; Guo et al., 2014; Koide et al., 2011; Koide et al., 2012).

NIR fluorescent proteins are among the most desired of developments for the field of imaging. No single molecule has made such an impact on biology as the Green Fluorescent Protein, and proteins that could absorb and emit NIR light would circumvent the problems associated with this marvel of science (Tsien, 1998; Zimmer, 2002). To date though, there are still very few of these molecules available. Little success has been achieved to manufacture GFP-type proteins that absorb in the NIR, although there are some that emit in the far-red (Wu et al., 2011). The greatest success thus far has been through the use of bacterial phytochrome photoreceptors (BphPs) (Shcherbakova and Verkhusha, 2013). These macromolecules are showing promise, but they tend to have very low

quantum yields and require an additional cofactor in order to become fluorescent (Shcherbakova and Verkhusha, 2013).

### **Flaws of NIR Fluorophores**

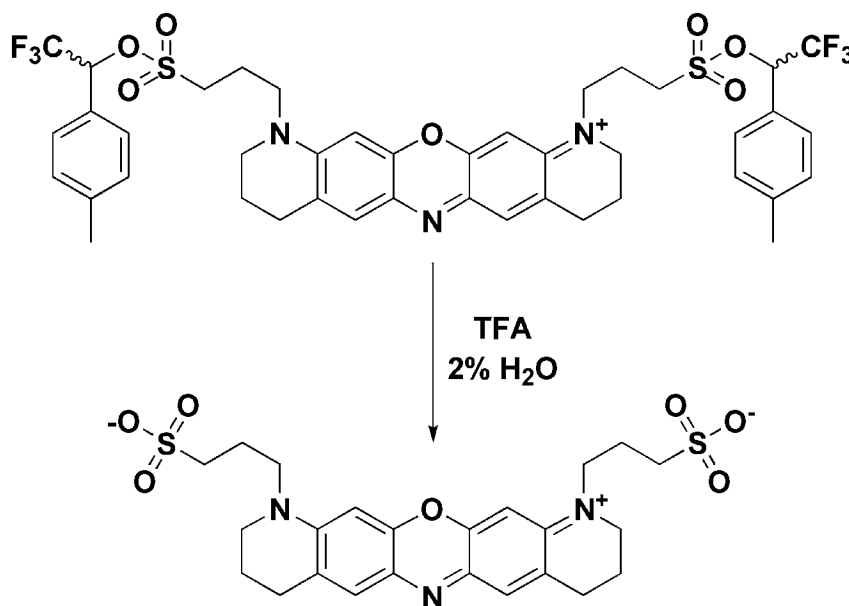
Although NIR light is ideal for imaging in live cells and organisms, it is clear from the above survey of those currently available, that NIR fluorophores are not ideal imaging reagents (Weissleder, 2001). Most of these molecules are poorly water soluble, which results from the high degree of conjugation and structural planarity required for the absorbance of low energy radiation (Sauer et al., 2011). Unfortunately, since cells and organisms are primarily aqueous, hydrophobic dyes are not a suitable imaging tool. Another problematic feature of NIR dyes is that they tend to be cationic (Figure 1.10). This presents a challenge for imaging live cells because these compounds will tend to be attracted to and localize in the negatively polarized mitochondrial membrane (Bunting et al., 1989). The hydrophobic and cationic nature of these molecules will therefore produce high background fluorescence resulting from membrane and mitochondrial staining (Bunting et al., 1989; Cunningham et al., 2010; Escobedo et al., 2010; Jiang et al., 2013; Johnson, 1998). The primary method used to increase water-solubility and eliminate the cationic charge of the dye is to modify the scaffold with highly polar sulfonate groups (Li et al., 2008; Morgan et al., 2011; Mujumdar et al., 1993; Niu et al., 2009; Panchuk-Voloshina et al., 1999).

While this is a successful strategy, it prevents the molecules from traversing cellular membranes (Stolz, 2001; Wuhrmann et al., 1980).

### **Summary**

Apart from the flaws discussed above, a key feature lacking in the NIR toolkit is diversity. While there are several different NIR scaffolds, most fluorophores targeted for use in imaging are indocyanine derivatives. This results in a very limited chemical palette. The feature most needed for biological imaging is a greater choice of imaging reagents. With choice comes opportunity and NIR imaging offers science the opportunity to examine live cells and organisms in much greater detail than can be obtained with visible light.

**CHAPTER II: A trifluoroacetic acid-labile sulfonate protecting group and its use in the synthesis of a near-IR fluorophore**



**Summary**

Sulfonated molecules exhibit high water solubility, a property which is valuable for many biological applications, but often complicates their synthesis and purification. Here, we report a sulfonate protecting group that is resistant to nucleophilic attack, but is readily removed with trifluoroacetic acid (TFA). The use of this protecting group improved the synthesis of a sulfonated near-IR fluorophore and the mild deprotection conditions allowed isolation of the product without requiring chromatography.

## ***Introduction***

Sulfonation of hydrophobic fluorescent dyes greatly improves both their solubility and fluorescence properties in aqueous media (Li et al., 2008; Morgan et al., 2011; Mujumdar et al., 1993; Niu et al., 2009; Panchuk-Voloshina et al., 1999). However, sulfonated molecules can be tedious to prepare and purify because their high polarity often necessitates the use of aqueous conditions during synthesis and purification. For example, we found that HPLC was required for purification of sulfonated oxazine near-IR fluorophores such as **1** (Figure 2.1) (Pauff and Miller, 2011). On the other hand, purification of stable sulfonate ester dyes such as **2** was possible via conventional silica gel flash chromatography (Figure 2.1) (Pauff and Miller, 2011). Thus, the synthesis of sulfonated molecules could be aided by a protecting group which allows solubility in standard organic solvents and purification by conventional chromatography, but is readily removed in a final cleavage step that does not itself require HPLC purification.

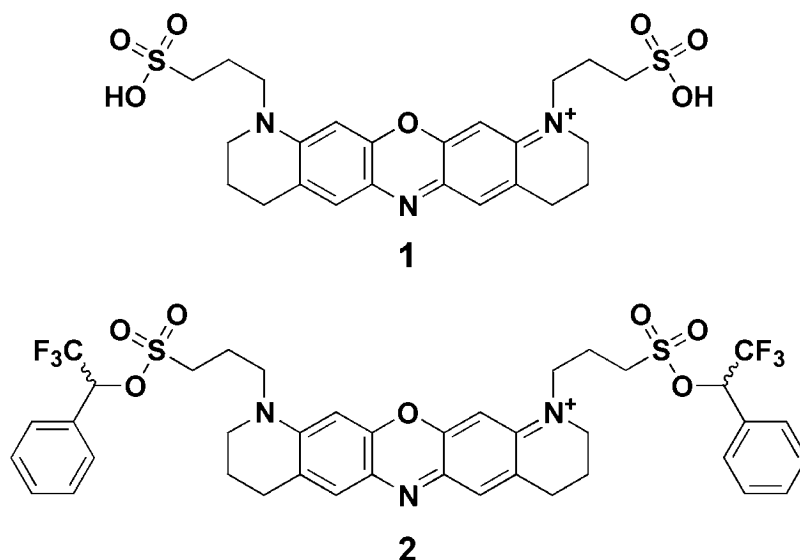


**Figure 2.1: Bis-sulfonate oxazine (1) and bis-sulfonate ester (2).**

Compared to carboxylates, there are relatively few choices for sulfonate protecting groups (Green and Wuts, 1999). Sulfonate esters are generally highly reactive electrophiles that alkylate a wide range of nucleophilic molecules. Protecting groups currently available for sulfonates all have caveats that limit their general applicability (Miller, 2010). Isopropyl (*i*Pr) and isobutyl (*i*Bu) sulfonates retain lability to nucleophiles, while trichloroethyl (TCE) sulfonates are unstable to mildly basic conditions (Ali et al., 2009; Musicki and Widlanski, 1990; Simpson and Widlanski, 2006; Xie and Widlanski, 1996). Neopentyl (Neo) groups are highly stable to nucleophiles but removal requires either strongly acidic conditions or heating in DMF with strong nucleophiles (Ali et al., 2009; Miller, 2010; Roberts et al., 1997; Simpson and Widlanski, 2006). Trifluoroethyl (TFE) sulfonates are stable to both nucleophilic and acidic conditions, but need strongly



basic conditions for removal (Miller, 2010). For our purposes, existing sulfonate protecting groups are either insufficiently stable, require cleavage conditions that are too harsh, and/or deprotection would require subsequent HPLC purification. For example, attempted cleavage of the sulfonate ester dye **2** with NaOH led to dye decomposition.

A convenient cleavage reagent for many protecting groups is trifluoroacetic acid (TFA) (Green and Wuts, 1999). While TFA-labile protecting groups for carboxylates, alcohols, amines, and other functionalities are common, most sulfonate esters that are stable to nucleophiles are also stable to TFA (Green and Wuts, 1999; Miller, 2010). An exception is the “triggered” TFA-labile sulfonate ester protecting group reported by Roberts et al., Neo N-B, which is stable to nucleophiles by virtue of its neopentyl structure (Roberts et al., 1997). However, cleavage of Neo N-B is a two-step process that requires initial cleavage of a Boc-protected amine followed by neutralization to effect release of the sulfonate. Isolation of the liberated sulfonate requires the chromatographic removal of non-volatile side-products, and the protecting group itself is not readily available, requiring a four-step synthesis from commercially available materials. Other related neopentyl-based protection strategies for sulfonates have similar limitations (Morgan et al., 2011; Seeberger et al., 2007). We therefore sought to develop a sulfonate protecting group which could satisfy three criteria: i) intrinsic TFA-lability not requiring any additional treatment for cleavage to occur; ii) easy

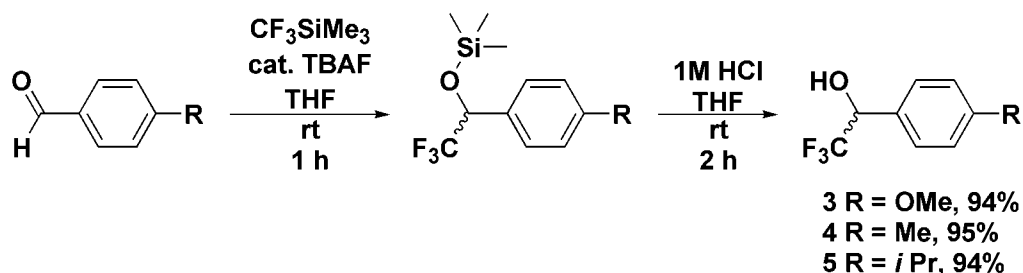
separation of the cleaved sulfonate from any byproducts; and iii) ready access from commercially available materials.

### **Results and Discussion**

In a recent survey of commercially available alcohols that could potentially serve as protecting groups for sulfonates, we found that  $\alpha$ -trifluoromethylbenzyl (TFMB) sulfonates are stable to nucleophiles and could function as a scaffold for the design of sulfonate ester protecting groups with engineered lability (as in **2**, Figure 2.1) (Miller, 2010). For example, we have prepared an esterase-labile sulfonate protecting group by incorporating an acetoxy group into the *para* position (Rusha and Miller, 2011). Thus, while TFMB sulfonates themselves are stable to TFA, we hypothesized that electron-rich variants could be created that would be labile to TFA yet retain stability to nucleophiles (Miller, 2010).

Solvolysis studies of 1-aryl-2,2,2-trifluoromethyl tosylates have shown that the rate of carbocation formation in ionizing solvents is dependent on the nature of the aryl group (Allen et al., 1983). We therefore introduced the strongly electron-donating *para*-methoxy group onto the TFMB scaffold by treating *p*-anisaldehyde with TMSCF<sub>3</sub> under Ruppert-Prakash conditions to afford **3** (Scheme 2.1) (Krishnamurti et al., 1991). More weakly electron-donating *p*-methyl and *p*-isopropyl substituents were similarly introduced to yield alcohols **4** and **5**, respectively (Scheme 2.1). Typically, the Ruppert-Prakash reaction is quenched with HCl to hydrolyze the initially-formed TMS ether, followed by

chromatographic purification (Krishnamurti et al., 1991). However, we found that the starting benzaldehydes and trifluoromethylated alcohol products closely elute during flash column purification. Thus, if the reaction is incomplete, purification becomes tedious. We therefore first purified the TMS ether, which was very well resolved from the starting aldehyde by flash chromatography. Subsequent treatment with aqueous acid cleanly cleaved the TMS ether to yield the desired product after extractive workup. We have adopted this improved synthesis protocol for all Ruppert-Prakash reactions with benzaldehydes.

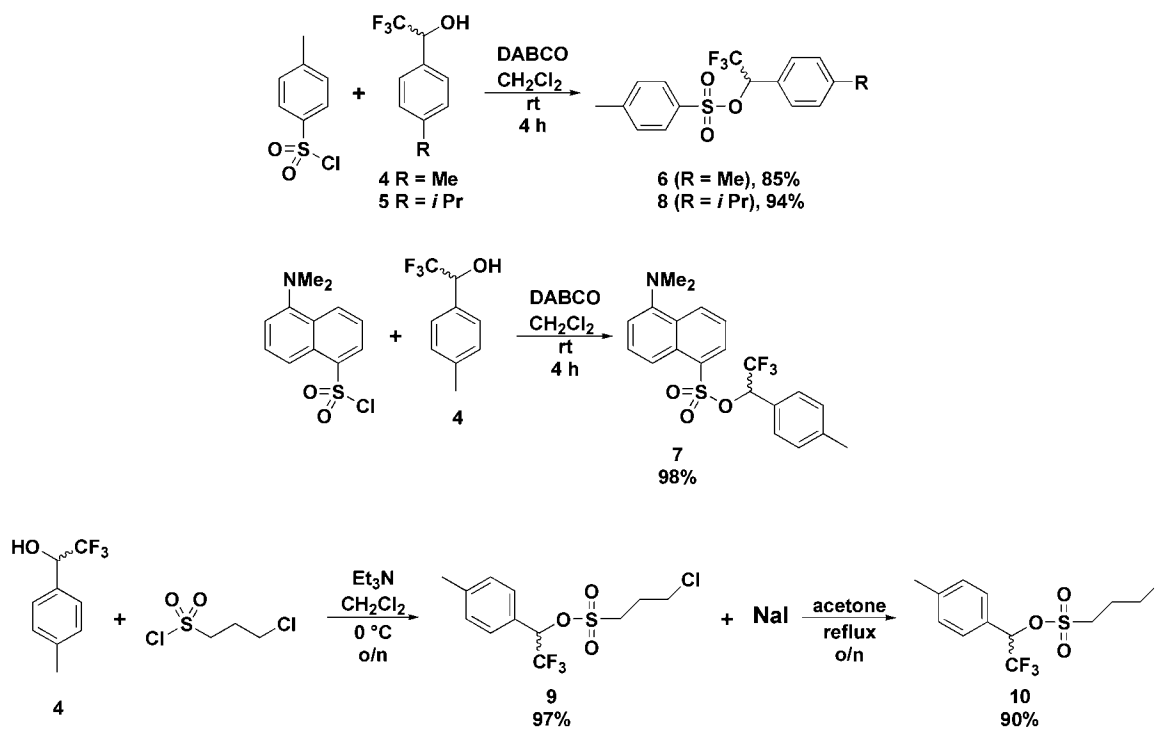


**Scheme 2.1: Ruppert-Prakash synthesis of potential reagents for the development of sulfonate protecting groups.**

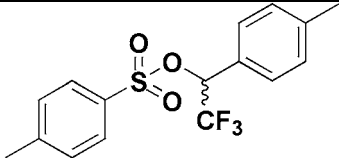
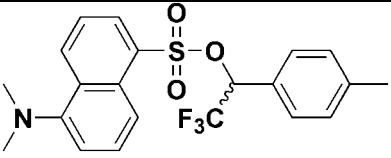
We next tested the suitability of **3-5** as sulfonate protecting groups.

Reaction of alcohol **3** with sulfonyl chlorides yielded sulfonate esters that were too labile to be easily isolated (e.g., the dansylate and 3-chloropropanesulfonate decomposed during purification on a silica gel column). On the other hand, sulfonate esters **6** and **7** derived from alcohol **4** (Scheme 2.2) were stable to isolation and to treatment with nucleophiles. Like the corresponding TFMB sulfonate esters, **6** and **7** were quantitatively recovered after 2 h treatment with

20% piperidine in DMF at room temperature or 4 h treatment with 1.1 eq of sodium iodide in refluxing acetone (Table 2.1, Figure 2.2) (Miller, 2010). While stable to nucleophilic attack, the *para*-methyl group is sufficiently electron-donating that sulfonate esters of **4**, dubbed "TFMT" sulfonates, can be cleaved by solvolysis in TFA (Table 2.2 and Table 2.3). Inclusion of water as a cation scavenging agent at 2% v/v or greater improves the cleavage yield in the case of the tosyl ester **6**. This may reflect the formation of a tight ion pair that can recombine unless quenched by water (Allen et al., 1995). Under these conditions, cleavage is readily achieved in 2 h at room temperature (Table 2.2), and the pure sulfonate could be conveniently isolated by extraction and evaporation, without requiring chromatography. Tosylate **8** derived from *p*-isopropyl alcohol **5** was also found to be TFA-labile and nucleophile stable, but provided no obvious advantages over TFMT. Finally, the TFMT sulfonate ester is stable to K<sub>2</sub>CO<sub>3</sub> in hot DMF and to hot dilute aqueous acidic conditions that cleave acetals and carboxylate esters (2M HCl/acetone, 70 °C), suggesting that TFMT sulfonates could survive similar conditions necessary for oxazine dye synthesis (Table 2.1) (Heiskanen and Hormi, 2009).



**Scheme 2.2: Synthesis of TFMT sulfonate esters.**

Condition		
20% Piperidine/DMF rt, 2h	100%	100%
1.1 eq NaI, Acetone reflux, 4h	100%	100%
1 eq K <sub>2</sub> CO <sub>3</sub> /DMF 65 °C, 24 h	92%	92%
1:1 2M HCl/Acetone 70 °C, 2h	93%	N/A

**Table 2.1: Stability of TFMT sulfonate esters.** The stability of compounds **6** (left) and **7** (right) was investigated in conditions known to cleave protecting groups or react with sulfonate esters. Percentages refer to the recovery of the starting material that was verified by <sup>1</sup>H- and <sup>19</sup>F-NMR and ESI-HRMS. N/A: compound not tested.

**Figure 2.2: Analytical HPLC traces of Compound 6 (A) and the purified material from cleavage (B) and stability (C) analyses of TFMT-sulfonate ester protecting group.** Cleavage/stability reactions (B/C, respectively) were performed and worked up as described in the experimental methods prior to HPLC analysis. Identity of the compounds were determined by  $^1\text{H}$ - and  $^{19}\text{F}$ -NMR and ESI-HRMS. Traces show absorbance detection at 224 nm. Detection at 262 nm was also obtained and replicated the above data.

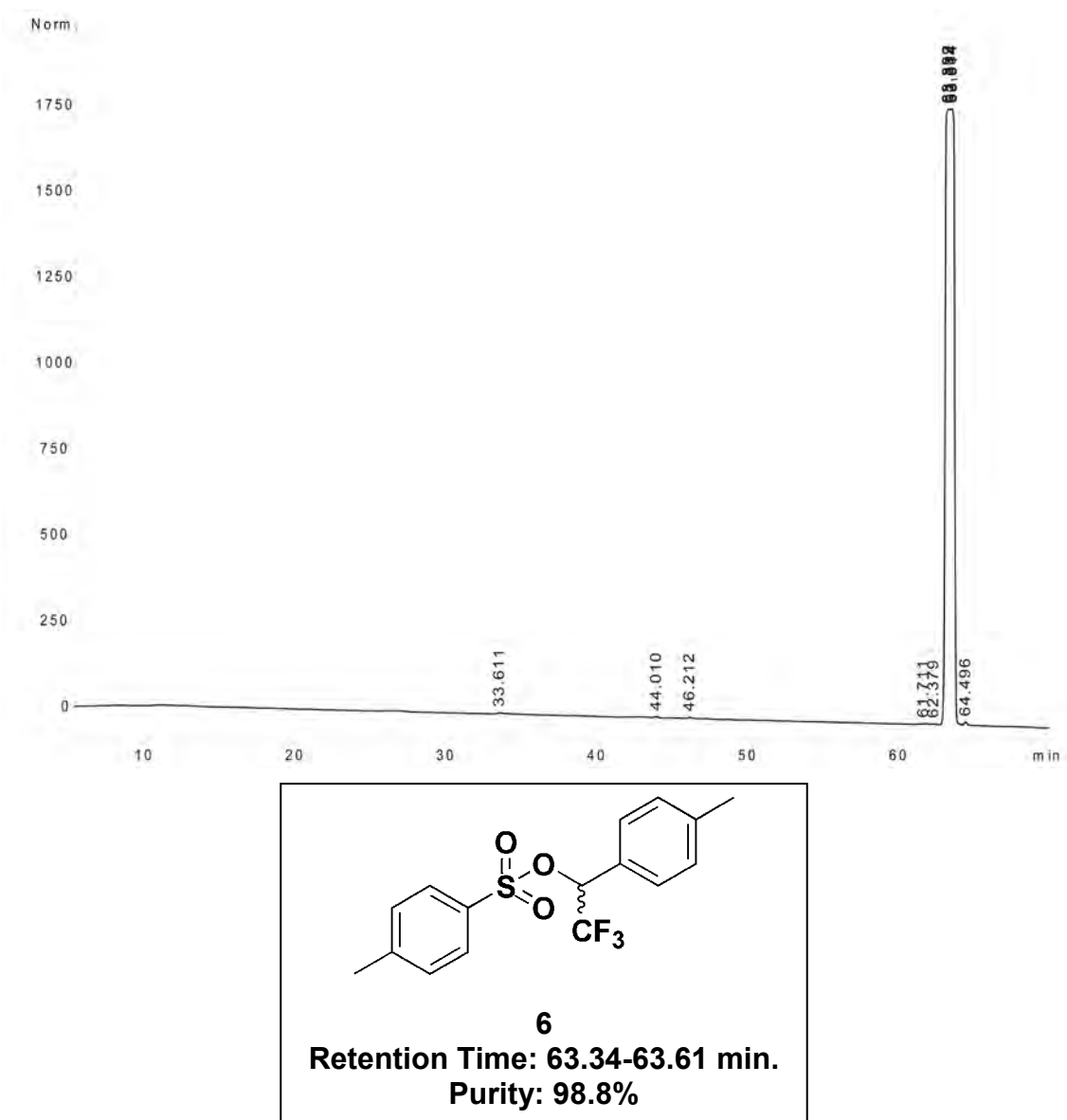


**Figure 2.2A.** HPLC trace of **6**.



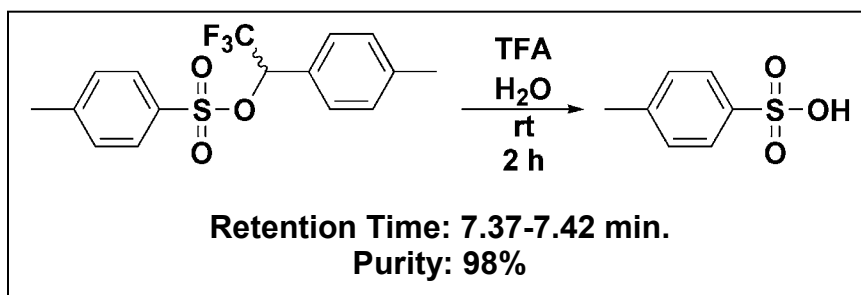
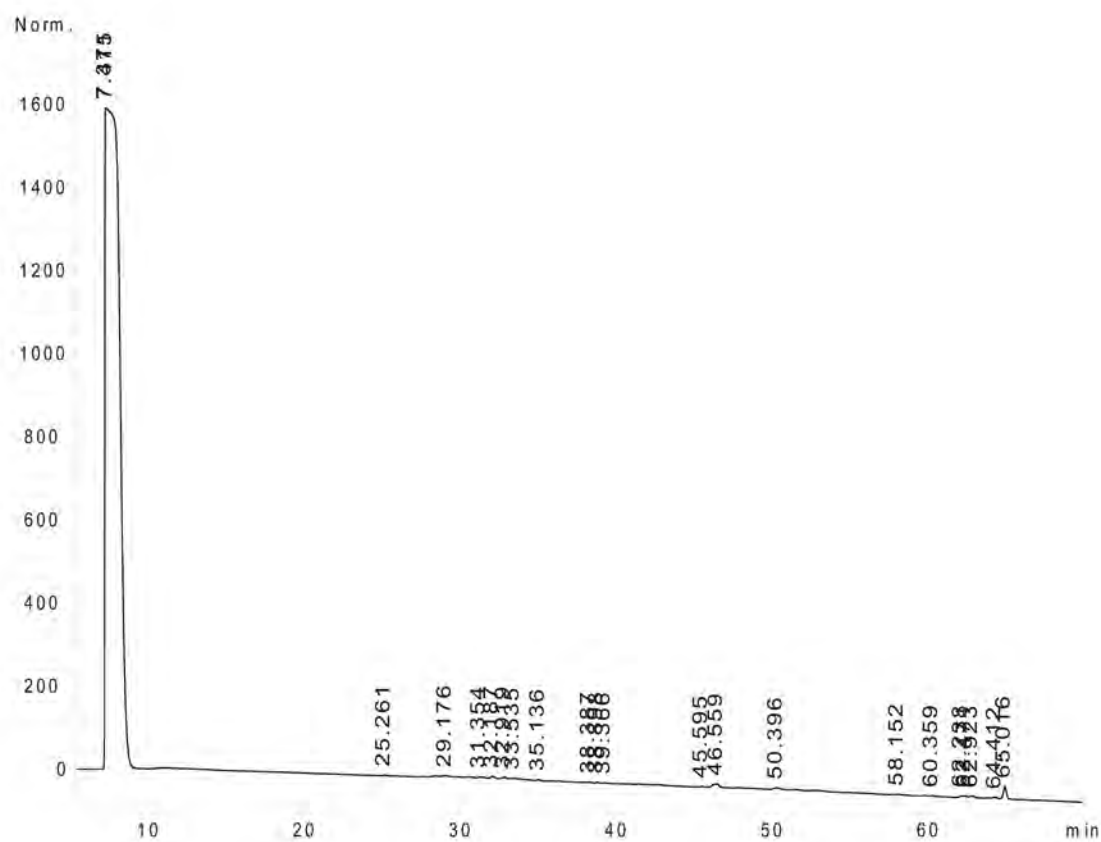
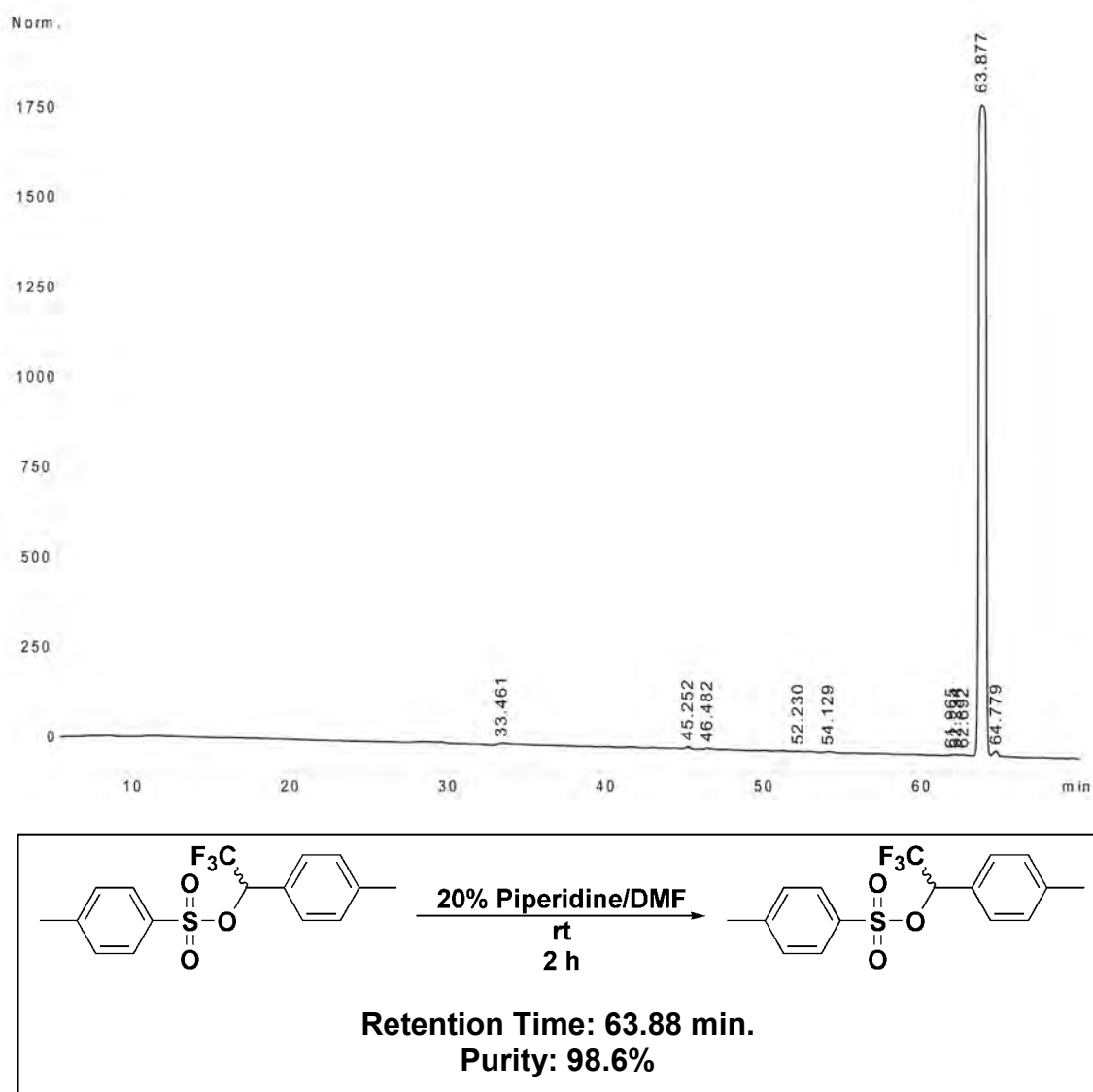
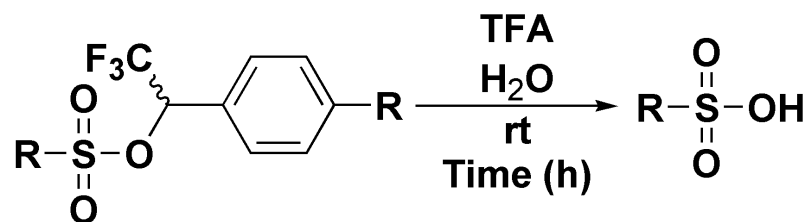


Figure 2.2B. HPLC trace of product from cleavage reaction with **6**.



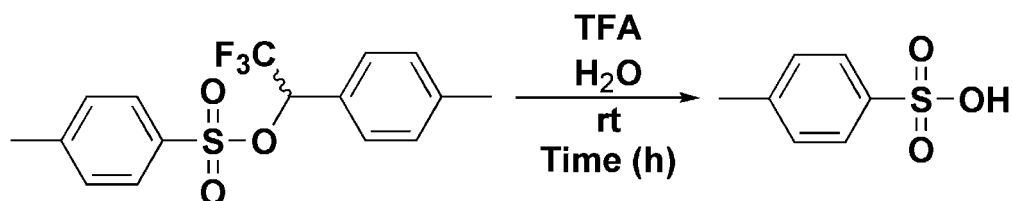
**Figure 2.2C.** HPLC trace of product from reaction of **6** with 20% piperidine in DMF.



Entry	Substrate	% Water	Time	Yield
1*	6	0	2h	39%
2	7	0	2h	84%
3**	6	1	2h	41%
4	7	1	2h	99%
5**	6	1	16h	88%
6†	6	2	2h	84%
7**	6	3	2h	82%
8	6	5	2h	89%

**Table 2.2: TFA cleavage of sulfonate esters 6 and 7.**

(\*): average of n = 3, (\*\*): n = 2, (†): n = 4. Entries without superscripts: n = 1.

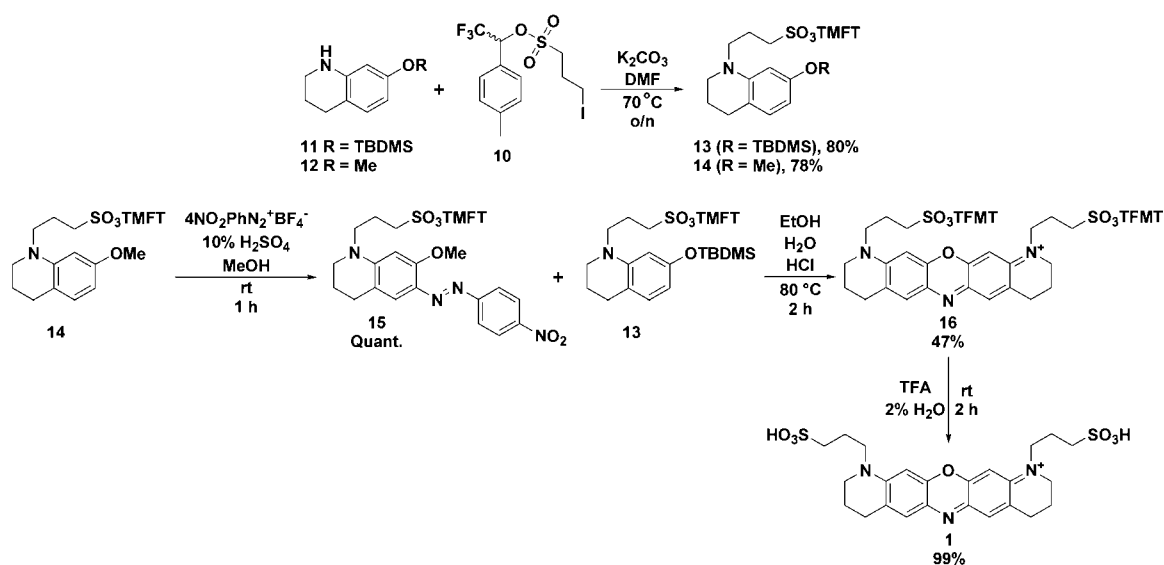


% H <sub>2</sub> O	Time (h)	Mass of <b>6</b> (mg)	Theoretical Yield of TosylSulfonate (mg)	Actual Yield of TosylSulfonate (mg)	% Yield
0	2	99	55	18	33
0	2	115	64	25	39
0	2	99	55	25	45
1	16	67	37	33	89
1	16	99	55	48	87
1	2	84	46	17	37
1	2	62	34	15	44
2	2	99	55	50	91
2	2	67	37	30	81
2	2	60	33	27	82
2	2	76	42	34	81
3	2	75	41	33	80
3	2	78	43	36	84
5	2	103	57	51	89

**Table 2.3: TFA cleavage of compound **6** employing different percentages of water as a cation scavenger.**

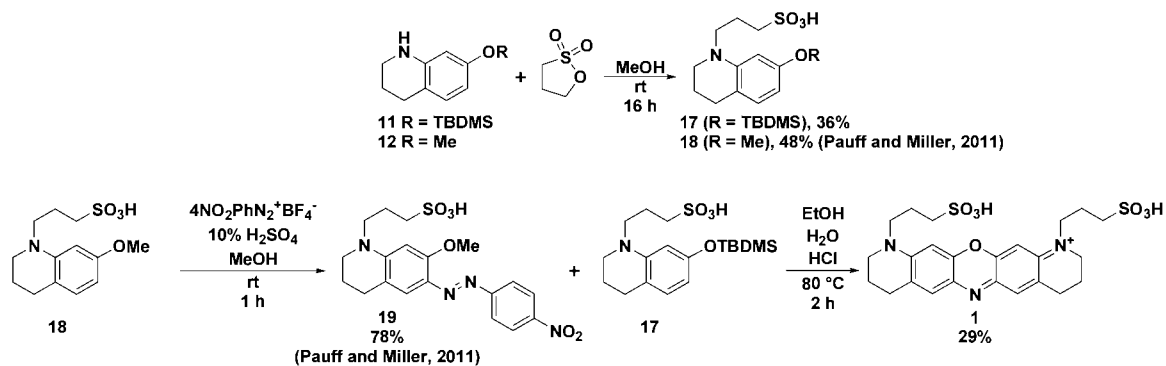
Having established that TFMT met our three criteria for a new sulfonate protecting group, we next sought to test its utility in the context of sulfonated near-IR fluorophore synthesis. To access the TFMT-protected sulfonated dyes, we first synthesized the TFMT-protected sulfopropyl iodide **10** (Scheme 2.2). As with TFMB, the remarkable stability of TFMT sulfonates to nucleophilic attack by iodide is manifestly demonstrated by the selective substitution of the chloride in **9** to cleanly afford **10** (Pauff and Miller, 2011). Iodide **10** was then used to alkylate

the tetrahydroquinolines **11** and **12** to afford **13** and **14** (Scheme 2.3) (Pauff and Miller, 2011). Like TFMB, the TFMT group was stable to these nucleophilic substitution reactions (Pauff and Miller, 2011). Similarly, acidic diazonium coupling conditions (10% aqueous H<sub>2</sub>SO<sub>4</sub>) and dye coupling conditions (hot acetic acid or HCl in refluxing aqueous ethanol) were tolerated, allowing access to the bis-TFMT protected oxazine dye **16** (Scheme 2.3), which could be purified by silica gel chromatography.



**Scheme 2.3: Synthesis of bis-sulfonated oxazine dye (1) using the TFA-labile TFMT sulfonate protecting group.**

Treatment of the purified bis-TFMT dye **16** with TFA and 2% H<sub>2</sub>O at rt for 2 h liberated the bis-sulfonate dye **1** (Scheme 2.3). After reaction, the volatiles were removed and the dye was extracted into water and lyophilized. Notably, complete cleavage was observed, and no impurities were introduced (Figure 2.3). Compared to the synthesis of the bis-sulfonated oxazine dye **1** using the conventional sulfopropylation reagent 1,3-propanesultone (Scheme 2.4), the TFMT approach was higher-yielding, easier to perform, and more rapid as all products could be purified by standard silica gel flash chromatography methods rather than HPLC.



**Scheme 2.4: Synthesis of bis-sulfonate oxazine dye (1) using 1,3-propanesultone.**

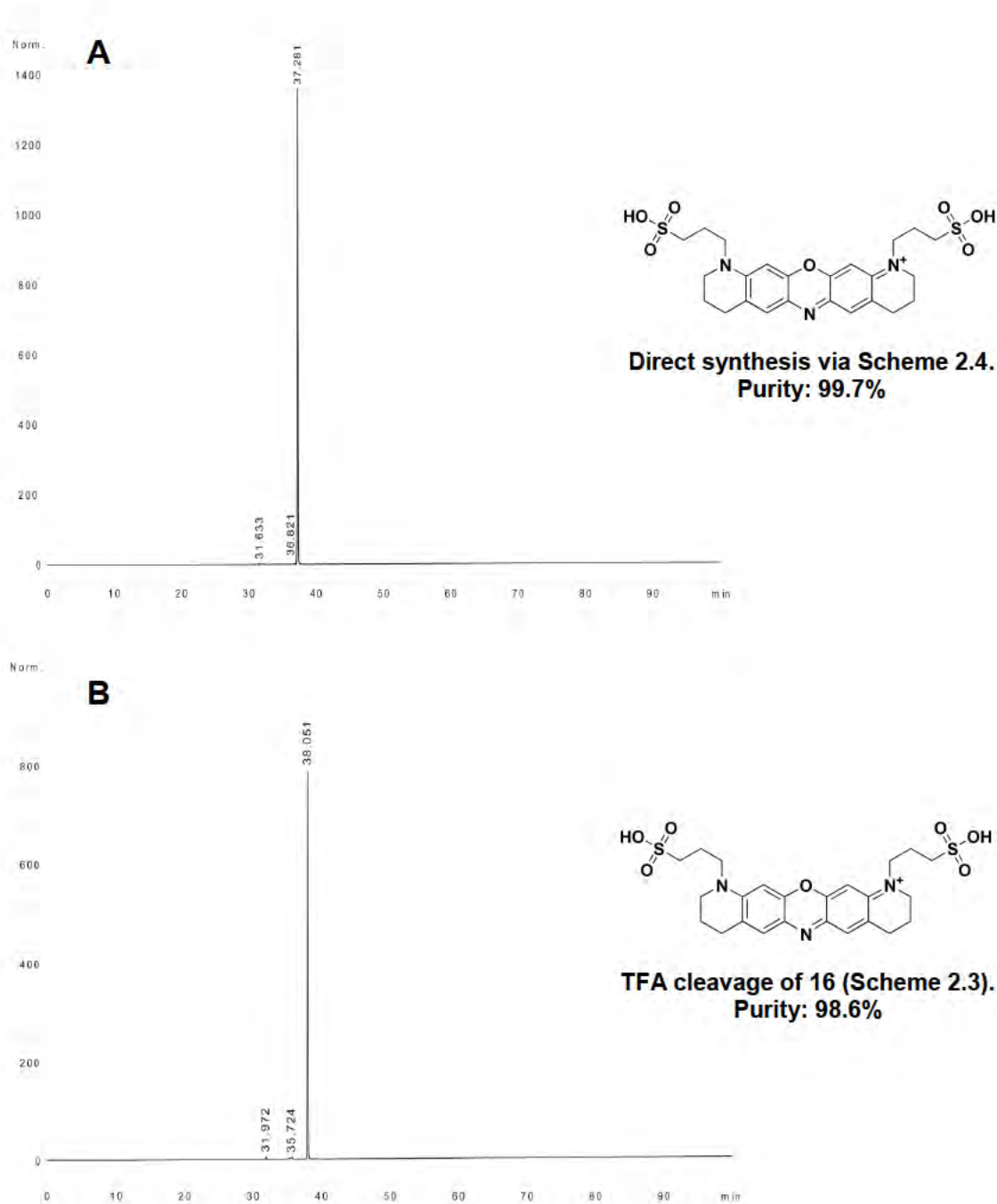


**Figure 2.3: Analytical HPLC of bis-sulfonated oxazine dye (1).** (A) Direct synthesis with purification by semi-preparative HPLC (Scheme 2.4). (B) TFA-cleavage of **16** without HPLC purification (Scheme 2.3). Traces show absorbance detection at 659 nm. Detection at 303 and 606 nm were also obtained and replicated the above data.

## ***Conclusions***

In conclusion, TFMT is a new sulfonate protecting group that is readily accessible in a single high-yield step from commercially available materials. TFMT-protected sulfonates are resistant to nucleophilic attack but can be unmasked under relatively mild conditions by treatment with TFA, and the cleavage product separated by extraction and evaporation. The TFMT group thus complements and expands the repertoire of practical and useful sulfonate protecting groups. We have found it to be advantageous for the synthesis and purification of sulfonated oxazine dyes and their intermediates, and anticipate that it will be generally useful for the synthesis of a wide variety of sulfonated molecules. For example, the stability of the TFMT group to 20% piperidine in DMF and facile cleavage by TFA suggests that it may also find application for the synthesis of sulfonated peptides under Fmoc solid-phase peptide synthesis (SPPS) conditions.

## ***Materials and Methods***

### **General Methods**

Chemicals for synthesis were from standard suppliers. NMR spectra were recorded at 400 MHz for  $^1\text{H}$ , 376 MHz for  $^{19}\text{F}$  and 101 MHz for  $^{13}\text{C}$ . Electrospray ionization mass spectra were acquired on a Q-TOF exact mass spectrometer. Melting points are uncorrected. Unless otherwise stated, all reactions were performed under argon.



## Analytical HPLC

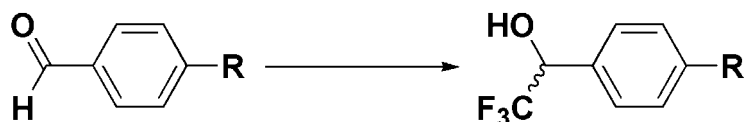
Purity of the compounds was analyzed via HPLC on a 4.6 x 250 mm C-18 column using a diode array detector. All purification methods used aqueous 0.1% trifluoroacetic acid as Solvent A and acetonitrile as Solvent B and were run at a flow rate of 1 mL/min. HPLC methods were as follows:

*Tosyl TFMT reactions (Figure 2.2):* Absorbance detector set at 224 and 262 nm. 10% B for 5 minutes, 10-100% B over 90 minutes, 100% B for 5 minutes.

*Oxazine dye 1 (Figure 2.3):* Absorbance detector set at 303, 606, 659 nm. 0% B for 5 minutes, 0-100% B over 100 minutes, 100% B for 5 minutes.

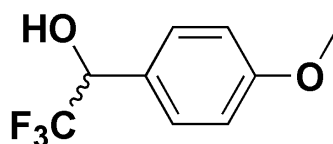
## Synthetic Procedures

*General procedure for Ruppert-Prakash reactions.*

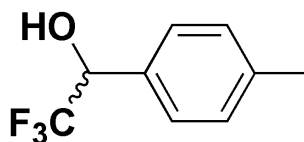


Trimethyl(trifluoromethyl)silane (1.4 eq) was added to a solution of the benzaldehyde (1.0 eq) in THF (0.5 M). The solution was cooled to 0 °C followed by the dropwise addition of a catalytic amount (~1 drop/mmol) of 1M tetra-*n*-butylammonium fluoride (TBAF) in THF. The reaction was brought to room temperature and stirred for 1 hour. The solution was then concentrated via rotary evaporation and purified by flash column chromatography (0-1% ethyl acetate/hexanes) giving the TMS-protected alcohol as a clear, pale-yellow liquid.

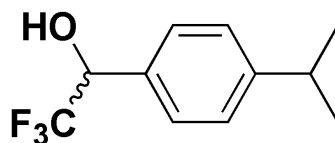
This intermediate was dried under vacuum and then dissolved in 1:1 THF–1 M HCl (0.25 M) and stirred for 2 hours at room temperature to cleave the TMS ether. The solution was then poured into water and the product was extracted with ethyl acetate. The combined organic phases were washed with 0.1 M HCl, water, brine, and then dried over Na<sub>2</sub>SO<sub>4</sub>. Removal of solvent *in vacuo* yielded the product.



**2,2,2-Trifluoro-1-(4-methoxy-phenyl)-ethanol (3)** (Song et al., 2005): yellow oil (1.4 g, 94%). <sup>1</sup>H-NMR (400 MHz, CDCl<sub>3</sub>): δ 7.40 (d, 2H, *J* = 8.9 Hz), 6.93 (d, 2H, *J* = 8.9 Hz), 4.97 (q, 1H, *J*<sub>HF</sub> = 6.7 Hz), 3.83 (s, 3H), 2.46 (br s, 1H). <sup>19</sup>F-NMR (376 MHz, CDCl<sub>3</sub>): δ -79.0 (d, *J* = 6.7 Hz). <sup>13</sup>C-NMR (100 MHz, CDCl<sub>3</sub>): δ 160.5, 129.1, 126.5, 124.6 (q, <sup>1</sup>*J*<sub>CF</sub> = 282 Hz), 114.2, 72.5 (q, <sup>2</sup>*J*<sub>CF</sub> = 32 Hz), 55.5. ESI-HRMS *m/z*: [M + H]<sup>+</sup> Calculated for C<sub>9</sub>H<sub>10</sub>F<sub>3</sub>O<sub>2</sub>: 207.0633, found: 207.0625.

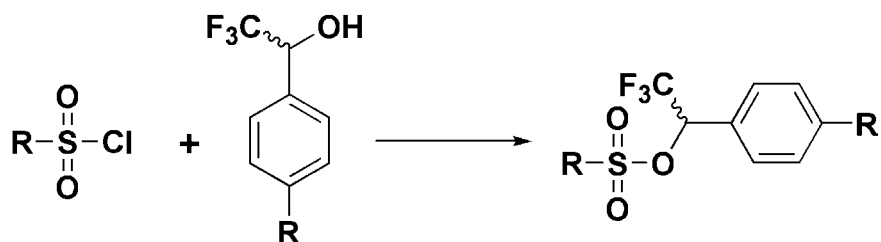


**2,2,2-Trifluoro-1-p-tolyl-ethanol (4)** (Allen et al., 1995): pale yellow oil (1.5 g, 95%). The product becomes a soft, off-white solid when stored at 4 °C.  $^1\text{H-NMR}$  (400 MHz,  $\text{CDCl}_3$ ):  $\delta$  7.36 (d, 2H,  $J = 8.2$  Hz), 7.22 (d, 2H,  $J = 7.9$  Hz), 5.02-4.96 (dq, 1H,  $J = 4.5$  Hz,  $J_{\text{HF}} = 6.7$  Hz), 2.48 (d, 1H,  $J = 4.6$  Hz), 2.37 (s, 3H).  $^{19}\text{F-NMR}$  (376 MHz,  $\text{CDCl}_3$ ):  $\delta$  -78.9 (d,  $J = 6.8$  Hz).  $^{13}\text{C-NMR}$  (100 MHz,  $\text{CDCl}_3$ ):  $\delta$  139.8, 131.3, 129.6, 127.6, 124.6 (q,  $^1J_{\text{CF}} = 282$  Hz), 72.9 (q,  $^2J_{\text{CF}} = 32$  Hz), 21.4. ESI-HRMS  $m/z$ :  $[\text{M} + \text{Na}]^+$  Calculated for  $\text{C}_9\text{H}_9\text{F}_3\text{ONa}$ : 213.0503, found: 213.0497.

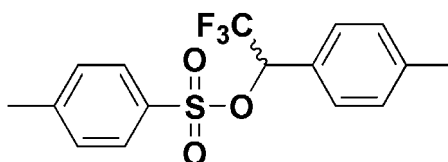


**2,2,2-Trifluoro-1-(4-isopropyl-phenyl)-ethanol (5)**: pale yellow oil (1.3 g, 94%).  $^1\text{H-NMR}$  (400 MHz,  $\text{CDCl}_3$ ):  $\delta$  7.46 (d, 2H,  $J = 8.2$  Hz), 7.38 (d, 2H,  $J = 8.2$  Hz), 4.92 (q, 1H,  $J_{\text{HF}} = 6.5$  Hz), 4.05 (br s, 1H), 3.11-3.00 (m, 1H), 1.40 (s, 3H), 1.38 (s, 3H).  $^{19}\text{F-NMR}$  (376 MHz,  $\text{CDCl}_3$ ):  $\delta$  -78.5 (d,  $J = 6.8$  Hz).  $^{13}\text{C-NMR}$  (100 MHz,  $\text{CDCl}_3$ ):  $\delta$  150.8, 131.7, 127.9, 127.0, 124.7 (q,  $^1J_{\text{CF}} = 282$  Hz), 72.9 (q,  $^2J_{\text{CF}} = 32$  Hz), 34.2, 24.0. ESI-HRMS  $m/z$ :  $[\text{M} + \text{H}]^+$  Calculated for  $\text{C}_{11}\text{H}_{14}\text{F}_3\text{O}$ : 219.0997, found: 219.0999.

General procedure for sulfonate ester formation.

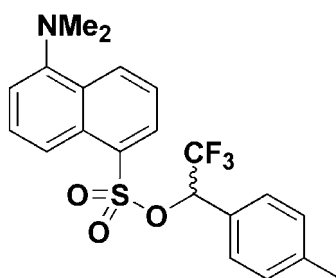


Sulfonyl chloride (1.1 equiv) and a trifluoromethyl benzyl alcohol (1 equiv) were dissolved in CH<sub>2</sub>Cl<sub>2</sub> (0.7 M). To this solution was added dropwise a solution of DABCO (1.2 equiv) in CH<sub>2</sub>Cl<sub>2</sub> (2 M), resulting in precipitate formation. The mixture was then stirred for 4 hours at room temperature. The reaction was quenched by the addition of 1M NaOH (1 mL) resulting in elimination of the precipitate. The solution was diluted into ethyl acetate and extracted with saturated NaHCO<sub>3</sub>, 0.1 M HCl, water, and brine. The organic phase was then dried over Na<sub>2</sub>SO<sub>4</sub> and the solvent was removed via rotary evaporation.

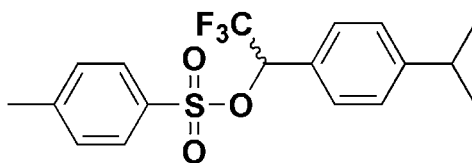


**Toluene-4-sulfonic acid 2,2,2-trifluoro-1-p-tolyl-ethyl ester (6)** (Allen et al., 1995): white solid (1.17 g, 85%). mp 83-85 °C; <sup>1</sup>H-NMR (400 MHz, CDCl<sub>3</sub>): δ 7.65 (d, 2H, *J* = 8.3 Hz), 7.23-7.20 (m, 4H), 7.11 (d, 2H, 7.7 Hz), 5.62 (q, 1H, *J*<sub>HF</sub> = 6.4 Hz), 2.40 (s, 3H), 2.33 (s, 3H). <sup>19</sup>F-NMR (376 MHz, CDCl<sub>3</sub>): δ -76.5 (d, *J* =

6.4 Hz).  $^{13}\text{C-NMR}$  (100 MHz,  $\text{CDCl}_3$ ):  $\delta$  145.5, 140.7, 133.3, 129.9, 129.5, 128.3, 128.1, 126.9, 122.5 (q,  $^1J_{\text{CF}} = 281$  Hz), 78.3 (q,  $^2J_{\text{CF}} = 34$  Hz), 21.8, 21.5. ESI-HRMS  $m/z$ :  $[\text{M} + \text{Na}]^+$  Calculated for  $\text{C}_{16}\text{H}_{15}\text{F}_3\text{O}_3\text{SNa}$ : 367.0592, found: 367.0583.

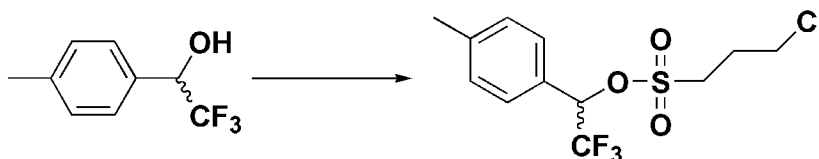


**5-Dimethylamino-naphthalene-1-sulfonic acid 2,2,2-trifluoro-1-p-tolyl-ethyl ester (7)**: yellow solid (436 mg, 98%). mp 97-99 °C;  $^1\text{H-NMR}$  (400 MHz,  $\text{CDCl}_3$ ):  $\delta$  8.46 (d, 1H,  $J = 8.5$  Hz), 8.23 (d, 1H,  $J = 8.7$  Hz), 8.08 (dd, 1H,  $J = 1.3$  Hz, 7.4 Hz), 7.56 (dd, 1H,  $J = 7.6$  Hz, 8.6 Hz), 7.37 (dd, 1H,  $J = 7.4$  Hz, 8.5 Hz), 7.16 (d, 1H,  $J = 7.1$  Hz), 6.98 (d, 2H,  $J = 8.0$  Hz), 6.81 (d, 2H,  $J = 7.9$  Hz), 5.6 (q, 1H,  $J_{\text{HF}} = 6.4$  Hz), 2.83 (s, 6H), 2.17 (s, 3H).  $^{19}\text{F-NMR}$  (376 MHz,  $\text{CDCl}_3$ ):  $\delta$  -76.3 (d,  $J = 6.4$  Hz).  $^{13}\text{C-NMR}$  (100 MHz,  $\text{CDCl}_3$ ):  $\delta$  151.8, 140.3, 132.1, 131.8, 130.4, 130, 129.8, 128.9, 128.2, 126.1, 122.9, 122.5 (q,  $^1J_{\text{CF}} = 281$  Hz), 119.7, 115.7, 78.8 (q,  $^2J_{\text{CF}} = 34$  Hz), 45.6, 21.3. ESI-HRMS  $m/z$ :  $[\text{M} + \text{H}]^+$  Calculated for  $\text{C}_{21}\text{H}_{21}\text{F}_3\text{NO}_3\text{S}$ : 424.1194, found: 424.1202.



**Toluene-4-sulfonic acid 2,2,2-trifluoro-1-(4-isopropyl-phenyl)-ethyl ester (8):**

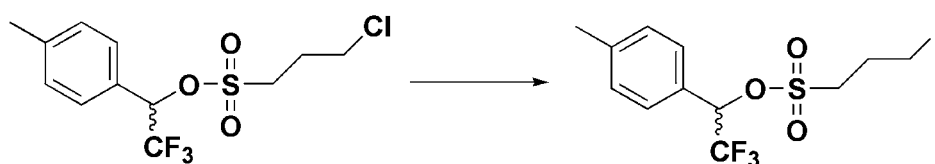
off-white solid (349 mg, 94%). mp 81-83 °C;  $^1\text{H-NMR}$  (400 MHz,  $\text{CDCl}_3$ ):  $\delta$  7.61 (d, 2H,  $J = 8.4$  Hz), 7.20 (d, 2H,  $J = 8.2$  Hz), 7.17 (d, 2H,  $J = 8$  Hz), 7.12 (d, 2H,  $J = 8.2$  Hz), 5.63 (q, 1H,  $J_{\text{HF}} = 6.4$  Hz), 2.92-2.82 (m, 1H), 2.37 (s, 3H), 1.22 (s, 3H), 1.20 (s, 3H).  $^{19}\text{F-NMR}$  (376 MHz,  $\text{CDCl}_3$ ):  $\delta$  -76.5 (d,  $J = 6.4$  Hz).  $^{13}\text{C-NMR}$  (100 MHz,  $\text{CDCl}_3$ ):  $\delta$  151.4, 145.3, 133.4, 129.8, 128.4, 128.1, 127.0, 126.9, 122.5 (q,  $^1J_{\text{CF}} = 281$  Hz), 78.5 (q,  $^2J_{\text{CF}} = 34$  Hz), 34.1, 24.04, 24, 21.8. ESI-HRMS  $m/z$ : [M + Na] $^+$  Calculated for  $\text{C}_{18}\text{H}_{19}\text{F}_3\text{O}_3\text{SNa}$ : 395.0905, found: 395.0899.



**3-Chloro-propane-1-sulfonic acid 2,2,2-trifluoro-1-p-tolyl-ethyl ester (9).**

Compound **4** (1 g, 5.3 mmol) was dissolved in anhydrous dichloromethane (48 mL) and cooled to 0 °C in an ice bath. Triethylamine (1.46 mL, 10.5 mmol) was then added to the solution. 3-Chloropropanesulfonyl chloride (0.83 mL, 6.8 mmol) dissolved in anhydrous dichloromethane (5 mL) was added dropwise via syringe to the reaction flask at a rate of 20 drops/min. Upon completion of compound

addition, the reaction was stirred at 4 °C overnight. The reaction was poured into 1 M HCl and the product was extracted with dichloromethane. The combined organic phases were washed with water, saturated sodium bicarbonate and brine, then dried over sodium sulfate. Removal of the solvent under vacuum resulted in a pale yellow oil. The crude product was purified by flash column chromatography (0-15% ethyl acetate/hexanes) to yield the product as a white solid (1.64 g, 97%). mp 61-63 °C;  $^1\text{H-NMR}$  (400 MHz,  $\text{CDCl}_3$ ):  $\delta$  7.38 (d, 2H,  $J = 8.0$  Hz), 7.26 (d, 2H,  $J = 7.8$  Hz), 5.74 (q, 1H,  $J_{\text{HF}} = 6.4$  Hz), 3.63-3.54 (m, 2H), 3.27-3.14 (m, 2H), 2.39 (s, 3H), 2.31-2.21 (m, 2H).  $^{19}\text{F-NMR}$  (376 MHz,  $\text{CDCl}_3$ ):  $\delta$  -76.3 (d,  $J = 6.4$  Hz).  $^{13}\text{C-NMR}$  (100 MHz,  $\text{CDCl}_3$ ):  $\delta$  141.4, 130.0, 128.3, 126.8, 122.5 (q,  $^1J_{\text{CF}} = 281$  Hz), 78.3 (q,  $^2J_{\text{CF}} = 35$  Hz), 49.8, 42.3, 26.7, 21.6. ESI-HRMS  $m/z$ :  $[\text{M} + \text{Na}]^+$  Calculated for  $\text{C}_{12}\text{H}_{14}\text{ClF}_3\text{O}_3\text{SNa}$ : 353.0202, found: 353.0190.

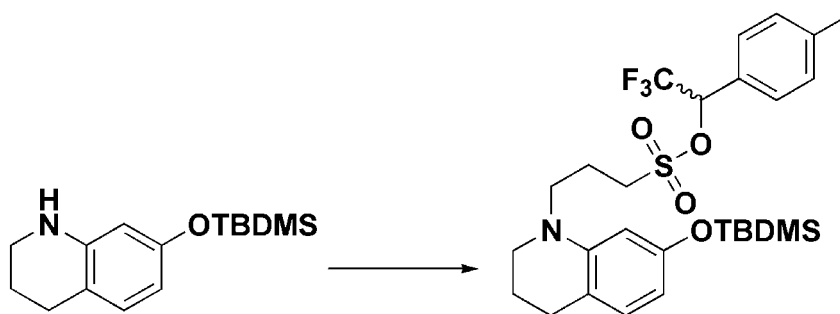


### 3-Iodo-propane-1-sulfonic acid 2,2,2-trifluoro-1-p-tolyl-ethyl ester (10).

Compound **9** (500 mg, 1.51 mmol) was added to a solution of sodium iodide (906 mg, 6.05 mmol) in acetone (5 mL). The reaction was heated to reflux and stirred for 16 hours. After cooling to room temperature, the mixture was filtered to

remove sodium chloride and the filtrand was washed with acetone (25 mL). Acetone was removed via rotary evaporation and the resulting residue was extracted between ethyl acetate and water. The organic phase was collected and the aqueous phase was washed with ethyl acetate. The combined organic phases were washed with brine, dried over sodium sulfate, and the solvent removed via rotary evaporation giving a bronze oil. The crude material was purified with flash column chromatography (0-10% ethyl acetate/hexanes) to yield the product as a viscous, pale yellow oil (571 mg, 90%).  $^1\text{H-NMR}$  (400 MHz,  $\text{CDCl}_3$ ):  $\delta$  7.39 (d, 2H,  $J = 8.1$  Hz), 7.27 (d, 2H,  $J = 7.9$  Hz), 5.73 (q, 1H,  $J_{\text{HF}} = 6.4$  Hz), 3.22-3.07 (m, 4H), 2.39 (s, 3H), 2.33-2.21 (m, 2H).  $^{19}\text{F-NMR}$  (376 MHz,  $\text{CDCl}_3$ ):  $\delta$  -76.3 (d,  $J = 6.4$  Hz).  $^{13}\text{C-NMR}$  (100 MHz,  $\text{CD}_3\text{OD}$ ):  $\delta$  141.5, 130.1, 128.4, 126.8, 122.5 (q,  $^1J_{\text{CF}} = 281$  Hz), 78.3 (q,  $^2J_{\text{CF}} = 34$  Hz), 53.2, 27.2, 21.6, 2.1. ESI-HRMS  $m/z$ :  $[\text{M} + \text{Na}]^+$  Calculated for  $\text{C}_{12}\text{H}_{14}\text{F}_3\text{IO}_3\text{SNa}$ : 444.9558, found: 444.9520.

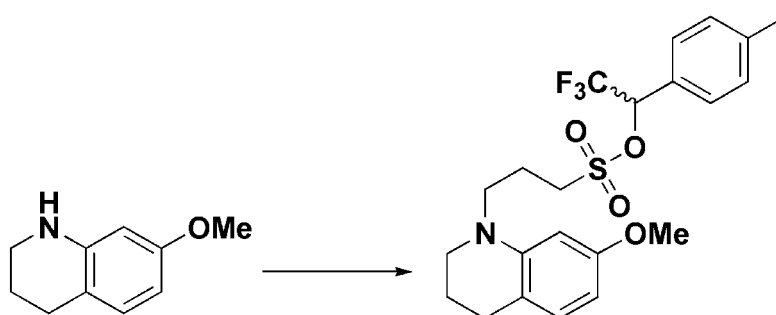




**3-[7-(*tert*-Butyl-dimethyl-silyloxy)-3,4-dihydro-2H-quinolin-1-yl]-propane-1-sulfonic acid 2,2,2-trifluoro-1-p-tolyl-ethyl ester (13). 7-(*t*-**

Butyldimethylsilyloxy)-1,2,3,4-tetrahydroquinoline **11** (Pauff and Miller, 2011) (200 mg, 0.76 mmol) was dissolved in DMF (0.8 mL). Compound **10** (641 mg, 1.5 mmol) dissolved in DMF (0.8 mL) and potassium carbonate (120 mg, 0.91 mmol) were added to the solution and the reaction was heated to 70 °C and stirred for 24 hours. The reaction was poured into water and acidified to pH 1 with 1M HCl. The product was extracted with ethyl acetate and the combined organic phases were washed with water and brine and dried over sodium sulfate. The solvent was removed by rotary evaporation and the crude material was purified by flash column chromatography (0-5% acetone/hexanes) to yield a viscous orange oil (337 mg, 80%). <sup>1</sup>H-NMR (400 MHz, CDCl<sub>3</sub>): δ 7.37 (d, 2H, *J* = 8.1 Hz), 7.22 (d, 2H, *J* = 7.9 Hz), 6.78 (d, 1H, *J* = 8.0 Hz), 6.12 (dd, 1H, *J* = 2.2 Hz, 8.0 Hz), 6.01 (d, 1H, *J* = 1.9 Hz), 5.73 (q, 1H, *J* = 6.4 Hz), 3.33-3.21 (m, 2H), 3.10 (t, 2H, *J* = 5.5 Hz), 3.12-2.99 (m, 2H), 2.65 (t, 2H, *J* = 6.3 Hz), 2.38 (s, 3H), 2.07 (p, 2H, *J* = 7.2 Hz), 1.88-1.82 (m, 2H), 0.98 (s, 9H), 0.19 (s, 6H). <sup>19</sup>F-NMR (376 MHz, CDCl<sub>3</sub>): δ -76.4 (d, *J* = 6.4 Hz). <sup>13</sup>C-NMR (100 MHz, CD<sub>3</sub>OD): δ 155.2, 145.7,

141.3, 130, 129.9, 128.3, 127, 122.6 (q,  $^1J_{CF} = 281$  Hz), 116, 108.2, 103.1, 78.2 (q,  $^2J_{CF} = 34$  Hz), 50.3, 49.7, 49.6, 27.5, 26, 22.5, 21.6, 21.1, 18.5, -4.1. ESI-HRMS  $m/z$ :  $[M + H]^+$  Calculated for  $C_{27}H_{39}F_3NO_4SSi$ : 558.2321, found: 558.2305.



**3-(7-Methoxy-3,4-dihydro-2H-quinolin-1-yl)propane-1-sulfonic acid 2,2,2-trifluoro-1-p-tolyl-ethyl ester (14).** 7-Methoxy-1,2,3,4-tetrahydroquinoline **12**

(Pauff and Miller, 2011) (100 mg, 0.61 mmol) was dissolved in DMF (0.5 mL).

Compound **10** (517 mg, 1.23 mmol) dissolved in DMF (0.8 mL) and potassium carbonate (96 mg, 0.74 mmol) were added to the solution and the reaction was

heated to 70 °C and stirred for 24 hours. The reaction was poured into water and

acidified to pH 1 with 1M HCl. The product was extracted with ethyl acetate and

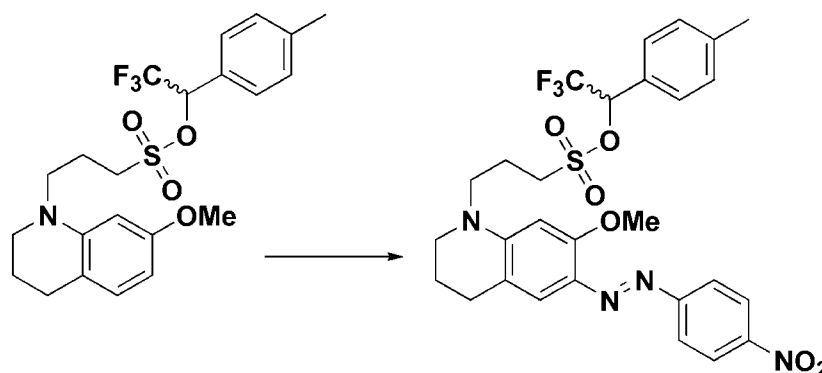
the combined organic phases were washed with water and brine and dried over

sodium sulfate. The solvent was removed by rotary evaporation and the crude

material was purified by flash column chromatography (0-10% ethyl

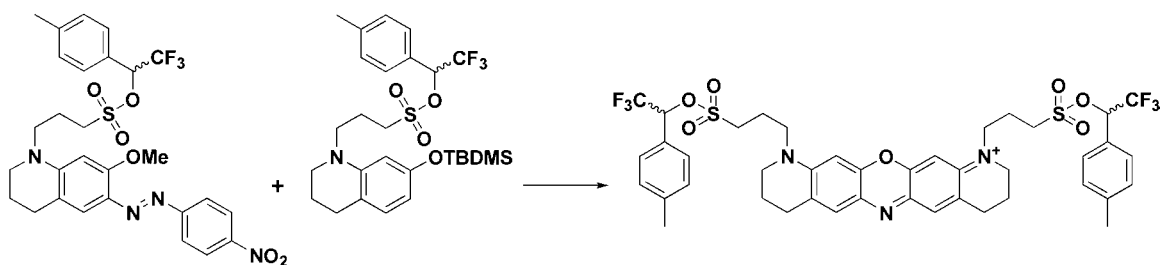
acetate/hexanes) to yield a viscous, pale yellow oil (217 mg, 78%).  $^1H$ -NMR (400

MHz, CD<sub>3</sub>OD):  $\delta$  7.37 (d, 2H,  $J$  = 8.1 Hz), 7.2 (d, 2H,  $J$  = 7.9 Hz), 6.76 (d, 1H,  $J$  = 8.1 Hz), 6.12 (dd, 1H,  $J$  = 2.4 Hz, 8.1 Hz), 6.07 (d, 1H,  $J$  = 2.4 Hz), 5.96 (q, 1H,  $J_{HF}$  = 6.5 Hz), 3.69 (s, 3H), 3.23-3.02 (m, 4H), 3.01 (t, 2H,  $J$  = 5.6 Hz), 2.58 (t, 2H,  $J$  = 6.1 Hz), 2.32 (s, 3H), 1.95-1.82 (m, 2H), 1.79-1.73 (m, 2H). <sup>19</sup>F-NMR (376 MHz, CD<sub>3</sub>OD):  $\delta$  -78.0 (d,  $J$  = 6.5 Hz). <sup>13</sup>C-NMR (100 MHz, CD<sub>3</sub>OD):  $\delta$  159.5, 145.7, 141.1, 129.5, 128.2, 127.3, 122.9 (q,  $^1J_{CF}$  = 280 Hz), 115.3, 100.9, 97.2, 77.8 (q,  $^2J_{CF}$  = 34 Hz), 54.4, 49.3, 49.1, 49, 27.2, 22.4, 20.5, 20.2. ESI-HRMS  $m/z$ : [M + H]<sup>+</sup> Calculated for C<sub>22</sub>H<sub>27</sub>F<sub>3</sub>NO<sub>4</sub>S: 458.1613, found: 458.1596.



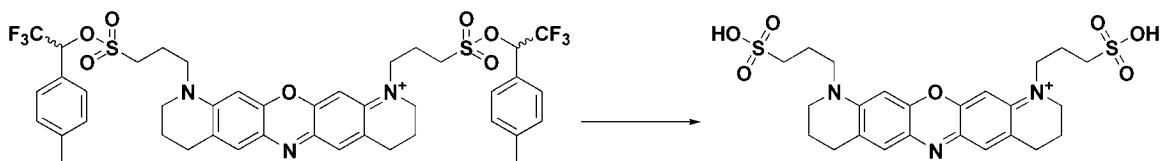
**3-[7-Methoxy-6-(4-nitro-phenylazo)-3,4-dihydro-2H-quinolin-1-yl]-propane-1-sulfonic acid 2,2,2-trifluoro-1-p-tolyl-ethyl ester (15).** Compound **14** (105 mg, 0.23 mmol) was dissolved in methanol (2.3 mL). 4-Nitrobenzenediazonium tetrafluoroborate (54 mg, 0.23 mmol) was suspended in 10% sulfuric acid (2.3 mL) with vigorous stirring. The organic solution was added to the aqueous mixture and stirred at ambient conditions for 1 hour. The solution was then neutralized with ammonium hydroxide, resulting in a deep red precipitate. The

mixture was filtered and the filtrand washed with water to give a blood red solid (140 mg, quantitative). This compound was dried *in vacuo* and used in the next reaction without further purification. NMR of the crude material revealed a contaminant of ammonium tetrafluoroborate salt. A small sample of the compound was therefore desalted by flash column chromatography (0-50% ethyl acetate/hexanes) to obtain NMR. mp 153-155 °C (dec.); <sup>1</sup>H-NMR (400 MHz, CDCl<sub>3</sub>): δ 8.27 (d, 2H, *J* = 9.0 Hz), 7.86 (d, 2H, *J* = 9.0 Hz), 7.58 (s, 1H), 7.37 (d, 2H, *J* = 7.8 Hz), 7.24 (d, 2H, *J* = 7.8 Hz), 6.17 (s, 1H), 5.76 (q, 1H, *J*<sub>HF</sub> = 6.3 Hz), 3.98 (s, 3H), 3.61-3.47 (m, 2H), 3.31 (t, 2H, *J* = 5.4 Hz), 3.16-3.05 (m, 2H), 2.72 (t, 2H, *J* = 5.9 Hz), 2.37 (s, 3H), 2.23-2.11 (m, 2H), 1.92 (p, 2H, *J* = 5.3 Hz). <sup>19</sup>F-NMR (376 MHz, CDCl<sub>3</sub>): δ -76.3 (d, *J* = 6.2 Hz). <sup>13</sup>C-NMR (100 MHz, CDCl<sub>3</sub>): δ 160.1, 157.8, 151, 147.0, 141.5, 134, 130.1, 128.3, 126.7, 124.9, 122.7, 122.6 (q, <sup>1</sup>*J*<sub>CF</sub> = 281 Hz), 117.8, 116.1, 93.5, 78.5 (q, <sup>2</sup>*J*<sub>CF</sub> = 34 Hz), 56.7, 50, 49.9, 49.7, 27.4, 22.1, 21.6, 20.7. ESI-HRMS *m/z*. [M + H]<sup>+</sup> Calculated for C<sub>28</sub>H<sub>30</sub>F<sub>3</sub>N<sub>4</sub>O<sub>6</sub>S: 607.1838, found: 607.1841.



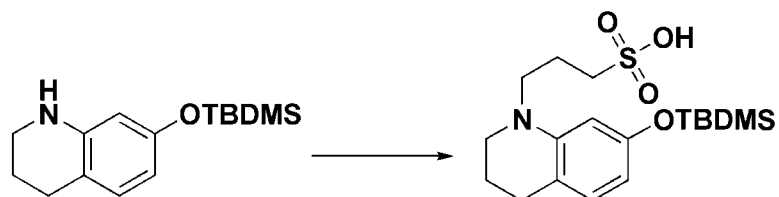
**1,11-Bis-[3-(2,2,2-trifluoro-1-p-tolyl-ethoxysulfonyl)-propyl]-3,4,8,9,10,11-hexahydro-2H-13-oxa-6,11-diaza-1-azonia-pentacene tetrafluoroborate (16).**

Compound **13** (44 mg, 79  $\mu\text{mol}$ ) and compound **15** (55 mg, 91  $\mu\text{mol}$ ) were dissolved in a solution of ethanol: water: hydrochloric acid (500  $\mu\text{L}$ : 50  $\mu\text{L}$ : 25  $\mu\text{L}$ ) and heated to 80  $^{\circ}\text{C}$  with stirring for 2 hours. Solvent was removed via rotary evaporation to give a fluorescent blue residue. The crude material was purified by flash column chromatography (0-10% methanol/dichloromethane) yielding the tetrafluoroborate salt as a blue solid (36 mg, 47%). mp 220-222  $^{\circ}\text{C}$  (dec.);  $^1\text{H}$ -NMR (400 MHz,  $\text{CD}_3\text{OD}$ ):  $\delta$  7.47 (s, 2H), 7.43 (d, 4H,  $J = 8.1$  Hz), 7.21 (d, 4H,  $J = 8$  Hz), 6.81 (s, 2H), 6.07 (q, 2H,  $J_{\text{HF}} = 6.5$  Hz), 3.74-3.61 (m, 4H), 3.55 (t, 4H,  $J = 5.5$  Hz), 3.45-3.33 (m, 4H), 2.90 (t, 4H,  $J = 6$  Hz), 2.28 (s, 6H), 2.15-2.07 (m, 4H), 1.99 (p, 4H,  $J = 5.5$  Hz).  $^{19}\text{F}$ -NMR (376 MHz,  $\text{CD}_3\text{OD}$ ):  $\delta$  -78.0 (d,  $J = 6.5$  Hz), -154.58 (s), -154.6 (s) ( $\text{BF}_4^-$  counterion).  $^{13}\text{C}$ -NMR (100 MHz,  $\text{CD}_3\text{OD}$ ):  $\delta$  154.6, 148.7, 141.1, 134.4, 130.8, 129.5, 129.4, 128.2, 127.4, 122.9 (q,  $^1J_{\text{CF}} = 280$  Hz), 95.0, 77.7 (q,  $^2J_{\text{CF}} = 34$  Hz), 50.64, 50.6, 27.2, 20.6, 20.5, 20.1. ESI-HRMS  $m/z$   $[\text{M}]^+$  Calculated for  $\text{C}_{42}\text{H}_{44}\text{F}_6\text{N}_3\text{O}_7\text{S}_2$ : 880.2525, found: 880.2511.



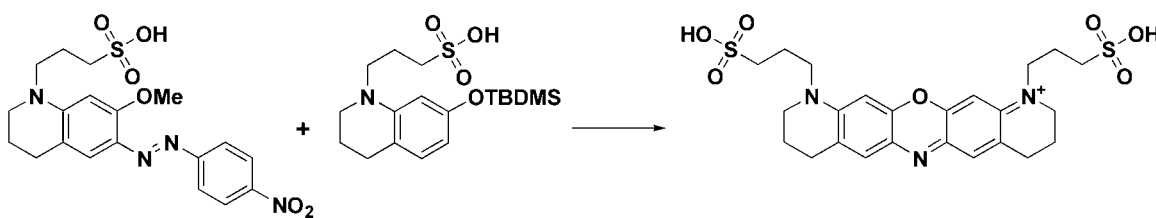
**1,11-Bis-(3-sulfo-propyl)-3,4,8,9,10,11-hexahydro-2H-13-oxa-6,11-diaza-1-azonia-pentacene tetrafluoroborate (1) by TFA cleavage of 16.** Compound **16**

(12 mg, 12  $\mu\text{mol}$ ) and water (20  $\mu\text{L}$ ) was dissolved in trifluoroacetic acid (1 mL) and stirred at room temperature for 2 hours. TFA was removed via rotary evaporation and the residue was dissolved in water (60 mL). The aqueous phase was extracted with ethyl acetate (1 x 40 mL, 4 x 20 mL) and lyophilized to give the pure blue compound as a tetrafluoroborate salt (8.1 mg, 99%). mp 365-367  $^{\circ}\text{C}$  (dec.);  $^1\text{H-NMR}$  (400 MHz,  $\text{D}_2\text{O}$ ):  $\delta$  6.99 (s, 2H), 6.6 (s, 2H), 3.5 (br s, 8H), 2.86 (t, 4H,  $J = 7.4$  Hz), 2.62 (br s, 4H), 1.99 (p, 4H,  $J = 7.0$  Hz), 1.82 (br s, 4H).  $^{19}\text{F-NMR}$  (376 MHz,  $\text{D}_2\text{O}$ ):  $\delta$  -150.9 (s), -151.0 (s) ( $\text{BF}_4^-$  counterion). ESI-HRMS  $m/z$ :  $[\text{M}]^+$  Calculated for  $\text{C}_{24}\text{H}_{30}\text{N}_3\text{O}_7\text{S}_2$ : 536.1525, found: 536.1507.



**3-[7-(*tert*-Butyl-dimethyl-silyloxy)-3,4-dihydro-2H-quinolin-1-yl]-propane-1-sulfonic acid monohydrate (17).** 7-*t*-Butyldimethylsilyloxy-1,2,3,4-tetrahydroquinoline **11** (Pauff and Miller, 2011) (214 mg, 0.812 mmol) and 1,3-

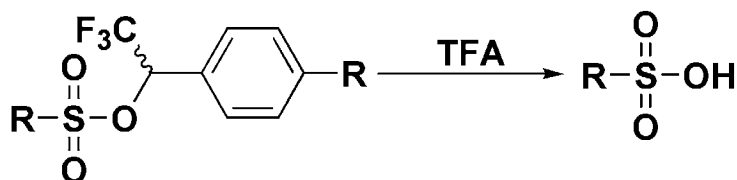
propanesultone (200 mg, 1.6 mmol) were dissolved in methanol (1.6 mL) and stirred overnight at room temperature. The solvent was removed via rotary evaporation and the crude material was purified by flash column chromatography (10 % methanol/dichloromethane) to yield a yellow-white solid (119 mg, 36%). mp 202-204 °C (dec.); <sup>1</sup>H-NMR (400 MHz, CD<sub>3</sub>OD): δ 6.73 (d, 1H, *J* = 8.0 Hz), 6.14 (br s, 1H), 6.05 (dd, 1H, *J* = 1.8 Hz, 8 Hz), 3.35 (t, 2H, *J* = 7.2 Hz), 3.27 (t, 2H, *J* = 5.5 Hz), 2.88 (t, 2H, *J* = 7.5 Hz), 2.64 (t, 2H, *J* = 6.3 Hz), 2.07 (p, 2H, *J* = 7.6 Hz), 1.9 (p, 2H, *J* = 6.3 Hz), 0.97 (s, 9H), 0.17 (s, 6H). <sup>13</sup>C-NMR (100 MHz, CD<sub>3</sub>OD): δ 155, 154.8, 145.5, 129.4, 116.3, 103.4, 50.5, 49.2, 49.1, 27.2, 25.2, 22.1, 21.9, 18, -5.2. ESI-HRMS *m/z*: [M + H]<sup>+</sup> Calculated for C<sub>18</sub>H<sub>32</sub>NO<sub>4</sub>SSi: 386.1821, found: 386.1821.



**1,11-Bis-(3-sulfo-propyl)-3,4,8,9,10,11-hexahydro-2H-13-oxa-6,11-diaza-1-azonia-pentacene trifluoroacetate (1).** Compound **17** (43 mg, 110 μmol) and 3-[7-Methoxy-6-(4-nitro-phenylazo)-3,4-dihydro-2H-quinolin-1-yl]-propane-1-sulfonic acid **19** (Pauff and Miller, 2011) (48 mg, 110 μmol) were dissolved in a solution of ethanol: water: hydrochloric acid (1 mL: 100 μL: 50 μL) and heated to 80 °C with stirring for 2 hours. The solvent was removed via rotary evaporation to

give a fluorescent blue residue. The crude material was purified to 99% purity by HPLC over a C18 column to yield a blue solid (22 mg, 29%). Solvent A and B were respectively aqueous 0.1% trifluoroacetic acid and acetonitrile/0.1% trifluoroacetic acid. The flow rate during purification was 5 mL/min. The absorbance detector was set at 294, 306, 383, 607, and 660 nm. Elution of the compound was obtained via the following method: 15% B for 5 minutes, 15-50% B over 35 minutes, 50-100% B over 5 minutes, 100% B for 10 minutes. mp 365-367 °C (dec.);  $^1\text{H-NMR}$  (400 MHz,  $\text{D}_2\text{O}$ ):  $\delta$  6.72 (s, 2H), 6.44 (s, 2H), 3.38 (br s, 8H), 2.81 (t, 4H,  $J = 6.8$  Hz), 2.48 (br s, 4H), 1.91 (br s, 4H), 1.73 (br s, 4H).  $^{19}\text{F-NMR}$  (376 MHz,  $\text{D}_2\text{O}$ ):  $\delta$  -76.1 (s) (TFA counterion).  $^{13}\text{C-NMR}$  (100 MHz,  $\text{D}_2\text{O}$ ):  $\delta$  153.9, 147.9, 132.4, 129.4, 129.2, 95.2, 51.4, 50.7, 48.0, 26.9, 21.7, 20.2. ESI-HRMS  $m/z$ :  $[\text{M} - 2\text{H}]^-$  Calculated for  $\text{C}_{24}\text{H}_{28}\text{N}_3\text{O}_7\text{S}_2$ : 534.1368, found: 534.1348.

*General procedure for TFA cleavage of sulfonate esters.*



Sulfonate ester (~0.2 mmol) and water (0-30  $\mu\text{L}$ ) were dissolved in TFA (1 mL) and stirred at room temperature for 2-16 h. After rotary evaporation of TFA, the residue was taken up into 80 mL water. The aqueous phase was extracted with ethyl acetate and lyophilized to yield the cleaved tosylate or dansylate.



## Stability Experiments

*General procedure for determining stability to 20% piperidine/DMF.*

Protected sulfonate (0.1-0.4 mmol) was dissolved in 1 mL of a freshly prepared 20% piperidine/DMF solution and stirred at room temperature for 2 hours. The reaction was then poured into 1 M HCl and extracted with ethyl acetate. The combined organic phases were washed with water and brine and then dried over sodium sulfate. The recovered compound was then isolated by removal of the solvent via rotary evaporation.

*General procedure for determining stability to NaI in refluxing acetone.*

0.1 mmol of the protected sulfonate was dissolved in a solution of NaI (16 mg, 0.11 mmol) in 0.2 mL acetone and refluxed for 4 hours. The reaction was diluted into 1:1 EtOAc:H<sub>2</sub>O and the organic phase was collected. The aqueous phase was further extracted with ethyl acetate and the combined organic phases were washed with brine and dried over sodium sulfate. The compound was then isolated by removal of the solvent via rotary evaporation.

*General procedure for determining stability to potassium carbonate.*

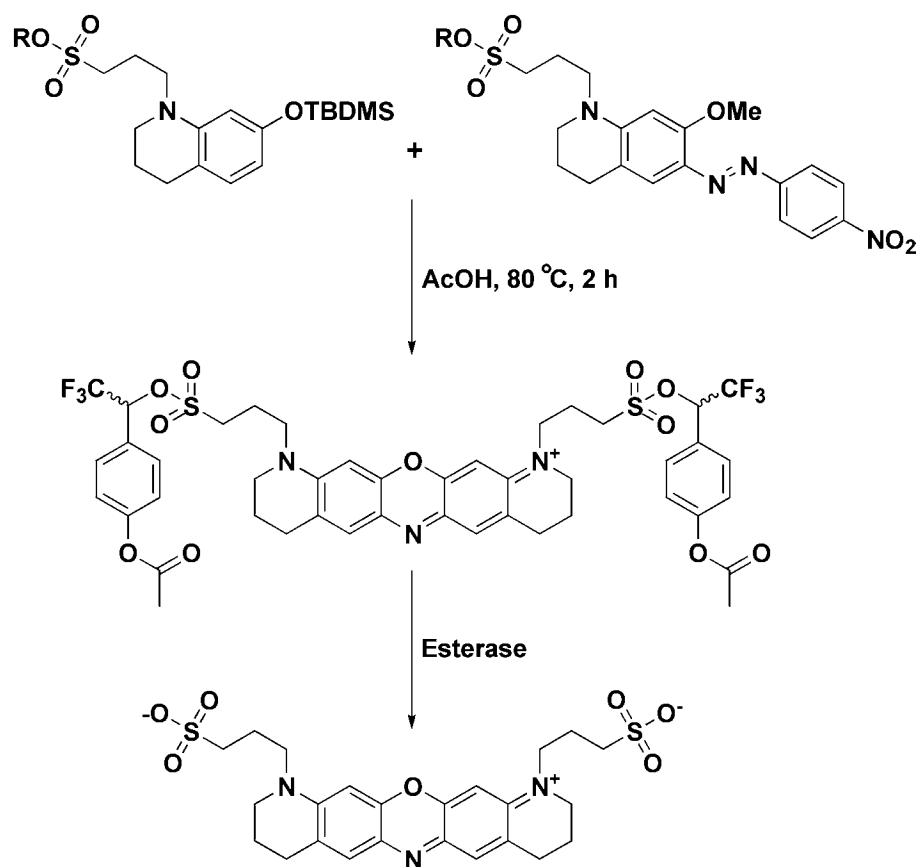
K<sub>2</sub>CO<sub>3</sub> (0.24 mmol) was added to a solution of the protected sulfonate (0.2 mmol) in DMF (0.4 mL) and the mixture was heated to 65 °C for 24 hours. The reaction was then poured into water and acidified with 1 M HCl. The aqueous phase was extracted with ethyl acetate and the combined organic phases were washed with

water and brine and then dried over sodium sulfate. The solvent was removed by rotary evaporation and the recovered material was purified by flash column chromatography (0-10% ethyl acetate/hexanes). Both **6** and **7** were recovered in 92% yield.

*Stability of **6** to hot dilute aqueous acid.*

Compound **6** (75 mg, 0.22 mmol) was dissolved in a 1 mL solution of 1:1 2 M HCl/acetone and heated to 70 °C for 2 hours. The reaction was then poured into ethyl acetate and the organic phase was washed with water and brine and dried over sodium sulfate. The solvent was removed by rotary evaporation and the recovered material was purified by flash column chromatography (0-10% ethyl acetate/hexanes) to return the starting material as a white solid (70 mg, 93%).

**CHAPTER III: Synthesis of near-IR fluorescent oxazine dyes with esterase-labile sulfonate esters**



**Summary**

Near-IR oxazine dyes are reported that contain sulfonate esters which are rapidly cleaved by esterase activity to unmask highly polar anionic sulfonates. Strategies for the synthesis of these dyes included the development of milder dye condensation conditions with improved functional compatibility, and the use of an

alkyl halide that allows for the introduction of esterase-labile sulfonates without the need for sulfonation of the target molecule.

### ***Introduction***

Cells and organisms are most transparent to near-IR light (650-900 nm), making this region of the electromagnetic spectrum optimal for optical imaging (Weissleder, 2001). Unfortunately, most organic near-IR dyes are not suitable for live intracellular applications. Dyes that are capable of diffusing across cell membranes typically give high background staining of cells because they accumulate in intracellular membranes and organelles (Cunningham et al., 2010; Johnson, 1998). Moreover, most near-IR dyes are cationic, which favors accumulation in the negatively-polarized membranes of mitochondria (Bunting et al., 1989). On the other hand, highly polar water-soluble sulfonated near-IR dyes (e.g., Alexa and Cy dyes) are unable to diffuse across cell membranes.

One potential strategy to overcome this problem is to design cell-permeable near-IR dyes that can be selectively unmasked to a more water-soluble form upon cellular entry. Toward this end, we recently reported a chemically-stable but esterase-labile sulfonate ester, AcOTFMB (Figure 3.1), that enables the delivery and unmasking of dansyl sulfonate within the cytoplasm of cells (Rusha and Miller, 2011)

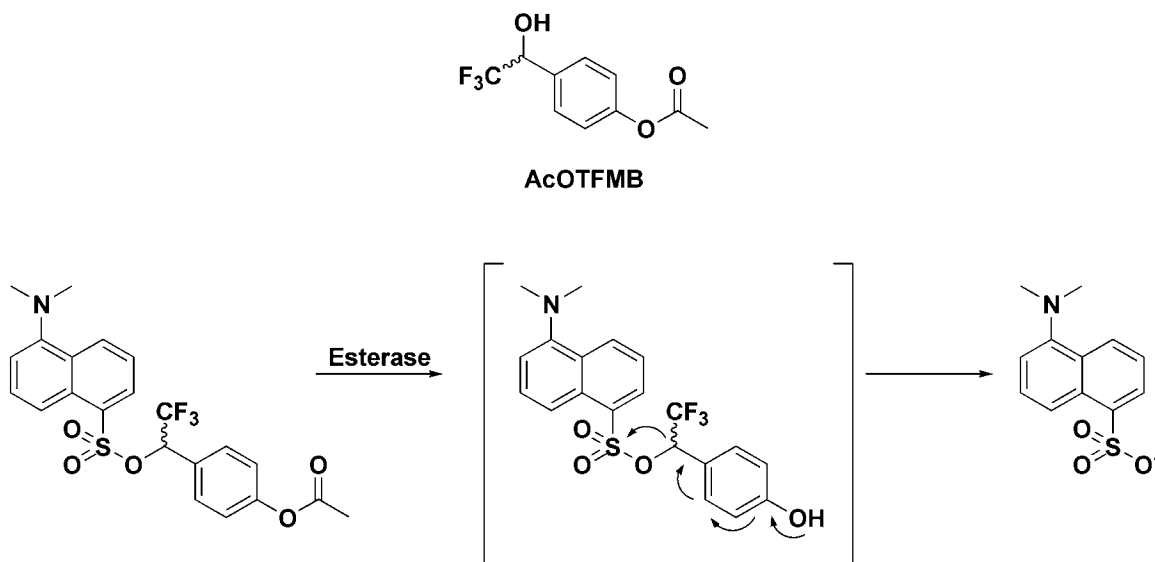


**Figure 3.1: Esterase-labile protecting group for sulfonates.** Top: Structure of AcOTFMB (Rusha and Miller, 2011). Bottom: Yellow-green fluorescent AcOTFMB dansyl sulfonate esters are stable to nucleophilic attack due to the electron-withdrawing properties of the trifluoromethyl group. The acetoxy trigger can be readily removed by esterase activity. Subsequent rapid 1,6-elimination affords the blue-fluorescent dansyl sulfonate anion.

Most sulfonate esters are potent electrophiles. Exceptions include neopentyl sulfonates (steric block of reactivity) and  $\alpha$ -trifluoromethylated sulfonates (electronic deactivation) (Miller, 2010). We have utilized these classes of sulfonate esters as platforms for the design of protecting groups that can be removed under specific conditions. In particular, we found that the incorporation of an acetoxy group into trifluoromethylbenzyl (TFMB) sulfonate esters maintained stability to nucleophiles but rendered these groups highly labile to esterase activity (Figure 3.1) (Rusha and Miller, 2011).

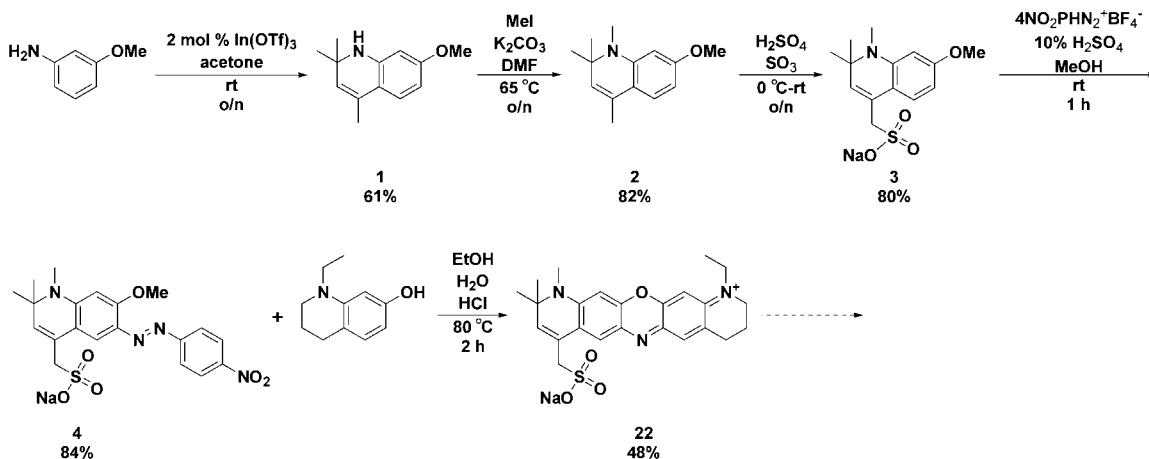
While this approach was facile for the small dansyl fluorophore, it was unclear whether the AcOTFMB group could be incorporated into near-IR dyes,

which are considerably larger and more challenging to synthesize. Here we report the successful synthesis of oxazine near-IR fluorophores bearing AcOTFMB esterase-labile sulfonate esters. We demonstrate that these dyes are chemically stable, but are readily cleaved to the free sulfonate by esterase activity, while the corresponding TFMB esters are unaffected.

### ***Results and Discussion***

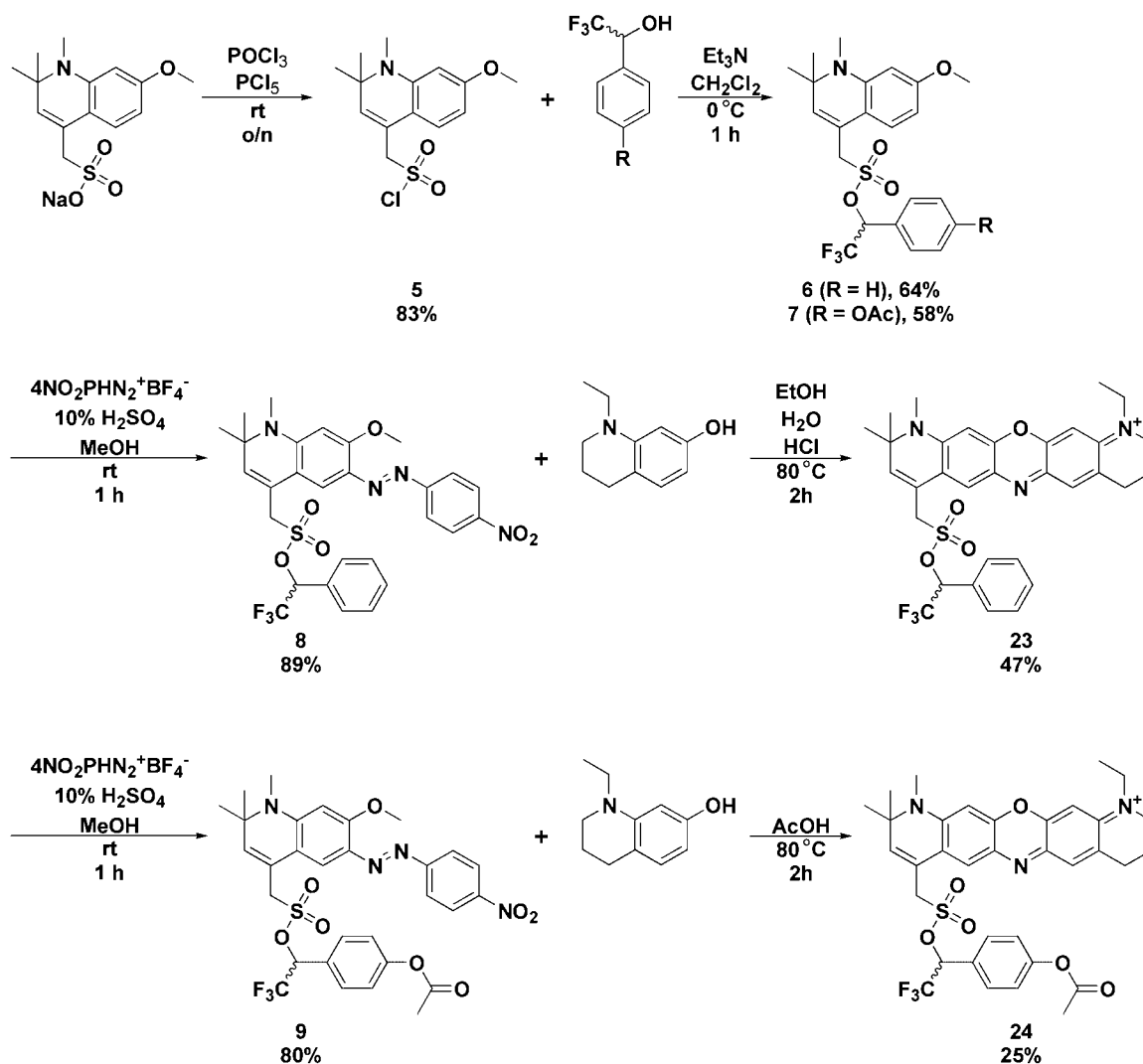
Examples of sulfonated near-IR fluorophores include cyanines, oxazines, and some rhodamine and BODIPY derivatives (Kolmanov et al., 2010; Mujumdar et al., 1993; Niu et al., 2009; Touthkine, 2009; Zilles et al., 2006). Among these dye classes, near-IR oxazines have the advantages of a compact structure, excitation and bright fluorescence in the 650-700 nm region, and high photostability (Eggeling et al., 2006; Hintersteiner et al., 2005; Wakata et al., 2010). To determine whether the AcOTFMB protection strategy was amenable to this class of near-IR fluorophores, we first synthesized the sulfonated oxazine dye **22** as shown in Scheme 3.1. Reaction of *m*-anisidine with acetone to form the dihydroquinoline **1** was facile in the presence of 2 mol % In(OTf)<sub>3</sub> (Theoclitou and Robinson, 2002). This product was then N-methylated and sulfonated to afford **3** (Zilles et al., 2006). Diazonium coupling yielded **4**, and subsequent acid-catalyzed condensation of this arylazo compound with a *m*-aminophenol yielded the sulfonated dye **22**, which exhibits maximal absorption at 673 nm and

emission at 689 nm in phosphate-buffered saline (PBS) (Kanitz and Hartmann, 1999).



### Scheme 3.1: Synthesis of a sulfonated oxazine dye.

With this sulfonated near-IR fluorophore in hand, the next synthetic challenge was determining how and when to incorporate the TFMB and AcOTFMB sulfonate esters. Our initial attempts to directly introduce TFMB and AcOTFMB sulfonate esters into **22** by formation and reaction of the sulfonyl chloride were unsuccessful. We therefore installed the sulfonate esters into the dye precursors (Scheme 3.2). Thus, the sodium sulfonate salt **3** was converted into the allylic sulfonyl chloride **5** and subsequently treated with the corresponding alcohol and  $\text{Et}_3\text{N}$  at  $0^\circ\text{C}$  to afford the sulfonate esters **6** and **7**.



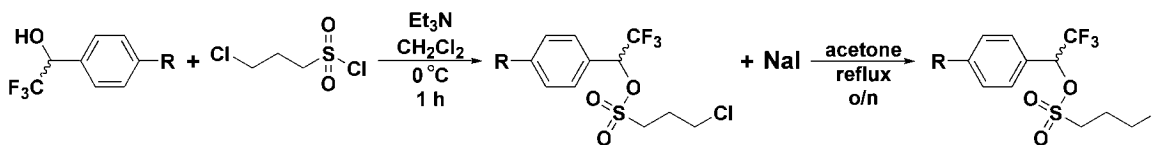
**Scheme 3.2: Incorporation of TFMB and AcOTFMB sulfonate esters into an oxazine dye.**

The sulfonate esters **6** and **7** were stable to diazonium coupling conditions in acidic aqueous methanol to afford **8** and **9**. Subsequent acid-catalyzed condensation of **8** with N-ethyl-7-hydroxy-tetrahydroquinoline yielded the desired TFMB-protected sulfonated oxazine **23**. However, the standard oxazine dye-



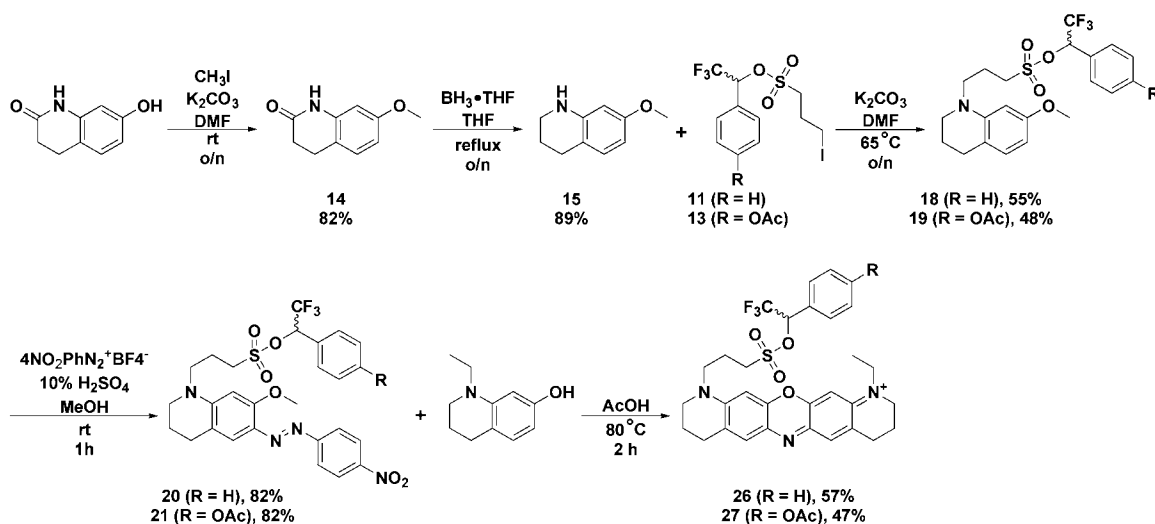
formation conditions of HCl in hot aqueous ethanol led to substantial deprotection of AcOTFMB, presumably because carboxylic esters are labile to these conditions. Gratifyingly, dye formation in hot acetic acid readily afforded the desired oxazine dye **24** with the AcOTFMB sulfonate ester intact (Scheme 3.2).

To facilitate the synthesis of more dyes containing a protected sulfonate, we constructed TFMB and AcOTFMB-protected iodopropyl sulfonates **11** and **13** (Scheme 3.3). Treatment of 3-chlorosulfonyl chloride with the corresponding alcohols and Et<sub>3</sub>N at 0°C yielded the respective chloropropyl sulfonates **10** and **12**. The chlorides were then selectively displaced with iodides. These compounds are especially notable because 1) their synthesis clearly demonstrates the remarkable stability of TFMB and AcOTFMB sulfonates to nucleophilic attack (chloro is displaced selectively even after overnight reflux with excess iodide), and 2) the iodide **13** can allow the introduction of an AcOTFMB-protected sulfonate into molecules with a suitable nucleophile, avoiding the need for sulfonation.

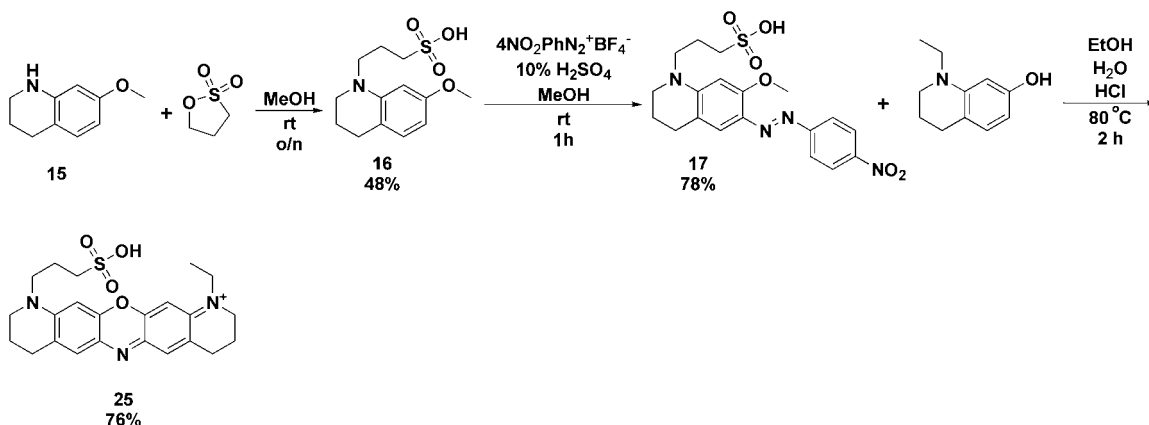


**Scheme 3.3: Synthesis of iodopropyl sulfonates.**

To make use of **11** and **13** for the construction of near-IR dyes, we synthesized sulfonated analogs of the oxazine dye MR121 (Scheme 3.4) (Herrmann et al., 1996; Lieberwirth et al., 1998). The tetrahydroquinoline **15** was dissolved in DMF and heated with **11** or **13** in the presence of excess  $K_2CO_3$  to yield **18** and **19**. Diazonium coupling followed by acid-catalyzed condensation with N-ethyl-7-hydroxy-tetrahydroquinoline yielded the desired oxazine dyes **26** and **27**. The corresponding free sulfonate dye was synthesized analogously by treatment of **15** with 1,3-propanesultone to afford **16** which was subsequently elaborated to yield the sulfonated dye **25** (Scheme 3.5). The excitation and emission wavelengths for this dye are similar to MR121, at 659 and 671 nm respectively.

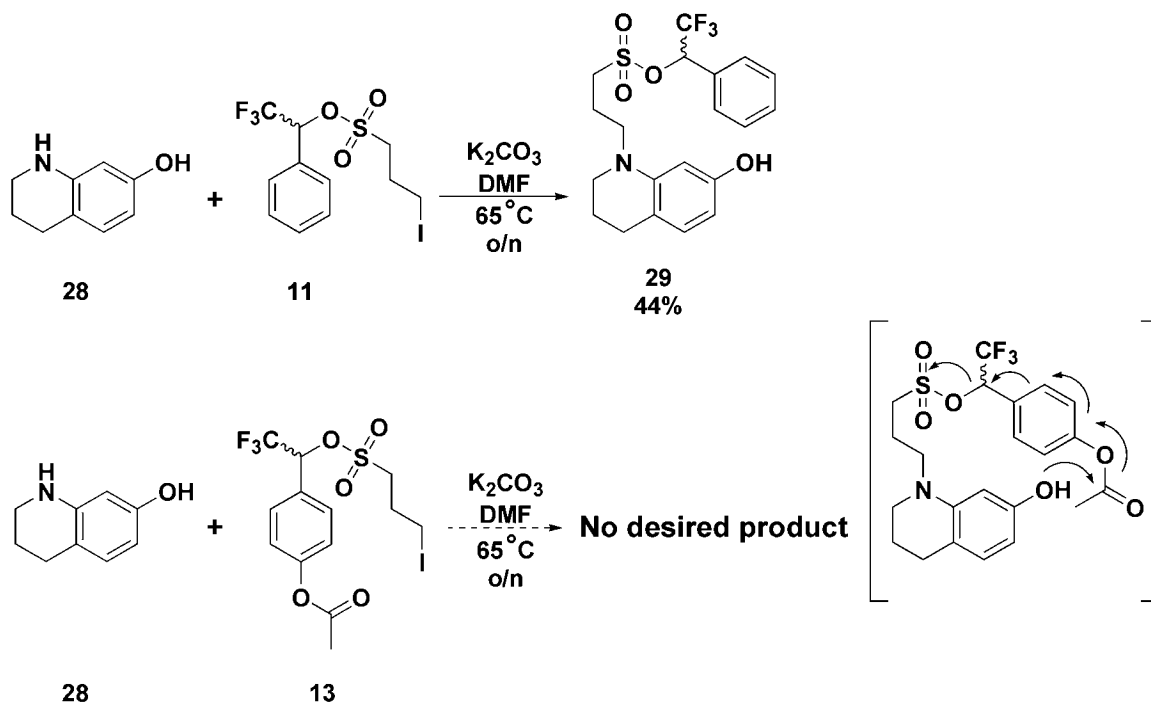


**Scheme 3.4: Synthesis of sulfonate ester derivatives of MR121.**



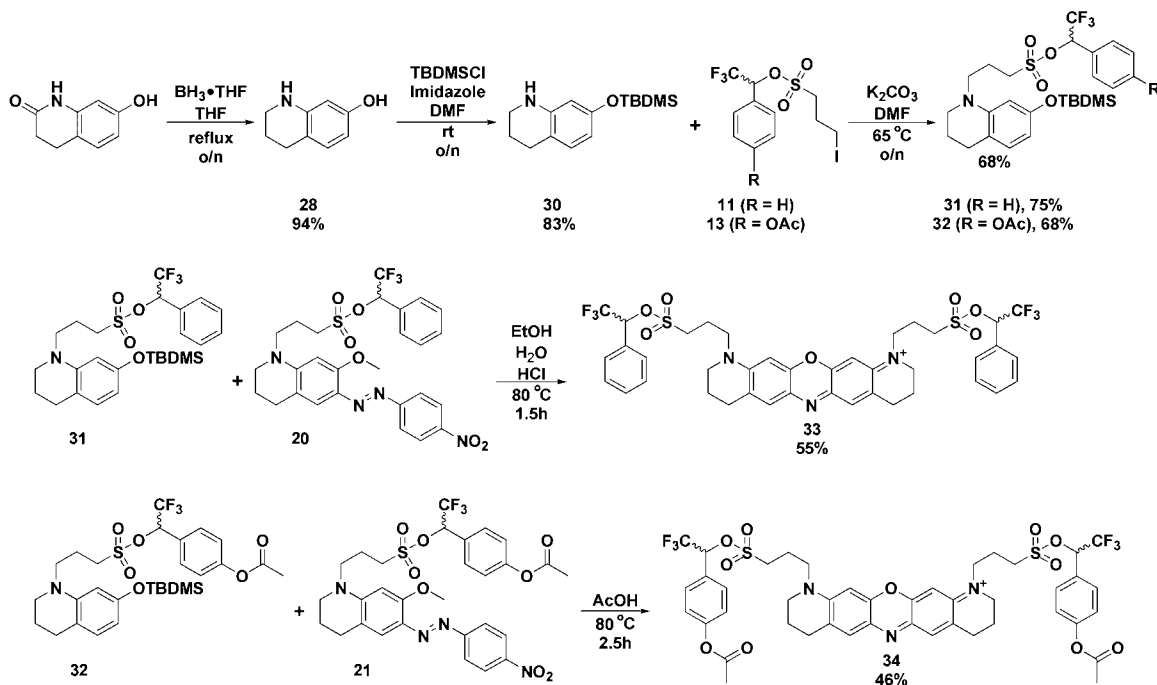
**Scheme 3.5: Synthesis of a sulfonated MR121 derivative.**

We next attempted to synthesize symmetrical oxazine dyes with two protected sulfonates, which would generate highly polar anionic molecules upon cleavage. Current synthetic approaches to such dyes require a phenolic intermediate such as **29** (Scheme 3.6) (Herrmann et al., 1996; Hintersteiner et al., 2005; Kanitz and Hartmann, 1999; Touthkine, 2009; Zilles et al., 2006). While the synthesis of the TFMB-protected sulfonate ester **29** was facile, we were unable to isolate the corresponding AcOTFMB-protected phenolic intermediate (Scheme 3.6). Because the corresponding TFMB-protected phenol **29** is stable, we surmise that the phenol promotes intramolecular deacetylation and self-immolation of the AcOTFMB group (Scheme 3.6). Indeed, the corresponding AcOTFMB-protected anisole **19** is stable and readily isolated (Scheme 3.4). Thus, derivatives of AcOTFMB bearing intramolecular nucleophiles may be prone to self-immolation.



**Scheme 3.6: Intramolecular nucleophiles can cause self-immolation of AcOTFMB sulfonates.**

In order to access symmetrical bis-sulfonated dyes without the need for the isolation of a phenolic intermediate such as **29**, we constructed the silyl ether **30**. We hypothesized that the AcOTFMB group would be stable in the presence of the silyl ether, and that the acidic conditions of dye synthesis would unmask the silyl ether and allow dye formation (Scheme 3.7). We were gratified to find that the silyl ether **32** was indeed stable, and that the silyl ethers **31** and **32** readily formed the desired symmetric bis-sulfonated oxazine dyes **33** and **34** when treated with **20** and **21** under acidic conditions (Scheme 3.7).



**Scheme 3.7: Bypassing phenols: formation of bis-sulfonated oxazine dyes from silyl ether and anisole starting materials.**

This method of oxazine dye synthesis has three key advantages over the classical methods that utilize condensation of one or more phenolic compounds (Herrmann et al., 1996; Hintersteiner et al., 2005; Kanitz and Hartmann, 1999; Toutchkine, 2009; Zilles et al., 2006). First, during the N-alkylation step, protection of the phenol avoids any undesired O-alkylation (Scheme 3.7), which improves yields and simplifies purification. Second, there is no need to deprotect prior to dye synthesis, eliminating a synthetic step. Finally, the use of silyl ethers expands the range of functionality that is compatible with oxazine dye synthesis. Typically, anisoles have been used for protection of phenolic intermediates in dye synthesis, and the requirement for HBr or  $\text{BBr}_3$  deprotection greatly limits

functional group compatibility (Herrmann et al., 1996; Hintersteiner et al., 2005; Toutchkine, 2009; Zilles et al., 2006). We anticipate that this method of dye synthesis will also find use in the preparation of rhodamine dyes bearing sensitive chemical functionality.

The AcOTFMB-protected sulfonated oxazine dyes **24** and **27** are readily unmasked by pig liver esterase (PLE) to afford the zwitterionic free sulfonate dyes **22** and **25**, respectively (Figure 3.2). Similarly, treatment of **34** with PLE rapidly formed the highly polar bis-sulfonate (Figure 3.3). In contrast, TFMB-protected dyes are stable to esterase activity (Figure 3.3), and both TFMB and AcOTFMB dyes are stable to treatment with biological nucleophiles such as 5 mM glutathione and 1 mg/mL ovalbumin (Figure 3.2 and 3.3). These findings are consistent with our results with dansyl dyes, and suggest that the AcOTFMB group is generally suitable as a chemically-stable, esterase-labile protecting group for dyes containing either aryl, allyl, or alkyl sulfonates (Rusha and Miller, 2011).

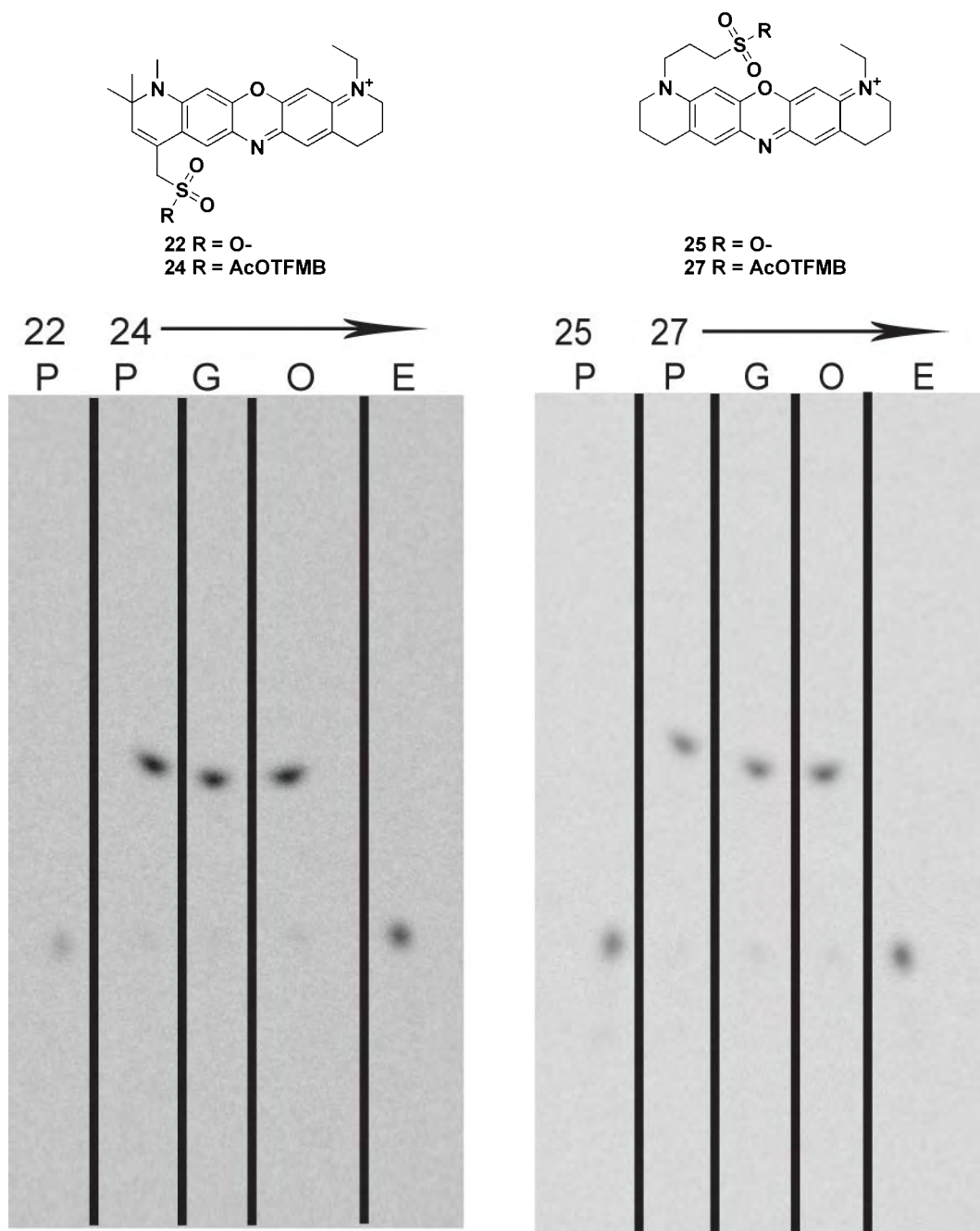


**Figure 3.2: NIR oxazines functionalized with AcOTFMB-sulfonate esters are cleaved to the free sulfonate dye *in vitro* by pig liver esterase.** AcOTFMB-oxazine dyes **24** and **27** were incubated in 1X PBS, pH 7.4 (P), 5 mM glutathione (G), 1 mg/mL ovalbumin (O) or 1U/mL pig liver esterase (E) for 30 minutes, then separated by TLC (10% MeOH/CH<sub>2</sub>Cl<sub>2</sub>) and imaged. The respective free sulfonate dyes **22** and **25** were incubated in PBS and used as a reference.

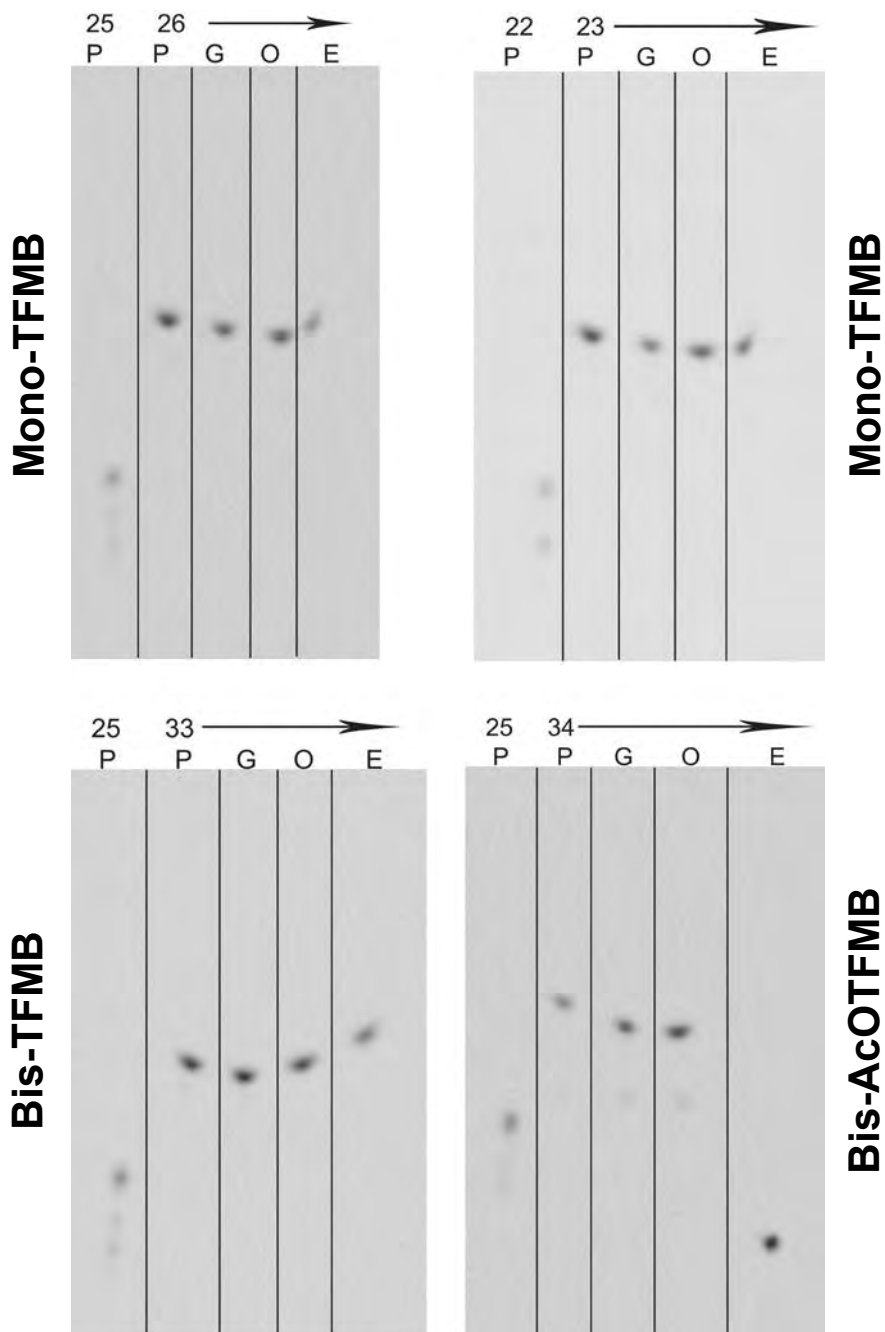


**Figure 3.3: Only the NIR oxazine dye functionalized with AcOTFMB-sulfonate esters (34) is cleaved to the free sulfonate dye upon treatment with pig liver esterase *in vitro*.** Oxazine dyes (1  $\mu$ M) were incubated in 1X PBS, pH 7.4 (P), 5 mM glutathione (G), 1 mg/mL ovalbumin (O) or 1 U/mL pig liver esterase (E) at room temperature for 30 minutes, then separated by TLC (10% MeOH/CH<sub>2</sub>Cl<sub>2</sub>) and imaged. Free mono-sulfonate oxazines (22 and 25) were incubated in PBS and used as a reference.



## **Conclusions**

We have described complex near-IR fluorophores that contain the esterase-labile sulfonate protecting group AcOTFMB. Moreover, intermediates such as **7**, **21**, and **32** are basic building blocks for the incorporation of esterase-labile sulfonates into oxazines and other dyes such as rhodamines, and intermediate **13** can allow the incorporation of the esterase-labile AcOTFMB sulfonate into an even wider variety of molecules. Further optimization of this approach and cell-based applications of these molecules are currently underway.

## **Materials and Methods**

### **General Methods**

3,4-Dihydro-7-hydroxy-2(1H)-quinolinone was purchased from TCI. Organic solvents were ACS grade (hexanes), AR<sup>®</sup> grade (acetone, ethyl acetate), and ChromAR<sup>®</sup> grade (methanol, dichloromethane, chloroform) and were purchased from BDH and Mallinckrodt. Dry solvents were purchased from Aldrich and Acros. NMR solvents were purchased from Cambridge Isotope Laboratories. All other chemicals were purchased from Aldrich, Acros, or Fisher Scientific.

NMR spectra were recorded with a Varian Mercury 400 MHz instrument. <sup>1</sup>H, <sup>19</sup>F and <sup>13</sup>C NMR spectra were recorded in CDCl<sub>3</sub>, CD<sub>3</sub>OD, or DMSO-D<sub>6</sub>. High-resolution mass spectra were obtained on a Waters QToF Premier. Fluorescence spectra were obtained using a Jobin Yvon Horiba SPEX FluoroMax-3.

### **Semi-preparative HPLC Purification**

Oxazine dyes were purified, as needed, by semi-preparative HPLC on a 22 x 250 mm C-18 column using a Hewlett Packard Agilent 1100 HPLC equipped with a G1315A DAD absorbance detector. All purification methods used aqueous 0.1% trifluoroacetic acid as Solvent A and acetonitrile/0.1% trifluoroacetic acid as Solvent B and were run at a flow rate of 5 mL/min. Acetonitrile and trifluoroacetic acid were HPLC grade and were purchased, respectively, from J. T. Baker and Aldrich. HPLC methods were as follows:

**Method A:** Absorbance detector set at 286, 354, 428, 626, and 675 nm. 40% B for 5 minutes, 40-65% B over 25 minutes, 65-100% B over 5 minutes, 100% B for 5 minutes.

**Method B:** Absorbance detector set at 290, 362, 615, and 667 nm. 60% B for 5 minutes, 60-90% B over 30 minutes, 90-100% B over 5 minutes, 100% B for 5 minutes.

**Method C:** Absorbance detector set at 285, 373, 452, 618, and 669 nm. 50% B for 5 minutes, 50-90% B over 40 minutes, 90-100% B over 5 minutes, 100% B for 5 minutes.

**Method D:** Absorbance detector set at 301, 354, 406, 608, and 657 nm. 40% B for 5 minutes, 40-70% B over 30 minutes, 70-100% B over 5 minutes, 100% B for 10 minutes.

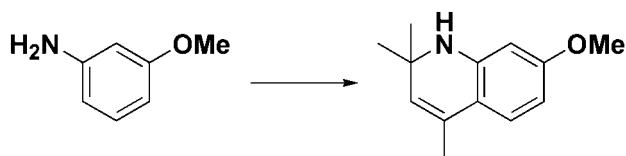
**Method E:** Absorbance detector set at 300, 456, 607, and 653 nm. 60% B for 5 minutes, 60-100% B over 40 minutes, 100% B for 5 minutes.

**Method F:** Absorbance detector set at 301, 454, 603, and 653 nm. 45% B for 5 minutes, 45-90% B over 45 minutes, 90-100% B over 5 minutes, 100% B for 5 minutes.

### Sulfonate Protecting Group Cleavage Assay.

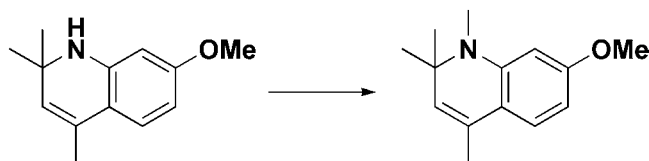
To determine the ability of the sulfonate esters to be unmasked by esterase activity, oxazine dyes were incubated at room temperature for 30 minutes in the following conditions: PBS, 5 mM glutathione (MP Biomedicals) in PBS, 1 mg/mL ovalbumin (Sigma) in PBS, 1 unit of pig liver esterase (Sigma) activity in PBS. Oxazine dyes were prepared as 10 mM stocks in DMSO (Aldrich) and diluted to 1  $\mu$ M for the experiments. After incubation, the samples were run on TLC plates in 10 % methanol/dichloromethane and analyzed using an LAS-3000 (FujiFilm) with a 670 nm long pass filter and excitation at 630 nm.

### Synthetic Procedures



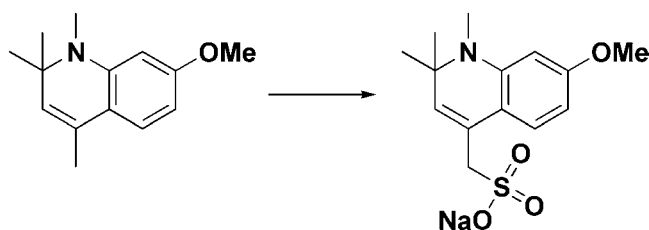
**7-methoxy-2,2,4-trimethyl-1,2-dihydroquinoline (1).** m-Anisidine (4 mL, 36 mmol) was added with stirring to a mixture of acetone (104 mL, 1.42 mol) and 2

mol %  $\text{In}(\text{OTf})_3$  (405 mg, 0.72 mmol). The reaction was stirred for 16 hours at room temperature. Evaporation of solvent via rotary evaporation yielded a viscous amber oil. The crude material was purified by flash column chromatography (0-3% ethyl acetate/hexanes) giving the product as a white solid (4.45 g, 61%).  $^1\text{H-NMR}$  ( $\text{CDCl}_3$ ):  $\delta$  6.97 (d, 1H,  $J = 8.4$  Hz), 6.20 (dd, 1H,  $J = 2.5$  Hz, 8.4 Hz), 6.01 (d, 1H,  $J = 2.5$  Hz), 5.19 (q, 1H,  $J = 1.3$  Hz), 3.75 (s, 3H), 3.69 (br. s, 1H), 1.96 (d, 3H,  $J = 1.3$  Hz), 1.26 (s, 6H).  $^{13}\text{C-NMR}$  ( $\text{CDCl}_3$ ):  $\delta$  160.4, 144.9, 128.4, 126.2, 124.9, 115.6, 102.5, 98.8, 55.3, 52.2, 31.3, 18.9. HR-EIMS:  $m/z$  calculated for  $\text{C}_{13}\text{H}_{18}\text{NO}$ : 204.1388, found: 204.1402.



**7-methoxy-1,2,2,4-tetramethyl-1,2-dihydroquinoline (2).** Compound **1** (3 g, 15 mmol) was dissolved in DMF (20 mL). Potassium carbonate (2.9 g, 21 mmol) was added, followed by methyl iodide (1.2 mL, 19 mmol), and the reaction mixture was heated to 50 °C with stirring for 20 hours. The mixture was cooled to room temperature, poured into water (200 mL) and the product extracted with ethyl acetate (4 X 50 mL). The combined organic layers were washed with water (3 X 50 mL), brine (1 X 125 mL), and dried over sodium sulfate. Removal of the solvent by rotary evaporation yielded a clear purple liquid. The crude material

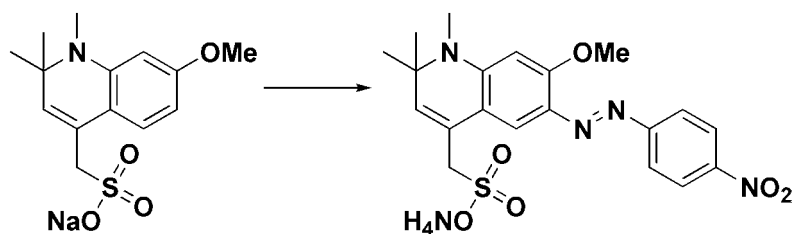
was purified by flash column chromatography (0-2% ethyl acetate/hexanes), yielding a viscous purple liquid (3.62 g, 82%).  $^1\text{H-NMR}$  ( $\text{CDCl}_3$ ):  $\delta$  6.98 (d, 1H,  $J = 8.3$  Hz), 6.20 (dd, 1H,  $J = 2.4$  Hz, 8.3 Hz), 6.11 (d, 1H,  $J = 2.4$  Hz), 5.18 (q, 1H,  $J = 1.3$  Hz), 3.80 (s, 3H), 2.79 (s, 3H), 1.96 (d, 3H,  $J = 1.4$  Hz), 1.29 (s, 6H).  $^{13}\text{C-NMR}$  ( $\text{CDCl}_3$ ):  $\delta$  160.8, 146.9, 128.1, 127.9, 124.2, 117.4, 99.8, 98.3, 56.5, 55.3, 30.9, 27.5, 18.9. HR-EIMS  $m/z$  calculated for  $\text{C}_{14}\text{H}_{20}\text{NO}$ : 218.1545, found: 218.1525.



**Sodium (7-methoxy-1,2,2-trimethyl-1,2-dihydroquinolin-4-yl)-**

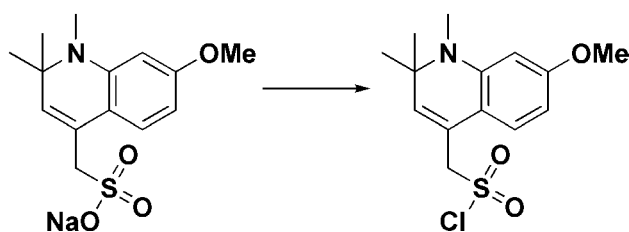
**methanesulfonate (3).** A 5:1 sulfuric acid:oleum solution (10 mL) was prepared with cooling in an ice bath. Compound **2** (2.3 g, 11 mmol) was dissolved in the cooled acid solution and the reaction was brought to room temperature and stirred for 20 hours. The reaction was poured onto ice, cooled in an ice/methanol bath, and adjusted to pH 12 with 5 M sodium hydroxide. Unreacted starting material was removed by extraction with chloroform (1 X 200 mL and 2 X 100 mL) and the aqueous phase was concentrated via rotary evaporation to yield a patchy white and brown solid. The solid was dissolved in 95% ethanol, filtered to

separate the product from the sodium sulfate salt, and the filtrate was concentrated under vacuum to yield a white solid. The crude compound was purified by flash column chromatography (0-50% methanol/chloroform) to give the product as a pale green solid (2.75 g, 80%).  $^1\text{H-NMR}$  (DMSO- $\text{D}_6$ ):  $\delta$  7.16 (d, 1H,  $J = 8.4$  Hz), 6.08 (dd, 1H,  $J = 2.5$  Hz, 8.4 Hz), 5.97 (d, 1H,  $J = 2.4$  Hz), 5.33 (s, 1H), 3.68 (s, 3H), 3.40 (s, 2H), 2.67 (s, 3H), 1.20 (s, 6H).  $^{13}\text{C-NMR}$  (DMSO- $\text{D}_6$ ):  $\delta$  160.4, 147.1, 131.3, 126.3, 126.1, 116.6, 100.4, 98.1, 56.5, 55.4, 54.5, 31.1, 27.4. HR-EIMS  $m/z$  calculated for  $\text{C}_{14}\text{H}_{20}\text{NO}_4\text{S}$ : 298.1113, found: 298.1100.



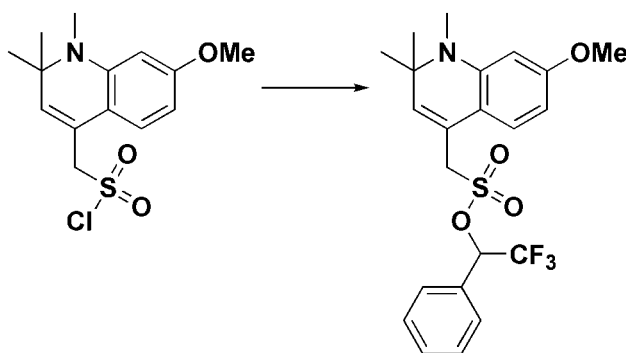
**Ammonium [7-Methoxy-1,2,2-trimethyl-6-(4-nitro-phenylazo)-1,2-dihydro-quinolin-4-yl]-methanesulfonate (4).** Compound **3** (405 mg, 1.27 mmol) was dissolved in methanol (13 mL). 4-Nitrobenzenediazonium tetrafluoroborate (301 mg, 1.27 mmol) was suspended in 10% sulfuric acid (13 mL) with vortexing. The organic solution was added to the aqueous mixture and stirred at ambient conditions for 1 hour. The solution was then neutralized with ammonium hydroxide, resulting in a purple precipitate. The mixture was filtered and the filtrand washed with chloroform (5 X 20 mL) to yield a purple solid (496 mg,

84%). This compound was dried *in vacuo* and used in the next reaction without further purification.  $^1\text{H-NMR}$  (DMSO- $\text{D}_6$ ):  $\delta$  8.29 (d, 2H,  $J = 9.1$  Hz), 7.83 (d, 2H,  $J = 9.1$  Hz), 7.74 (s, 1H), 6.17 (s, 1H), 5.61 (s, 1H), 3.97 (s, 3H), 3.44 (s, 2H), 3.00 (s, 3H), 1.36 (s, 6H).  $^{13}\text{C-NMR}$  (DMSO- $\text{D}_6$ ):  $\delta$  161.6, 157.9, 152.6, 146.4, 133.2, 132.9, 125.5, 124.8, 122.8, 115.4, 112.7, 93.9, 58.7, 56.6, 53.6, 32.5, 29.0. HR-EIMS  $m/z$  calculated for  $\text{C}_{20}\text{H}_{23}\text{N}_4\text{O}_6\text{S}$ : 447.1338, found: 447.1337.



**(7-methoxy-1,2,2-trimethyl-1,2-dihydroquinolin-4-yl)-methanesulfonyl chloride (5).** Compound **3** (616 mg, 1.93 mmol) was suspended in  $\text{POCl}_3$  (9.2 mL) and stirred at room temperature.  $\text{PCl}_5$  (401 mg, 1.93 mmol) was added to the mixture and the reaction was stirred at room temperature overnight. The reaction was poured into ice water (200 mL) which resulted in the product crashing out as a red oil. Upon neutralizing with  $\text{NaHCO}_3$  (400 mL), the oil became a sticky solid which floated to the top of the solution. The product was then extracted with dichloromethane (800 mL), washed with brine (500 mL), and dried over sodium sulfate. Removal of the solvent under vacuum yielded the product as a viscous amber oil (504 mg, 83%). This compound was used without further purification.

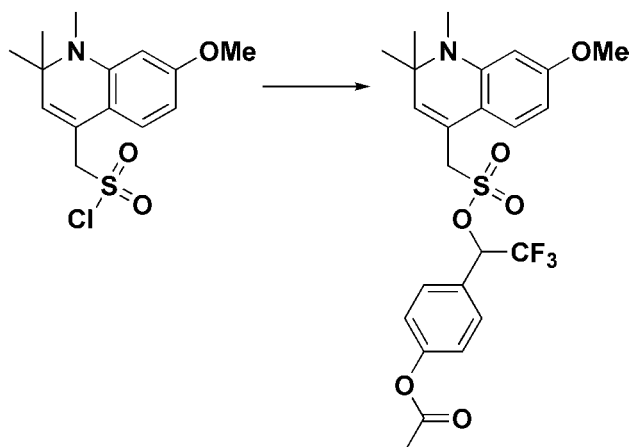
$^1\text{H-NMR}$  ( $\text{CDCl}_3$ ):  $\delta$  7.07 (d, 1H,  $J$  = 8.5 Hz), 6.24 (dd, 1H,  $J$  = 2.3 Hz, 8.4 Hz), 6.14 (br s, 1H), 5.67 (s, 1H), 4.67 (d, 2H,  $J$  = 0.5 Hz), 3.80 (s, 3H), 2.80 (s, 3H), 1.37 (s, 6H).  $^{13}\text{C-NMR}$  ( $\text{CDCl}_3$ ):  $\delta$  161.6, 147.0, 137.4, 124.9, 120.7, 113.4, 100.7, 99.2, 77.5, 68.2, 55.4, 30.0, 26.7. HR-EIMS  $m/z$  calculated for  $\text{C}_{14}\text{H}_{19}\text{ClNO}_3\text{S}$ : 316.0774, found: 316.0764.



**(7-methoxy-1,2,2-trimethyl-1,2-dihydroquinolin-4-yl)-methanesulfonic acid 2,2,2-trifluoro-1-phenyl-ethyl ester (6).**  $\alpha$ -(Trifluoromethyl)-benzyl alcohol (0.18 mL, 1.3 mmol) was dissolved in anhydrous dichloromethane (3 mL) and cooled to 0 °C in an ice bath. Triethylamine (0.12 mL, 0.84 mmol) was then added to the reaction. Compound **5** (132 mg, 0.418 mmol) dissolved in anhydrous dichloromethane (1.2 mL) was added dropwise via syringe to the reaction flask at a rate of 20 drops/min. Upon completion of the dropwise addition, the reaction was stirred at 0 °C for 1 hour. The reaction was poured into 1 M hydrochloric acid (40 mL) and extracted with dichloromethane (1 X 50 mL and 3 X 20 mL). The organic phases were combined, washed with water (50 mL), sodium

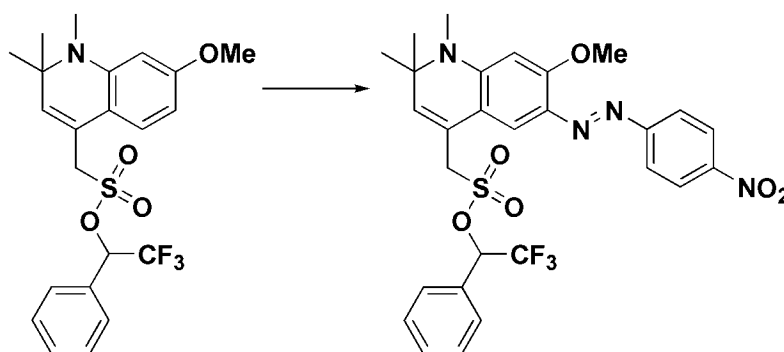


bicarbonate (50 mL), brine (50 mL) and dried over sodium sulfate. The solvent was evaporated and the crude material was purified by flash column chromatography (0-10% ethyl acetate/hexanes) to yield the product as a viscous, lime-green oil (122 mg, 64%).  $^1\text{H-NMR}$  ( $\text{CDCl}_3$ ):  $\delta$  7.48-7.39 (m, 5H), 6.96 (d, 1H,  $J = 8.5$  Hz), 6.19 (dd, 1H,  $J = 2.4$  Hz, 8.5 Hz), 6.09 (d, 1H,  $J = 2.4$  Hz), 5.80 (q, 1H,  $J_{\text{HF}} = 6.3$  Hz), 5.43 (s, 1H), 4.10 (d of ABq, 2H,  $\Delta\delta_{\text{AB}} = 0.03$ ,  $J_{\text{AB}} = 14.8$  Hz,  $J = 0.7$  Hz), 3.79 (s, 3H), 2.74 (s, 3H), 1.27 (s, 3H), 1.24 (s, 3H).  $^{19}\text{F-NMR}$  ( $\text{CDCl}_3$ ):  $\delta$  -76.2 (d,  $J = 6.3$  Hz).  $^{13}\text{C-NMR}$  ( $\text{CD}_3\text{OD}$ ):  $\delta$  161.4, 147.1, 135.1, 130.5, 130.4, 128.8, 128.3, 124.8, 122.9 (q,  $^1J_{\text{CF}} = 281$  Hz), 120.9, 114.2, 100.5, 98.4, 77.4 (q,  $^2J_{\text{CF}} = 34$  Hz), 56.3, 54.3, 54.1, 29.8, 25.4, 25.3. HR-EIMS  $m/z$  calculated for  $\text{C}_{22}\text{H}_{25}\text{F}_3\text{NO}_4\text{S}$ : 456.1456, found: 456.1457.



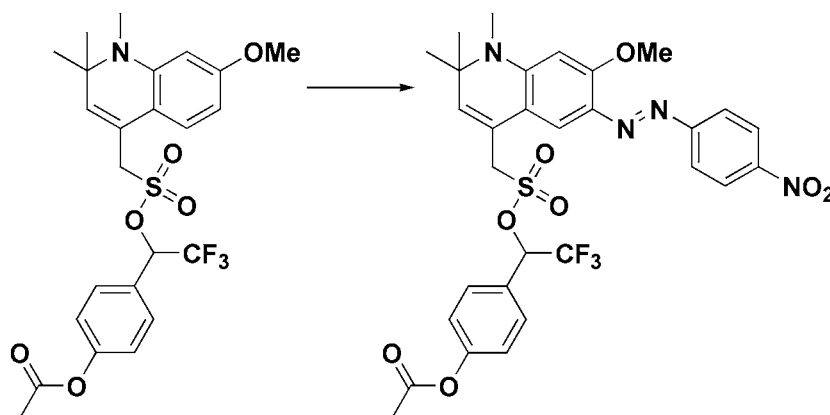
**Acetic acid 4-[2,2,2-trifluoro-1-(7-methoxy-1,2,2-trimethyl-1,2-dihydroquinolin-4-ylmethanesulfonyloxy)-ethyl]-phenyl ester (7).** Acetic acid 4-(2,2,2-trifluoro-1-hydroxy-ethyl)-phenyl ester (AcOTFMB, Rusha and Miller, 2011) (212 mg, 0.904 mmol) was dissolved in anhydrous dichloromethane (4 mL) and cooled to 0 °C in an ice bath. Triethylamine (0.101 mL, 0.723 mmol) was then added to the reaction. Compound **5** (190 mg, 0.602 mmol) dissolved in anhydrous dichloromethane (2 mL, 31 mmol) was added dropwise via syringe to the reaction flask at a rate of 20 drops/min. Upon completion of dropwise addition, the reaction was stirred at 0 °C for 1 hour. The reaction was poured into 1 M hydrochloric acid (60 mL) and extracted with dichloromethane (1 X 60 mL and 4 X 20 mL). The organic phases were combined, washed with 0.1 M hydrochloric acid (4 X 20 mL), sodium bicarbonate (40 mL), brine (80 mL) and dried over sodium sulfate. The solvent was evaporated and the crude material was purified by flash column chromatography on two successive columns. The purest fractions from the first column (0-25% ethyl acetate/hexanes) were

separated on a second column with 0-2% methanol/dichloromethane to yield the product as a viscous, green oil (178 mg, 58%).  $^1\text{H-NMR}$  ( $\text{CDCl}_3$ ):  $\delta$  7.45 (d, 2H,  $J = 8.7$  Hz), 7.14 (d, 2H,  $J = 8.8$  Hz), 6.97 (d, 1H,  $J = 8.4$  Hz), 6.20 (dd, 1H,  $J = 2.4$  Hz, 8.4 Hz), 6.09 (d, 1H,  $J = 2.3$  Hz), 5.80 (q, 1H,  $J_{\text{HF}} = 6.2$  Hz), 5.45 (s, 1H), 4.14 (d of ABq, 2H,  $\Delta\delta_{\text{AB}} = 0.03$ ,  $J_{\text{AB}} = 14.8$  Hz,  $J = 0.7$  Hz), 3.79 (s, 3H), 2.74 (s, 3H), 2.31 (s, 3H), 1.27 (s, 3H), 1.24 (s, 3H).  $^{19}\text{F-NMR}$  ( $\text{CDCl}_3$ ):  $\delta$  -76.2 (d,  $J = 6.2$  Hz).  $^{13}\text{C-NMR}$  ( $\text{CD}_3\text{OD}$ ):  $\delta$  169.5, 161.4, 152.6, 147.1, 135.1, 129.5, 127.9, 124.7, 122.8 (q,  $^1J_{\text{CF}} = 280$  Hz), 122.2, 122.14, 121.5, 120.9, 114.2, 100.5, 98.4, 76.6 (q,  $^2J_{\text{CF}} = 34$  Hz), 56.3, 54.3, 53.9, 29.8, 25.4, 25.2, 19.7. HR-EIMS  $m/z$  calculated for  $\text{C}_{24}\text{H}_{27}\text{F}_3\text{NO}_6\text{S}$ : 514.1506, found: 514.1491.



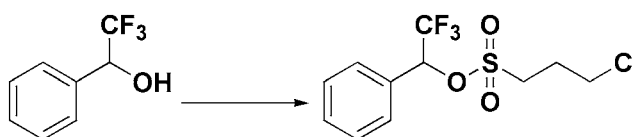
**[7-Methoxy-1,2,2-trimethyl-6-(4-nitro-phenylazo)-1,2-dihydro-quinolin-4-yl]-methanesulfonic acid 2,2,2-trifluoro-1-phenyl-ethyl ester (8)**. Compound **6** (121 mg, 0.267 mmol) was dissolved in methanol (3 mL). 4-Nitrobenzenediazonium tetrafluoroborate (63.1 mg, 0.267 mmol) was suspended in 10% sulfuric acid (3 mL) with vortexing. The organic solution was added to the

aqueous mixture and stirred at ambient conditions for 1 hour. The solution was then neutralized with ammonium hydroxide, resulting in a reddish-purple precipitate. The mixture was filtered and the filtrand washed with water (3 X 20 mL) to yield a deep purple-black solid (144 mg, 89 %). This compound was dried *in vacuo* and used in the next reaction without further purification.  $^1\text{H-NMR}$  ( $\text{CDCl}_3$ ):  $\delta$  8.31 (d, 2H,  $J = 9.1$  Hz), 7.90 (d, 2H,  $J = 9.1$  Hz), 7.68 (s, 1H), 7.46-7.33 (m, 5H), 6.06 (s, 1H), 5.81 (q, 1H,  $J_{\text{HF}} = 6.3$  Hz), 5.62 (s, 1H), 4.18 (ABq, 2H,  $\Delta\delta_{\text{AB}} = 0.05$ ,  $J_{\text{AB}} = 14.8$  Hz), 4.05 (s, 3H), 2.96 (s, 3H), 1.40 (s, 3H), 1.38 (s, 3H).  $^{19}\text{F-NMR}$  ( $\text{CDCl}_3$ ):  $\delta$  -76.1 (d,  $J = 6.3$  Hz). HR-EIMS:  $m/z$  calculated for  $\text{C}_{28}\text{H}_{28}\text{F}_3\text{N}_4\text{O}_6\text{S}$ : 605.1676, found: 605.1653.



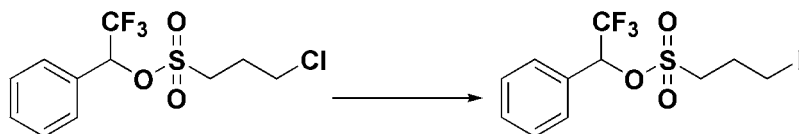
**Acetic acid 4-{2,2,2-trifluoro-1-[7-Methoxy-1,2,2-trimethyl-6-(4-nitrophenylazo)-1,2-dihydro-quinolin-4-ylmethanesulfonyloxy]-ethyl)-phenyl ester (9).** Compound 7 (179 mg, 0.35 mmol) was dissolved in methanol (4 mL). 4-Nitrobenzenediazonium tetrafluoroborate (83 mg, 0.35 mmol) was suspended

in 10% sulfuric acid (4 mL) with vortexing. The organic solution was added to the aqueous mixture and stirred at ambient conditions for 1 hour. The solution was then neutralized with ammonium hydroxide, resulting in a reddish-purple precipitate. The mixture was filtered and the filtrand washed with water (3 X 25 mL) to yield a purple solid (185 mg, 80%). This compound was dried *in vacuo* and used in the next reaction without further purification.  $^1\text{H-NMR}$  ( $\text{CD}_3\text{OD}$ ):  $\delta$  8.32 (d, 2H,  $J = 9.1$  Hz), 7.90 (d, 2H,  $J = 9.1$  Hz), 7.70 (s, 1H), 7.47 (d, 2H,  $J = 8.6$  Hz), 7.09 (d, 2H,  $J = 8.7$  Hz), 6.15 (s, 1H), 6.12 (q, 1H,  $J_{\text{HF}} = 6.4$  Hz), 5.65 (s, 1H), 4.40 (s, 2H), 4.03 (s, 3H), 2.98 (s, 3H), 2.27 (s, 3H), 1.37 (s, 3H), 1.36 (s, 3H).  $^{19}\text{F-NMR}$  ( $\text{CD}_3\text{OD}$ ):  $\delta$  -78.0 (d,  $J = 6.4$  Hz). HR-EIMS:  $m/z$  calculated for  $\text{C}_{30}\text{H}_{30}\text{F}_3\text{N}_4\text{O}_8\text{S}$ : 663.1736, found: 663.1730.



**3-Chloro-propane-1-sulfonic acid 2,2,2-trifluoro-1-phenyl-ethyl ester (10).**  $\alpha$ -(Trifluoromethyl)-benzyl alcohol (1.29 mL, 9.47 mmol) was dissolved in anhydrous dichloromethane (29 mL) and cooled to 0 °C in an ice bath. Triethylamine (0.879 mL, 6.31 mmol) was then added to the reaction. 3-Chloropropanesulfonyl chloride (0.386 mL, 3.15 mmol) dissolved in anhydrous dichloromethane (2 mL) was added dropwise via syringe to the reaction flask at a rate of 20 drops/min. Upon completion of dropwise addition, the reaction was

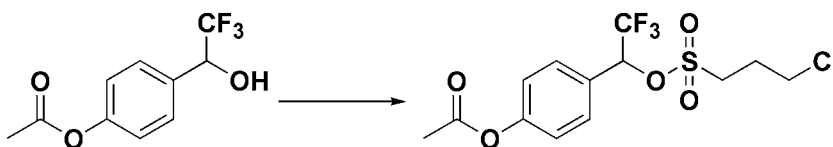
stirred at 0 °C for 1 hour. The reaction was poured into 1 M hydrochloric acid (300 mL) and extracted with dichloromethane (1 X 300 mL and 4 X 60 mL). The combined organic phases were washed with water (200 mL), brine (250 mL) and dried over sodium sulfate. Removal of the solvent under vacuum yielded the product as a white solid (886 mg, 89%). <sup>1</sup>H-NMR (CDCl<sub>3</sub>): δ 7.53-7.44 (m, 5H), 5.78 (q, 1H, *J*<sub>HF</sub> = 6.4 Hz), 3.59 (t, 2H, *J* = 6.1 Hz), 3.30-3.17 (m, 2H), 2.31-2.22 (m, 2H). <sup>19</sup>F-NMR (CDCl<sub>3</sub>): δ -76.3 (d, *J* = 6.3 Hz). <sup>13</sup>C-NMR (CD<sub>3</sub>OD): δ 130.6, 130.5, 128.9, 128.2, 122.9 (q, <sup>1</sup>*J*<sub>CF</sub> = 280 Hz), 77.6 (q, <sup>2</sup>*J*<sub>CF</sub> = 34 Hz), 48.9, 41.9, 26.7. HR-EIMS *m/z* calculated for C<sub>11</sub>H<sub>12</sub>ClF<sub>3</sub>O<sub>3</sub>SNa: 339.0045, found: 339.0060.



### **3-Iodo-propane-1-sulfonic acid 2,2,2-trifluoro-1-phenyl-ethyl ester (11).**

Sodium iodide (757 mg, 5.05 mmol) was dissolved in acetone (5 mL). Compound **10** (400 mg, 1.26 mmol) was added to the solution and the reaction was heated to reflux and stirred overnight. After cooling to room temperature, the mixture was filtered to remove sodium chloride and the filtrand was washed with acetone (40 mL). The filtrate was concentrated under vacuum and the resulting residue was extracted between 75 mL ethyl acetate and 75 mL water. The organic phase was collected, dried over sodium sulfate, and the solvent removed via rotary

evaporation giving an amber oil. The crude material was purified by flash column chromatography (15% ethyl acetate/hexanes) to yield the compound as a yellow liquid (488 mg, 95%).  $^1\text{H-NMR}$  ( $\text{CDCl}_3$ ):  $\delta$  7.53-7.45 (m, 5H), 5.77 (q, 1H,  $J_{\text{HF}} = 6.3$  Hz), 3.24-3.11 (m, 4H), 2.33-2.24 (m, 2H).  $^{19}\text{F-NMR}$  ( $\text{CDCl}_3$ ):  $\delta$  -76.3 (d,  $J = 6.3$  Hz).  $^{13}\text{C-NMR}$  ( $\text{CD}_3\text{OD}$ ):  $\delta$  130.7, 130.5, 130.4, 128.9, 128.23, 128.22, 122.9 (q,  $^1J_{\text{CF}} = 280$  Hz), 77.6 (q,  $^2J_{\text{CF}} = 34$  Hz), 52.2, 27.5, 0.8. HR-EIMS  $m/z$  calculated for  $\text{C}_{11}\text{H}_{12}\text{F}_3\text{O}_3\text{SiNa}$ : 430.9402, found: 430.9382.



**Acetic acid 4-[1-(3-chloro-propane-1-sulfonyloxy)-2,2,2-trifluoro-ethyl]-phenyl ester (12).** Acetic acid 4-(2,2,2-trifluoro-1-hydroxy-ethyl)-phenyl ester (AcOTFMB, Rusha and Miller, 2011) (537 mg, 2.29 mmol) was dissolved in anhydrous dichloromethane (9 mL) and cooled to 0 °C in an ice bath. Triethylamine (0.32 mL, 2.29 mmol) was added to the reaction. 3-Chloropropanesulfonyl chloride (0.14 mL, 1.13 mmol) dissolved in anhydrous dichloromethane (2 mL) was added dropwise via syringe to the reaction flask at a rate of 20 drops/min. Upon completion of dropwise addition, the reaction was stirred at 0 °C for 1 hour. The reaction was poured into 1 M hydrochloric acid (110 mL) and extracted with dichloromethane (1 X 110 mL and 4 X 20 mL). The combined organic phases were washed with water (75 mL), brine (90 mL), and

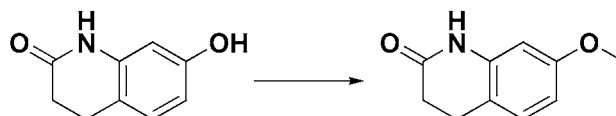
dried over sodium sulfate. Removal of the solvent under vacuum resulted in a yellowish oil. The crude product was purified by flash column chromatography (0-2% methanol/dichloromethane) to yield the product as a clear viscous oil (386 mg, 91%).  $^1\text{H-NMR}$  ( $\text{CDCl}_3$ ):  $\delta$  7.52 (d, 2H,  $J = 8.8$  Hz), 7.21 (d, 2H,  $J = 8.8$  Hz), 5.79 (q, 1H,  $J_{\text{HF}} = 6.3$  Hz), 3.61 (t, 2H,  $J = 6.2$  Hz), 3.33-3.20 (m, 2H), 2.32 (s, 3H), 2.31-2.24 (m, 2H).  $^{19}\text{F-NMR}$  ( $\text{CDCl}_3$ ):  $\delta$  -76.3 (d,  $J = 6.3$  Hz).  $^{13}\text{C-NMR}$  ( $\text{CDCl}_3$ ):  $\delta$  169.5, 152.8, 129.5, 128, 122.8 (q,  $^1J_{\text{CF}} = 280$  Hz), 122.4, 76.9 (q,  $^2J_{\text{CF}} = 34$  Hz), 48.9, 41.9, 26.7, 19.7. HR-EIMS  $m/z$  calculated for  $\text{C}_{13}\text{H}_{14}\text{ClF}_3\text{O}_5\text{SNa}$ : 397.0100, found: 397.0097.



**Acetic acid 4-[2,2,2-trifluoro-1-(3-iodo-propyl-sulfonyloxy)-ethyl]-phenyl ester (13).** Sodium iodide (398 mg, 2.66 mmol) was dissolved in acetone (2 mL). Compound **12** (249 mg, 0.664 mmol) was added to the solution and the reaction was heated to reflux and stirred for 17 hours. After cooling to room temperature, the mixture was filtered to remove sodium chloride and the filtrand was washed with acetone (25 mL). Acetone was removed via rotary evaporation and the resulting residue was extracted between 60 mL ethyl acetate and 60 mL water. The organic phase was collected and the aqueous phase was washed with ethyl acetate (2 X 50 mL). The combined organic phases were washed with brine (75



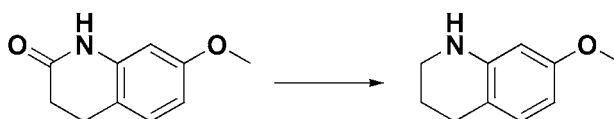
mL), dried over sodium sulfate, and the solvent removed via rotary evaporation giving an amber oil. The crude material was purified by flash column chromatography (15% ethyl acetate/hexanes) to yield the product as a viscous yellow oil (300 mg, 97%).  $^1\text{H-NMR}$  ( $\text{CDCl}_3$ ):  $\delta$  7.52 (d, 2H,  $J = 8.8$  Hz), 7.21 (d, 2H,  $J = 8.8$  Hz), 5.78 (q, 1H,  $J_{\text{HF}} = 6.3$  Hz), 3.24-3.17 (m, 4H), 2.33-2.26 (m, 5H), 2.32 (s, 3H).  $^{19}\text{F-NMR}$  ( $\text{CDCl}_3$ ):  $\delta$  -76.3 (d,  $J = 6.3$  Hz).  $^{13}\text{C-NMR}$  ( $\text{CD}_3\text{OD}$ ):  $\delta$  169.6, 152.8, 129.6, 127.9, 122.8 (q,  $^1J_{\text{CF}} = 280$  Hz), 122.5, 77.0 (q,  $^2J_{\text{CF}} = 34$  Hz), 52.3, 27.5, 19.9, 1.1. HR-EIMS  $m/z$  calculated for  $\text{C}_{13}\text{H}_{14}\text{F}_3\text{O}_5\text{SiNa}$ : 488.9456, found: 488.9482.



**7-Methoxy-3,4-dihydro-1H-quinolin-2-one (14)** (Tsuritani et al., 2009). 7-Hydroxy-3,4-dihydroquinolin-2(1H)-one (1.5 g, 9.2 mmol) was dissolved in DMF (10 mL) and potassium carbonate (1.85 g, 13.4 mmol) was added. Methyl iodide (0.7 mL, 11 mmol) was added to the mixture and the reaction was stirred at room temperature overnight. The reaction was poured into water (100 mL) and neutralized with 1 M HCl. The compound was extracted with ethyl acetate (6 X 50 mL) and the combined organic phases were washed with water (200 mL), 1:1 saturated  $\text{Na}_2\text{S}_2\text{O}_3$ : brine (200 mL), and brine (200 mL). The organic phase was dried over sodium sulfate and solvent was removed via rotary evaporation. The

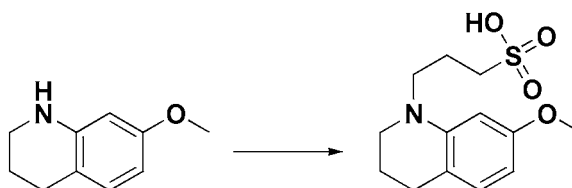
crude material was purified by flash column chromatography (50% ethyl acetate/hexanes) to yield the product as a white crystalline solid (1.34 g, 82%).

$^1\text{H-NMR}$  ( $\text{CDCl}_3$ ):  $\delta$  7.77 (br s, 1H), 7.06 (d, 1H,  $J = 8.3$  Hz), 6.53 (dd, 1H,  $J = 2.5$  Hz, 8.3 Hz), 6.30 (d, 1H,  $J = 2.4$  Hz), 3.78 (s, 3H), 2.90 (t, 2H,  $J = 7.9$  Hz), 2.62 (t, 2H,  $J = 7.8$  Hz). HR-EIMS  $m/z$  calculated for  $\text{C}_{10}\text{H}_{12}\text{NO}_2$ : 178.0868, found: 178.0867.



**7-Methoxy-1,2,3,4-tetrahydroquinoline (15).** Compound **14** (1 g, 5.6 mmol) was dissolved in THF (10 mL) and cooled to 0 °C. 1M  $\text{BH}_3 \cdot \text{THF}$  (70 mL, 70 mmol) was added to the solution dropwise through an addition funnel over 1 hour and the reaction was refluxed overnight. The reaction was then cooled to 0 °C and quenched by the slow addition of methanol (24 mL). After quenching, the reaction was acidified with concentrated hydrochloric acid (10 mL) and heated to 65 °C for 1 hour. The reaction was then cooled to 0 °C, neutralized with concentrated sodium hydroxide, and extracted with ethyl acetate (1 X 300 mL and 3 X 50 mL). The organic phases were combined, washed with brine (300 mL) and dried over sodium sulfate. Solvent was removed via rotary evaporation and crude material was purified by flash column chromatography (25% ethyl acetate/hexanes) to yield the product as a bright yellow oil (820 mg, 89%).  $^1\text{H-}$

NMR (CDCl<sub>3</sub>):  $\delta$  6.83 (d, 1H,  $J$  = 8.2 Hz), 6.20 (dd, 1H,  $J$  = 2.5 Hz, 8.2 Hz), 6.03 (d, 1H,  $J$  = 2.5 Hz), 3.80 (br s, 1H), 3.73 (s, 3H), 3.28 (t, 2H,  $J$  = 5.5 Hz), 2.69 (t, 3H,  $J$  = 6.4 Hz), 1.95-1.88 (m, 2H). <sup>13</sup>C-NMR (CDCl<sub>3</sub>):  $\delta$  159.2, 146.0, 130.4, 114.3, 103.0, 99.7, 55.4, 42.3, 26.7, 22.8. HR-EIMS  $m/z$  calculated for C<sub>10</sub>H<sub>14</sub>NO: 164.1075, found: 164.1075.



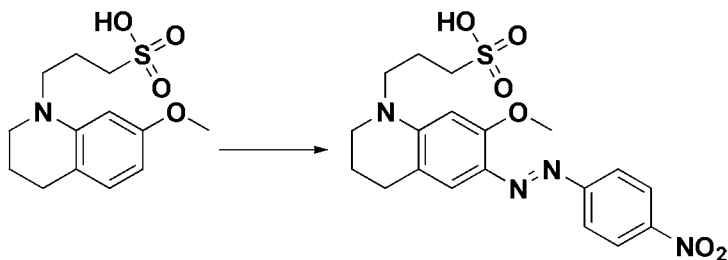
### 3-(7-Methoxy-3,4-dihydro-2H-quinolin-1-yl)-propane-1-sulfonic acid (**16**).

Compound **15** (100 mg, 0.61 mmol) and 1,3-Propanesultone (300 mg, 2.5 mmol) were dissolved in methanol (2 mL) and stirred overnight at room temperature.

The solvent was removed via rotary evaporation and the crude material purified by flash column chromatography (0-20 % methanol/dichloromethane) to give an orange oil. This material was dissolved in deuterated methanol and concentrated under vacuum five times to remove residual methanol and dichloromethane,

yielding the compound as a white solid (83 mg, 48%). <sup>1</sup>H-NMR (CD<sub>3</sub>OD):  $\delta$  6.74 (d, 1H,  $J$  = 8.1 Hz), 6.19 (d, 1H,  $J$  = 2.4 Hz), 6.07 (dd, 1H,  $J$  = 2.4 Hz, 8.1 Hz), 3.70 (s, 3H), 3.36 (t, 2H,  $J$  = 7.3 Hz), 3.25 (t, 2H,  $J$  = 5.5 Hz), 2.89 (t, 2H,  $J$  = 7.6 Hz), 2.63 (t, 2H,  $J$  = 6.3 Hz), 2.05 (p, 2H,  $J$  = 7.6 Hz), 1.91-1.85 (m, 2H). <sup>13</sup>C-

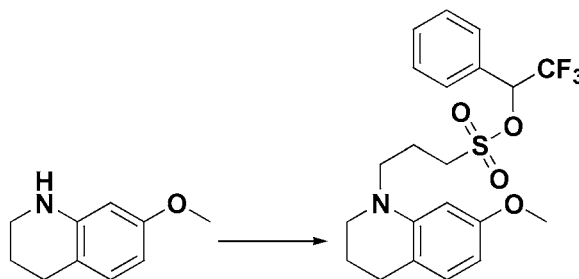
NMR (CD<sub>3</sub>OD):  $\delta$  159.5, 146.0, 129.3, 115.3, 97.4, 54.3, 49.9, 49.2, 49.0, 27.3, 22.5, 21.7. HR-EIMS  $m/z$  calculated for C<sub>13</sub>H<sub>20</sub>NO<sub>4</sub>S: 286.1113, found: 286.1134.



**3-[7-Methoxy-6-(4-nitro-phenylazo)-3,4-dihydro-2H-quinolin-1-yl]-propane-1-sulfonic acid (17).** Compound **16** (200 mg, 0.7 mmol) was dissolved in methanol (7 mL). 4-Nitrobenzenediazonium tetrafluoroborate (165 mg, 0.696 mmol) was suspended in 10% sulfuric acid (7 mL) with vortexing. The organic solution was added to the aqueous mixture and stirred at ambient conditions for 1 hour. The solution was then neutralized with ammonium hydroxide, resulting in a purple precipitate. The mixture was filtered and the filtrand washed with chloroform (10 X 10 mL) to yield a deep purple solid. The solid was then washed with ethanol (600 mL) to separate the product from ammonium sulfate. The filtrate was concentrated under vacuum to yield the product as a purple solid (239 mg, 78%). This compound was used in the next reaction without further purification. <sup>1</sup>H-NMR (CD<sub>3</sub>OD):  $\delta$  8.27 (d, 2H,  $J$  = 9.2 Hz), 7.83 (d, 2H,  $J$  = 9.1 Hz), 7.50 (s, 1H), 6.44 (s, 1H), 4.02 (s, 3H), 3.68 (t, 2H,  $J$  = 7.7 Hz), 3.47 (t, 2H,  $J$  = 6.3 Hz), 2.91 (t,

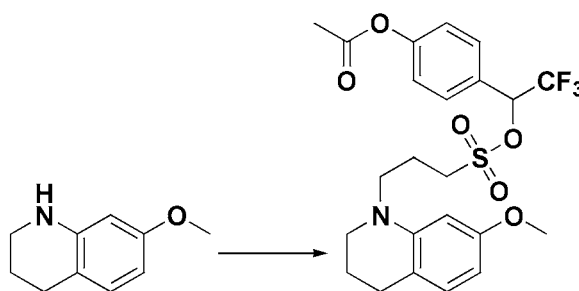
2H,  $J = 6.9$  Hz), 2.71 (m, 2H), 2.16 (p, 2H,  $J = 7$  Hz), 1.94 (p, 2H,  $J = 6.4$  Hz).

HR-EIMS  $m/z$  calculated for  $C_{19}H_{23}N_4O_6S$ : 435.1338, found: 435.1336.



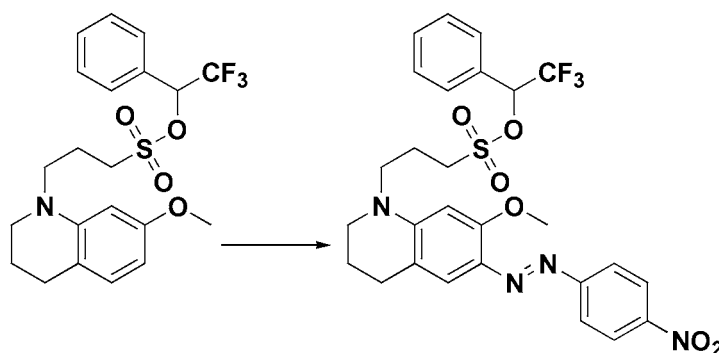
**3-(7-Methoxy-3,4-dihydro-2H-quinolin-1-yl)propane-1-sulfonic acid 2,2,2-trifluoro-1-phenylethyl ester (18).** Compound **15** (163 mg, 0.996 mmol) was dissolved in DMF (3 mL). Compound **11** (488 mg, 1.2 mmol) and potassium carbonate (193 mg, 1.39 mmol) were added to the solution and the reaction was heated to 65 °C and stirred overnight. The reaction was poured into 0.5 M hydrochloric acid (40 mL) and extracted with ethyl acetate (1 X 40 mL and 4 X 20 mL). The combined organic phases were washed with brine (75 mL) and dried over sodium sulfate. The solvent was removed by rotary evaporation to give a thick orange residue. The crude material was purified by flash column chromatography (20% ethyl acetate/hexanes) to yield the product as a viscous, red oil (244 mg, 55%).  $^1\text{H-NMR}$  ( $\text{CDCl}_3$ ):  $\delta$  7.51-7.40 (m, 5H), 6.86 (d, 1H,  $J = 8.2$  Hz), 6.18 (dd, 1H,  $J = 2.4$  Hz, 8.2 Hz), 6.05 (d, 1H,  $J = 2.4$  Hz), 5.76 (q, 1H,  $J_{\text{HF}} = 6.4$  Hz), 3.76 (s, 3H), 3.32-3.26 (m, 2H), 3.13 (t, 2H,  $J = 5.5$  Hz), 3.10-3.00 (m, 2H), 2.66 (t, 2H,  $J = 6.2$  Hz), 2.07 (p, 2H,  $J = 7.3$  Hz), 1.90-1.83 (m, 2H).  $^{19}\text{F-}$

NMR (CDCl<sub>3</sub>):  $\delta$  -76.3 (d,  $J$  = 6.3 Hz). <sup>13</sup>C-NMR (CD<sub>3</sub>OD):  $\delta$  159.5, 145.7, 130.6, 130.4, 129.6, 128.9, 128.2, 122.9 (q, <sup>1</sup> $J_{CF}$  = 280 Hz), 115.4, 100.9, 97.3, 77.7 (q, <sup>2</sup> $J_{CF}$  = 34 Hz), 54.4, 49.3, 49.1, 49, 27.2, 22.4, 20.4. HR-EIMS:  $m/z$  calculated for C<sub>21</sub>H<sub>25</sub>F<sub>3</sub>NO<sub>4</sub>S: 444.1456, found: 444.1470.



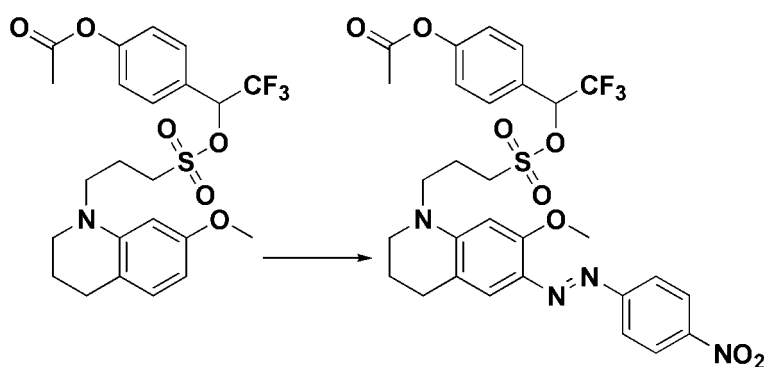
**Acetic acid 4-{2,2,2-trifluoro-1-[3-(7-methoxy-3,4-dihydro-2H-quinolin-1-yl)propane-1-sulfonyloxy]-ethyl}-phenyl ester (19).** Compound **15** (100 mg, 0.613 mmol) was dissolved in DMF (1.2 mL). Compound **13** (343 mg, 0.735 mmol) and potassium carbonate (119 mg, 0.858 mmol) were added to the solution and the reaction was heated to 65 °C and stirred overnight. The reaction was poured into 0.5 M hydrochloric acid (30 mL) and extracted with ethyl acetate (1 X 30 mL and 5 X 10 mL). The combined organic phases were washed with brine (40 mL) and dried over sodium sulfate. Solvent was removed by rotary evaporation to give a thick orange residue. The crude material was purified by flash column chromatography (0-25% ethyl acetate/hexanes) to yield the product as an extremely viscous, amber oil (149 mg, 48%). <sup>1</sup>H-NMR (CDCl<sub>3</sub>):  $\delta$  7.50 (d, 2H,  $J$  = 8.7 Hz), 7.18 (d, 2H,  $J$  = 8.7 Hz), 6.86 (d, 1H,  $J$  = 8.2 Hz), 6.18 (dd, 1H,  $J$

= 2.4 Hz, 8.1 Hz), 6.08 (d, 1H,  $J = 2.4$  Hz), 5.77 (q, 1H,  $J_{HF} = 6.3$  Hz), 3.76 (s, 3H), 3.32 (t, 2H,  $J = 6.6$  Hz), 3.15 (t, 2H,  $J = 5.5$  Hz), 3.12-3.03 (m, 2H), 2.67 (t, 2H,  $J = 6.3$  Hz), 2.32 (s, 3H), 2.10 (p, 2H,  $J = 7.3$  Hz), 1.92-1.84 (m, 2H).  $^{19}\text{F}$ -NMR ( $\text{CDCl}_3$ ):  $\delta$  -76.3 (d,  $J = 6.3$  Hz).  $^{13}\text{C}$ -NMR ( $\text{CD}_3\text{OD}$ ):  $\delta$  169.5, 159.5, 152.8, 145.7, 129.55, 129.5, 127.9, 122.8 (q,  $^1J_{CF} = 280$  Hz), 122.4, 115.4, 100.8, 97.3, 77.0 (q,  $^2J_{CF} = 34$  Hz), 54.4, 49.3, 49.1, 49.0, 27.2, 22.4, 20.4, 19.8. HR-EIMS:  $m/z$  calculated for  $\text{C}_{23}\text{H}_{27}\text{F}_3\text{NO}_6\text{S}$ : 502.1506, found: 502.1492.



**3-[7-Methoxy-6-(4-nitro-phenylazo)-3,4-dihydro-2H-quinolin-1-yl]-propane-1-sulfonic acid 2,2,2-trifluoro-1-phenylethyl ester (20).** Compound **18** (120 mg, 0.271 mmol) was dissolved in methanol (2.7 mL). 4-Nitrobenzenediazonium tetrafluoroborate (64.2 mg, 0.271 mmol) was suspended in 10% sulfuric acid (2.7 mL) with vortexing. The organic solution was added to the aqueous mixture and stirred at ambient conditions for 1 hour. The solution was then neutralized with ammonium hydroxide, resulting in a purple precipitate. The mixture was filtered and the filtrand washed with water (3 X 25 mL) and dried *in vacuo* to yield a

shiny, green and purple solid (132 mg, 82%). This compound was used in the next reaction without further purification.  $^1\text{H-NMR}$  ( $\text{CDCl}_3$ ):  $\delta$  8.29 (d, 2H,  $J = 9.1$  Hz), 7.87 (d, 2H,  $J = 8.9$  Hz), 7.59 (s, 1H), 7.50-7.42 (m, 5H), 6.18 (s, 1H), 5.79 (q, 1H,  $J_{\text{HF}} = 6.3$  Hz), 3.99 (s, 3H), 3.62-3.49 (m, 2H), 3.32 (t, 2H,  $J = 5.5$  Hz), 3.13 (t, 2H,  $J = 6.9$  Hz), 2.73 (t, 2H,  $J = 6.0$  Hz), 2.25-2.13 (m, 2H), 1.93 (p, 2H,  $J = 6.1$  Hz).  $^{19}\text{F-NMR}$  ( $\text{CDCl}_3$ ):  $\delta$  -76.2 (d,  $J = 6.3$  Hz). HR-EIMS:  $m/z$  calculated for  $\text{C}_{27}\text{H}_{28}\text{F}_3\text{N}_4\text{O}_6\text{S}$ : 593.1676, found: 593.1666.

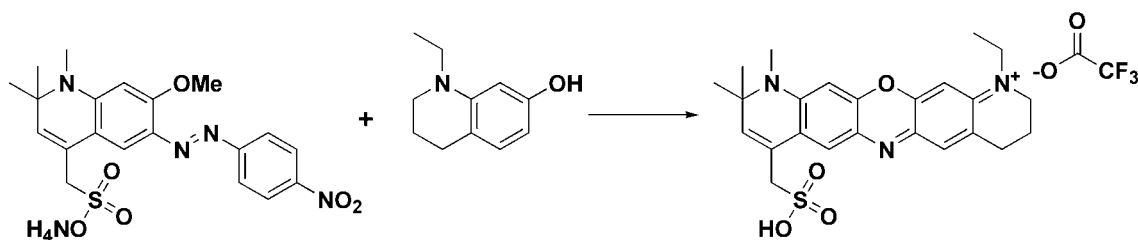


**Acetic acid 4-(2,2,2-trifluoro-1-{3-[7-methoxy-6-(4-nitro-phenylazo)-3,4-dihydro-2H-quinolin-1-yl]-propane-1-sulfonyloxy}-ethyl)-phenyl ester (21).**

Compound **19** (85 mg, 0.17 mmol) was dissolved in methanol (2 mL). 4-Nitrobenzenediazonium tetrafluoroborate (40 mg, 0.17 mmol) was suspended in 10% sulfuric acid (2 mL) with vortexing. The organic solution was added to the aqueous mixture and stirred at ambient conditions for 1 hour. The solution was neutralized with ammonium hydroxide resulting in a purple precipitate. The mixture was filtered and the filtrand washed with water (4 X 20 mL) and dried *in*

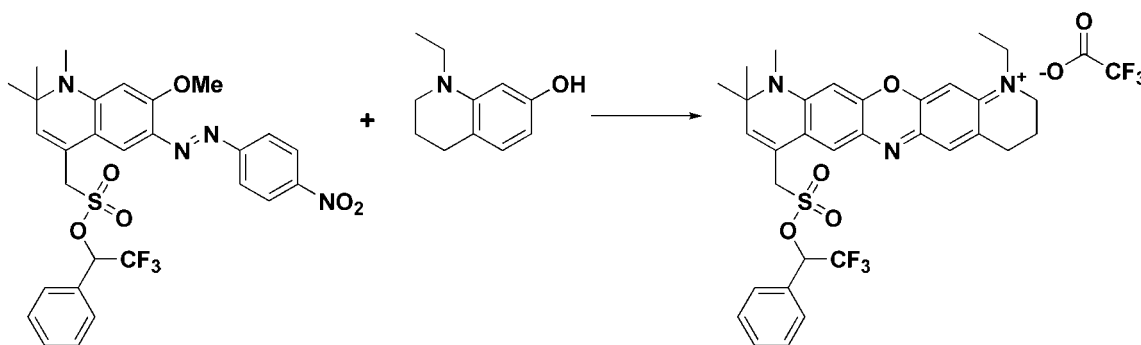


*vacuo* to yield a sticky, deep-purple solid with greenish spots (91 mg, 82%). This compound was used in the next reaction without further purification.  $^1\text{H-NMR}$  ( $\text{CDCl}_3$ ):  $\delta$  8.29 (d, 2H,  $J = 9.1$  Hz), 7.87 (d, 2H,  $J = 9$  Hz), 7.59 (s, 1H), 7.51 (d, 2H,  $J = 8.5$  Hz), 7.19 (d, 2H,  $J = 8.7$  Hz), 6.19 (s, 1H), 5.80 (q, 1H,  $J_{\text{HF}} = 6.2$  Hz), 4.00 (s, 3H), 3.63-3.49 (m, 2H), 3.33 (t, 2H,  $J = 5.5$  Hz), 3.15 (t, 2H,  $J = 6.8$  Hz), 2.73 (t, 2H,  $J = 6.1$  Hz), 2.32 (s, 3H), 2.26-2.13 (m, 2H), 1.94 (p, 2H,  $J = 6.1$  Hz).  $^{19}\text{F-NMR}$  ( $\text{CDCl}_3$ ):  $\delta$  -76.2 (d,  $J = 6.2$  Hz). HR-EIMS:  $m/z$  calculated for  $\text{C}_{29}\text{H}_{30}\text{F}_3\text{N}_4\text{O}_8\text{S}$ : 651.1731, found: 651.1714.



**1-Ethyl-10,10,11-trimethyl-8-sulfomethyl-3,4,10,11-tetrahydro-2H-13-oxa-6,11-diaza-1-azonia-pentacene trifluoroacetate (22).** Compound 4 (150 mg, 0.324 mmol) and 1-Ethyl-1,2,3,4-tetrahydroquinolin-7-ol (Miller, 2009) (57.4 mg, 0.324 mmol) were dissolved in a solution of ethanol: water: hydrochloric acid (3.24 mL: 324  $\mu\text{L}$ : 162  $\mu\text{L}$ ) and heated to 80 °C with stirring for 2 hours. Solvent was removed via rotary evaporation to give a fluorescent blue residue. The crude material was purified by flash column chromatography (0-25% methanol/dichloromethane) yielding the product as a blue solid (chloride

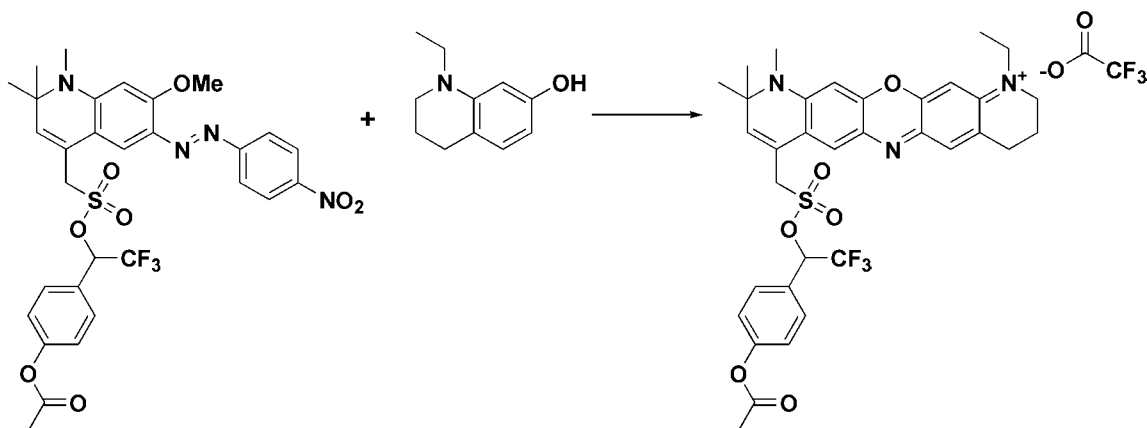
counterion) (76 mg, 48%). This compound was further purified by HPLC (Method A) to yield the product (trifluoroacetate counterion) in 99% purity.  $^1\text{H-NMR}$  ( $\text{CD}_3\text{OD}$ ):  $\delta$  7.77 (s, 1H), 7.41 (s, 1H), 6.88 (s, 1H), 6.78 (s, 1H), 6.04 (s, 1H), 4.00 (s, 2H), 3.73-3.65 (m, 4H), 3.25 (s, 3H), 2.91 (t, 2H,  $J = 6$  Hz), 2.04 (p, 2H,  $J = 6.6$  Hz), 1.60 (s, 6H), 1.34 (t, 3H,  $J = 7.1$  Hz).  $^{13}\text{C-NMR}$  ( $\text{CD}_3\text{OD}$ ):  $\delta$  154.6, 154.4, 154.3, 148.7, 138.4, 134.8, 134.2, 130.6, 129.5, 126.2, 124.0, 123.1, 95.0, 94.97, 63.5, 61.2, 53.1, 50.0, 33.1, 27.6, 27.2, 20.8, 10.5. HR-EIMS  $m/z$  calculated for  $\text{C}_{24}\text{H}_{28}\text{N}_3\text{O}_4\text{S}$ : 454.1801, found: 454.1785.



**1-Ethyl-10,10,11-trimethyl-8-(2,2,2-trifluoro-1-phenyl-ethoxysulfonylmethyl)-3,4,10,11-tetrahydro-2H-13-oxa-6,11-diaza-1-azonia-pentacene**

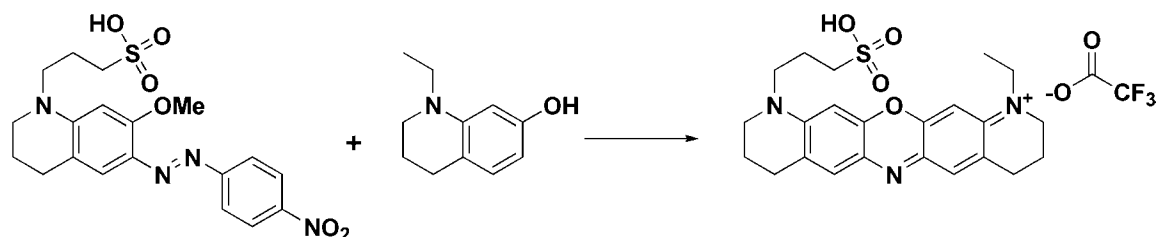
**trifluoroacetate (23).** Compound 8 (44 mg, 73  $\mu\text{mol}$ ) and 1-Ethyl-1,2,3,4-tetrahydro-quinolin-7-ol (Miller, 2009) (13 mg, 73  $\mu\text{mol}$ ) were dissolved in acetic acid (0.5 mL) and heated to 80  $^{\circ}\text{C}$  with stirring for 2 hours. Acetic acid was removed by azeotropeing with toluene under rotary evaporation to give a fluorescent blue residue. The crude material was purified by flash column

chromatography (0-10% methanol/dichloromethane) yielding the product as a blue solid (acetate counterion) (23 mg, 47%). This compound was further purified by HPLC (Method B) to yield the product (trifluoroacetate counterion) in 99% purity.  $^1\text{H-NMR}$  ( $\text{CD}_3\text{OD}$ ):  $\delta$  7.60 (s, 1H), 7.52-7.5 (m, 2H), 7.45 (s, 1H), 7.43-7.36 (m, 2H), 6.93 (s, 1H), 6.73 (s, 1H), 6.17 (q, 1H,  $J_{\text{HF}} = 6.4$  Hz), 6.04 (s, 1H), 4.59 (ABq, 2H,  $\Delta\delta_{\text{AB}} = 0.05$ ,  $J_{\text{AB}} = 14.8$  Hz), 3.77-3.70 (m, 4H), 3.18 (s, 3H), 2.94 (t, 2H,  $J = 5.7$  Hz), 2.05 (p, 2H,  $J = 6.1$  Hz), 1.53 (s, 3H), 1.50 (s, 3H), 1.35 (t, 3H,  $J = 7.1$  Hz).  $^{19}\text{F-NMR}$  ( $\text{CD}_3\text{OD}$ ):  $\delta$  -77.3 (br s), -77.7 (d,  $J = 6.4$  Hz).  $^{13}\text{C-NMR}$  ( $\text{CD}_3\text{OD}$ ):  $\delta$  155.1, 153.5, 149.7, 149.1, 141.0, 135.9, 133.1, 130.8, 130.5, 130.4, 130.3, 128.8, 128.3, 125.9, 122.0, 121.4, 119.1, 112.6, 112.0, 95.4, 95.3, 77.4, 60.9, 53.0, 50.3, 32.9, 27.5, 27.4, 27.2, 20.7, 10.6. HR-EIMS  $m/z$  calculated for  $\text{C}_{32}\text{H}_{33}\text{F}_3\text{N}_3\text{O}_4\text{S}$ : 612.2144, found: 612.2162.



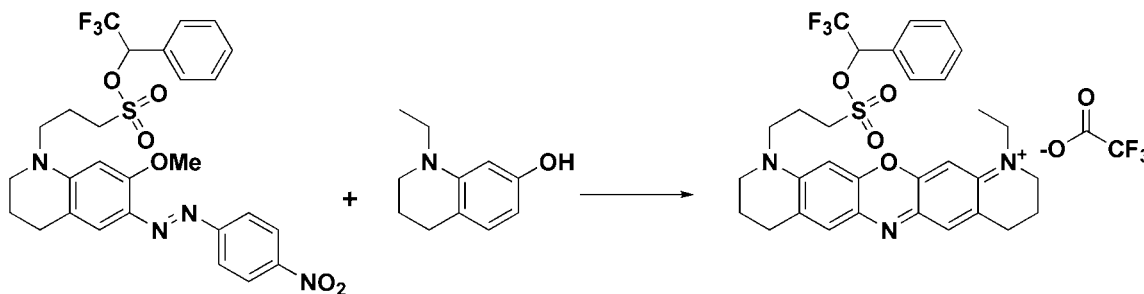
**8-[1-(4-Acetoxy-phenyl)-2,2,2-trifluoro-ethoxysulfonylmethyl]-1-ethyl-10,10,11-trimethyl-3,4,10,11-tetrahydro-2H-13-oxa-6,11-diaza-1-azonia-pentacene trifluoroacetate (24).** Compound **9** (60 mg, 90  $\mu$ mol) and 1-Ethyl-1,2,3,4-tetrahydro-quinolin-7-ol (Miller, 2009) (16.1 mg, 90  $\mu$ mol) were dissolved in acetic acid (0.5 mL) and heated to 80 °C with stirring for 70 minutes. Acetic acid was removed by azeotrope with toluene under rotary evaporation to give a fluorescent blue residue. The crude material was purified by flash column chromatography (0-10% methanol/dichloromethane) yielding the acetate salt as a blue solid (17 mg, 25%). This compound was further purified by HPLC (Method C) to yield the product (trifluoroacetate counterion) in 99% purity.  $^1\text{H-NMR}$  ( $\text{CD}_3\text{OD}$ ):  $\delta$  7.60 (s, 1H), 7.54-7.5 (m, 3H), 7.12 (d, 2H,  $J = 8.7$  Hz), 6.96 (s, 1H), 6.75 (s, 1H), 6.19 (q, 1H,  $J_{\text{HF}} = 6.3$  Hz), 6.04 (s, 1H), 4.62 (s, 2H), 3.79-3.72 (m, 4H), 3.20 (s, 3H), 2.96 (t, 2H,  $J = 5.7$  Hz), 2.25 (s, 3H), 2.07 (p, 2H,  $J = 6$  Hz), 1.53 (s, 3H), 1.51 (s, 3H), 1.37 (t, 3H,  $J = 7.2$  Hz).  $^{19}\text{F-NMR}$  ( $\text{CD}_3\text{OD}$ ):  $\delta$  -77.3 (br s), -77.9 (d,  $J = 6.3$  Hz).  $^{13}\text{C-NMR}$  ( $\text{CD}_3\text{OD}$ ):  $\delta$  169.3, 155.1, 153.5, 152.7, 149.8,

149.1, 141.0, 135.9, 133.2, 130.9, 130.3, 129.7, 127.6, 125.9, 122.2, 122.1,  
 119.1, 95.4, 95.3, 77.1, 61.0, 52.8, 50.3, 32.9, 27.5, 27.4, 27.2, 20.7, 19.7, 10.6.  
 HR-EIMS  $m/z$  calculated for  $C_{34}H_{35}F_3N_3O_6S$ : 670.2198, found: 670.2176.



**1-Ethyl-11-(3-sulfo-propyl)-3,4,8,9,10,11-hexahydro-2H-13-oxa-6,11-diaza-1-azonia-pentacene trifluoroacetate (25).** Compound **17** (25 mg, 56  $\mu$ mol) and 1-Ethyl-1,2,3,4-tetrahydro-quinolin-7-ol (Miller, 2009) (10 mg, 56  $\mu$ mol) were dissolved in a solution of ethanol: water: hydrochloric acid (0.5 mL: 50  $\mu$ L: 25  $\mu$ L) and heated to 80  $^{\circ}$ C with stirring for 2 hours. Solvent was removed via rotary evaporation to give a fluorescent blue residue. The crude material was purified by flash column chromatography (0-10% methanol/dichloromethane) yielding the product as a blue solid (chloride counterion) (21 mg, 76%). This compound was further purified by HPLC (Method D) to yield the product (trifluoroacetate counterion) in 99% purity.  $^1\text{H-NMR}$  ( $\text{CD}_3\text{OD}$ ):  $\delta$  7.40 (s, 1H), 7.39 (s, 1H), 7.03 (s, 1H), 6.88 (s, 1H), 6.04 (s, 1H), 3.82 (t, 2H,  $J = 7.9$  Hz), 3.73-3.67 (m, 6H), 2.94-2.9 (m, 6H), 2.18 (p, 2H,  $J = 5.0$  Hz), 2.04 (p, 4H,  $J = 5.4$  Hz), 1.34 (t, 3H,  $J = 7.1$  Hz).  $^{13}\text{C-NMR}$  ( $\text{CD}_3\text{OD}$ ):  $\delta$  154.5, 154.3, 148.9, 148.7, 134.2, 133.9, 130.5,

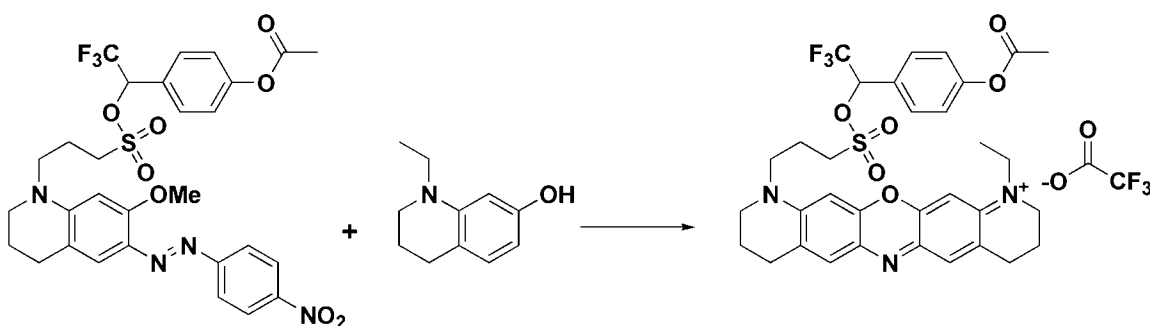
130.48, 129.3, 128.9, 95.4, 94.9, 51.7, 50.6, 50, 27.3, 22, 20.8, 20.7, 10.5. HR-EIMS  $m/z$  calculated for  $C_{23}H_{28}N_3O_4S$ : 442.1801, found: 442.1779.



**1-ethyl-11-[3-(2,2,2-trifluoro-1-phenylethoxysulfonyl)propyl]-3,4,8,9,10,11-hexahydro-2H-13-oxa-6,11-diaza-1-azonia-pentacene trifluoroacetate (26).**

Compound **20** (33 mg, 56  $\mu$ mol) and 1-Ethyl-1,2,3,4-tetrahydroquinolin-7-ol (Miller, 2009) (10 mg, 56  $\mu$ mol) were dissolved in acetic acid (0.5 mL) and heated to 80 °C with stirring for 110 minutes. Acetic acid was removed by azeotroping with toluene under rotary evaporation to give a fluorescent blue residue. The crude material was purified by flash column chromatography (0-10% methanol/dichloromethane) yielding the acetate salt as a blue solid (21 mg, 57%). This compound was further purified by HPLC (Method E) to yield the product (trifluoroacetate counterion) in 99% purity.  $^1H$ -NMR ( $CD_3OD$ ):  $\delta$  7.57-7.56 (m, 2H), 7.51-7.5 (m, 2H), 7.43-7.4 (m, 3H), 6.95 (s, 1H), 6.82 (s, 1H), 6.14 q, 1H,  $J_{HF}$  = 6.5 Hz), 3.78- 3.65 (m, 6H), 3.54 (t, 2H,  $J$  = 5 Hz), 3.45-3.34 (m, 2H), 2.97-2.90 (m, 4H), 2.16-1.96 (m, 6H), 1.36 (t, 3H,  $J$  = 7.1 Hz).  $^{19}F$ -NMR ( $CD_3OD$ ):  $\delta$  -77.3 (br s), -78.1 (d,  $J$  = 6.4 Hz).  $^{13}C$ -NMR ( $CD_3OD$ ):  $\delta$  154.9, 154.0, 149.1,

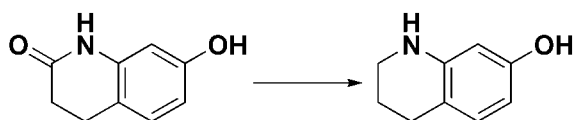
148.5, 135.2, 133.5, 130.8, 130.7, 130.54, 130.5, 130, 128.9, 128.5, 128.2, 122.9 (q,  $^1J_{CF} = 280$  Hz), 95, 94.9, 77.6 (q,  $^2J_{CF} = 34$  Hz), 73.9, 50.5, 50.4, 50.2, 34.1, 27.22, 27.2, 20.7, 20.6, 20.5, 10.6 . HR-EIMS  $m/z$  calculated for  $C_{31}H_{33}F_3N_3O_4S$ : 600.2144, found: 600.2152.



**11-{3-[1-(4-acetoxy-phenyl)-2,2,2-trifluoro-ethoxysulfonyl]-propyl}-1-ethyl-3,4,8,9,10,11-hexahydro-2H-13-oxa-6,11-diaza-1-azonia-pentacene**

**trifluoroacetate (27).** Compound **21** (42 mg, 65  $\mu$ mol) and 1-Ethyl-1,2,3,4-tetrahydro-quinolin-7-ol (Miller, 2009) (12 mg, 65  $\mu$ mol) were dissolved in acetic acid (0.5 mL) and heated to 80  $^{\circ}$ C with stirring for 70 minutes. Acetic acid was removed by azeotropeing with toluene under rotary evaporation to give a fluorescent blue residue. The crude material was purified by flash column chromatography (0-10% methanol/dichloromethane) yielding the acetate salt as a blue solid (22 mg, 47%). This compound was further purified by HPLC (Method F) to yield the product (trifluoroacetate counterion) in 99% purity.  $^1$ H-NMR ( $CD_3OD$ ):  $\delta$  7.62 (d, 2H,  $J = 8.6$  Hz), 7.473-7.457 (m, 2H), 7.18 (d, 2H,  $J = 8.7$

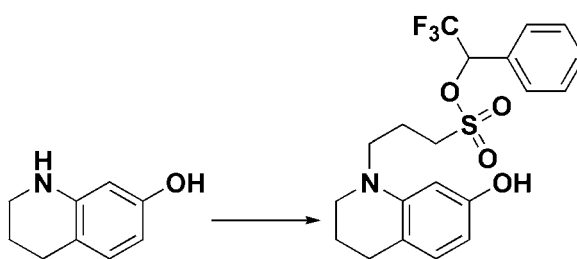
Hz), 6.92 (s, 1H), 6.77 (s, 1H), 6.19 (q, 1H,  $J_{HF} = 6.4$  Hz), 3.76-3.58 (m, 6H), 3.53 (t, 2H,  $J = 5.4$  Hz), 3.46-3.3 (m, 2H), 2.96-2.88 (m, 4H), 2.22 (s, 3H), 2.12-1.95 (m, 6H) 1.35 (t, 3H,  $J = 7.1$  Hz).  $^{19}\text{F}$ -NMR ( $\text{CD}_3\text{CN}$ ):  $\delta$  -76 (br s), -77.4 (d,  $J = 6.3$  Hz).  $^{13}\text{C}$ -NMR ( $\text{CD}_3\text{OD}$ ):  $\delta$  169.4, 154.8, 154.0, 152.8, 149.1, 148.5, 135.1, 133.5, 130.74, 130.7, 130, 129.6, 128.6, 127.9, 122.8 (q,  $^1J_{\text{CF}} = 281$  Hz), 122.4, 95, 94.9, 77 (q,  $^2J_{\text{CF}} = 34$  Hz), 50.5, 50.4, 50.2, 27.22, 27.2, 20.7, 20.6, 20.5, 19.7, 10.5. HR-EIMS  $m/z$  calculated for  $\text{C}_{33}\text{H}_{35}\text{F}_3\text{N}_3\text{O}_6\text{S}$ : 658.2198, found: 658.2165.



**1,2,3,4-tetrahydroquinolin-7-ol (28).** 7-hydroxy-3,4-dihydroquinolin-2(1H)-one (2.19 g, 13.4 mmol) was dissolved in THF (20 mL) and cooled to 0 °C. 1 M  $\text{BH}_3 \cdot \text{THF}$  (136 mL, 136 mmol) was added to the solution dropwise via an addition funnel. The reaction flask was then fitted with a condenser and refluxed overnight. The solution was cooled to 0 °C and excess borane was quenched by the slow addition of methanol (24 mL). The solution was then acidified with concentrated hydrochloric acid (12 mL) and heated to 60 °C for 1 hour. The reaction was then neutralized with concentrated sodium hydroxide and extracted with ethyl acetate (1 X 200 mL and 3 X 50 mL). The combined organic phases were washed with water (2 X 100 mL), brine (1 X 80 mL and 3 X 50 mL), and dried over sodium sulfate. Evaporation of the solvent resulted in a viscous yellow

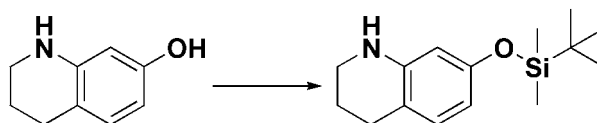


oil. This crude material was purified by flash column chromatography (0-25% ethyl acetate/hexanes) to yield the product as a white crystalline solid (1.91 g, 94%).  $^1\text{H-NMR}$  ( $\text{CDCl}_3$ ):  $\delta$  6.79 (d, 1H,  $J = 8.1$  Hz), 6.09 (dd, 1H,  $J = 2.5$  Hz, 8.1 Hz), 5.97 (d, 1H,  $J = 2.5$  Hz), 4.19 (br s, 1H), 3.27 (t, 2H,  $J = 5.5$  Hz), 2.68 (t, 2H,  $J = 6.4$  Hz), 1.94-1.88 (m, 2H).  $^{13}\text{C-NMR}$  ( $\text{CDCl}_3$ ):  $\delta$  155, 145.4, 130.6, 114.7, 105.7, 101.9, 42.2, 26.4, 22.6. HR-EIMS:  $m/z$  calculated for  $\text{C}_9\text{H}_{12}\text{NO}$ : 150.0919, found: 150.0938.



**3-(7-Hydroxy-3,4-dihydro-2H-quinolin-1-yl)-propane-1-sulfonic acid 2,2,2-trifluoro-1-phenylethyl ester (29).** Compound **28** (50 mg, 0.34 mmol) was dissolved in DMF (0.7 mL). Compound **11** (164 mg, 0.4 mmol) and potassium carbonate (56 mg, 0.4 mmol) were added to the solution and the reaction was heated to 65 °C and stirred overnight. The reaction was poured into 0.5 M hydrochloric acid (10 mL) and extracted with ethyl acetate (1 X 12 mL and 4 X 10 mL). The combined organic phases were washed with water (10 mL), brine (10 mL) and dried over sodium sulfate. The solvent was removed by rotary evaporation to give a red-purple oil. The crude material was purified by flash

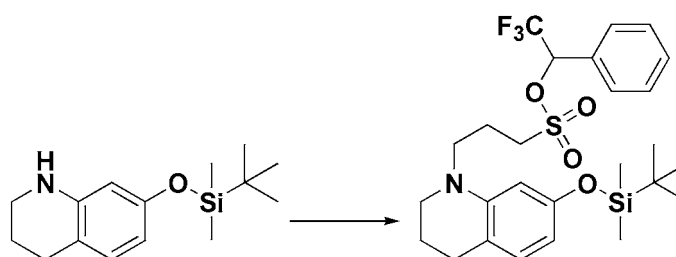
column chromatography (0-25% ethyl acetate/hexanes) to yield the product as a viscous, amber oil (63 mg, 44%).  $^1\text{H-NMR}$  ( $\text{CDCl}_3$ ):  $\delta$  7.52-7.41 (m, 5H), 6.79 (d, 1H,  $J = 8.0$  Hz), 6.07 (dd, 1H,  $J = 2.3$  Hz, 7.9 Hz), 5.98 (d, 1H,  $J = 2.4$  Hz), 5.76 (q, 1H,  $J_{\text{HF}} = 6.3$  Hz), 3.29-3.25 (m, 2H), 3.14-3 (m, 4H), 2.65 (t, 2H,  $J = 6.2$  Hz), 2.10-2.03 (m, 2H), 1.89-1.83 (m, 2H).  $^{19}\text{F-NMR}$  ( $\text{CDCl}_3$ ):  $\delta$  -76.3 (d,  $J = 6.3$  Hz).  $^{13}\text{C-NMR}$  ( $\text{CD}_3\text{OD}$ ):  $\delta$  156.3, 145.8, 130.6, 130.4, 129.6, 128.9, 128.2, 122.9 (q,  $^1J_{\text{CF}} = 280$  Hz), 114.2, 103.0, 98, 77.7 (q,  $^2J_{\text{CF}} = 35$  Hz), 49.4, 49.2, 49.0, 27.2, 22.5, 20.7. HR-EIMS:  $m/z$  calculated for  $\text{C}_{20}\text{H}_{23}\text{F}_3\text{NO}_4\text{S}$ : 430.1300, found: 430.1316.



**7-(*tert*-Butyl-dimethyl-silyloxy)-1,2,3,4-tetrahydro-quinoline (30).**

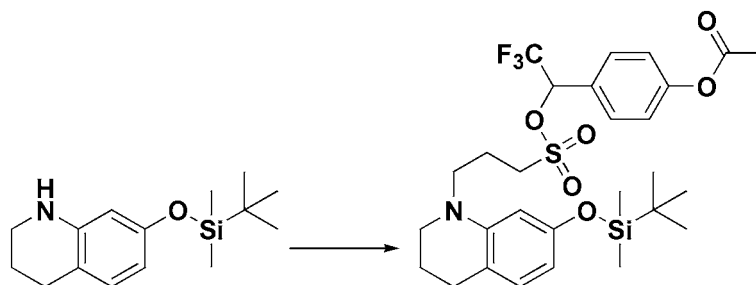
Compound **28** (1 g, 6.7 mmol) was dissolved in DMF (14 mL). Imidazole (1.14 g, 16.8 mmol) and *tert*-butyldimethylchlorosilane (1.2 g, 8.0 mmol) were added to the solution and the reaction was stirred at room temperature overnight. The reaction was then poured into 5%  $\text{NaHCO}_3$  (200 mL) and extracted with ethyl acetate (6 X 75 mL). The combined organic phases were washed with brine (175 mL) and dried over sodium sulfate. The solvent was removed by rotary evaporation and the crude material was purified by flash column chromatography (0-10% ethyl acetate/hexanes) yielding the product as a yellow-white solid (1.5 g,

83%).  $^1\text{H-NMR}$  ( $\text{CDCl}_3$ ):  $\delta$  6.76 (d, 1H,  $J = 8.1$  Hz), 6.11 (dd, 1H,  $J = 2.4$  Hz, 8.1 Hz), 5.98 (d, 1H,  $J = 2.4$  Hz), 3.73 (br s, 1H), 3.26 (t, 2H,  $J = 5.5$  Hz), 2.68 (t, 2H,  $J = 6.4$  Hz), 1.94-1.88 (m, 2H), 0.96 (s, 9H), 0.17 (s, 6H).  $^{13}\text{C-NMR}$  ( $\text{CDCl}_3$ ):  $\delta$  154.8, 145.9, 130.2, 114.8, 109.1, 105.8, 42.2, 26.8, 26.2, 22.8, 18.6, -4. HR-EIMS:  $m/z$  calculated for  $\text{C}_{15}\text{H}_{26}\text{NOSi}$ : 264.1784, found: 264.1752.



**3-[7-(*tert*-Butyl-dimethyl-silanyloxy)-3,4-dihydro-2H-quinolin-1-yl]-propane-1-sulfonic acid 2,2,2-trifluoro-1-phenyl-ethyl ester (31).** Compound **30** (100 mg, 0.38 mmol) was dissolved in DMF (0.75 mL). Compound **11** (186 mg, 0.46 mmol) and potassium carbonate (63 mg, 0.46 mmol) were added to the solution and the reaction was heated to 65 °C and stirred overnight. The reaction was poured into 0.5 M hydrochloric acid (30 mL) and extracted with ethyl acetate (1 X 30 mL and 4 X 20 mL). The combined organic phases were washed with water (30 mL), brine (50 mL) and dried over sodium sulfate. The solvent was removed by rotary evaporation and the crude material was purified by flash column chromatography (0-10% ethyl acetate/hexanes) to yield a yellow liquid. This material was further purified by gravity column chromatography (25%

acetone/hexanes) to yield the product as a viscous, yellow oil (155 mg, 75%).  $^1\text{H-NMR}$  ( $\text{CDCl}_3$ ):  $\delta$  7.49-7.4 (m, 5H), 6.77 (d, 1H,  $J = 8.0$  Hz), 6.10 (dd, 1H,  $J = 2.3$  Hz, 8.0 Hz), 5.98 (d, 1H,  $J = 2.3$  Hz), 5.78 (q, 1H,  $J_{\text{HF}} = 6.4$  Hz), 3.28-3.24 (m, 2H), 3.13-3 (m, 4H), 2.64 (t, 2H,  $J = 6.3$  Hz), 2.07 (p, 2H,  $J = 7.3$  Hz), 1.85 (p, 2H,  $J = 6.5$  Hz), 0.97 (s, 9H), 0.18 (s, 6H).  $^{19}\text{F-NMR}$  ( $\text{CDCl}_3$ ):  $\delta$  -76.3 (d,  $J = 6.4$  Hz).  $^{13}\text{C-NMR}$  ( $\text{CD}_3\text{OD}$ ):  $\delta$  154.9, 145.7, 130.6, 130.4, 129.5, 128.9, 128.2, 122.9 (q,  $^1J_{\text{CF}} = 280$  Hz), 116.0, 107.7, 102.9, 77.7 (q,  $^2J_{\text{CF}} = 34$  Hz), 49.3, 49.13, 49.1, 27.2, 25.1, 22.3, 20.5, 17.9, -5.3. HR-EIMS:  $m/z$  calculated for  $\text{C}_{26}\text{H}_{37}\text{F}_3\text{NO}_4\text{SSi}$ : 544.2165, found: 544.2128.

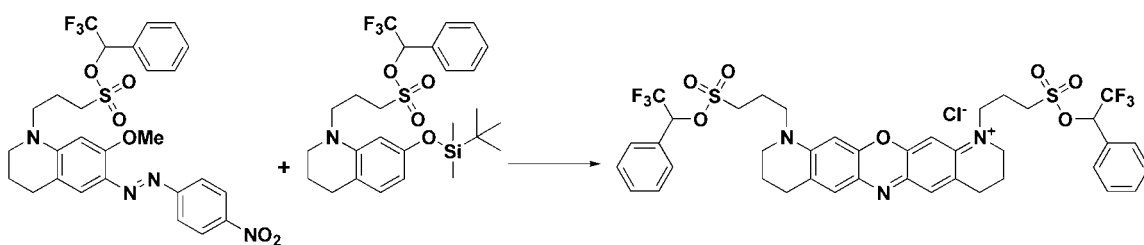


**Acetic acid 4-(1-{3-[7-(*tert*-butyl-dimethyl-silyloxy)-3,4-dihydro-2H-quinolin-1-yl]-propane-1-sulfonyloxy}-2,2,2-trifluoro-ethyl)-phenyl ester**

**(32)**. Compound **30** (156 mg, 0.59 mmol) was dissolved in DMF (1.1 mL).

Compound **13** (303 mg, 0.65 mmol) and potassium carbonate (98 mg, 0.71 mmol) were added to the solution and the reaction was heated to 65 °C and stirred overnight. The reaction was poured into 0.5 M hydrochloric acid (20 mL) and extracted with ethyl acetate (1 X 20 mL and 6 X 10 mL). The combined

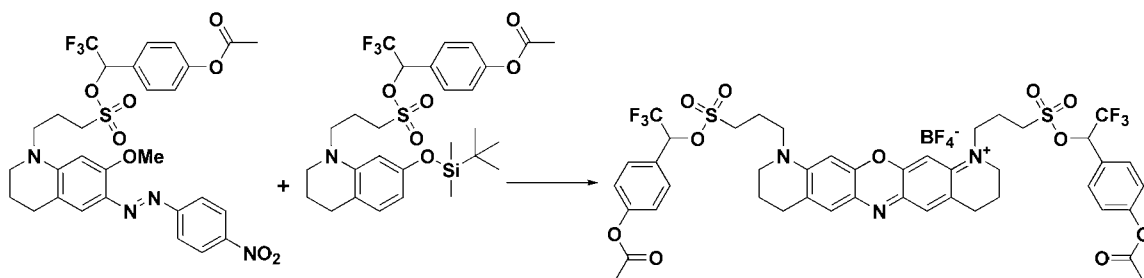
organic phases were washed with water (30 mL), brine (30 mL) and dried over sodium sulfate. The solvent was removed by rotary evaporation and the crude material was purified by flash column chromatography (0-20% ethyl acetate/hexanes) to yield the product as a viscous, orange oil (241 mg, 68%).  $^1\text{H-NMR}$  ( $\text{CDCl}_3$ ):  $\delta$  7.50 (d, 2H,  $J = 8.7$  Hz), 7.17 (d, 2H,  $J = 8.7$  Hz), 6.79 (d, 1H,  $J = 8$  Hz), 6.12 (dd, 1H,  $J = 2.2$  Hz, 8 Hz), 6.04 (d, 1H,  $J = 2.3$  Hz), 5.79 (q, 1H,  $J_{\text{HF}} = 6.3$  Hz), 3.32-3.27 (m, 2H), 3.21-3.05 (m, 4H), 2.66 (t, 2H,  $J = 6.3$  Hz), 2.32 (s, 3H), 2.09 (p, 2H,  $J = 7.1$  Hz), 1.89-1.84 (m, 2H), 0.99 (s, 9H), 0.20 (s, 6H).  $^{19}\text{F-NMR}$  ( $\text{CDCl}_3$ ):  $\delta$  -76.3 (d,  $J = 6.3$  Hz).  $^{13}\text{C-NMR}$  ( $\text{CDCl}_3$ ):  $\delta$  169.1, 155.2, 152.6, 145.8, 130, 129.6, 127.5, 122.6, 122.5 (q,  $^1J_{\text{CF}} = 281$  Hz), 116, 108.1, 103, 77.4 (q,  $^2J_{\text{CF}} = 35$  Hz), 50.3, 49.63, 49.6, 27.5, 26.0, 22.6, 21.4, 21.1, 18.5, -4.1. HR-EIMS:  $m/z$  calculated for  $\text{C}_{28}\text{H}_{39}\text{F}_3\text{NO}_6\text{SSi}$ : 602.2219, found: 602.2197.



**1,11-Bis-[3-(2,2,2-trifluoro-1-phenylethoxysulfonyl)-propyl]-3,4,8,9,10,11-hexahydro-2H-13-oxa-6,11-diaza-1-azonia-pentacene chloride (33).**

Compounds **20** (47 mg, 79  $\mu\text{mol}$ ) and **31** (43 mg, 79  $\mu\text{mol}$ ) were dissolved in a solution of ethanol: water: hydrochloric acid (750  $\mu\text{L}$ : 75  $\mu\text{L}$ : 35  $\mu\text{L}$ ) and heated to

80 °C with stirring for 1.5 hours. Solvent was removed via rotary evaporation to give a fluorescent blue residue. The crude material was purified by flash column chromatography (0-10% methanol/dichloromethane) yielding the pure product as a blue solid (39 mg, 55%).  $^1\text{H-NMR}$  ( $\text{CD}_3\text{OD}$ ):  $\delta$  7.57-7.55 (m, 4H), 7.46 (s, 2H), 7.43-7.38 (m, 6H), 6.80 (s, 2H), 6.14 (q, 2H,  $J_{\text{HF}} = 6.4$  Hz), 3.76-3.63 (m, 4H), 3.56 (t, 4H,  $J = 5.2$  Hz), 3.46-3.34 (m, 4H), 2.91 (t, 4H,  $J = 5.9$  Hz), 2.12 (p, 4H,  $J = 7.7$  Hz), 2.00-1.98 (m, 4H).  $^{19}\text{F-NMR}$  ( $\text{CD}_3\text{OD}$ ):  $\delta$  -77.9 (d,  $J = 6.4$  Hz).  $^{13}\text{C-NMR}$  ( $\text{CD}_3\text{OD}$ ):  $\delta$  154.6, 148.6, 134.4, 130.9, 130.6, 130.4, 129.4, 128.9, 128.2, 122.8 (q,  $^1J_{\text{CF}} = 280$  Hz), 95, 77.7 (q,  $^2J_{\text{CF}} = 35$  Hz), 50.7, 50.6, 27.2, 20.6. HR-EIMS  $m/z$  calculated for  $\text{C}_{40}\text{H}_{40}\text{F}_6\text{N}_3\text{O}_7\text{S}_2$ : 852.2212, found: 852.2180.

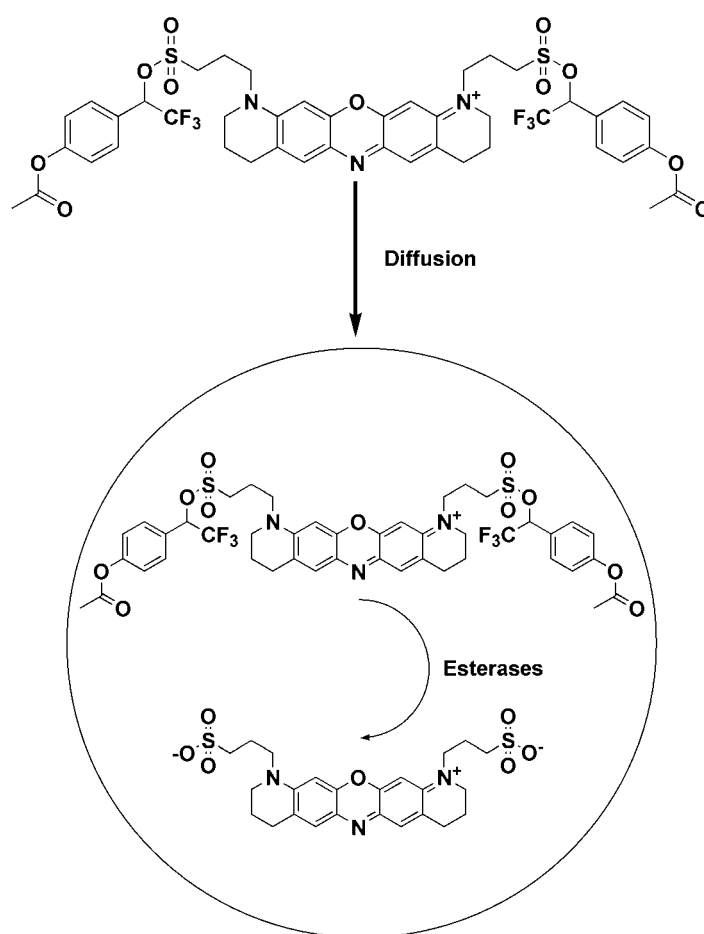


**1,11-Bis-{3-[1-(4-acetoxy-phenyl)-2,2,2-trifluoro-ethoxysulfonyl]-propyl}-3,4,8,9,10,11-hexahydro-2H-13-oxa-6,11-diaza-1-azonia-pentacene**

**tetrafluoroborate (34).** Compounds **21** (46 mg, 71  $\mu\text{mol}$ ) and **32** (43 mg, 71  $\mu\text{mol}$ ) were dissolved in acetic acid (0.7 mL) and heated to 80 °C with stirring for 2.5 hours. Acetic acid was removed by azeotroping with toluene under rotary evaporation to give a fluorescent blue residue. The crude material was purified

by flash column chromatography (0-10% methanol/dichloromethane) yielding the pure product as a blue solid (35 mg, 46%). During the preparation of compound **21** for this reaction, the compound was washed with water as described but the washing did not remove all  $\text{BF}_4^-$ . Upon spectral analysis,  $\text{BF}_4^-$  was found to be the counterion for compound **34**.  $^1\text{H-NMR}$  ( $\text{CD}_3\text{OD}$ ):  $\delta$  7.61 (d, 4H,  $J = 8.6$  Hz), 7.42 (s, 2H), 7.17 (d, 4H, 8.7 Hz), 6.74 (s, 2H), 6.18 (q, 2H,  $J_{\text{HF}} = 6.3$  Hz), 3.71-3.59 (m, 4H), 3.54 (t, 4H,  $J = 5.4$  Hz), 3.50-3.35 (m, 4H), 2.88 (t, 4H,  $J = 5.6$  Hz), 2.21 (s, 6H), 2.08 (p, 4H,  $J = 7.7$  Hz), 2.02-1.96 (m, 4H).  $^{19}\text{F-NMR}$  ( $\text{CD}_3\text{OD}$ ):  $\delta$  -78 (d,  $J = 6.3$  Hz), [-154.28, -154.34] (1:4 ratio,  $^{10}\text{B}/^{11}\text{B}$  isotope effect) (Falcone, 2011).  $^{13}\text{C-NMR}$  ( $\text{CD}_3\text{OD}$ ):  $\delta$  169.5, 154.5, 152.8, 148.6, 134.4, 130.8, 129.6, 129.4, 127.9, 122.8 (q,  $^1J_{\text{CF}} = 280$  Hz), 122.4, 94.9, 77.0 (q,  $^2J_{\text{CF}} = 35$  Hz), 50.7, 50.6, 48.4, 27.2, 20.5, 19.7. HR-EIMS  $m/z$  calculated for  $\text{C}_{44}\text{H}_{44}\text{F}_6\text{N}_3\text{O}_{11}\text{S}_2$ : 968.2322, found: 968.2305.

## Chapter IV: Delivery of sulfonated near-IR oxazines into the cytoplasm of living cells



### Summary

Near-infrared (NIR) light is the ideal optical window for imaging in live cells and organisms. However, most NIR dyes are poorly suited for use in the aqueous cytosol due to their hydrophobicity. We have developed NIR oxazines functionalized with sulfonate esters that are converted to highly water-soluble



sulfonated dyes upon interaction with esterases *in vitro*. Here we show that these functionalized oxazines can diffuse into live cells, are cleaved to the free sulfonate dye by intracellular esterases, and are able to access the entire aqueous environment of the cell. We have characterized the behavior of our oxazines within cells and explore how these features will be useful in studying the intracellular environment. Additionally, we show that our dyes are suitable for use *in vivo* by imaging in live mice and compare the results with that of the FDA approved NIR dye, Indocyanine Green.

### ***Introduction***

The near-infrared (NIR) region of the electromagnetic spectrum (650-900 nm) is ideal for imaging in live cells and organisms. This is due to the poor absorbance and minimal emission of NIR light by endogenous biological molecules, which allows for deeper photon penetration and decreased autofluorescence background as compared to visible wavelength imaging (Escobedo et al., 2010; Frangioni, 2003; Guo et al., 2014; Hilderbrand and Weissleder, 2010; König, 2000). Unfortunately, with the exception of a limited number of bacterial phytochromes, fluorescent proteins do not absorb light above 650 nm (Piatkevich et al., 2013; Tasler et al., 2005; Wu et al., 2011). Moreover, although there are organic dyes that absorb and emit NIR light, most are not suitable for applications in live cells. The primary obstacles faced by NIR organic fluorophores are the hydrophobic and cationic nature of these molecules. These

features cause accumulation within cellular membranes and organelles, especially the negatively polarized membrane of the mitochondria, resulting in non-specific background staining (Bunting et al., 1989; Cunningham et al., 2010; Escobedo et al., 2010; Jiang et al., 2013; Johnson, 1998).

To improve both their solubility and fluorescence properties within aqueous environments, hydrophobic fluorophores are often sulfonated (Li et al., 2008; Morgan et al., 2011; Mujumdar et al., 1993; Niu et al., 2009; Panchuk-Voloshina et al., 1999). The addition of the negatively charged sulfonate group also has the benefit of neutralizing the positive charge of NIR dyes. The increased hydrophilicity and loss of cationic character should make sulfonated NIR fluorophores ideal intracellular imaging reagents. Unfortunately, the highly polar, water-soluble sulfonated dyes are generally unable to diffuse across the lipophilic cell membrane and thus cannot access the intracellular environment (Stolz, 2001; Wuhrmann et al., 1980).

Previously, our lab reported a number of chemically-stable, esterase-labile sulfonate esters, and showed that one of these groups (AcOTFMB) could be used to deliver dansyl sulfonate into live cells (Figure 4.1) (Miller, 2010; Rusha and Miller, 2011). We subsequently reported the synthesis of a family of NIR oxazines functionalized with AcOTFMB-sulfonate esters and showed that *in vitro* treatment with pig liver esterase converts these fluorophores to their sulfonated counterparts (Figure 4.2) (Pauff and Miller, 2011). We now present the delivery

and intracellular characterization of our sulfonated NIR oxazines in live cells and explore how these fluorophores can be employed in the study of both live cells and organisms.

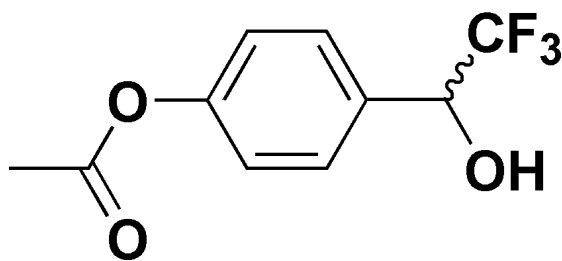


**Figure 4.1: Structure of AcOTFMB (Miller, 2010; Rucha and Miller, 2011).**

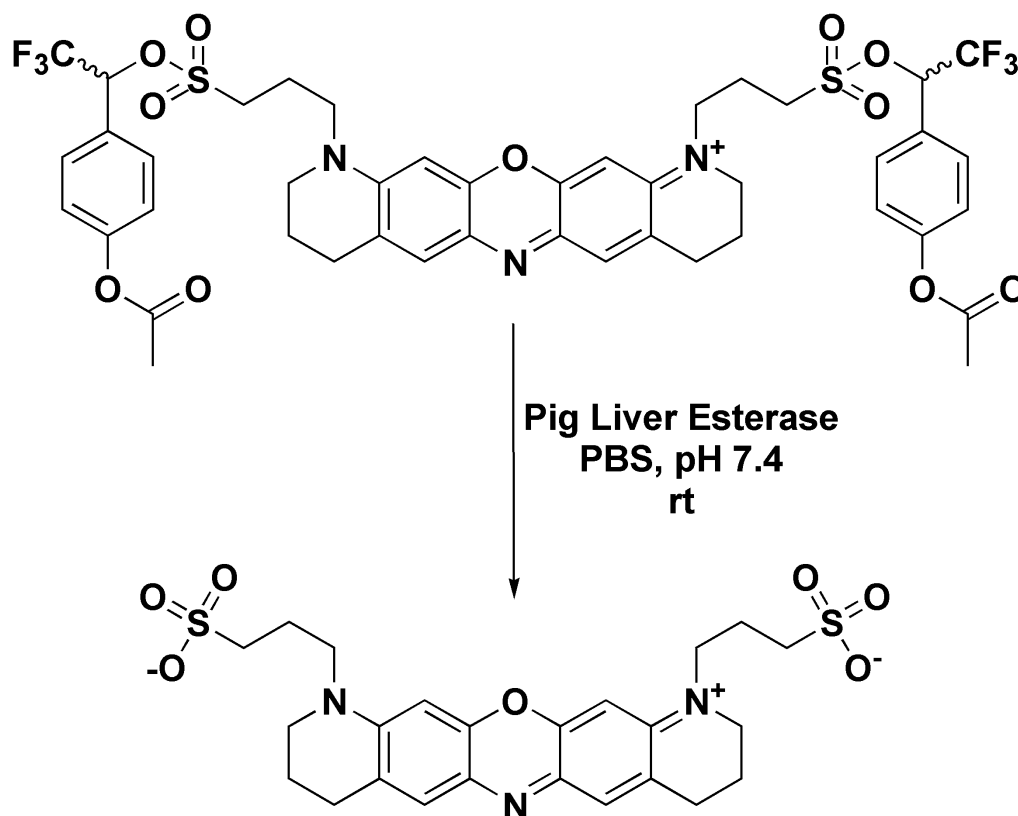


**Figure 4.2:** NIR oxazines functionalized with AcOTFMB-sulfonate esters are converted to sulfonated NIR oxazines upon *in vitro* treatment with pig liver esterase (Pauff and Miller 2011).

### ***Results and Discussion***

We previously synthesized a family of NIR oxazines bearing free sulfonates (**Sulf-Ox1** and **Sulf-Ox2**), esterase-stable sulfonate esters (**TFMB-Ox1** and **TFMB-Ox2**), or esterase-labile sulfonate esters (**AcOTFMB-Ox1** and **AcOTFMB-Ox2**) (Figure 4.3) (Pauff and Miller, 2011; Pauff and Miller, 2013). We next sought to determine whether our cellular sulfonate-delivery strategy, successfully applied to the small fluorophore dansyl sulfonate, could be applied

to these NIR dyes. To investigate this, we treated the human osteosarcoma cell line, U2-OS, with 1  $\mu$ M solutions of our dyes for 10 minutes and monitored the cells for an increase in intracellular fluorescence via wide field fluorescence microscopy (Figure 4.4). We were excited to see a high degree of intracellular accumulation of **AcOTFMB-Ox1** and **2** and **TFMB-Ox1** and **2** as this confirmed that our fluorophores were indeed traversing the plasma membrane (Figure 4.4). In fact, real time monitoring of dye import using spinning disc confocal microscopy indicated that uptake of our oxazine dyes begins to occur immediately upon addition of the dyes to the cell media (Movies 4.1-4.8). As expected, **Sulf-Ox1** and **2** were completely excluded from the cells due to the presence of the negatively-charged sulfonate moieties (Figure 4.4). The rapid import of our cationic sulfonate ester oxazines and exclusion of the highly polar free sulfonate oxazines suggests that the dyes are diffusing through the membrane, as expected for small organic molecules.

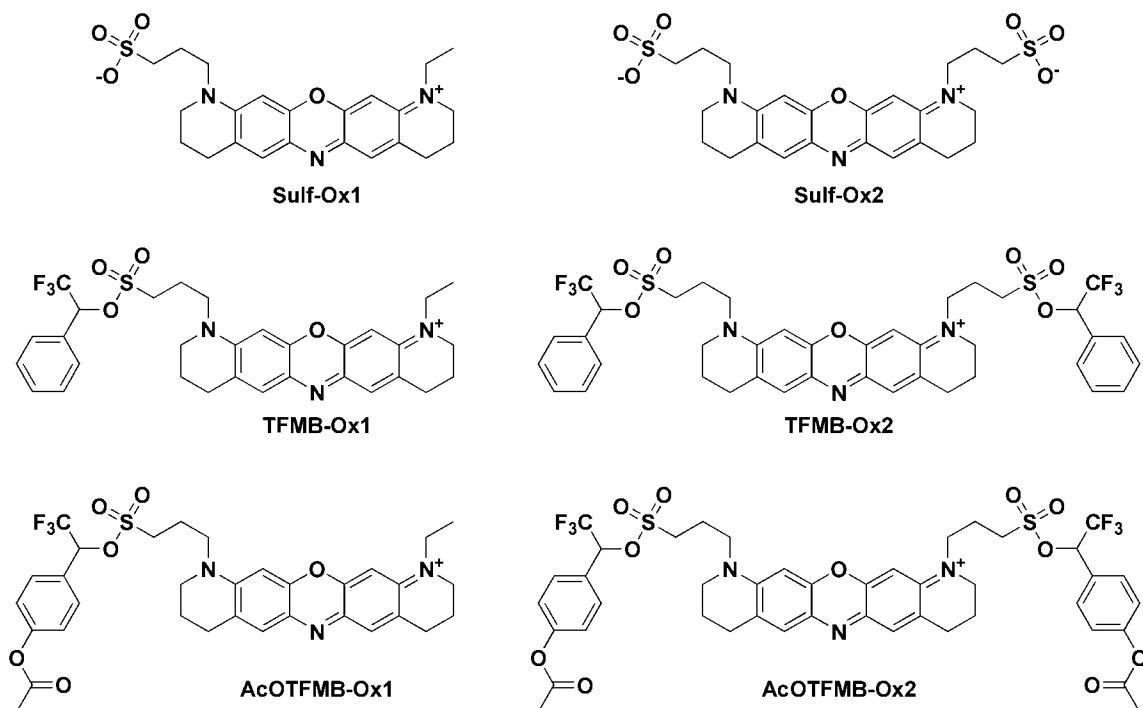


**Figure 4.3: Pentacyclic NIR oxazines functionalized with sulfonates and sulfonate esters (Pauff and Miller, 2011; Pauff and Miller, 2013).**

**Figure 4.4: The lipophilic NIR oxazines AcOTFMB-Ox and TFMB-Ox diffuse into live U2-OS cells while the hydrophilic Sulf-Ox NIR oxazines are excluded from the cytoplasm.** U2-OS cells were incubated with 1  $\mu$ M dye solutions in OPTI-MEM I for 10 minutes at 37 °C, 5% CO<sub>2</sub>. Following aspiration of dye solution and washing, the cells were treated with fresh OPTI-MEM I for imaging. A) Mono-sulfonate ester oxazines **TFMB/AcOTFMB-Ox1**. B) Bis-sulfonate ester oxazines **TFMB/AcOTFMB-Ox2**. C) Sulfonated oxazines **Sulf-Ox1** and **2**.

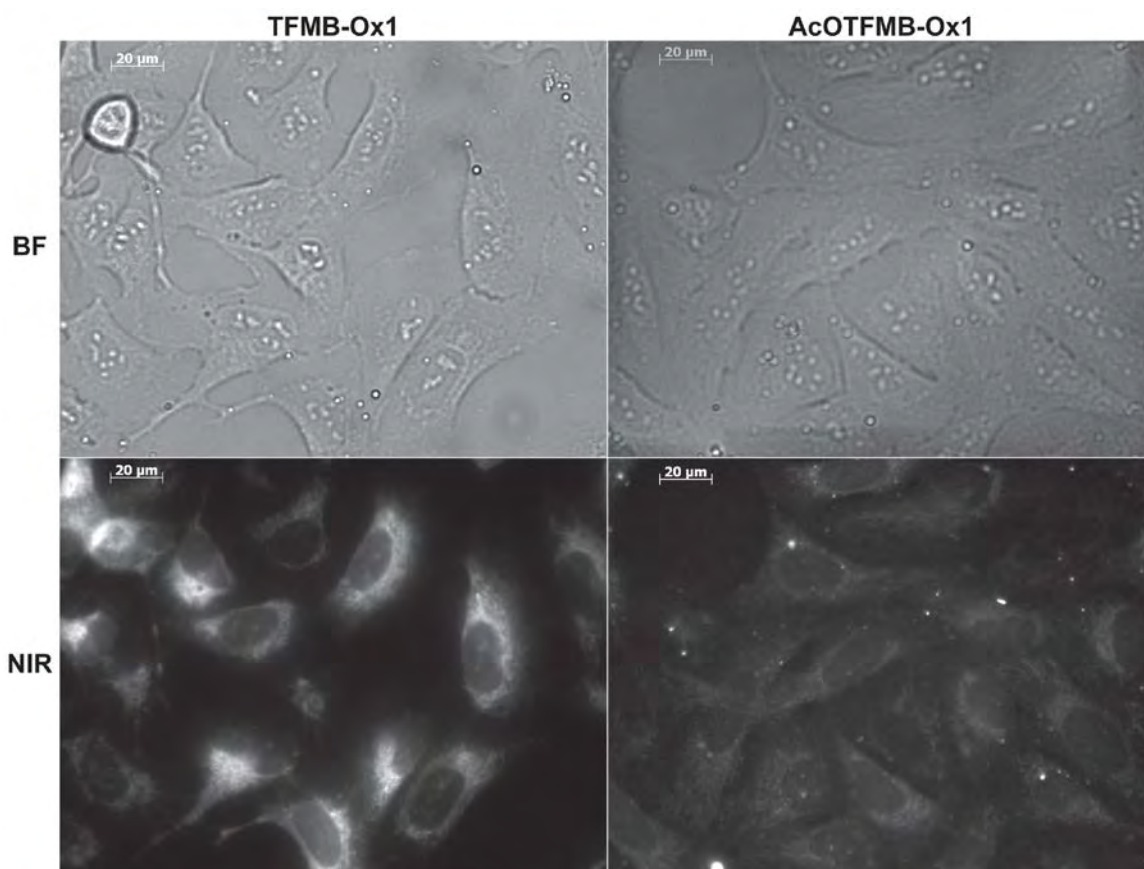


**Figure 4.4A.** Mono-sulfonate ester functionalized NIR oxazines. Top: Bright Field (BF) images. Bottom: NIR images. Exposure time for **TFMB-Ox1** NIR image (bottom left) was 10 ms. Exposure time for **AcOTFMB-Ox1** NIR image (bottom right) was 150 ms.



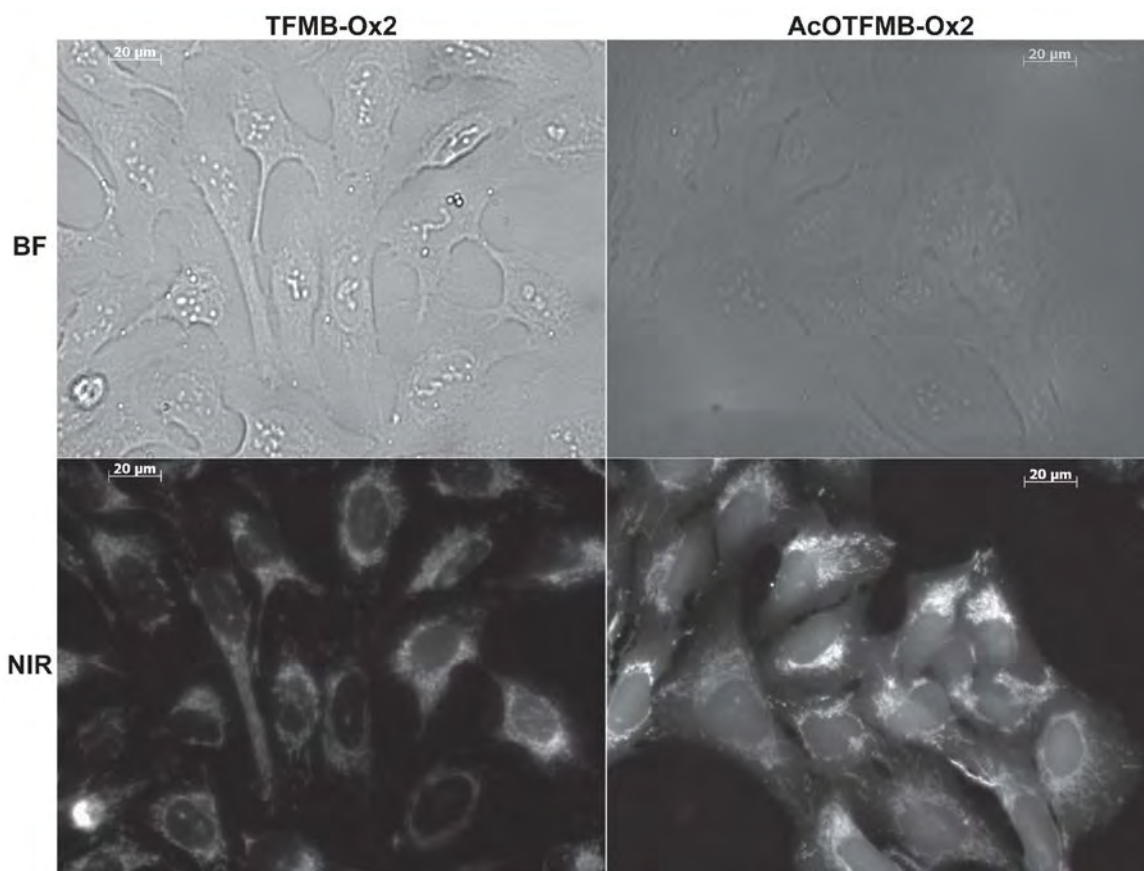


**Figure 4.4B.** Bis-sulfonate ester functionalized NIR oxazines. Top: Bright Field (BF) images. Bottom: NIR images. Exposure time for **TFMB-Ox2** NIR image (bottom left) was 10 ms. Exposure time for **AcOTFMB-Ox2** NIR image (bottom right) was 60 ms.

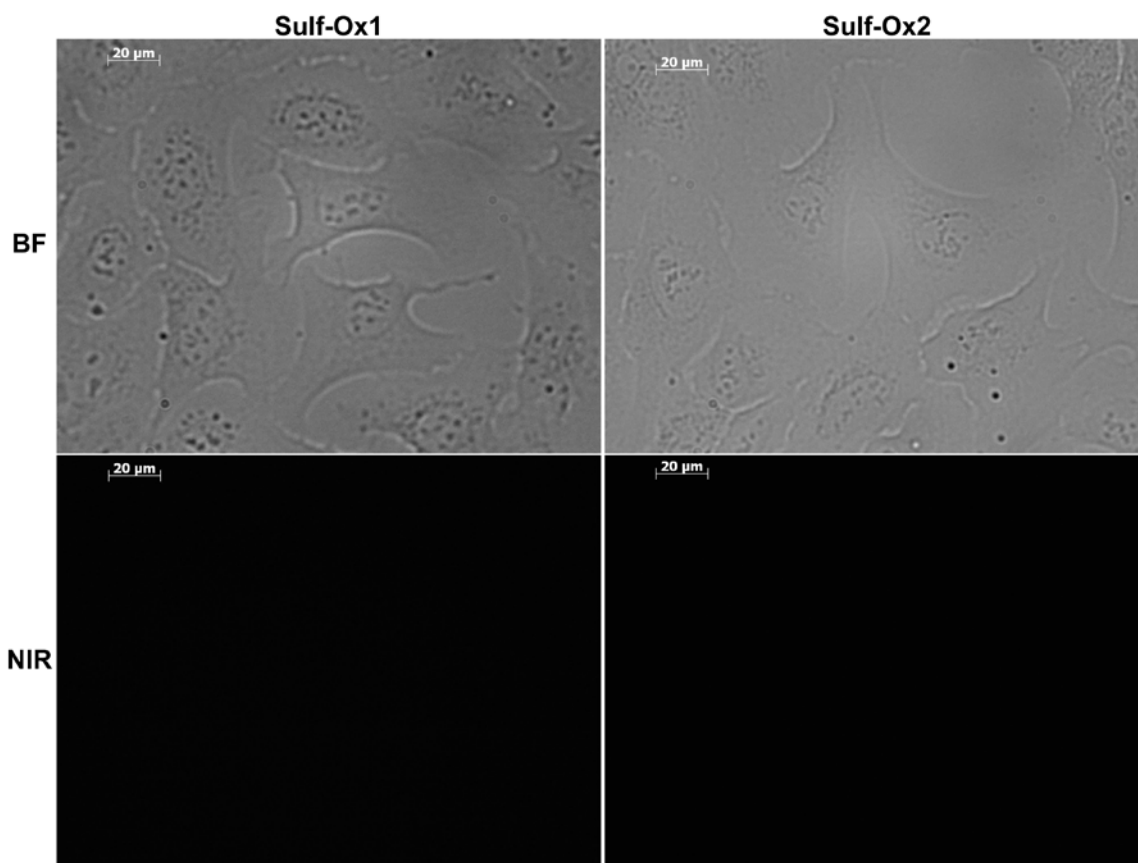


**Figure 4.4C.** Mono/Bis-sulfonated NIR oxazines. Top: Bright Field (BF) images. Bottom: NIR images. Exposure time for NIR images was 150 ms.

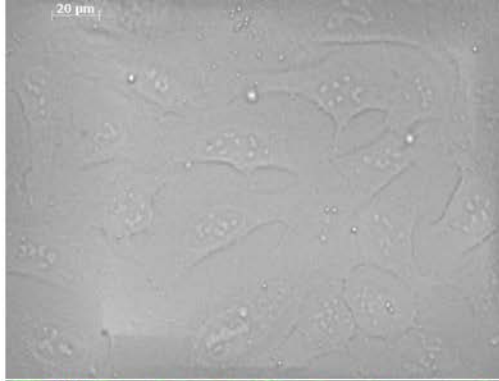
Upon initial entry into the cell, the fluorescence of both the **AcOTFMB-Ox** and **TFMB-Ox** dyes has a distinct cellular localization (Figure 4.4). Small cationic compounds, including many dyes, have a tendency to accumulate in the mitochondria due to the negative potential across the mitochondrial membrane (Bunting et al., 1989). Since our sulfonate-ester oxazines bear an overall positive charge, we hypothesized that the localized fluorescence we observed results from ionic attractions between our dye and the mitochondria (Figure 4.3). This

hypothesis was confirmed by costaining U2-OS cells with our NIR oxazines and the mitochondrial stain, MitoTracker® Green FM (Figure 4.5). The overlaid images show that the fluorescence of all of our NIR oxazines initially colocalizes with the fluorescence from MitoTracker® Green (Figure 4.5: bottom images). This finding is consistent with the rapid uptake of these cationic dyes and their subsequent interaction with the negatively polarized mitochondrial membrane.

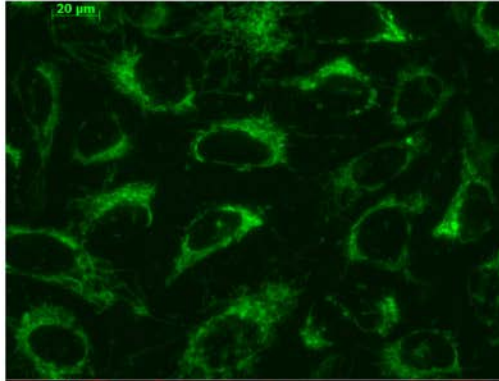
**Figure 4.5: Sulfonate ester NIR oxazines localize to mitochondria upon entry into the cytoplasm.** U2-OS cells were incubated at 37 °C, 5% CO<sub>2</sub> with 100 nM MitoTracker® Green FM for 30 minutes followed by incubation with 1 μM **AcOTFMB-Ox1** (A), **TFMB-Ox1** (B), **TFMB-Ox2** (C), **AcOTFMB-Ox2** (D) for 10 minutes. Following aspiration of dye solution and washing, the cells were treated with fresh OPTI-MEM I for imaging. BF: Bright Field. Overlay images were prepared using ImageJ software.

**A**

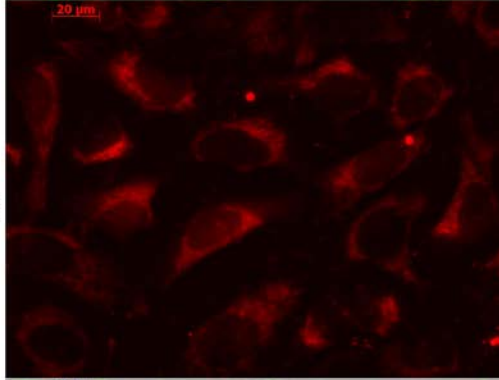
**BF**



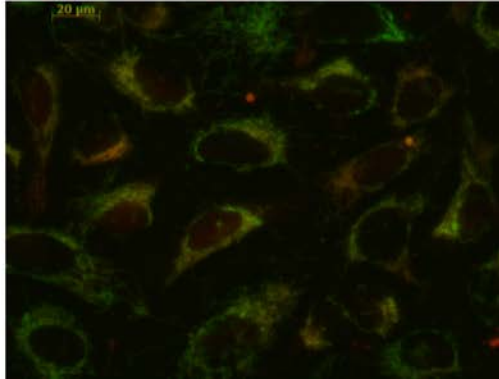
**Mitotracker  
100 ms exposure**



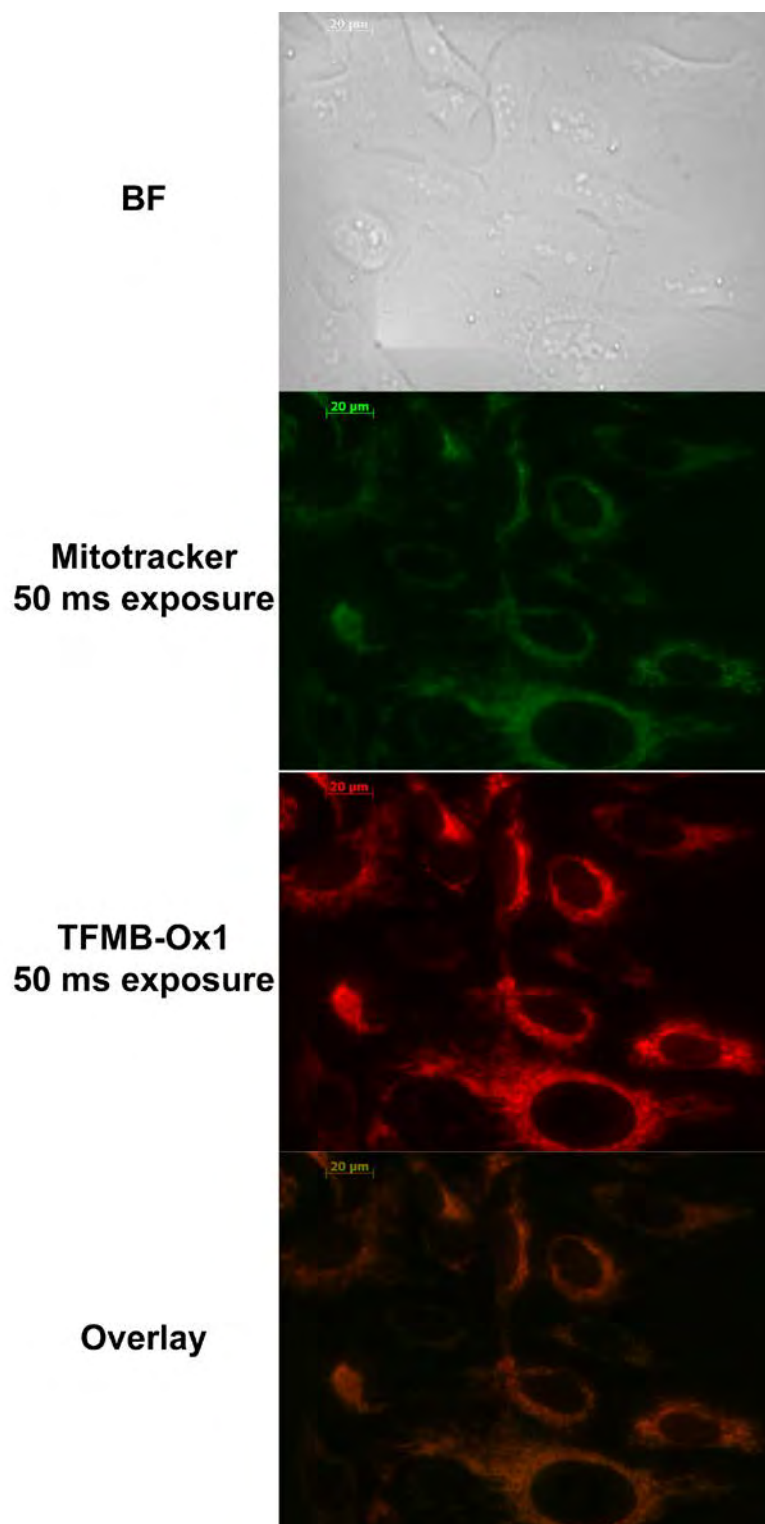
**AcOTFMB-Ox1  
100 ms exposure**



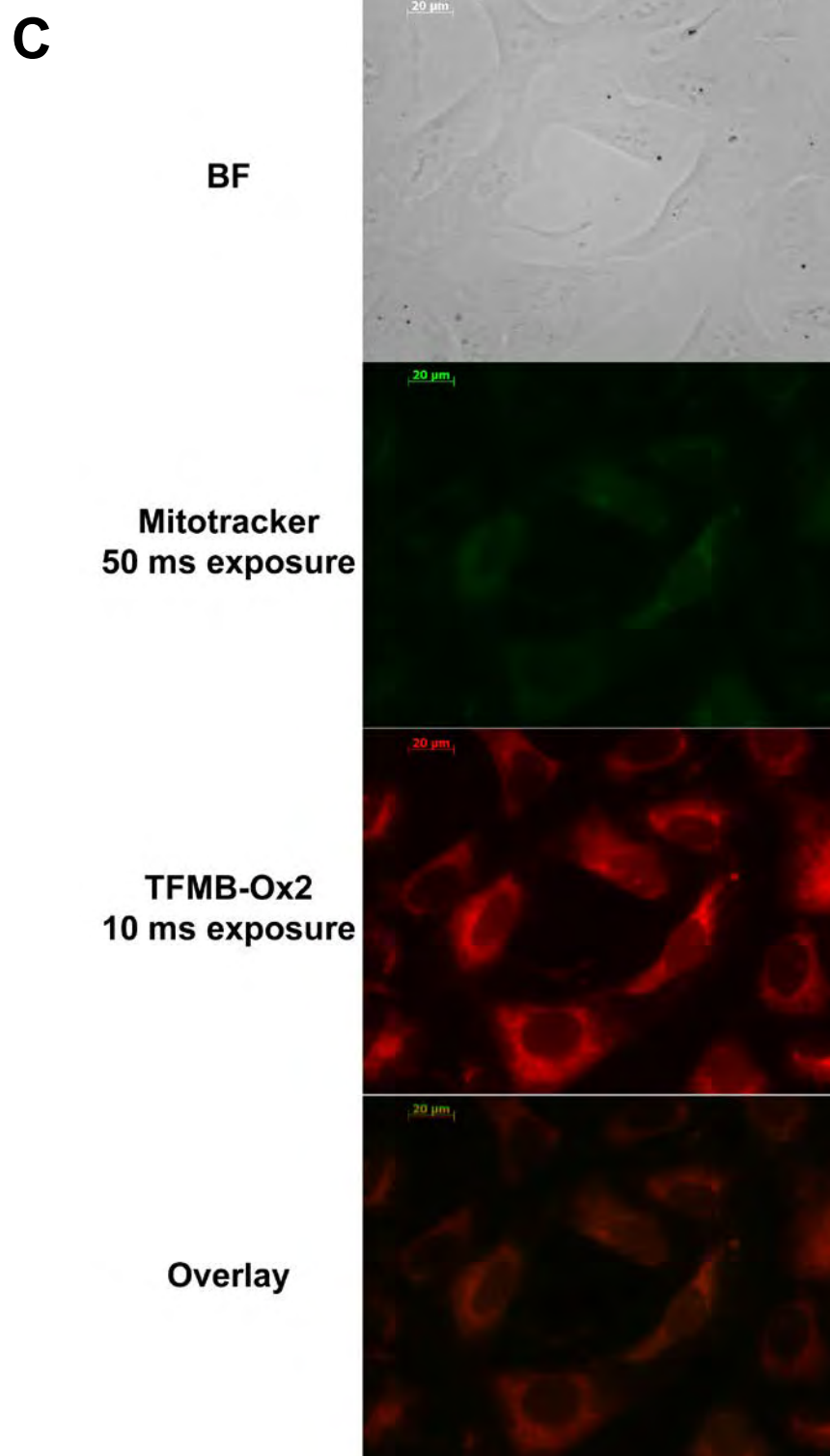
**Overlay**



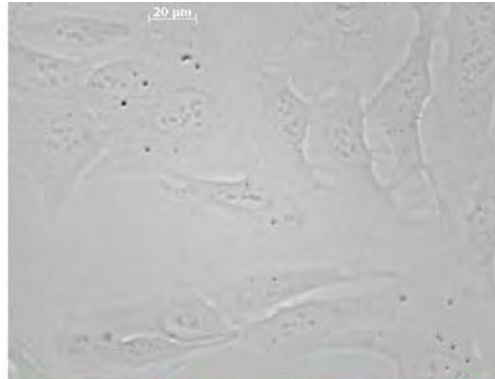
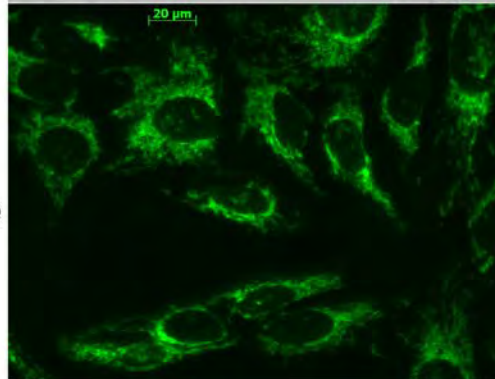
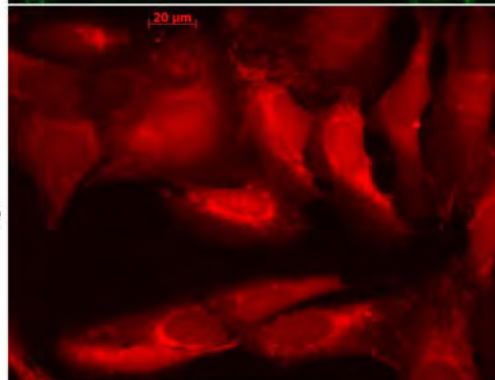
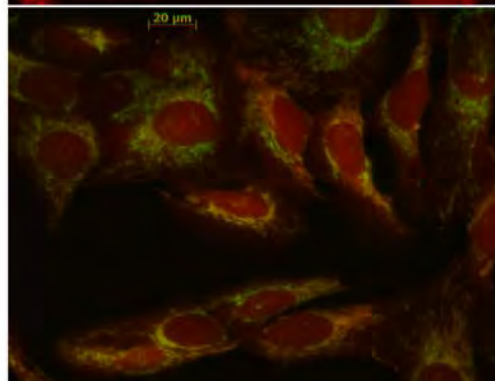
**Figure 4.5A.** U2-OS cells costained with MitoTracker® Green FM and AcOTFMB-Ox1.

**B**

**Figure 4.5B.** U2-OS cells costained with MitoTracker® Green FM and **TFMB-Ox1**.



**Figure 4.5C.** U2-OS cells costained with MitoTracker® Green FM and **TFMB-Ox2**.

**D****BF****Mitotracker  
60 ms exposure****AcOTFMB-Ox2  
60 ms exposure****Overlay**

**Figure 4.5D.** U2-OS cells costained with MitoTracker® Green FM and AcOTFMB-Ox2.



Although the initial localization of our NIR oxazines to mitochondria was expected, this was not the ultimate fate for which our esterase-labile sulfonate ester dyes were designed. Upon interaction with cellular esterases, we expect that **AcOTFMB-Ox1** and **2** would be converted to their free sulfonate counterparts and would be able to freely access the entire cell. To confirm that our esterase cleavage strategy works in live cells, we followed the fates of the **TFMB-Ox** and **AcOTFMB-Ox** dyes in U2-OS cells over three hours using wide field fluorescence microscopy (Figure 4.6 and 4.7). At all times throughout the imaging, **TFMB-Ox1** and **2** remain localized at the mitochondria, as expected for dyes which are always cationic (Figure 4.6). Excitingly, within 5 minutes following the dye treatment, the fluorescence from the esterase-labile **AcOTFMB-Ox2** begins to become diffuse (see **AcOTFMB-Ox2** images in Figures 4.4 and 4.5), and at 20 minutes post-dye treatment, cells treated with **AcOTFMB-Ox2** displayed completely diffuse fluorescence, accessing both nucleus and cytoplasm (Figure 4.7B, left side). On the other hand, while **AcOTFMB-Ox1** fluorescence did become diffuse, localized punctate staining remained throughout the duration of the experiment (Figure 4.7A, left side). This persistent mitochondrial localization of **AcOTFMB-Ox1** likely results from the fact that, when the mono-sulfonate ester dye is converted to its sulfonate form, the overall charge on the dye is neutral rather than negative. It is therefore possible that the localized negative charge on the sulfonate is not sufficient to overcome the attraction of the positively-charged oxazine scaffold to the high negative potential

of the mitochondrial membrane. Although we were somewhat disappointed by the results of the **AcOTFMB-Ox1** treatment, the rapid conversion of **AcOTFMB-Ox2** fluorescence from localized to cell-encompassing was overwhelmingly encouraging.

**Figure 4.6: NIR oxazines functionalized with esterase-stable TFMB sulfonate esters (TFMB-Ox) display persistent mitochondrial localization over 3 hours.** U2-OS cells were incubated at 37 °C, 5% CO<sub>2</sub> with 100 nM MitoTracker® Green FM for 30 minutes followed by incubation with 1 μM **TFMB-Ox1** (A) or **TFMB-Ox2** (B) for 10 minutes. Following aspiration of dye solution and washing, the cells were incubated in OPTI-MEM I and imaged periodically over 3 hours. BF: Bright Field. Overlay images were prepared using ImageJ software.

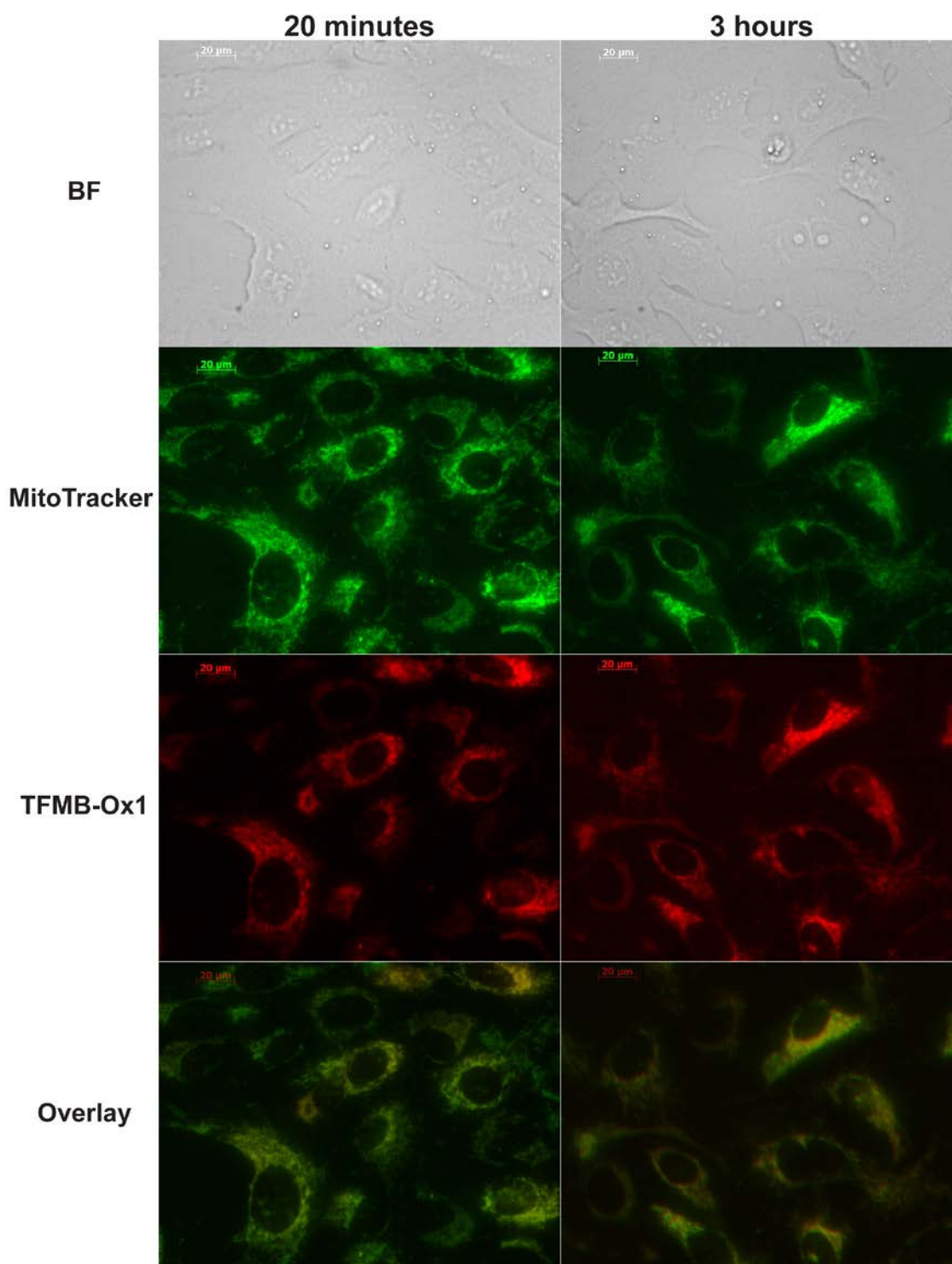


**Figure 4.6A.** Exposure times for MitoTracker® Green FM and **TFMB-Ox1** were 50 ms.

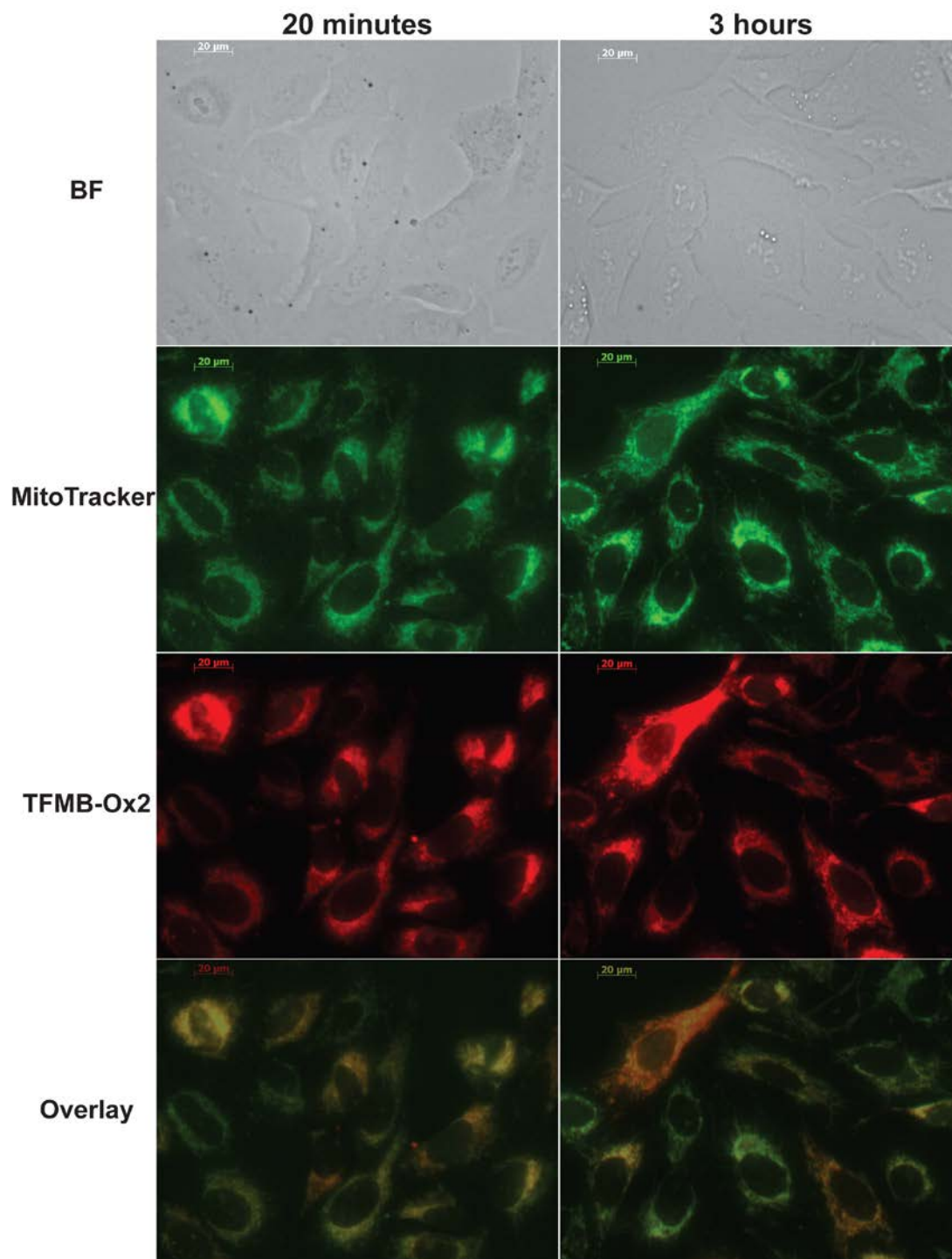


**Figure 4.6B.** Exposure times for MitoTracker® Green FM were 50 ms (20-minute incubation) and 100 ms (3-hour incubation). Exposure times for **TFMB-Ox2** were 10 ms (20-minute incubation) and 50 ms (3-hour incubation).

**Figure 4.7: U2-OS cells treated with NIR oxazines functionalized with esterase-labile AcOTFMB sulfonate esters (AcOTFMB-Ox) display diffuse fluorescence within 20 minutes of dye treatment but lose intracellular NIR fluorescence within 90 minutes of dye treatment.** U2-OS cells were incubated at 37 °C, 5% CO<sub>2</sub> with 100 nM MitoTracker® Green FM for 30 minutes followed by incubation with 1 µM **AcOTFMB-Ox1** (A) or **AcOTFMB-Ox2** (B) for 10 minutes. Following aspiration of dye solution and washing, the cells were incubated in OPTI-MEM I and imaged periodically until no NIR fluorescence was observed. Fluorescent signal for the mono-sulfonate ester **AcOTFMB-Ox1** treated cells ceased after 90 minutes. Fluorescent signal for the bis-sulfonate ester **AcOTFMB-Ox2** treated cells ceased after 60 minutes. BF: Bright Field. Overlay images were prepared using ImageJ software

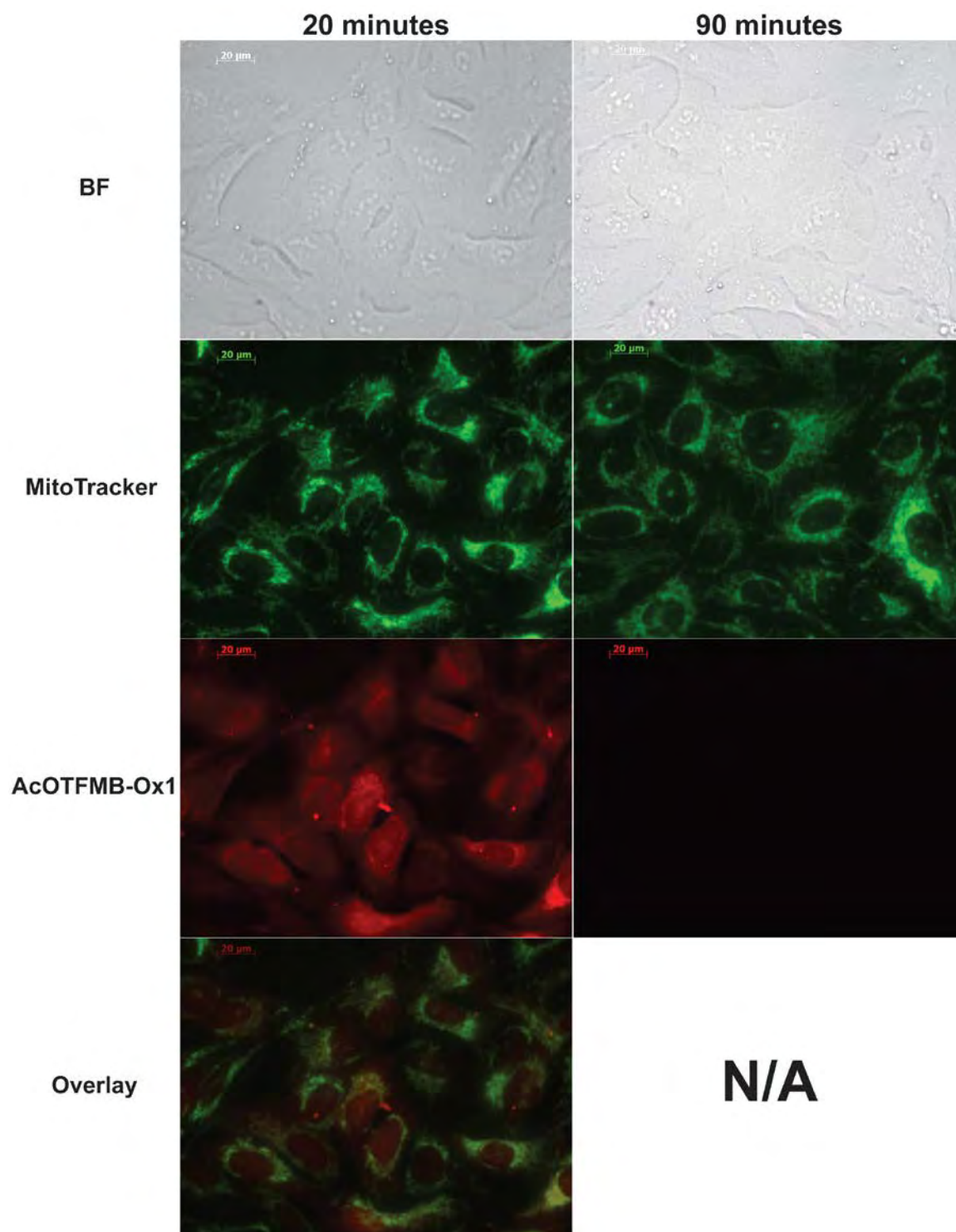


**Figure 4.7A.** Exposure times for MitoTracker® Green FM and **AcOTFMB-Ox1** were 100 ms.

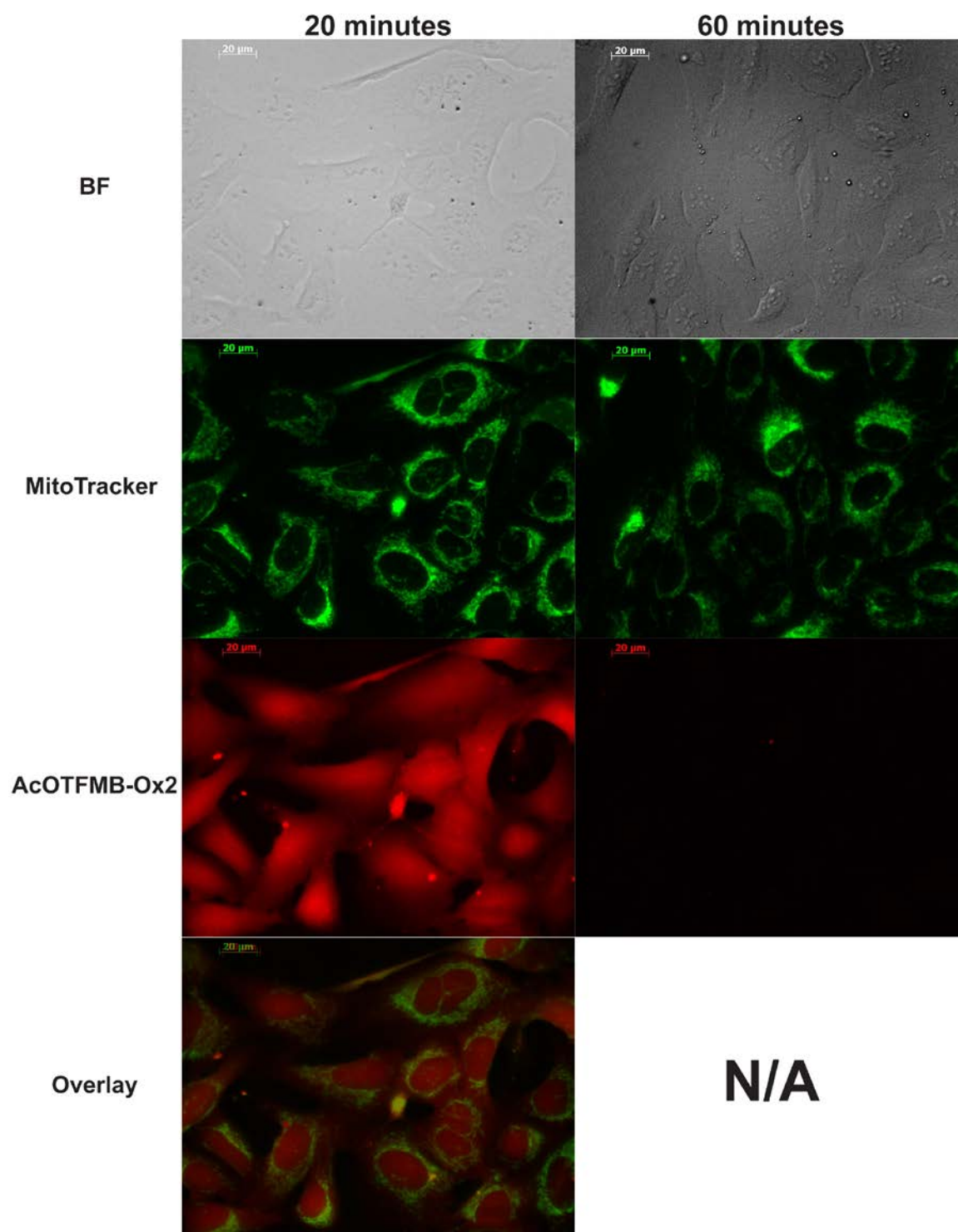
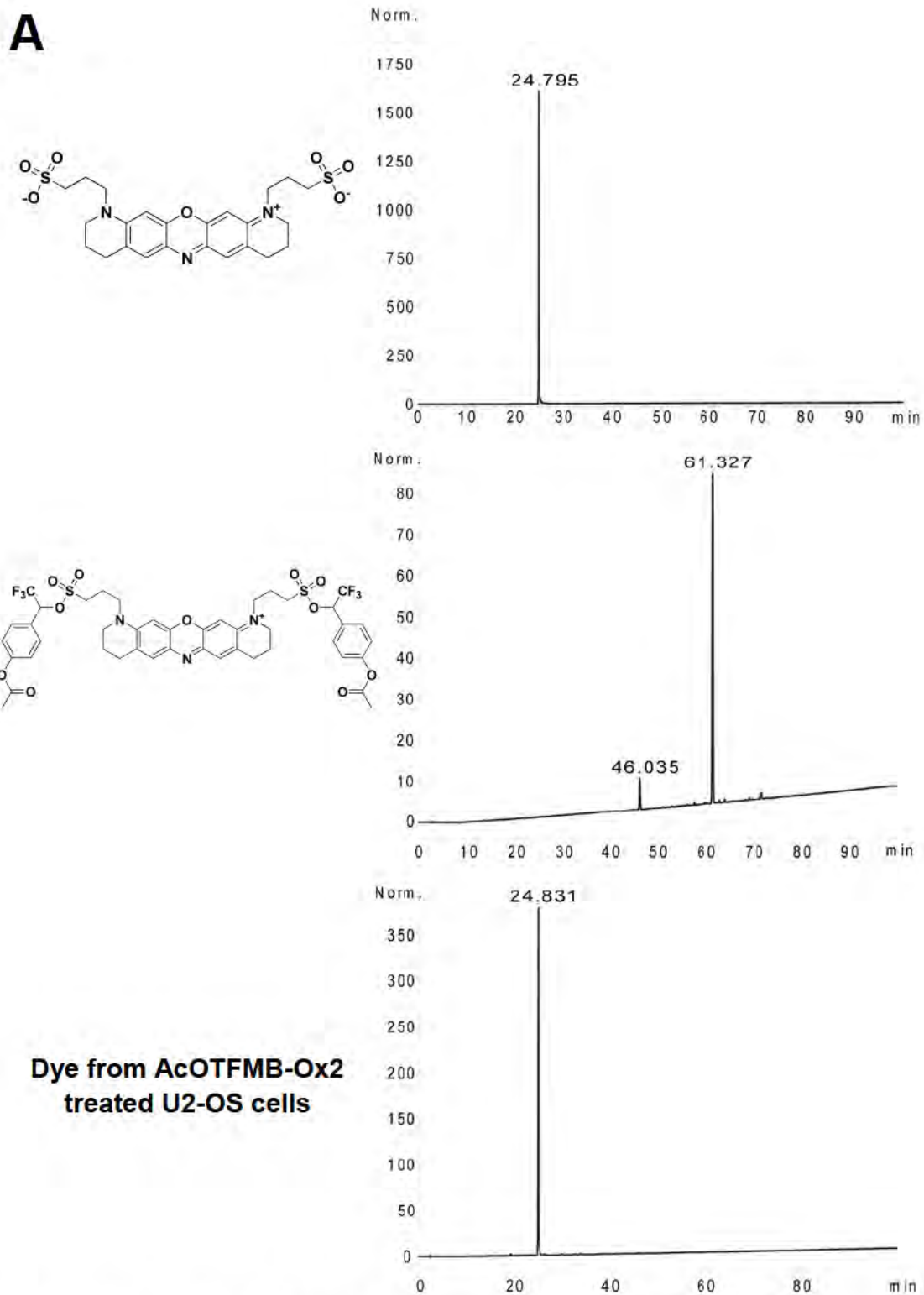


**Figure 4.7B.** Exposure times for MitoTracker® Green FM and **AcOTFMB-Ox2** were 60 ms.

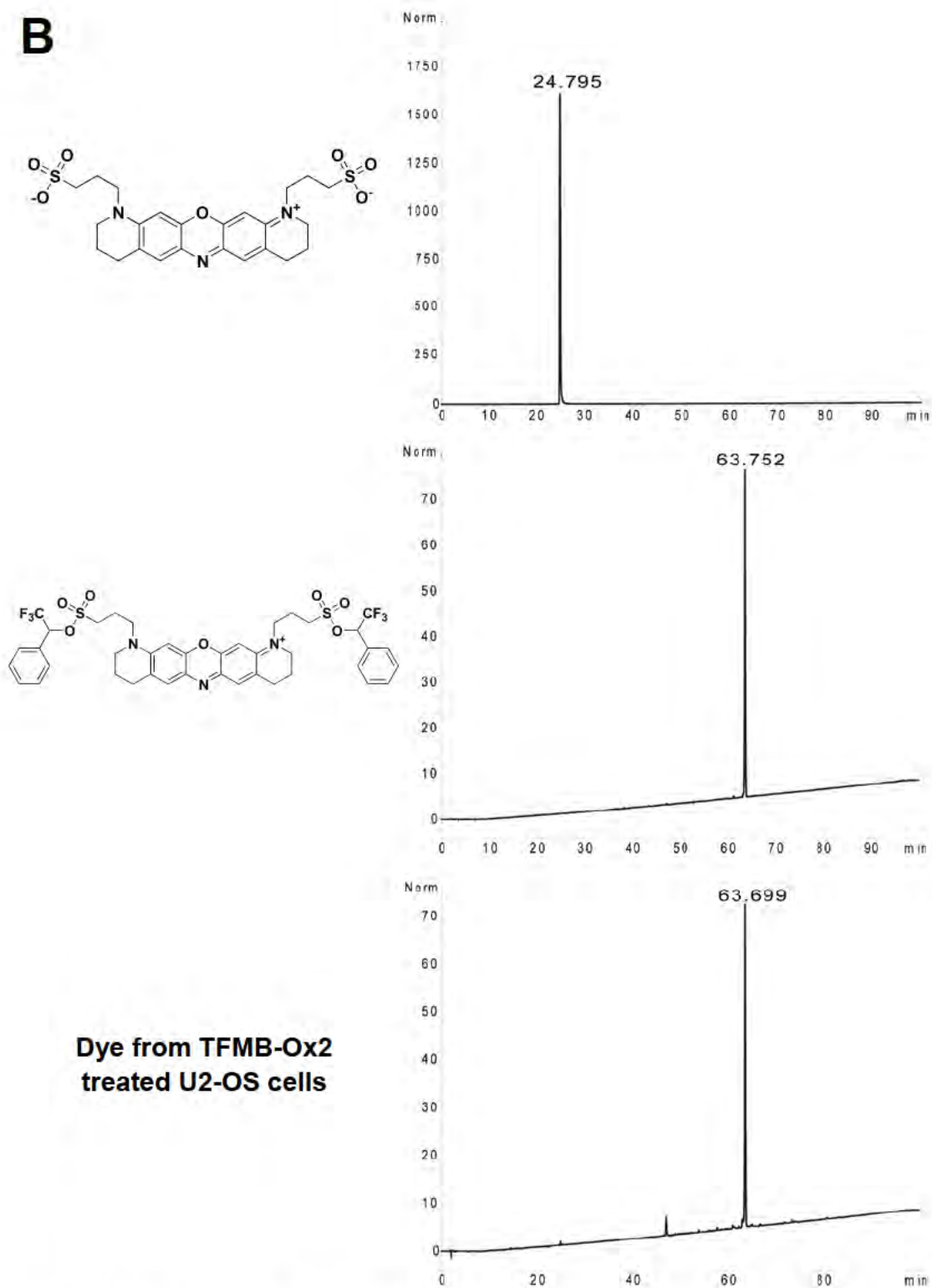


The conversion of localized to diffuse fluorescence observed in the **AcOTFMB-Ox2** treated U2-OS cells supports the hypothesis that the positively-charged sulfonate ester is cleaved to the negatively-charged bis-sulfonated oxazine, **Sulf-Ox2**, by cellular esterases. To prove, beyond a reasonable doubt, that the dye associated with diffuse cellular fluorescence was indeed the bis-sulfonated NIR oxazine, we incubated U2-OS cells with 1  $\mu$ M **AcOTFMB-Ox2** and periodically imaged the cells until diffuse fluorescence was observed. The cells were then lysed and the dye was collected via centrifugation. The collected dye was subsequently analyzed via RP-HPLC and ESI-HRMS (Figure 4.8A and Table 4.1). The HPLC traces show that the dye collected from the U2-OS cells elutes as **Sulf-Ox2** (Figure 4.8A). Additionally, HRMS confirmed that the dye collected from the cells has the same molecular mass as **Sulf-Ox2** (Table 4.1). A similar result was found for **AcOTFMB-Ox1**, confirming that this dye is cleaved to the mono-sulfonated NIR oxazine **Sulf-Ox1** within the cytoplasm of live U2-OS cells (Figure 4.8B). Dyes collected from **TFMB-Ox1** and **2** treated cells eluted as the respective parent dye on HPLC, confirming, as expected, that there was no change to the esterase-stable TFMB sulfonate ester (Figures 4.8C and D).

**Figure 4.8: Esterase-labile AcOTFMB-Ox dyes are converted to Sulf-Ox within living cells while esterase-stable TFMB-Ox dyes are unaffected by the cellular environment.** U2-OS cells were incubated at 37 °C, 5% CO<sub>2</sub> with 1 μM **AcOTFMB-Ox2** (A), **TFMB-Ox2** (B), **AcOTFMB-Ox1** (C), **TFMB-Ox1** (D), allowing sufficient time for dye uptake and delocalized fluorescence to be observed within the cells (where applicable). Oxazine dyes were retrieved from the cells as described (See Methods). The collected dye samples were then analyzed via HPLC as described (See Methods). As controls, DMSO stocks of **Sulf-Ox**, **TFMB-Ox**, and **AcOTFMB-Ox** dyes were also subjected to analytical HPLC.



**Figure 4.8A.** Top trace: 660 nm. Middle/Bottom trace: 653 nm.

**B**

**Figure 4.8B.** Top trace: 660 nm. Middle/Bottom trace: 653 nm.

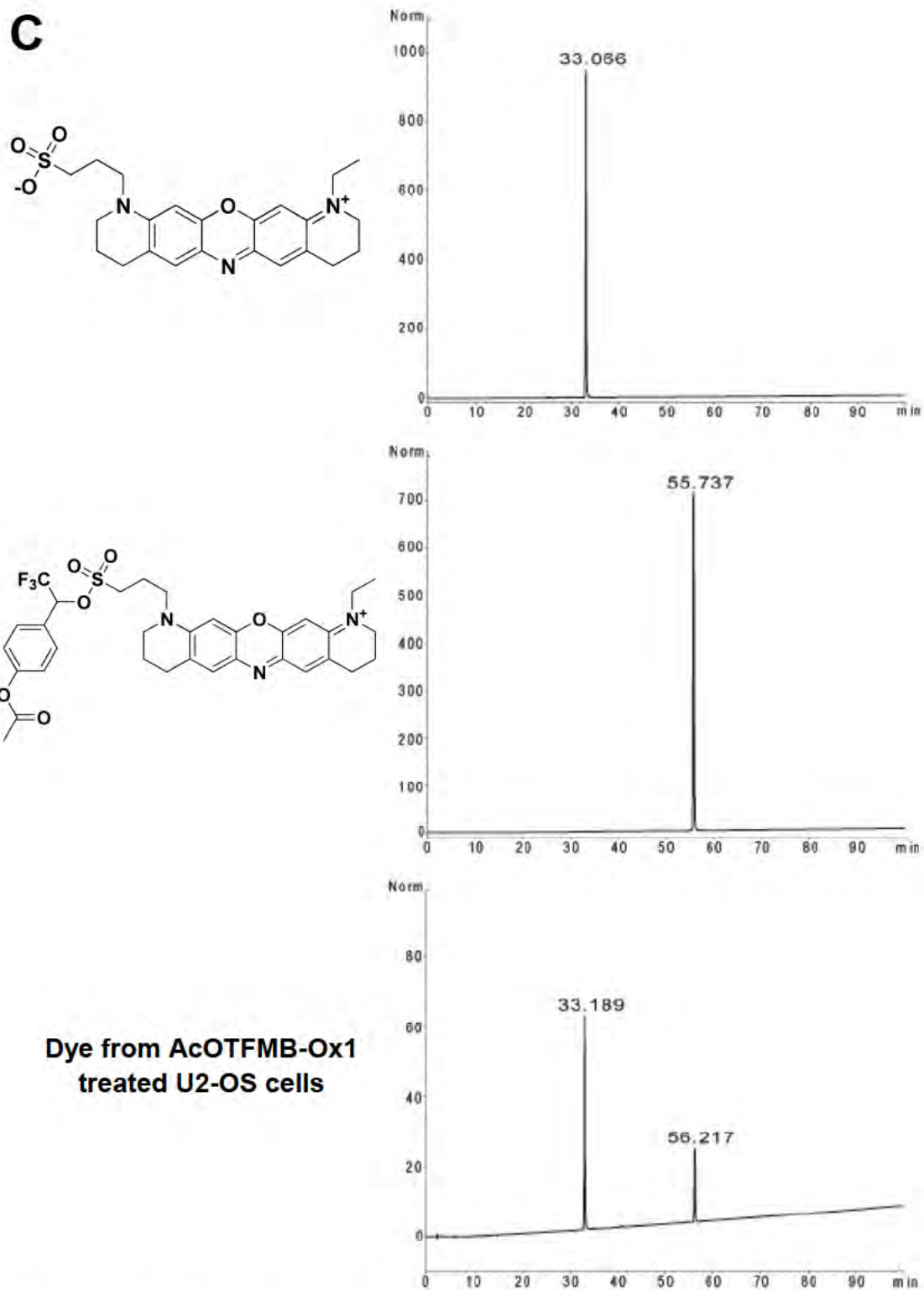


**Figure 4.8C.** Top trace: 657 nm. Middle/Bottom trace: 653 nm.

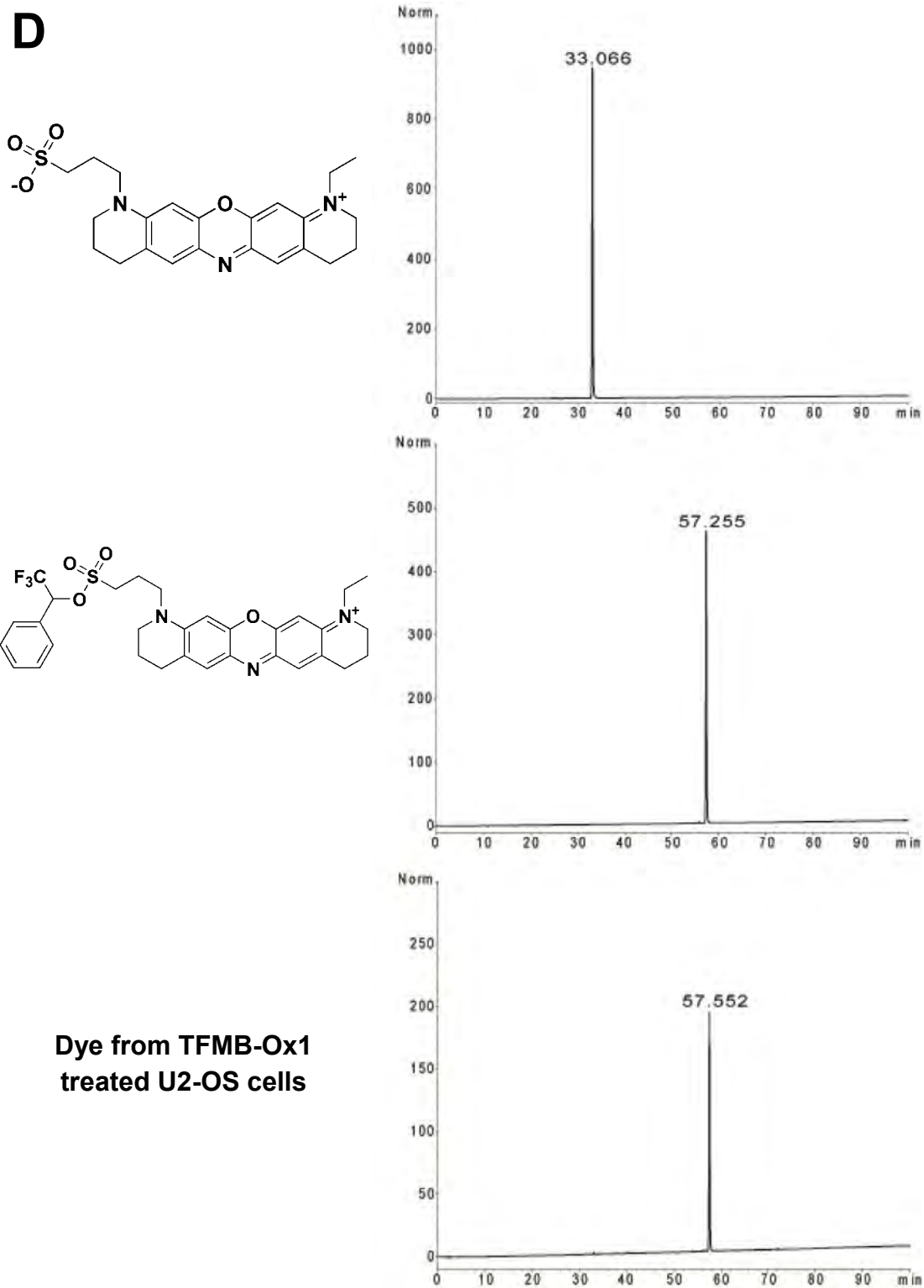


**Figure 4.8D.** Top trace: 657 nm. Middle/Bottom trace: 653 nm.

Compound	Retention Time (min)	ESI-HRMS (m/z)
<b>Sulf-Ox2</b>	24.795	534.1348
<b>AcOTFMB-Ox2</b>	61.327	968.2305
<b>AcOTFMB-Ox2 from cells</b>	<b>24.831</b>	<b>534.1392</b>
<b>TFMB-Ox2</b>	63.752	852.2180
<b>TFMB-Ox2 from cells</b>	<b>63.699</b>	<b>852.2214</b>
<b>Sulf-Ox1</b>	33.066	442.1779
<b>AcOTFMB-Ox1</b>	55.737	658.2165
<b>AcOTFMB-Ox1 from cells</b>	<b>33.189</b>	<b>442.1789</b>
<b>AcOTFMB-Ox1 from cells</b>	<b>56.217</b>	<b>658.2188</b>
<b>TFMB-Ox1</b>	57.255	600.2152
<b>TFMB-Ox1 from cells</b>	<b>57.552</b>	<b>600.2122</b>

**Table 4.1: ESI-HRMS m/z values for NIR oxazine fluorophores collected from U2-OS cells (Figure 4.8).** Retention times and observed masses for dyes collected from cells are shown in bold. Retention times and observed masses for control dyes are shown for comparison.

Since the sulfonated NIR oxazines, **Sulf-Ox1** and **2**, are unable to diffuse into the cells, the sulfonated NIR oxazines formed by interaction of the **AcOTFMB-Ox** dyes with intracellular esterases will be unable to passively diffuse out of the cell. However, we observed that the intracellular fluorescence intensity of **AcOTFMB-Ox2** treated cells decreases substantially after fluorescence becomes diffuse. In fact, one hour after dye treatment, little to no fluorescence is observed in **AcOTFMB-Ox2** treated U2-OS cells (Figure 4.7B). The situation is far different for U2-OS cells treated with the esterase-stable **TFMB-Ox2** (Figure 4.6B). While there is some flux in fluorescence intensity due to diffusion of the cationic **TFMB-Ox2**, bright mitochondrial-localized fluorescence is consistently observed over the 3 hour imaging period (Figure 4.6B). Based on this observation, it is unlikely that the loss of fluorescence in the **AcOTFMB-Ox2** treated U2-OS cells is due to fluorescence quenching or photobleaching. Since diffusion through the plasma membrane is inconsistent with the behavior of highly polar, sulfonated dyes, we hypothesized that the intracellular sulfonated NIR oxazines were being actively transported out of the cells.

A diverse array of molecules including drugs, peptides, and nucleotides are actively pumped out of the cell by ATP-binding cassette (ABC) transporters (Borst and Elferink, 2002). A small subset of these ABC transporters have been implicated in the phenomenon of multidrug resistance: permeability glycoprotein (ABCB1, MDR1, Pgp); multidrug resistance associated proteins 1, 2, and 4



(ABCC1/2/4, MRP1/2/4); and the breast cancer resistance protein (ABCG2, BCRP) (Lebedeva et al., 2011; Russel et al., 2008; Sharom, 2008). Three of these transporters, Pgp, MRP1, and BCRP, commonly referred to as the multidrug efflux pumps, have also been found to remove small organic fluorophores including: calcein (MRP1), Hoechst 33342 (MDR1, BCRP), and rhodamine 123 (MDR1) (Sharom, 2008). From these observations, we considered the possibility that our bis-sulfonated oxazine dye was also being effluxed by one or more of these transporters.

To identify which, if any, of the multidrug efflux pumps were involved in dye export, we treated U2-OS cells with inhibitors of Pgp (verapamil), MRP1 (MK-571), or BCRP (Ko143). We then incubated the cells with **AcOTFMB-Ox2** and monitored the cells for 30 minutes to determine the effect of pump inhibition on fluorescence retention (Figure 4.9). We found that cells treated with Ko143 showed no difference in fluorescence retention compared with the untreated control (Figure 4.9B). Ko143 is one of the most potent and specific inhibitors of BCRP and thus the loss of intracellular fluorescence from Ko143 treated cells indicates that BCRP is not necessary for efflux of our bis-sulfonated dye (Allen et al., 2002; Pick et al., 2010). On the other hand, cells treated with either verapamil or MK-571 retained observably more intracellular fluorescence than untreated U2-OS cells, suggesting that both Pgp and MRP1 are involved in intracellular clearance of **Sulf-Ox2** (Figure 4.9B).

**Figure 4.9: Inhibition of the efflux transporters MRP1 and Pgp results in increased retention of bis-sulfonated NIR oxazines.** U2-OS cells were pretreated with 50  $\mu$ M verapamil (Pgp inhibitor), 50  $\mu$ M MK-571 (MRP1 inhibitor), 0.5  $\mu$ M Ko143 (BCRP inhibitor), or no inhibitor (control). Cells were then incubated with 1  $\mu$ M **AcOTFMB-Ox2** plus inhibitor for 30 minutes to allow for dye uptake and conversion into the bis-sulfonated oxazine. Following aspiration of dye solution and washing, the cells were treated with fresh inhibitor-supplemented OPTI-MEM I and imaged (A). Cells were then incubated in inhibitor-supplemented media and imaged after 30 minutes (B). To confirm that treatment did not affect cell viability, cells were washed with inhibitor-free HBSS, incubated in inhibitor-free media for an additional 30 minutes to allow for return of efflux activity and then imaged (C). BF: bright field.

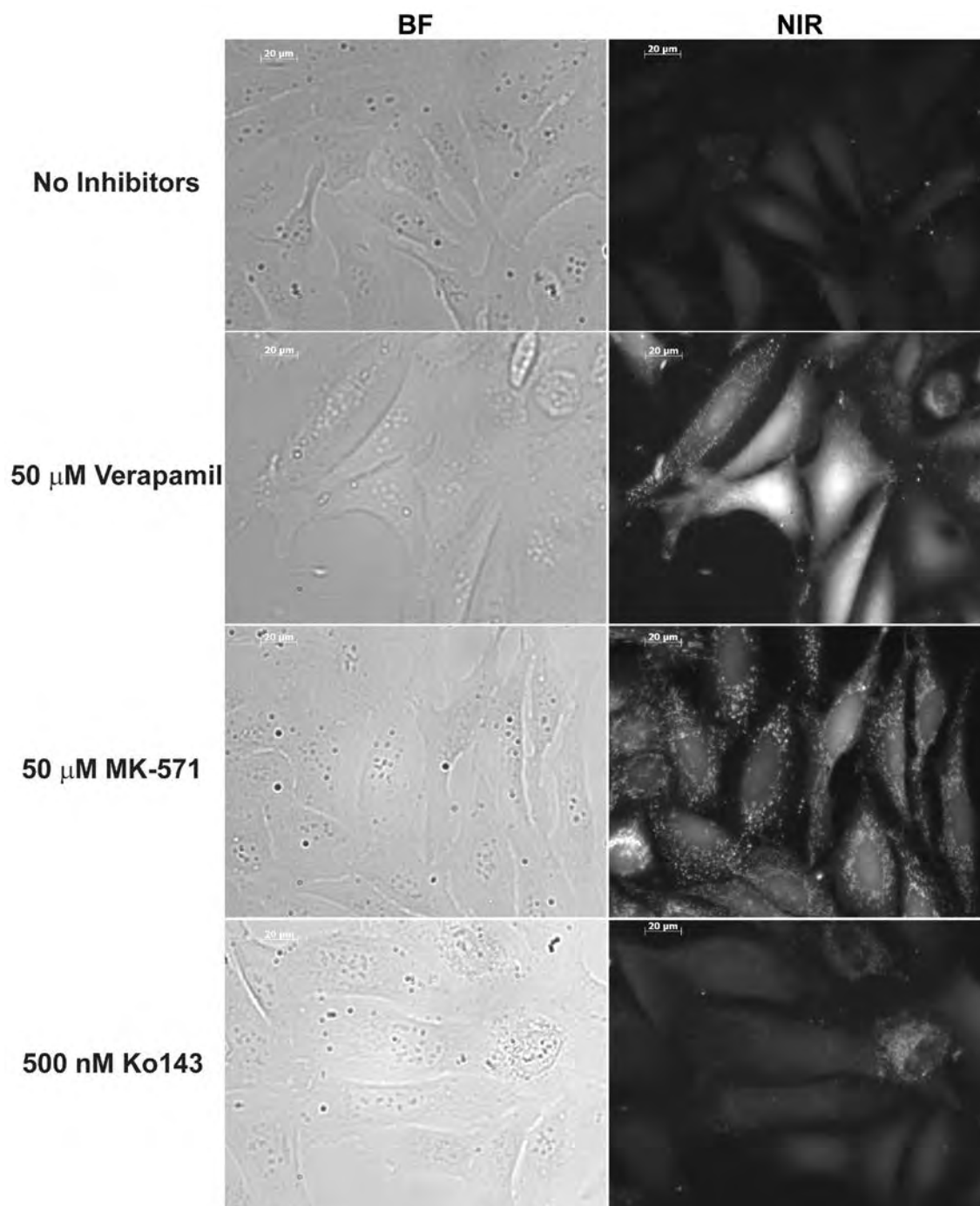


**Figure 4.9A.** Immediately after dye treatment. NIR exposure time: 50 ms.

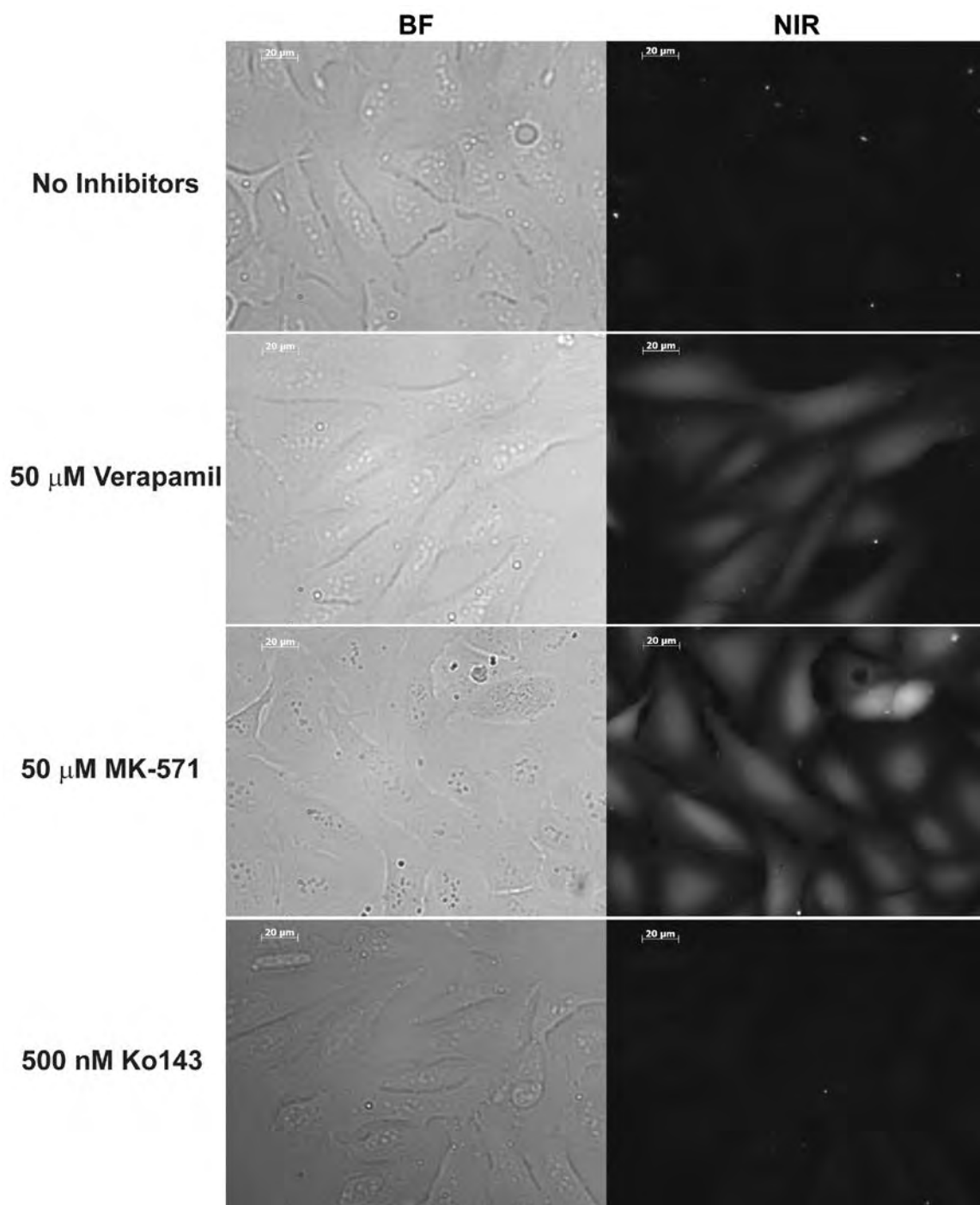


**Figure 4.9B.** 30 minutes post-dye treatment. NIR exposure time: 54 ms.

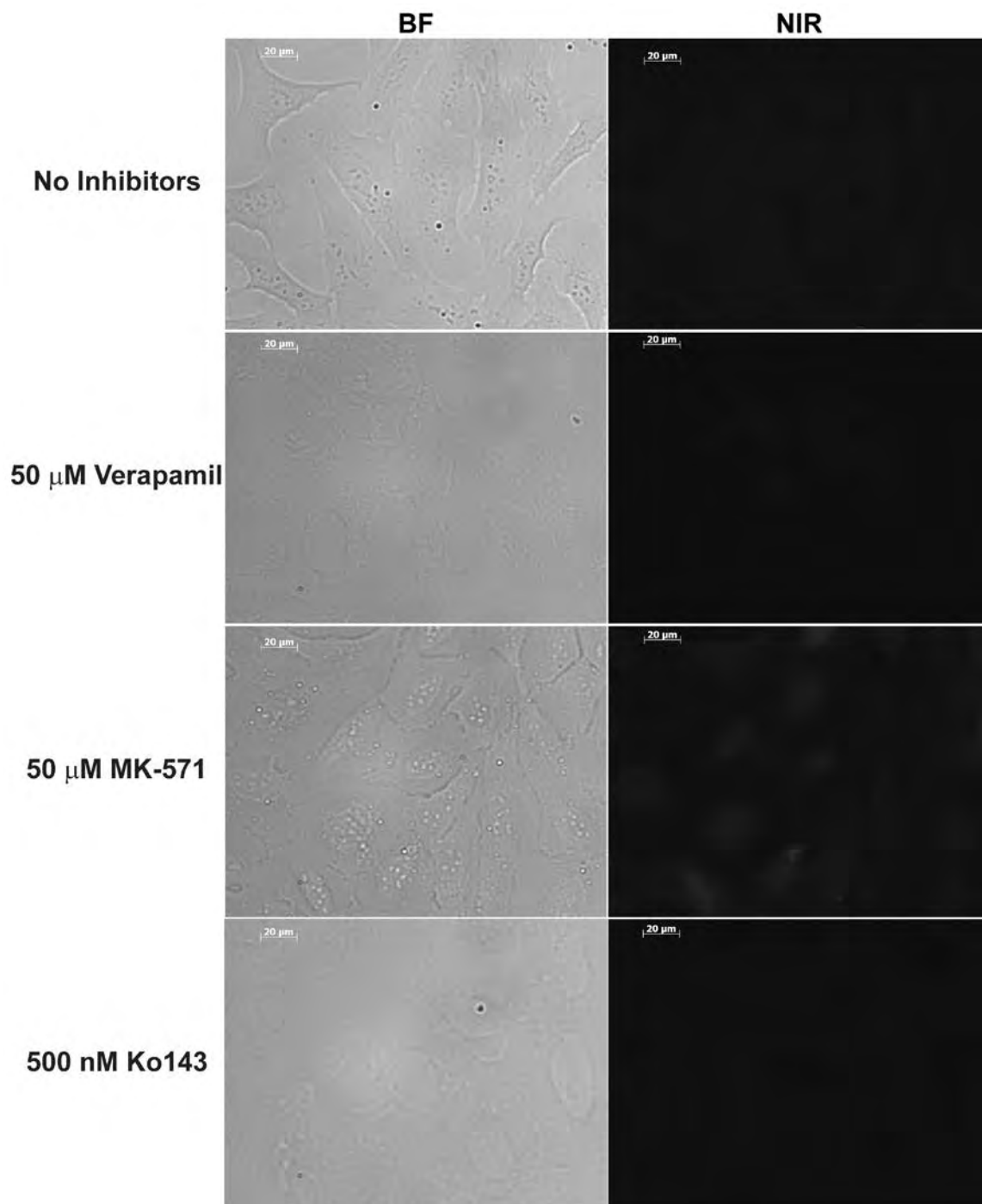


**Figure 4.9C.** 30 minutes post-inhibitor wash-out. 1 hour post dye treatment. NIR exposure time: 54 ms.

It was not surprising to find that both Pgp and MRP1 could be involved in efflux of our bis-sulfonated dye since substrate overlap between multidrug efflux transporters is common (Munoz et al., 2007). However, Pgp is most well known for clearing hydrophobic substrates, whereas MRP1 has been linked to organic anion efflux (Munoz et al., 2007; Sharom, 2014). Moreover, while verapamil is considered to be a potent inhibitor of Pgp, there have been observations that it also has some indirect effects on the activity of MRP1 (Cole et al., 1994; Loe et al., 2000; Pauli-Magnus et al., 2000). To confirm the contributions of MRP1 and Pgp to efflux of our NIR oxazines, we depleted MRP1 or Pgp expression in U2-OS cells via stable expression of shRNA. We then incubated our knockdown cells with **AcOTFMB-Ox2** and monitored the loss of intracellular fluorescence over 2 hours using wide field fluorescence microscopy (Figure 4.10). Over the first hour, the Pgp-knockdown cells are slightly more fluorescent than the control, whereas the MRP1-knockdown cells retain observably more fluorescence than either the control or Pgp-knockdowns (Figure 4.10B and C). This suggests that MRP1 is the primary efflux transporter for the sulfonated oxazine. However, by the end of the second hour, the control and knockdown cells all have very little intracellular fluorescence (Figure 4.10D). Since MRP1 and Pgp expression are reduced but not eliminated, the loss of fluorescence could be due to the residual activity of the transporters that are present. However, since the knockdown of Pgp does appear to have some effect on fluorescence retention, it is possible that some of the loss of fluorescence from the MRP1-knockdown cells results

from Pgp activity. It is also possible that other members of the MRP family are also involved in efflux of our dyes, such as MRP2 or MRP4. These transporters should have been inactivated by treatment with MK571 but are unaffected by MRP1-specific shRNA knockdown (Reid et al., 2003; Williams et al., 2002). Yet, the extended duration of intracellular fluorescence retention in our MRP1-knockdown U2-OS cells clearly displays the primary role of MRP1 in efflux of our sulfonated oxazines and relegates Pgp to a secondary pathway. The contribution of the other MRP family members to dye efflux was not investigated.

**Figure 4.10: shRNA knockdown of MRP1 and Pgp results in the increased retention of bis-sulfonated NIR oxazines.** U2-OS cells stably expressing shRNA against Pgp or MRP1 were prepared as described (see Methods). U2-OS cells not expressing shRNA were used as a negative control. Cells were incubated with 1  $\mu$ M **AcOTFMB-Ox2** for 15 minutes to allow for dye uptake. Following aspiration of dye solution and washing, cells were treated with fresh OPTI-MEM I and imaged (A). Cells were then incubated in OPTI-MEM I and imaged periodically over 2 hours (B-D). KD: knockdown. BF: bright field. NIR exposure time: 50 ms.



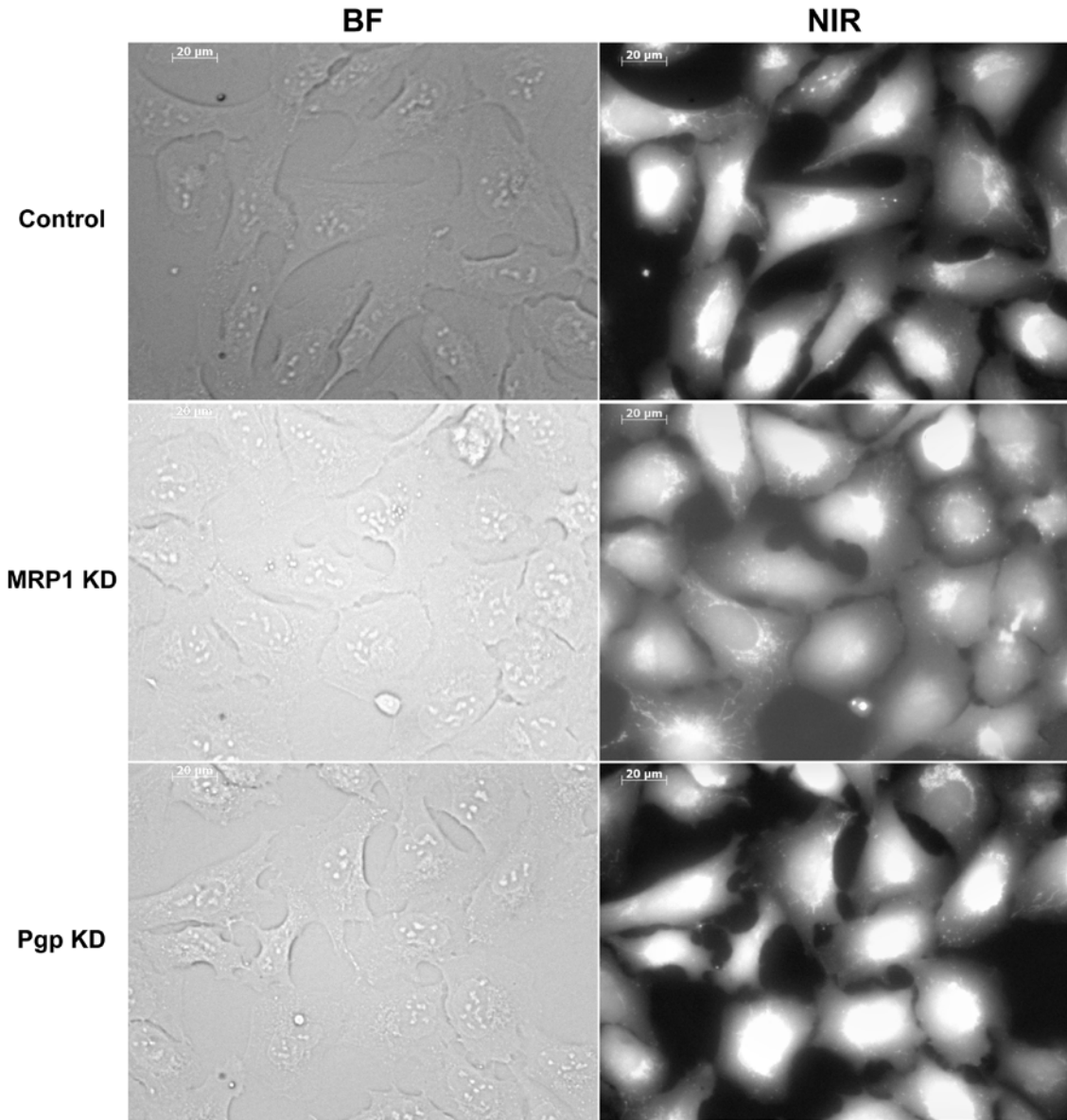


**Figure 4.10A.** Immediately after dye treatment.

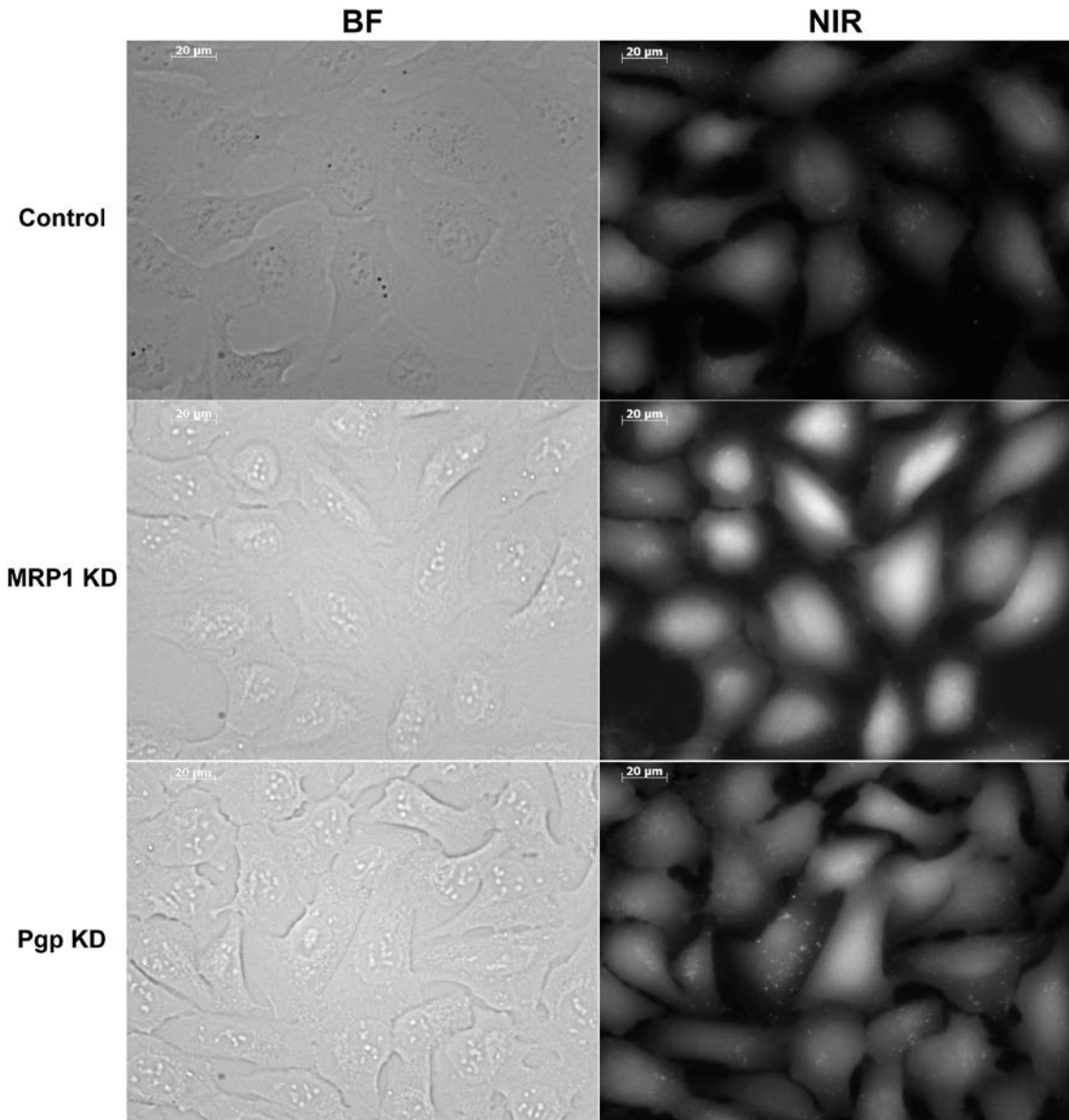


**Figure 4.10B.** 20 minutes post-dye treatment.

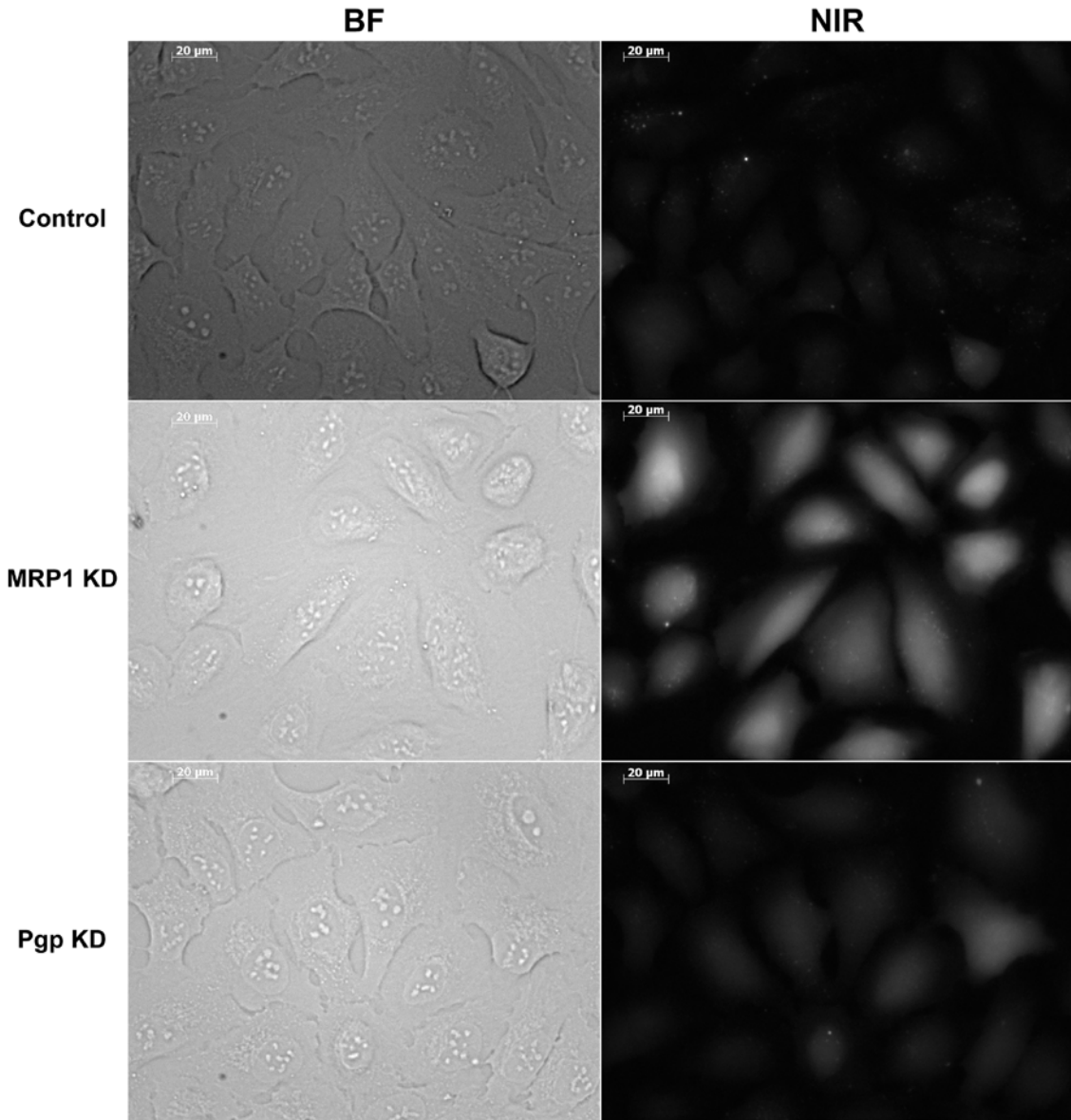


**Figure 4.10C.** 50 minutes post-dye treatment.

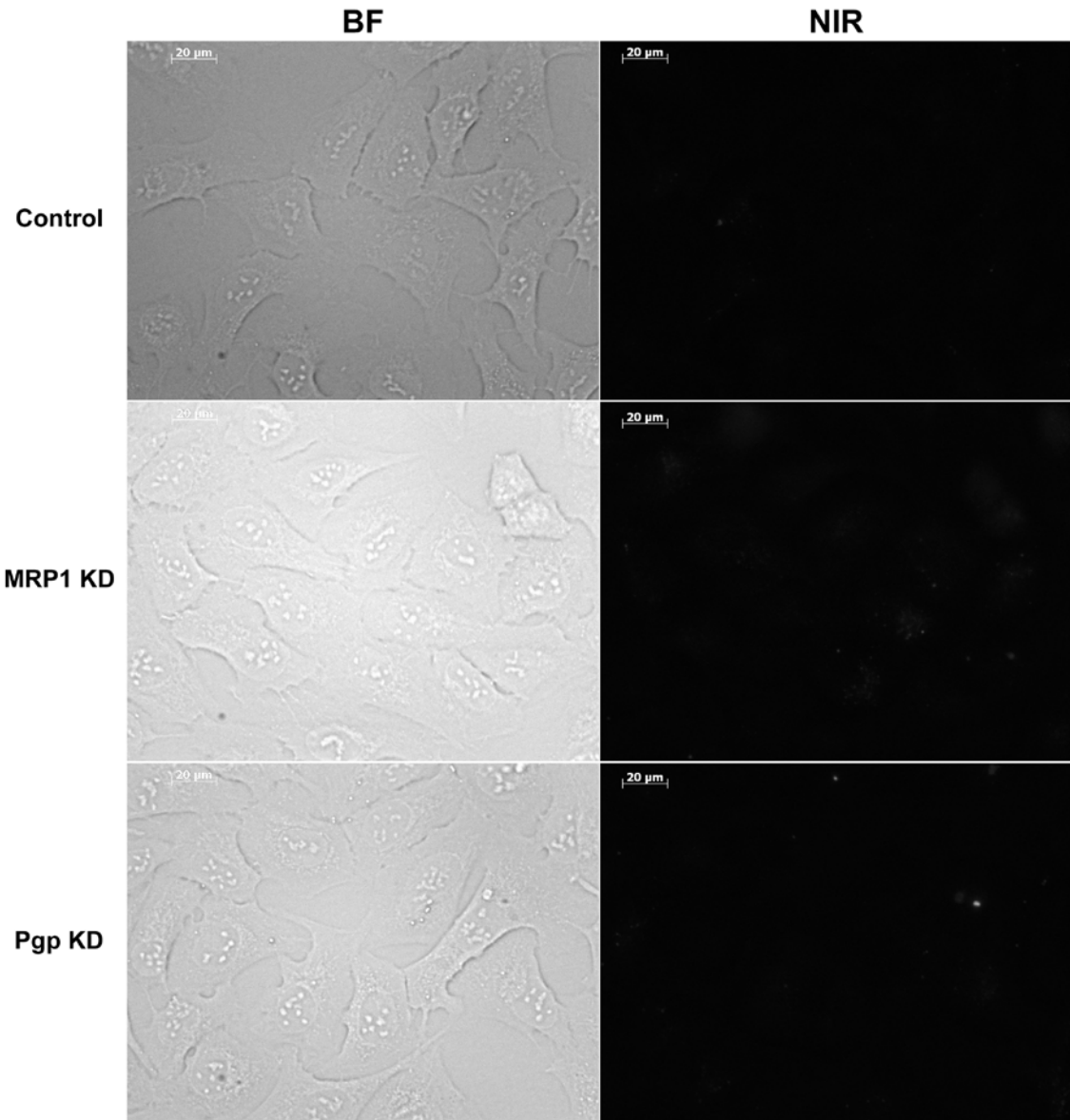


**Figure 4.10D.** 110 minutes post-dye treatment.

Having confirmed that our sulfonate ester delivery strategy is able to deliver sulfonated NIR oxazines into live cells, we wanted to show that these dyes could be used for imaging in whole organisms. Since the esterase-labile bis-sulfonate ester **AcOTFMB-Ox2** gives the highest degree of diffuse intracellular fluorescence, we limited this work to the **Ox-2** group of our NIR oxazines. Research involving NIR oxazines and live animal imaging is sparse (Hintersteiner et al., 2005; Park et al., 2014) and almost no work has been done on the performance of sulfonated NIR oxazines in whole organisms; therefore, we first sought to characterize the *in vivo* behavior of the bis-sulfonated **Sulf-Ox2**.

To investigate the activity of **Sulf-Ox2** *in vivo*, we treated albino C57BL/6 mice with 320 fmol/kg dye via intraperitoneal injection (IP) or intravenous tail vein injection (IV) and imaged the mice at two time points over a 4-hour period (Figure 4.11; Sulf-IP and Sulf-IV, respectively). Immediately following injection, bright fluorescence can be observed within the mice at the site of introduction (Figure 4.11A and B; top panels). This result was expected as **Sulf-Ox2** is a NIR fluorophore and organisms are known to be highly transparent to NIR light (Frangioni, 2003; Weissleder, 2001). However, we were still delighted by this observation as it confirmed that our dye could be successfully used to image within a living organism.

**Figure 4.11: *in vivo* imaging in mice with NIR bis-sulfonated oxazines.**

Albino C57BL/6 mice were treated with 320 fmol/kg oxazine dye in PBS via IP or IV injection and imaged at two time points over 4 hours using an IVIS-100 as described in Methods. Control mouse was not injected. Images were obtained using Cy5.5 excitation (615-665 nm) and emission (695-770 nm) filters. Images shown have been background subtracted and were prepared using Living Image 4.3.1 software. (A) Dorsal view. (B) Ventral view. Upper image is approximately 5 minutes after dye injection. Lower image is 3.5 hours after dye injection. Photon output is recorded as radiant efficiency, which is defined as the fluorescence emission radiance per incident excitation irradiance.

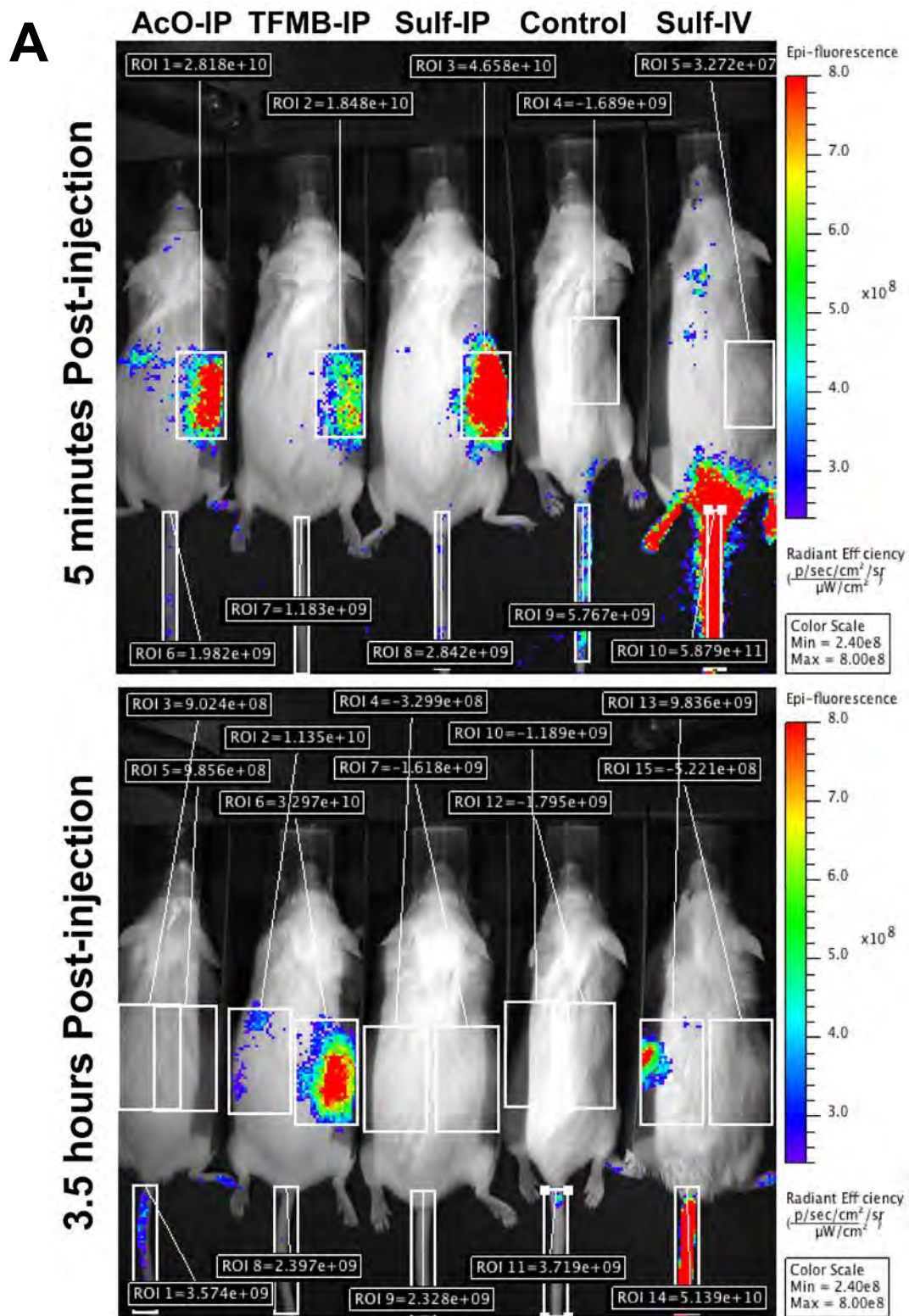


Figure 4.11A. Dorsal view.

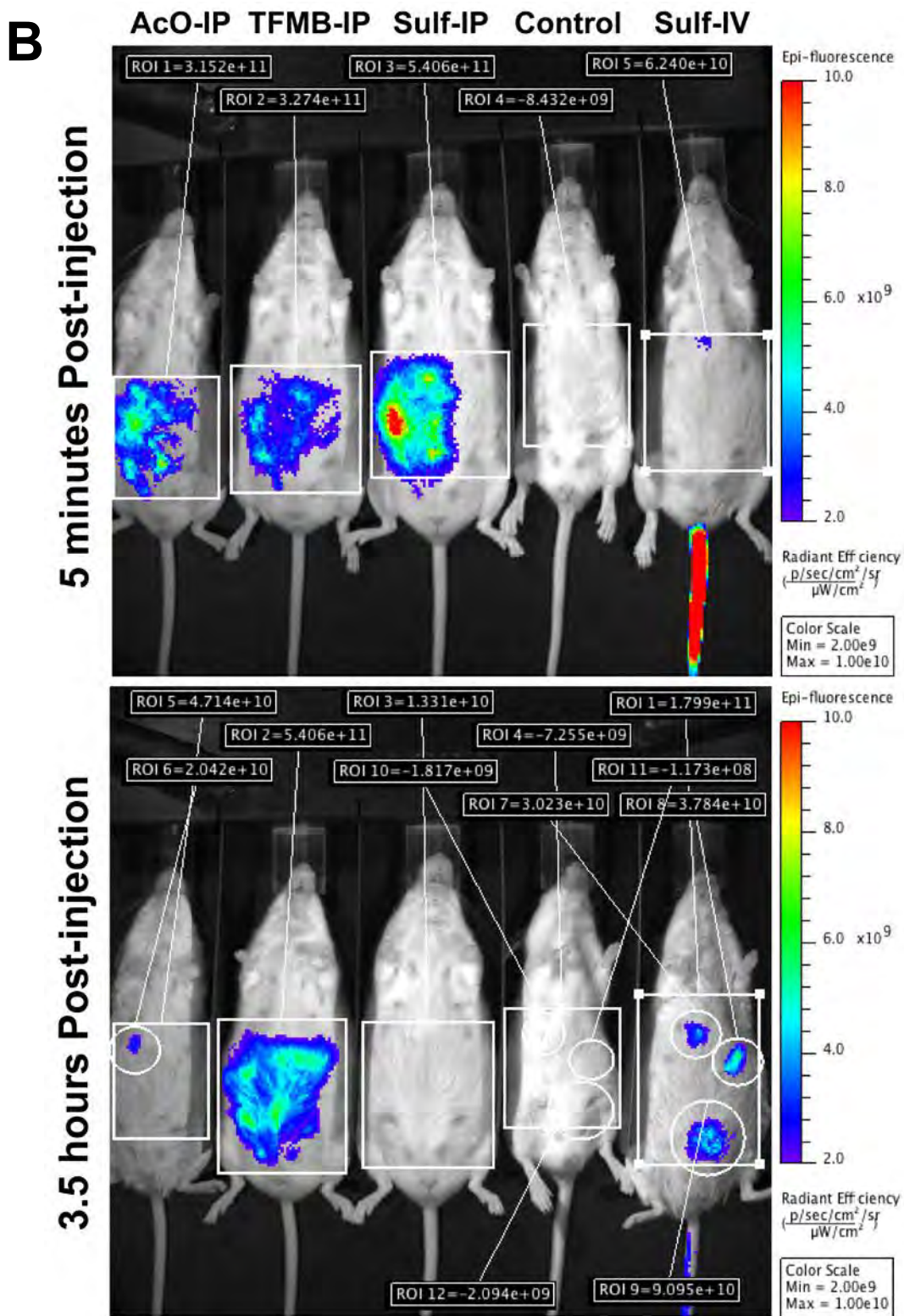


Figure 4.11B. Ventral view.



Compared to the initial behavior of **Sulf-Ox2** *in vivo*, the long-term fate of our bis-sulfonated dye was not as easily predicted. We observed two key features of **Sulf-Ox2** behavior when imaging the mice 3.5 hours post-injection (Figure 4.11A and B; bottom panels). First, the method of dye delivery (IP or IV) affects the long-term behavior of the dye. The Sulf-IP mouse emits relatively little NIR light and visually resembles the untreated control (Figure 4.11B; bottom panel, 3<sup>rd</sup> mouse from left). Contrast this to the Sulf-IV mouse that emits approximately 14 times more light than Sulf-IP and appears to have fluorescence localized at several organs throughout the mouse (Figure 4.11B; bottom panel, mouse on right). Often, *in vivo* pharmacokinetic studies find that molecules behave differently depending on how they are introduced into an organism, so these results are not unexpected (Guichard et al., 1998; Sim et al., 2011; Zhao et al., 2012).

Second, and of greater interest, is the distinct biodistribution of **Sulf-Ox2** in the IV treated mouse (Figure 4.11B; bottom panel, Sulf-IV). Although no confirmatory *ex vivo* imaging was performed, the image in Figure 4.11B suggests that over the 4-hour imaging period, **Sulf-Ox2** localizes to organs consistent with the heart and intestines. The medical diagnostic NIR dye, Indocyanine Green, is rapidly cleared by the liver, and IV injection primarily illuminates this organ (Ma et al., 2008; Soons et al., 1991). Our preliminary results with **Sulf-Ox2** suggests that, rather than being rapidly removed from the blood stream by the liver and kidneys, our NIR dye can actually be employed in the imaging of other tissues.

Having evaluated the *in vivo* characteristics of **Sulf-Ox2**, we were able to analyze the actions of its cell-permeable counterparts, **AcOTFMB-Ox2** and **TFMB-Ox2**. Similar to **Sulf-Ox2**, albino C57BL/6 mice were treated with 320 fmol/kg **AcOTFMB-Ox2** or **TFMB-Ox2** and imaged at two time points over a 4-hour period (Figure 4.11 AcO-IP and TFMB-IP, respectively). However, due to poor solubility in the aqueous buffer, these dyes were only introduced via IP injection. While this limited the comparison between these dyes and the **Sulf-Ox2** introduced IV, it eliminated the need to include a higher percentage of DMSO (see Methods) and thus provided a greater degree of experimental consistency.

As with Sulf-IP, bright fluorescence was observed about the injection site from both AcO-IP and TFMB-IP mice immediately following treatment (Figure 4.11A and B, Top panels). Three and a half hours post-injection, the AcO-IP mouse closely resembles the Sulf-IP mouse; i.e., relatively little fluorescence was detected (Figure 4.11A and B; Bottom panels, mice on left and center). This result is notably distinct from that of the **TFMB-Ox2** treated mouse. For example, at 3.5 hours post-injection, the TFMB-IP mouse was emitting more fluorescence than the AcO-IP mouse (11 times greater), the Sulf-IP mouse (41 times greater) or the Sulf-IV mouse (3 times greater) (Figure 4.11B, Bottom panel). More interestingly, the TFMB-IP mouse appeared to emit a higher degree of fluorescence at 3.5 hours than when it was first injected: approximately 2-fold both dorsally and ventrally (Figure 4.11A and B). Lastly, unlike the Sulf-IV or

AcO-IP mice, fluorescence from the **TFMB-Ox2** treated mouse remains localized about the site of injection (Figure 4.11B).

The results from the AcO-IP and TFMB-IP *in vivo* treatments are consistent with the design of these molecules. Since the **AcOTFMB-Ox2** dye is esterase-labile, interaction with esterases within the mouse should convert it into the **Sulf-Ox2** dye. Once the **AcOTFMB-Ox2** has lost its sulfonate protecting groups, its activity *in vivo* should resemble that of **Sulf-Ox2**. The similar appearance of the AcO-IP and Sulf-IP mice 3.5 hours post-injection indicates that this is indeed occurring and thus suggests that our strategy to deliver sulfonated NIR dyes into cells can be successfully applied *in vivo* as well (Figure 4.11). Conversely, the **TFMB-Ox2** dye was designed to be esterase-stable and is unaffected by esterase activity both *in vitro* and in live cells (Figure 4.8B and Pauff and Miller, 2011). The extended retention of fluorescence in the TFMB-IP mouse compared to both the Sulf-IV and Sulf-IP treatments suggests that this stability holds *in vivo* as well (Figure 4.11B). Furthermore, since **TFMB-Ox2** tends to accumulate and remain within mitochondria, it is no surprise that the fluorescence of this dye remains localized at the site of injection over the 4-hour imaging period (Figure 4.6B). This simply indicates that IP-injected **TFMB-Ox2** is diffusing into cells at the area it was first introduced into the animal. Lastly, the increase in fluorescence in the TFMB-IP mouse from the initial to the 3.5-hour time-point likely results from the relative hydrophobicity of the dye (Figure 4.11A, ROI 2 and 6; Figure 4.11B, ROI 2). In other words, since the dye is somewhat

hydrophobic, it may tend to self-aggregate in aqueous solution, which could result in fluorescence quenching. Once the dye diffuses into cells and travels to mitochondria, this aggregation would be minimized and bright fluorescence would be restored.

### **Conclusions**

It is widely accepted that NIR light is optimal for imaging live cells and organisms. However, NIR fluorophores are extremely hydrophobic and require the addition of highly charged moieties, such as sulfonate groups, when used in aqueous environments. Unfortunately, the lipophilic cellular membrane prevents the diffusion of sulfonated molecules into cells, preventing the use of sulfonated NIR dyes in live cell imaging. In this work, we have shown that we can deliver sulfonated near-IR oxazines into both live cells and mice using our AcOTFMB delivery method (Figures 4.8 and 4.11). One dye in particular, the bis-sulfonate ester **AcOTFMB-Ox2**, shows very high promise for use in cellular imaging.

**AcOTFMB-Ox2** rapidly diffuses into cells and, upon interaction with cellular esterases, is converted into the anionic bis-sulfonate, **Sulf-Ox2**, which has the ability to access the entire cell (Figures 4.4B, 4.7B, and 4.8A). This is one of the first examples of a NIR dye displaying truly diffuse localization, a feature which would allow it be employed for any number of imaging purposes. For example, since intracellular **Sulf-Ox2** has access to both the nucleus and cytoplasm, addition of a protein-labeling moiety to **AcOTFMB-Ox2** would allow

the study of nuclear and cytoplasmic proteins. Furthermore, since **AcOTFMB-Ox2** absorbs and emits in the NIR, protein localization studies using our fluorophore would not suffer from the cellular autofluorescence observed when using visible wavelength fluorescent proteins like GFP.

The intracellular fate of **AcOTFMB-Ox2** highlights another exceptional feature of our NIR oxazines. After diffusing throughout the cytoplasm, we observed that the newly formed **Sulf-Ox2** is quickly cleared from the cell by the multidrug efflux transporters MRP1 and Pgp (Figures 4.9 and 4.10). In fact, within an hour following dye treatment, cells treated with **AcOTFMB-Ox2** displayed little to no intracellular fluorescence (Figure 4.7B). This is no little feat as fluorophores in general, and NIR dyes in particular, are often associated with non-specific background labeling resulting from their inherent cationic and hydrophobic nature (Bunting et al., 1989; Cunningham et al., 2010; Escobedo et al., 2010; Jiang et al., 2013; Johnson, 1998). **AcOTFMB-Ox2** functionalized with a protein-labeling tag could thus provide a system for live cell imaging without the autofluorescence and background noise too commonly associated with fluorescence imaging. Additionally, the interaction of **Sulf-Ox2** with ABC transporters offers the ability to study the activity of these pharmacologically-relevant proteins in a very straightforward manner. For example, intracellular drug activity is often reduced due to their removal from cells by efflux transporters (Borst and Elferink, 2002; Glavinas et al., 2004). Inhibitors of these proteins could easily be assayed by evaluating their function with relation to the fluorescence retention of **Sulf-Ox2**.

Some of the most exciting results of this work came from exploring the *in vivo* behavior of our NIR oxazines. The intravenously delivered **Sulf-Ox2** has several *in vivo* characteristics which may favor its use over the commonly employed NIR fluorophore Indocyanine Green (ICG). For example, IV-injected ICG is rapidly removed from the bloodstream by the liver, followed by excretion into the bile (Ma et al., 2008; Soons et al., 1991). We confirmed this biodistribution by imaging albino C57BL/6 mice with 320 fmol/kg ICG (Figure 4.12). This limits the use of ICG. On the other hand, IV-injected **Sulf-Ox2** appears to travel through the bloodstream to several distinct organ systems, a feature that could be useful when imaging in organs other than the liver is desired (Figure 4.11B; bottom, Sulf-IV). Along with their biodistribution, ICG and **Sulf-Ox2** have a distinct temporal footprint. We found that, at 66 minutes post injection, the ICG-treated mouse was 26-fold less fluorescent than the **Sulf-Ox2**-treated mouse imaged 3.5 hours post injection (Figure 4.11B, bottom, ROI 1; Figure 4.12, ROI 2). This finding was no surprise as the half-life of IV-injected ICG is reported to be 2-4 minutes (Ma et al., 2008). This feature is viewed as one of the benefits of ICG since the short lifetime permits consecutive injections of the compound. However, in situations where longer imaging periods rather than consecutive treatments are favored, it is clear that our **Sulf-Ox2** fluorophore would be preferable.

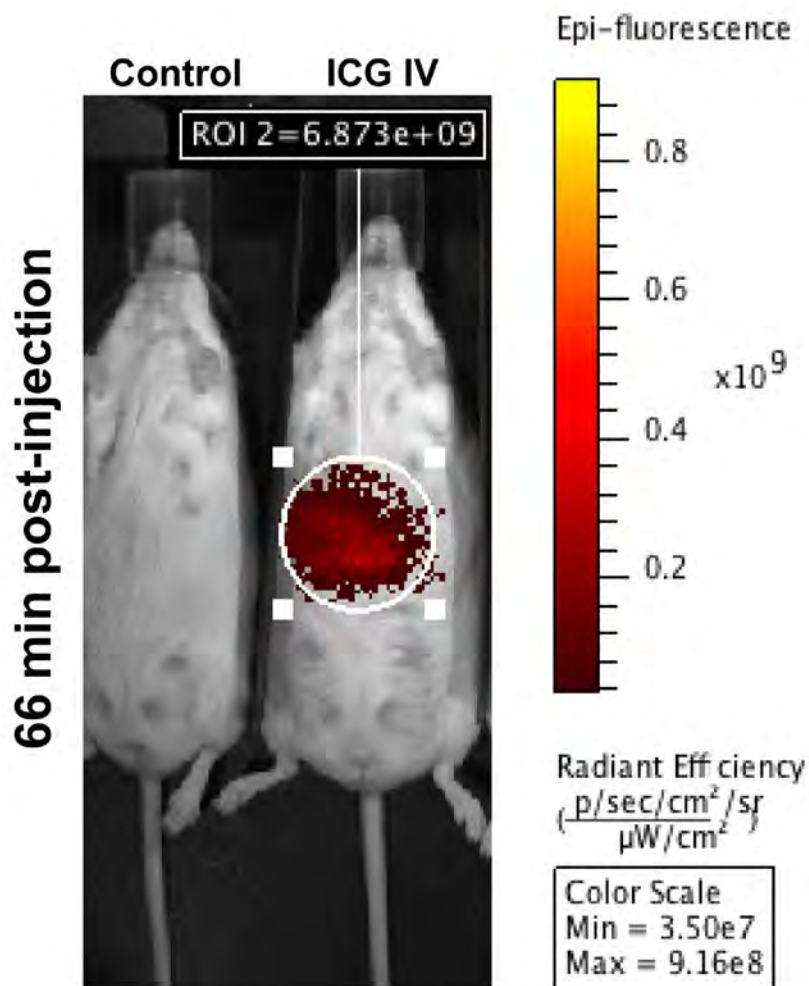


**Figure 4.12: *in vivo* imaging with Indocyanine Green.** An albino C57BL/6 mouse was treated with 320 fmol/kg ICG in PBS via IV injection and imaged at two time points over 2 hours using an IVIS-100 as described in Methods. Control mouse was not injected. Image was obtained using ICG excitation (710-760 nm) and emission (810-875 nm) filters and analyzed using Living Image 4.3.1 software following background subtraction. Photon output is recorded as radiant efficiency.

While we are enthusiastic about the diagnostically-important features displayed by **Sulf-Ox2**, we were more excited to observe the *in vivo* behavior of our cell-permeable NIR fluorophore, **AcOTFMB-Ox2**. Since this dye has the

ability to deliver NIR sulfonates into live cells, it offers the potential to study *in vivo* intracellular functions. From our proof of principle experiment, it does appear that **AcOTFMB-Ox2** functions similarly *in vivo* as in live cells. For example, while the esterase stable **TFMB-Ox2** remains localized to mouse abdomen throughout the time course, **AcOTFMB-Ox2** is cleared from the mouse in a manner similar to the IP-injected **Sulf-Ox2** (Figure 4.11). The question could be raised however, of whether **AcOTFMB-Ox2** is being converted into **Sulf-Ox2** within the cells or by extracellular esterases within the mouse. One observation favoring the intracellular conversion of **AcOTFMB-Ox2** to **Sulf-Ox2** is the higher degree of fluorescence emitted by the AcO-IP mouse 3.5 hours post injection (Figure 4.11B; bottom, ROIs 3 and 5). Compared to Sulf-IP treatment, AcO-IP results in 3.5 times more fluorescence at the later time point. This suggests a temporal aspect to the Sulf-IP-like behavior of **AcOTFMB-Ox2**. In other words, time is required for **AcOTFMB-Ox2** to enter the mouse cells, be converted into **Sulf-Ox2** by esterases, get exported back into the bloodstream, and be cleared from the mouse. This temporal requirement could also explain the appearance of fluorescence in the AcO-IP mouse at a location distant from the injection site, as some dye may have traveled through the mouse before it diffused into cells (Figure 4.11B, bottom, ROI 6). While these results are promising, further experiments must be performed to confirm that the dye is indeed accessing the intracellular regions of the mouse. One method to confirm this would be the *ex vivo* analysis of organs to determine whether **AcOTFMB-Ox2** has become



localized within cells. Alternatively, and less invasively, would be the possibility of co-treating mice with **AcOTFMB-Ox2** and an *in vivo* mitochondrial probe, such as the hypochlorite probe recently developed by the Yu group, and imaging the mice to determine if there is any co-localization of fluorescence (Hou et al., 2014). In either scenario, a positive result could open the door for the use of our **AcOTFMB-Ox2** as an *in vivo* intracellular imaging reagent.

In this work, I have shown the successful delivery of our sulfonated NIR oxazines into live cells and mice and characterized the intracellular and *in vivo* behavior of our dyes. While we expect that our fluorophores could be effectively utilized in imaging experiments, there are implications from our findings that reach beyond the limited focus of our dyes. As mentioned earlier, sulfonation is a common strategy employed for increasing the water-solubility of NIR fluorophores (Li et al., 2008; Morgan et al., 2011; Mujumdar et al., 1993; Niu et al., 2009; Panchuk-Voloshina et al., 1999). Our AcOTFMB sulfonate-protecting group is not specific to our oxazines and its application to sulfonated cyanines, BODIPYs and other dye families would allow many water-soluble NIR dyes to find employment in intracellular studies. In like manner, AcOTFMB can be applied to any sulfonated molecule and would therefore allow drugs that are too hydrophobic to be used within aqueous environments to be solubilized by sulfonation and delivered via AcOTFMB-mediated diffusion. With the correct application of our delivery method, we believe that it would be possible to tune the molecular structure of a myriad of biologically- relevant organic molecules

with minimal concern for cell permeability, as this permeability could be maximized by implementing a strategy with the seductive simplicity of AcOTFMB.

## ***Materials and Methods***

### **General Methods**

Chromasolv<sup>®</sup> HPLC grade acetonitrile, methanol, and trifluoroacetic acid were purchased from Sigma-Aldrich. Molecular biology grade dimethyl sulfoxide (DMSO) was purchased from Sigma-Aldrich. MK-571 sodium salt was purchased from Cayman Chemical and prepared as a 50 mM stock solution in DMSO. Ko143 was purchased from Tocris Bioscience and prepared as a 5 mM stock solution in DMSO. (±)-Verapamil hydrochloride was purchased from Sigma-Aldrich and was freshly prepared as a 50 mM stock solution in DMSO. MitoTracker<sup>®</sup> Green FM was purchased from Life Technologies. Indocyanine Green sodium salt was purchased from TCI America.

Cell culture supplies were purchased from the University of Massachusetts Medical School's Tissue Culture and Enzyme Freezer Supply. Dulbecco's Modified Eagle's Medium (DMEM) (with L-glutamine and pyruvate), Hank's Balanced Salt Solution (HBSS) (with calcium and magnesium, without phenol red), and fetal bovine serum (FBS) (USDA certified) were CellGro<sup>®</sup> from Mediatech. OPTI-MEM I reduced serum media, penicillin/streptomycin, and trypsin 0.25% were Invitrogen<sup>™</sup> from Life Technologies.

Wide-field fluorescence imaging was performed on a Zeiss Axiovert 200 fluorescence microscope with a 40X dry objective using a Hamamatsu ORCA-ER digital camera and excitation from an X-Cite 120 light source. MitoTracker<sup>®</sup> Green FM images were obtained using Zeiss filter set 38 (Endow GFP shift free (E) BP 470/40 excitation filter, beam splitter FT495, BP 525/50 emission filter). NIR images were obtained using Semrock BrightLine Basic<sup>™</sup> single-band filter set (BP 630/38 excitation filter, beam splitter FF655, BP 694/44 emission filter). Cell images were processed using ImageJ with images set to 32 bit followed by 1000 pixel background subtraction.

### **Cell Culture**

The human osteosarcoma cell line U2-OS (ATCC number HTB-96) was donated by Dr. Eric Swanson from the Lawrence lab at the University of Massachusetts Medical School and were employed for all experiments in this work. Cells were maintained in DMEM supplemented with 10% FBS, 100 units/mL penicillin and 100 µg/mL streptomycin (herein referred to as complete media) and grown at 37 °C in a 5% CO<sub>2</sub> atmosphere. Cells were subcultured at a ratio of 1:4 when plates reached 85-90% confluency using standard cell culture protocols. Cells were incubated at 37 °C in a 5% CO<sub>2</sub> atmosphere for all experiments.

## **Near-infrared Dye Treatment and Live Cell Imaging**

### *Preparation of NIR Dyes*

NIR dyes were prepared as 10 mM stocks in DMSO, aliquoted, and stored at -20 °C. Aliquoted preparations were used only once then discarded. Dye-labeling media (1  $\mu$ M NIR dye in OPTI-MEM I) was prepared immediately prior to treatment.

### *Dye Treatment and Imaging*

Cells were subcultured into 6-well plates at a seeding density of  $0.3 \times 10^6$  cells and grown to 80% confluency in complete media. Growth media was aspirated and cells were washed twice with HBSS. Cells were then incubated with 1  $\mu$ M NIR dye in OPTI-MEM I for 10-30 minutes, after which the dye-labeling media was aspirated and the cells were washed twice with HBSS. The cells were treated with fresh OPTI-MEM I, and then subjected to bright field and fluorescence microscopy.

### *Repeated Imaging*

After initial imaging, OPTI-MEM I was aspirated, replaced with fresh OPTI-MEM I, and cells were incubated until needed. Prior to imaging, cells were washed twice with HBSS and treated with fresh OPTI-MEM I. This series was repeated until imaging was no longer desired.

## **Costaining Cells with MitoTracker<sup>®</sup>**

### *Preparation of MitoTracker<sup>®</sup> Green FM*

MitoTracker<sup>®</sup> Green FM was freshly prepared as a 1 mM stock solution in DMSO. Dye-labeling media (100 nM in OPTI-MEM I) was prepared immediately prior to treatment.

### *Dye Treatment and Imaging*

Cells were subcultured as described for NIR experiments. Growth media was aspirated and cells were washed twice with HBSS. Cells were then incubated with 100  $\mu$ M MitoTracker<sup>®</sup> Green FM in OPTI-MEM I for 30 minutes. Upon completion of mitochondrial-labeling, the dye-labeling media was aspirated and the cells were washed twice with HBSS. Cells were then treated with NIR dye-labeling media (1  $\mu$ M in OPTI-MEM I) and incubated for 10 minutes. Imaging was performed as described above. Overlaid images were prepared with ImageJ.

## **Multidrug Efflux Pump Inhibition**

### *Inhibitor and NIR Dye Preparation*

Complete media, HBSS, and OPTI-MEM I containing either 0.5  $\mu$ M Ko143, 50  $\mu$ M MK-571, or 50  $\mu$ M verapamil were prepared prior to experiment by dilution of the stock compound into the appropriate medium. Dye-labeling media (1  $\mu$ M NIR dye in OPTI-MEM I plus inhibitor) was prepared immediately prior to treatment.

### *Initial Treatment with Inhibitors*

Cells were subcultured as described for NIR experiments. Growth media was aspirated and cells were washed twice with HBSS. Cells were then incubated with inhibitor in complete media for 5 minutes to allow for pump inhibition.

### *Dye Treatment and Imaging*

Complete media containing inhibitors was aspirated and cells were washed twice with inhibitor-supplemented HBSS. Cells were then incubated with 1  $\mu$ M NIR dye + inhibitor in OPTI-MEM I for 30 minutes. Upon completion of dye treatment, the dye-labeling media was aspirated and the cells were washed twice with inhibitor-supplemented HBSS. After layering in fresh inhibitor-supplemented OPTI-MEM I, bright field and NIR images were collected.

After initial imaging, inhibitor-supplemented OPTI-MEM I was aspirated and cells were washed twice with inhibitor-supplemented HBSS. The cells were then incubated for 30 minutes in complete media containing inhibitors. Upon completion of incubation, the cells were washed twice with inhibitor-supplemented HBSS, treated with fresh inhibitor-supplemented OPTI-MEM I, and subjected to bright field and fluorescence microscopy.

Upon completion of the second imaging, the inhibitor-supplemented OPTI-MEM I was aspirated. Efflux pump activity was then restored by washing the cells twice with inhibitor-free HBSS and incubating the cells in inhibitor-free complete media

for 30 minutes. The cells were then washed twice with inhibitor-free HBSS, treated with fresh inhibitor-free OPTI-MEM I, and then subjected to bright field and fluorescence microscopy.

### **shRNA Knockdown of ABCB1 (Pgp) and ABCC1 (MRP1) Efflux Pumps**

#### *shRNA Knockdown Cells*

U2-OS cells expressing shRNA against ABC transporters ABCB1 and ABCC1 were prepared by Poshen Chen in the Fazio lab at the University of Massachusetts Medical School as described in (Chen et al., 2013). Five potential shRNA sequences against each gene were chosen for analyses. The shRNA sequence which produced the highest degree of mRNA repression by RT-qPCR was then utilized for fluorescence experiments (Figure 4.13). The shRNA sequences chosen were ABCB1 clone B4 (CCGAACACATTGGAAGGAAAT: 94% decrease in expression) and ABCC1 clone E10 (CCACATGAAGAGCAAAGACAA: 71% decrease in expression). shRNA expressing U2-OS cells were selected for by maintenance in complete media supplemented with 2 µg/mL puromycin. Apart from this addition, culturing and subculturing of these cell lines was performed as described for normal U2-OS cells.

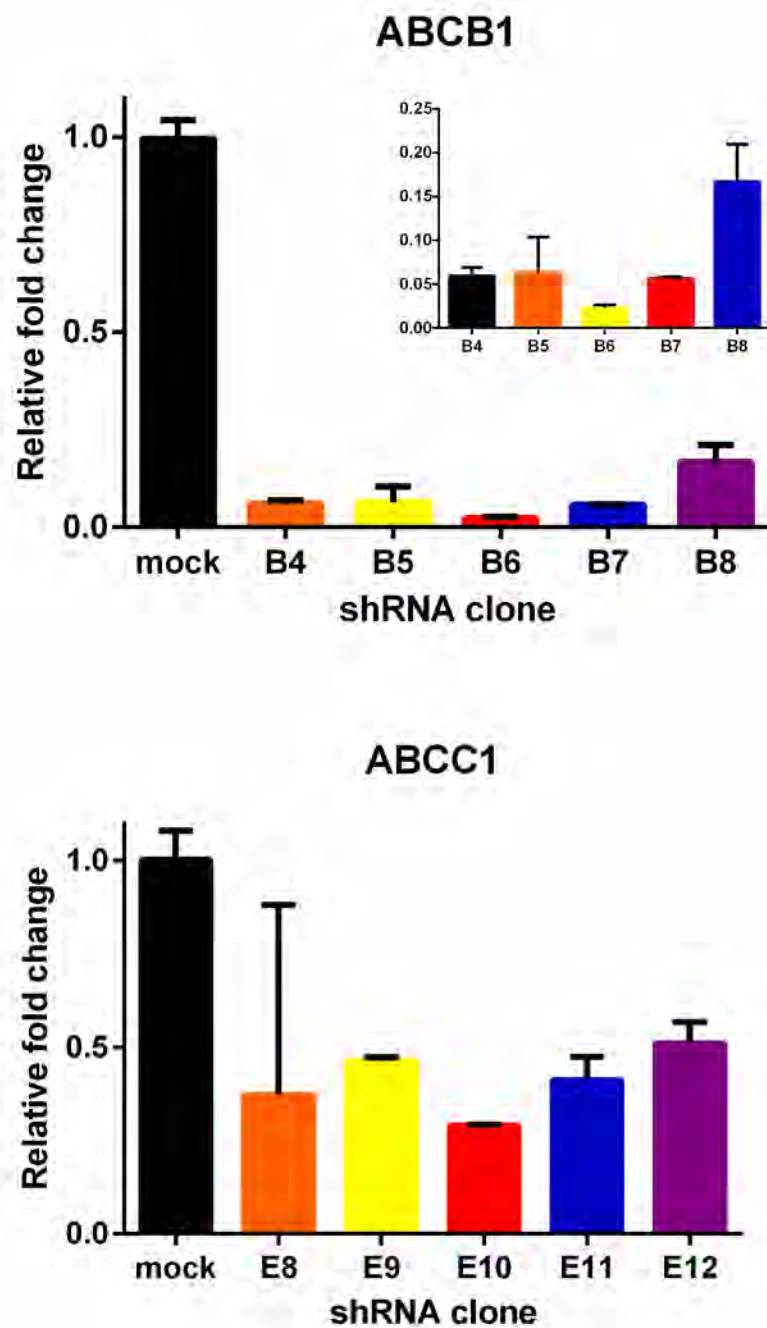


**Figure 4.13: RT-qPCR results of ABCB1 (top) and ABCC1 (bottom) expression in U2-OS cells expressing shRNA against the transporter. Mock: empty vector. Clones obtained from the University of Massachusetts Medical School RNAi Core Facility.**



### *Dye Treatment and Imaging*

Cells were subcultured as described for NIR experiments with the exception that growth media was supplemented with 2 µg/mL puromycin (provided by the Fazio Lab). No puromycin was used upon initiation of the experiment. Growth media was aspirated and cells were washed twice with HBSS. Cells were then incubated with 1 µM NIR dye in OPTI-MEM I for 15 minutes. Upon completion of dye treatment, the dye-labeling media was aspirated and the cells were washed twice with HBSS. After layering in fresh OPTI-MEM I, bright field and NIR images were collected. OPTI-MEM I was then aspirated, replaced with fresh OPTI-MEM I, and cells were incubated for an additional 20 minutes. OPTI-MEM I was aspirated and the cells were washed twice with HBSS, treated with fresh OPTI-MEM I, and then subjected to bright field and fluorescence microscopy. This process was repeated until imaging was concluded at 2 hours post dye treatment.

### **Spinning Disk Confocal Microscopy**

Prior to experiments, cells were subcultured into 35 mm plates fitted with a 14 mm collagen coated glass coverslip (MatTek) at a seeding density of  $0.05 \times 10^6$  cells. Cells were then incubated in complete media overnight.

Preceding dye treatment, growth media was aspirated and cells were washed twice with HBSS. Cells were then layered in 1 mL OPTI-MEM I and placed in a stage top incubator with a 5% CO<sub>2</sub> atmosphere and temperature maintained at

37 °C. DIC and NIR images were then collected for 2 to 5 minutes at a rate of 1 image/minute on a Nikon TE-2000E2 inverted microscope with a 40X Plan Apo oil objective using a Photometrics Coolsnap HQ2 camera. NIR emission was obtained by excitation with an argon ion laser (25 mW, 636 nm). During these initial images, a 2  $\mu$ M solution of NIR dye was prepared in OPTI-MEM I. Imaging of the cells was ceased and 1 mL of dye-labeling media was added to the cells to give a final dye concentration of 1  $\mu$ M. Cell imaging was immediately restarted and DIC/NIR images were collected at a rate of 1 image/minute for 30 to 40 minutes. Cell movies were then prepared using the Universal Imaging Metamorph software with playback at 1.5 frames/second.

### **Live Cell Cleavage of AcOTFMB-Sulfonate Ester**

#### *Dye Treatment*

Prior to experiments, cells were subcultured into 6-well plates at a seeding density of  $0.3 \times 10^6$  cells and grown to 80% confluency in complete media. Growth media was aspirated and cells were washed twice with HBSS. Cells were then incubated with 1  $\mu$ M NIR dye in OPTI-MEM I for 15-30 minutes. Dye uptake was monitored by wide field microscopy. Upon completion of dye treatment, the dye-labeling media was aspirated and the cells were washed twice with HBSS. Cells were then layered in fresh OPTI-MEM I and quickly imaged to confirm presence of intracellular dye fluorescence.

### *Cell Lysis and Dye Collection*

After imaging, OPTI-MEM I was removed by aspiration and the cells were covered with 2 mL 50% methanol/water and incubated at room temperature for 30 minutes. The cells were then lifted from the plate by scraping and transferred to eppendorf tubes. The wells of the plate were then washed twice with 1 mL 50% methanol/water with additional scraping and the washes were transferred to fresh eppendorf tubes. To complete lysis, the cell collections were voraciously vortexed and then frozen in liquid nitrogen. After freezing, the cell tubes were set aside to thaw at room temperature. The vortex/freeze/thaw cycle was then repeated two more times followed by centrifugation at 14,000 rpm for 15 minutes at room temperature. The supernatant containing the retrieved NIR dye was then concentrated on a SpeedVac while the pellet containing cell debris was discarded. The concentrated dye collections were then dissolved in 50% methanol/water, combined, and reconcentrated on a SpeedVac.

### *Reversed Phase-High Performance Liquid Chromatography Analysis*

Retrieved dye was analyzed by RP-HPLC on a 4.6 x 250 mm C-18 column using a Hewlett Packard Agilent 1100 HPLC equipped with a G1315A DAD absorbance detector. Absorbance detector was set at 800 nm for reference. Analysis was performed using aqueous 0.1% trifluoroacetic acid as Solvent A and acetonitrile/0.1% trifluoroacetic acid as Solvent B and were run at a flow rate of 1.4 mL/min. Retrieved dye samples were loaded onto column as 50%

acetonitrile/water solutions. **AcOTFMB-Ox**, **TFMB-Ox**, and **Sulf-Ox** dyes were used as controls for the analysis and were prepared from dilutions of the 10 mM DMSO stock in 50% acetonitrile/water.

Analytical HPLC method for all samples was 10% B for 5 minutes, 10-100% B over 90 minutes, 100% B for 10 minutes. Absorbances were measured at the following wavelengths:

**Ox-1** dyes: 280, 360, 603, 653, and 657 nm.

**Ox-2** dyes: 280, 360, 607, 653, and 660 nm.

#### *Electrospray Ionization-High-Resolution Mass Spectrometry*

ESI-HRMS spectra of samples collected from analytical HPLC were obtained on a Waters QToF Premier exact mass spectrometer. Data was used in combination with RP-HPLC to confirm the identity of the retrieved dye.

#### **NIR Imaging in Live Mice**

Live animal imaging was performed by Spencer Adams Jr. of the Miller lab at the University of Massachusetts Medical School. All protocols were performed within compliance with the Institutional Animal Care and Use Committee (IACUC) of the University of Massachusetts Medical School (IACUC: A-2474).

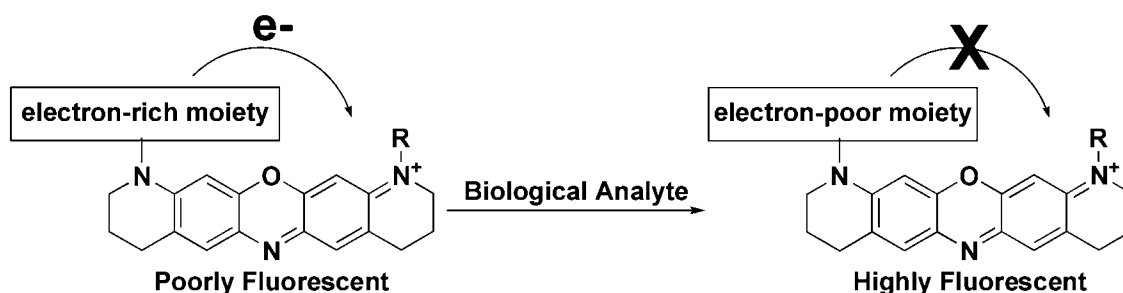
### *Dye Preparation*

Prior to mouse imaging, dyes were prepared in sterile PBS (Amicon<sup>®</sup> 10X PBS diluted 1:9 in Amicon<sup>®</sup> nuclease-free water). Each solution was then filtered through a 0.22 µm filter (Millex<sup>®</sup> GV 4mm filters).

### *Dye Treatment and Imaging*

C57BL/6 mice were weighed and then anesthetized with 2% isoflurane. Mice were transferred to the IVIS-100 imaging system from Xenogen<sup>®</sup>, (now a Perkin-Elmer company). Fluorescence imaging of the mice was performed with Cy5.5 filters (excitation: 615-665 nm, emission: 695-770 nm) or indocyanine green (ICG) filters (excitation: 710-760 nm, emission: 810-875 nm). Background subtraction was performed per the IVIS-100 manual. After collecting pre-injection images, mice were injected with 320 fm/kg dye, either intraperitoneally (ip) or into the tail vein (iv). Injections were performed with 27<sup>1/2</sup> gauge insulin syringes (Terumo<sup>®</sup> 0.5cc insulin syringes). Tails were pre-cleaned with alcohol-prep pads before injections and the alcohol-prep pad was used to apply pressure to the injection site post-injection to stop bleeding. Mice were imaged with the above filters immediately following injection and then again at a later time point (between 2 to 4 hours). Between the initial and final imaging periods, mice were returned to their cages and allowed to recover before re-inducing anesthesia. Imaging analysis was performed with Living Image 4.3.1 software (Caliper Life Sciences Inc.<sup>®</sup>, now Perkin-Elmer).

## Chapter V: Synthesis and characterization of near-IR oxazine sensors of pH and nitric oxide



### Summary

Fluorescence based biological sensors commonly employ photoinduced electron transfer (PET) to quench the sensor until it encounters its analyte of interest. The fluorescence of near-infrared (NIR) oxazine dyes is known to be efficiently modulated by PET, yet there are almost no fluorescence sensors using this scaffold. Here, we report the synthesis and *in vitro* evaluation of NIR oxazines that function as fluorescent sensors of either nitric oxide or changes in pH.

### Introduction

Fluorescent sensors are useful reagents for reporting on cellular conditions. For example, biologically relevant ions such as sodium, calcium and zinc have been monitored with fluorescein and rhodamine derivatives (Kikuchi et al., 2004; Martin et al., 2004; Martin et al., 2005; Minta et al., 1989). Reactive

oxygen and nitrogen species have also been detected using derivatives of fluorescein, rhodamine and BODIPY (Barta et al., 2002; Gabe et al., 2006; Koide et al., 2007; Kojima et al., 1998; Kojima et al., 2001). Yet, despite the variety of sensors available for biology, most of these fluorophores are poorly suited for use within cells and organisms. This is because most commonly used fluorophores absorb and emit visible light. The presence of endogenous fluorophores in cells (e.g., NADPH and flavins) that also absorb and emit visible light results in high autofluorescence background (Andersson-Engels et al., 1997; Monici, 2005). The situation is exacerbated *in vivo* due to the presence of hemoglobin, which strongly absorbs visible light and dramatically decreases the signal to noise ratio (Hilderbrand and Weissleder, 2010; König, 2000). Together, these factors render visible wavelength fluorophores essentially useless for detecting cellular changes in living organisms. Near-infrared (NIR) light (650-900 nm) is more suited for biological applications than visible light as cells do not fluoresce in the NIR and few endogenous molecules absorb long wavelength light (Escobedo et al., 2010; Frangioni, 2003; Guo et al., 2014; Hilderbrand and Weissleder, 2010 ). Due to the poor absorption of NIR light by biological molecules, NIR light penetrates deeper into tissue and is less phototoxic than visible light (Escobedo et al., 2010; Frangioni, 2003; Ghoroghchian et al., 2009; Guo et al., 2014; Hilderbrand and Weissleder, 2010; Kobayashi et al., 2010). Thus, NIR light is considered to be in the optimal spectral window for cellular and

*in vivo* imaging and it follows that NIR fluorophores are the most suited for detecting changes within cellular environments.

Most NIR probes are derived from four primary scaffolds: BODIPYs, indocyanines, oxazines, and most recently, silicon-functionalized rhodamines (Si-rhodamines). Of these scaffolds, heptamethine indocyanines, such as IR780 and IR783, have been exhaustively employed in biology as both stains and sensors (Figure 5.1) (Karton-Lifshin et al., 2011; Li et al., 2011; Sasaki et al., 2005; Tian et al., 2011; Xu et al., 2012; Yang et al., 2010; Zhang et al., 2010). This is due both to the photophysical properties of the dyes (peak absorbance of 780 nm or higher) and the synthetic ease with which these dyes can be functionalized. However, despite their extensive use as imaging reagents, NIR indocyanines have several drawbacks. First, non-sulfonated, IR780 type dyes are large, planar, hydrophobic molecules that tend to aggregate within aqueous environments, such as the cytosol (Peng and Draney, 2004; Mishra et al., 2000). Second, these dyes are cationic and, inside cells, will accumulate within the negatively polarized membrane of the mitochondria (Bunting et al., 1989; Perry et al., 2011). These features limit the cellular imaging utility of indocyanine dyes. On the other hand, sulfonated indocyanines, such as IR-783, are water-soluble; yet, the negative charge of the dye prevents the compound from traversing the plasma membrane (Berridge et al., 2005; Stolz, 2001; Wuhrmann et al., 1980).



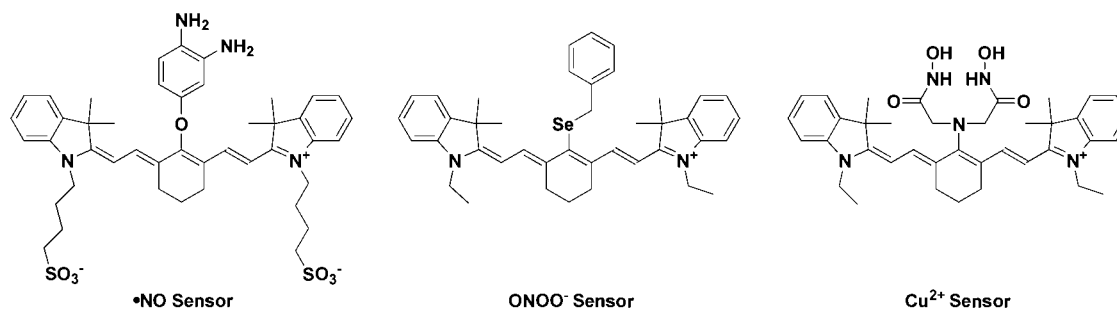


**Figure 5.1: IR780/783-derived fluorescent sensors** (Li et al., 2011; Sasaki et al., 2005; Tian et al., 2011).

Along with the need to circumvent the negative aspects associated with NIR indocyanines, there is a need to expand the palette of NIR tools for biological imaging in general. Some efforts to do this have focused on functionalizing the BODIPY scaffold, both to red shift the wavelength and enable the dye to interact with ions and small molecules (Figure 5.2) (Coskun et al., 2007; Hall et al., 2006; Matsui et al., 2011; Ni and Wu, 2014). Visible light emitting BODIPYs have very favorable photophysical characteristics including high extinction coefficients and high quantum yields (Gabe et al., 2006, Karolin et al., 1994). While some of these features are observed in NIR BODIPYs, these molecules tend to be extremely hydrophobic, and thus suffer the same problems associated with indocyanines (Ni and Wu, 2014).

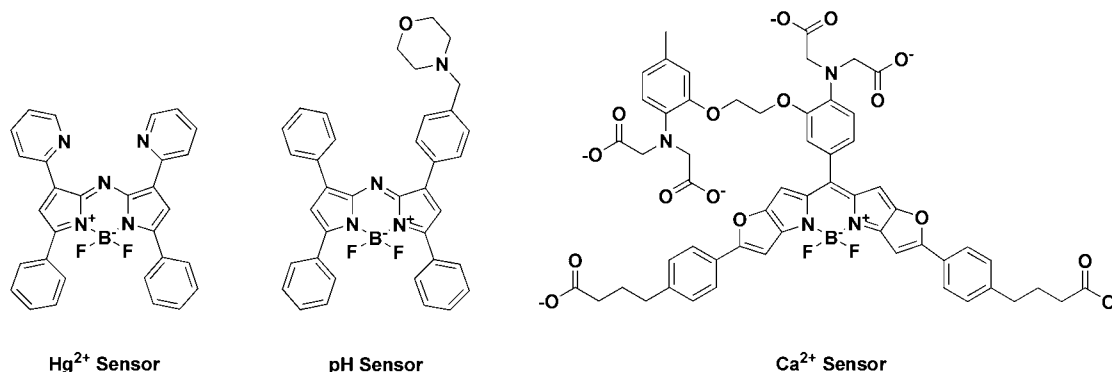


**Figure 5.2: NIR BODIPY and Aza-BODIPY fluorescent sensors** (Coskun et al., 2007; Hall et al., 2006; Matsui et al., 2011).

Although the majority of NIR dyes derivatized for biological sensing are based on cyanines and BODIPYs, another NIR scaffold, pentacyclic oxazine, has several characteristics that would favor its use for sensing small molecules (Figure 5.3). The NIR oxazine scaffold is more compact than either NIR indocyanines or BODIPYs. This reduces the hydrophobic surface area available for undesirable dye dimerization and binding to serum proteins observed among cyanines (Grabolle et al., 2014; Moody, et al., 1999; Muckle, 1976). Oxazines also exhibit higher photostability than cyanines, which is desirable when imaging for extended periods (Anzalone et al., 2013; Vogelsang et al., 2009). NIR oxazines have also been successfully employed for both live cell and *in vivo* imaging (Hintersteiner et al., 2005, Stöhr et al., 2010; van de Linde et al., 2012). Despite all these beneficial features, NIR oxazines are rarely employed as fluorescent sensors.

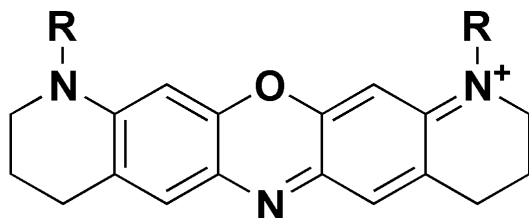


**Figure 5.3: NIR oxazine scaffold.**

The essential feature of fluorescent sensors is a measurable change in fluorescence, e.g. emission intensity or wavelength, upon interaction with the analyte of interest (Lemke and Schultz, 2011; Schäferling, 2012). An increase in fluorescence intensity upon analyte detection is a favored strategy for fluorescent sensors. One simple and highly utilized way to prepare a NIR fluorophore with reversibly quenched fluorescence is through photoinduced electron transfer (PET) (Ni and Wu, 2014; Song et al., 2005). PET is a non-destructive form of fluorescence quenching which employs an electron rich functionality (PET donor) to prevent radiative relaxation of a fluorophore's excited electron after photon absorption (Figure 5.4) (Bryan et al., 1989; Doose et al., 2009; Fox, 1990). PET-based turn-on fluorescent sensors function by using a PET donor that reacts with the target analyte, converting it to an electron-poor moiety (Bryan et al., 1989). This electron-poor moiety is unable to quench fluorescence thus permitting the fluorophore to relax radiatively.

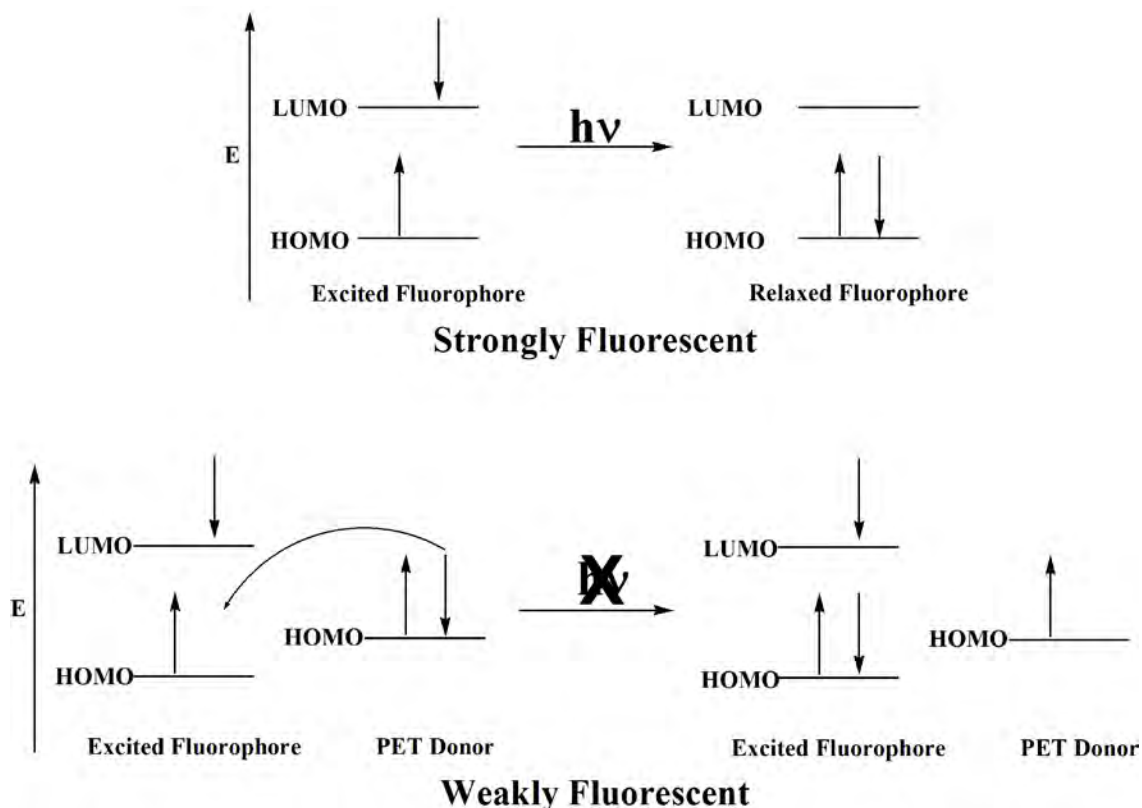


**Figure 5.4: Quenching of fluorescence via photoinduced electron transfer (PET).** Photon absorption results in electron promotion from the ground state HOMO to a singlet LUMO. Top: An unquenched fluorophore will relax via photon emission after absorbing light. Bottom: The PET donor, having ground state electrons in a HOMO of higher energy than the ground state of the fluorophore, can donate an electron to the evacuated fluorophore orbital thus preventing the excited electron from relaxing via photon emission.

Despite the use of PET as a quenching mechanism for numerous fluorescent sensors, it is generally less effective in modulating the fluorescence of long wavelength emitting fluorophores compared to visible light emitting dyes (Ozmen and Akkaya, 2000; Song et al., 2005). However, NIR oxazines are an exception to that rule. The fluorescence of NIR oxazines is known to be well modulated by PET (Doose et al., 2009; Marmé et al., 2003; Stöhr et al., 2010;

Valana et al., 2003). Sauer's group found that the fluorescence of the NIR oxazines MR121 and ATTO655 is efficiently quenched by tryptophan (Marmé et al., 2003). His group has also shown that the nucleotide guanosine can modulate the fluorescence of MR121 and another oxazine derivative, JA242, (Lieberwith et al., 1998; Sauer et al., 1995). Based on this feature, the Herten lab successfully developed a low background NIR oxazine probe for labeling intracellular proteins by conjugating the dye to an O<sup>6</sup>-benzylguanine moiety (Stöhr et al., 2010). Fluorescence of the dye is only restored upon removal of the guanine by SNAP tag fused-proteins (Keppler et al., 2003; Stöhr et al., 2010). Clearly, the modulatable fluorescence, high photostability, and favorable structural features of the pentacyclic oxazine make this a desirable scaffold for use in sensing technology. Seeing an opportunity to expand the palette of NIR fluorescent sensors, we set out to develop oxazine-based sensors of nitric oxide and pH.

### ***Results and Discussion***

Due to its role as a biological second messenger in a plethora of cellular pathways, the small radical nitric oxide (NO) has long been a target for sensing technologies (Akaike et. al., 2000, Hall and Garthwaite, 2009). The concentration of nitric oxide in living cells is very low and thus detecting NO in living systems requires methods with a high degree of sensitivity (Hall and Garthwaite, 2009). Fluorescence imaging has the high sensitivity desired for detecting low concentrations of a substance and NIR fluorescence imaging is aptly suited for

use in cells (Lakowicz, 2006). We therefore sought to develop a NIR oxazine-derived NO sensor.

One compound commonly employed as a PET donor for nitric oxide sensors is *o*-diaminobenzene (Figure 5.5) (Pluth et al., 2011). The unbound electron pairs of the two exocyclic amines make this an electron rich molecule. However, in the presence of NO, *o*-diaminobenzene reacts to form the electron-poor benzotriazole, which cannot function as a PET donor due to the electron withdrawing -N=N- and resonance -C=N- functionalities (Figure 5.5). This reaction provides the mechanism by which fluorescence can be modulated. The Nagano lab utilized this strategy in the preparation of NO sensors derived from fluorescein, rhodamine, BODIPY and indocyanine dyes (Gabe et al., 2004; Gabe et al., 2006; Hirotsu et al., 2000; Kojima et al., 2001; Sasaki et al., 2005); several of these compounds, diaminofluorescein-FM (DAF-FM), diaminorhodamine-FM (DAR-FM), and diaminorhodamine-4M (DAR-4M), are now commercially available. It should be noted that the *o*-diaminobenzene group does not directly react with nitric oxide, but with NO oxidation products that are rapidly formed in aqueous, aerobic environments (Figure 5.5) (Ignarro et al., 1993; Kojima et al., 1998; Kojima et al., 2001; Pluth et al., 2011). It has also been observed that *o*-diaminobenzene-based NO sensors are sensitive to dehydroascorbic acid and ascorbic acid (Pluth et al., 2011; Zhang et al., 2002). However, the focus of our work was to determine whether NIR oxazines could function as sensors for biological analytes; therefore, despite the limitations associated with the *o*-

diaminobenzene PET donor, we choose to functionalize our sensors with this moiety.

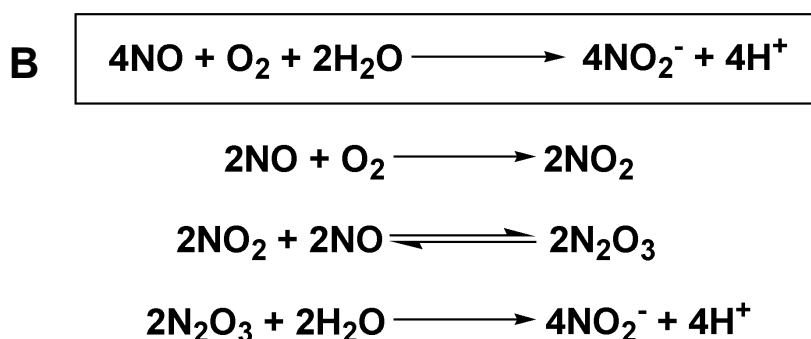
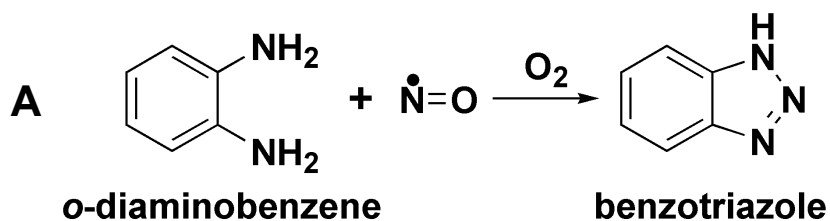


**Figure 5.5: The electron rich o-diaminobenzene reacts with nitric oxide to produce the electron poor benzotriazole.** A) Aerobic reaction of o-diaminobenzene with NO. o-Diaminobenzene actually reacts with oxidation products of NO, such as N<sub>2</sub>O<sub>3</sub> (Kojima et al., 2001). B) Oxidation reactions of NO in water.

PET is a short distance interaction, generally requiring van der Waals contact between donor and acceptor for effective quenching (Hush et al., 1985; Marmé et al., 2003). A commonly employed design used for fluorescent sensors to provide this contact is the fluorophore-spacer-PET donor structure (Figure 5.6) (Bryan et al., 1989; Hall et al., 2006). We thus modeled our sensor with the PET

donor separated from the dye by spacers of 1 to 3 methylene groups (Figure 5.7). Molecular modeling suggested that the three carbon propylene spacer would allow the closest approach between donor and fluorophore with a predicted separation of 5.4 Å. Based off of this design, we set out to synthesize our NIR oxazine-based NO sensor.

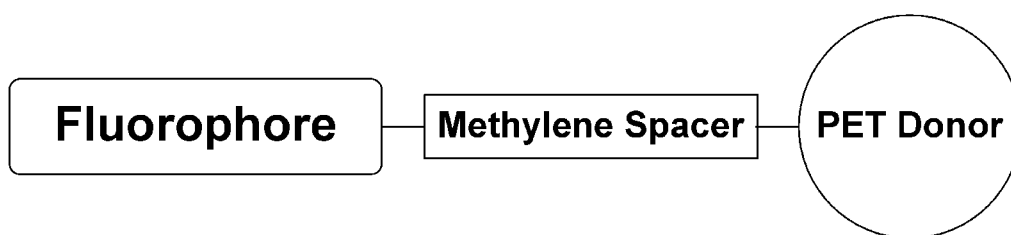


**Figure 5.6: General architecture for design of fluorescent sensor.**



**Figure 5.7: Molecular modeling reveals that a 3-carbon spacer between the NIR oxazine scaffold and o-diaminobenzene allows the closest approach between PET donor and acceptor.** A. Methylene spacer; B. Ethylene spacer; C. Propylene spacer. i. Chemical structure. ii. Ball and stick model showing closest distance obtainable between PET donor and dye scaffold. iii. van der Waals surface of PET-quenched dye structure. Molecular modeling performed by Brendan Hilbert.

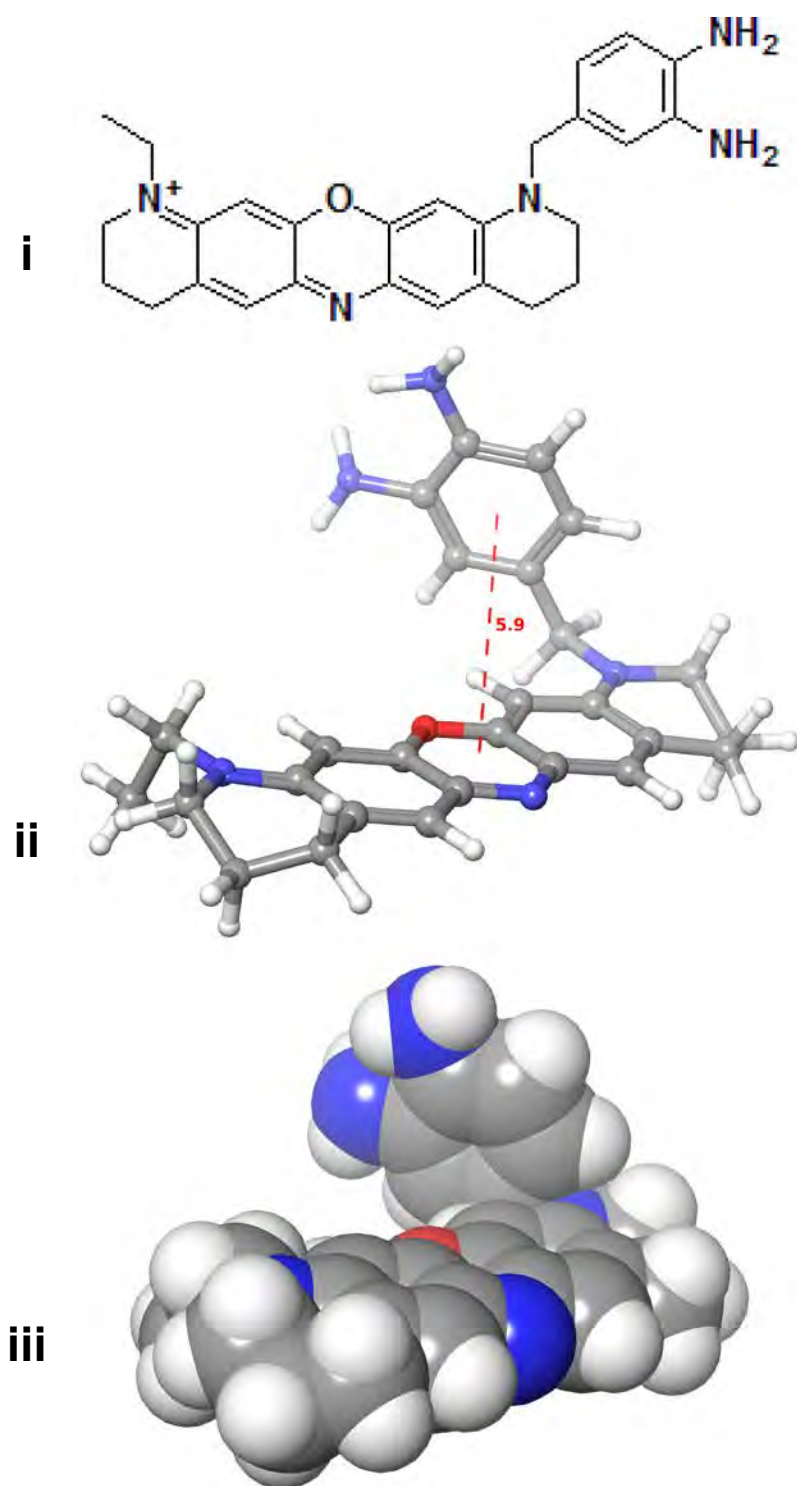


**Figure 5.7A.** *in silico* model of NO sensor with PET donor and dye separated by methylene spacer.

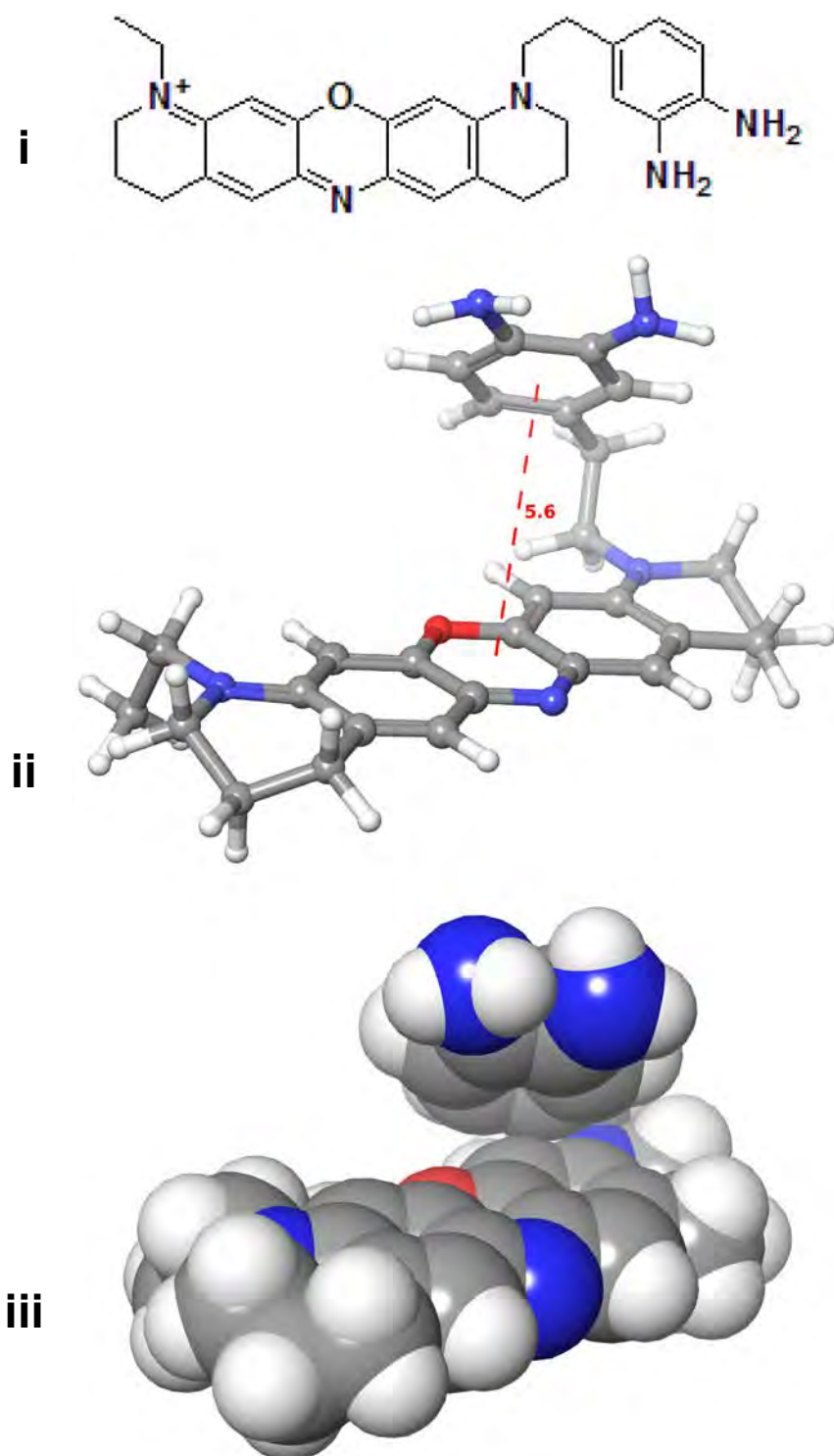


**Figure 5.7B.** *in silico* model of NO sensor with PET donor and dye separated by ethylene spacer.

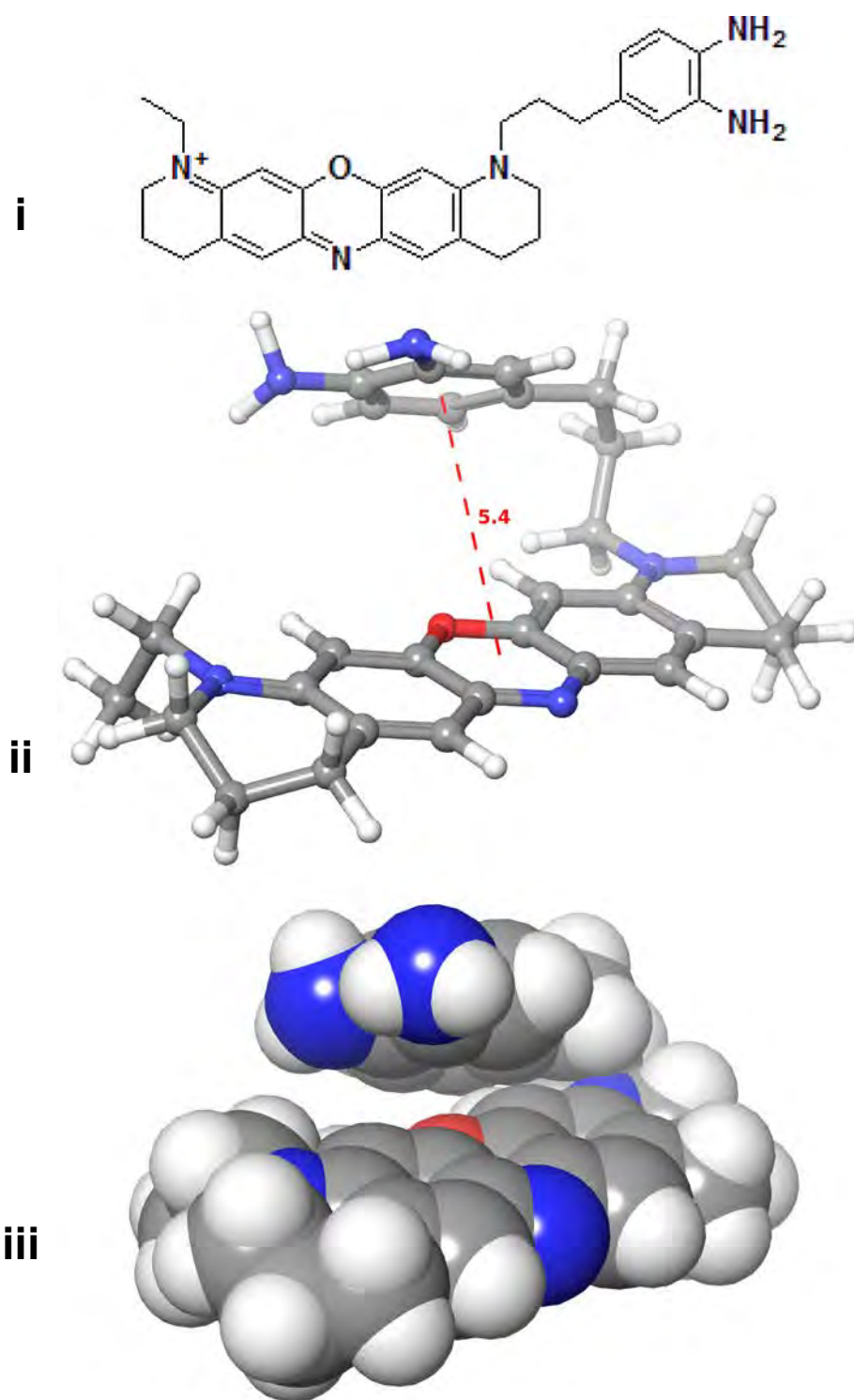
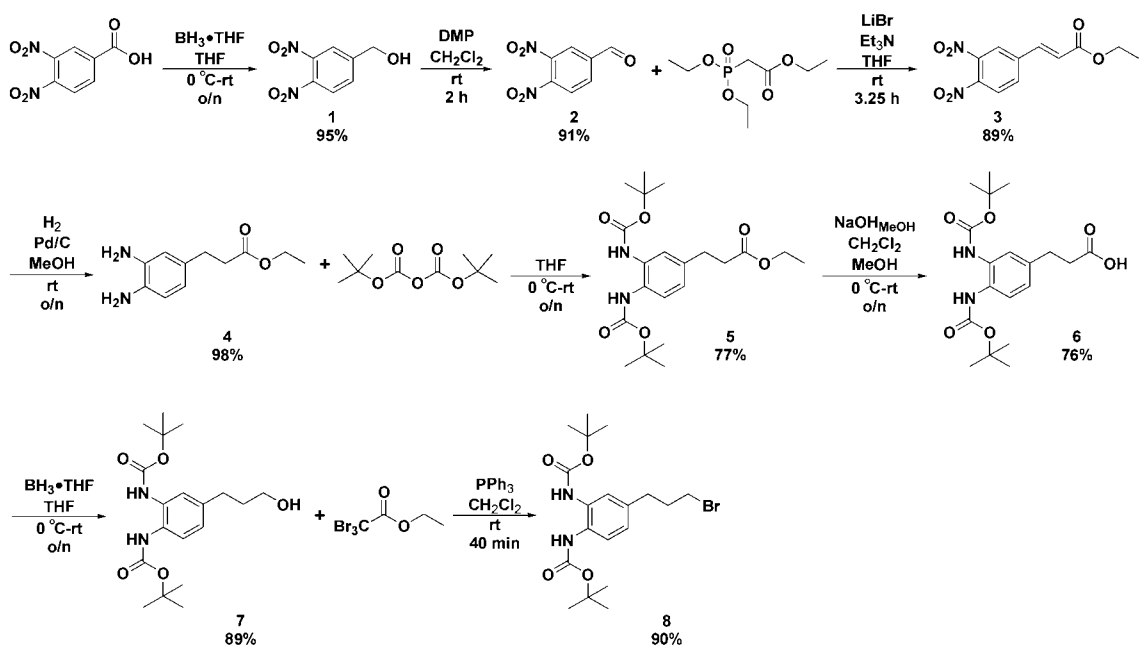


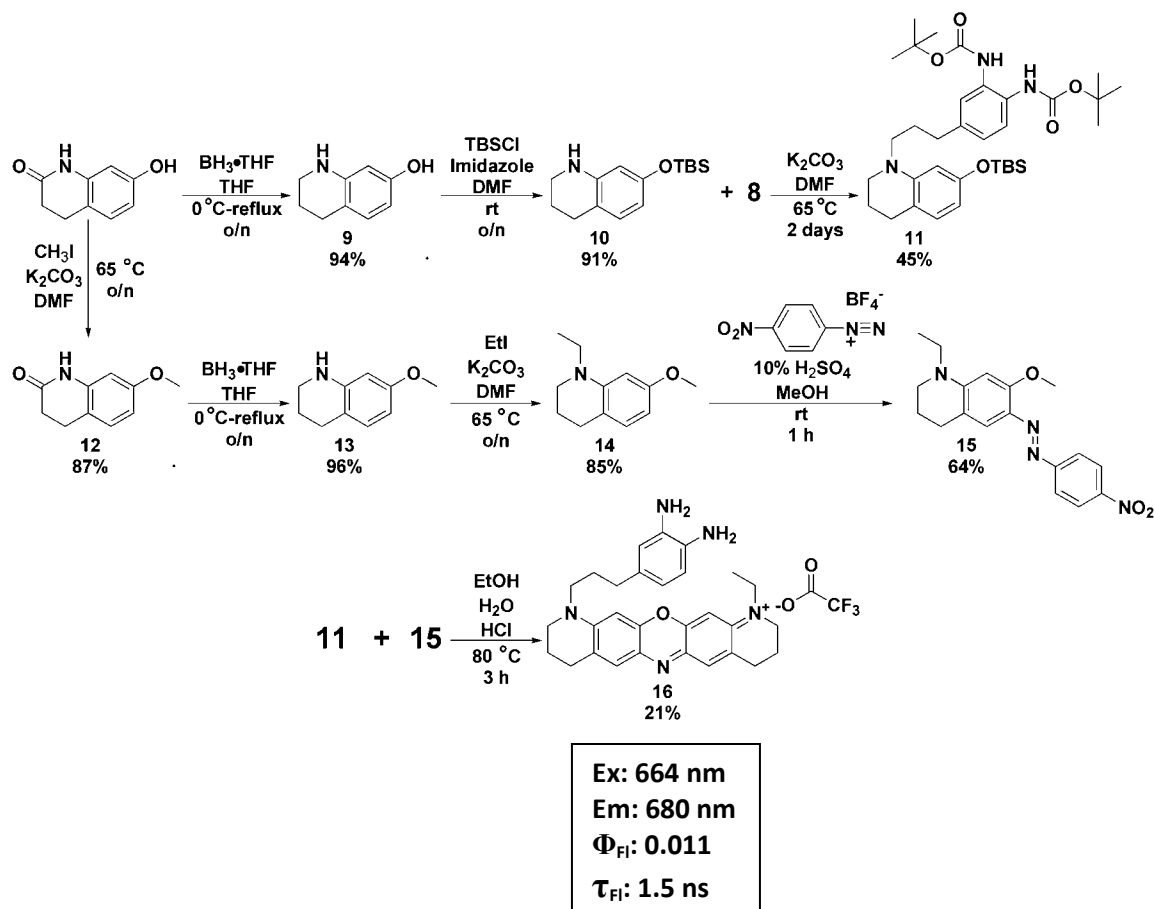
**Figure 5.7C.** *in silico* model of NO sensor with PET donor and dye separated by propylene spacer.

We first prepared the PET donor-spacer portion of the sensor (Scheme 5.1). Beginning with 3,4-dinitrobenzoic acid, the corresponding benzaldehyde **2** was prepared via borane reduction and Dess-Martin oxidation. 3,4-Dinitrobenzaldehyde was homologated via a Horner-Wadsworth-Emmons reaction **3** to prepare the 3-carbon linker needed for attachment to the dye core. Palladium catalyzed hydrogenation resulted in alkene and nitro reduction to give 3-(3,4-diamino-phenyl)-propionic acid ethyl ester **4**. To prevent further reaction at the aromatic exocyclic amines, the compound was Boc-protected **5**. Finally, saponification, borane reduction, and bromination resulted in the Boc-protected PET donor **8** in high yield.



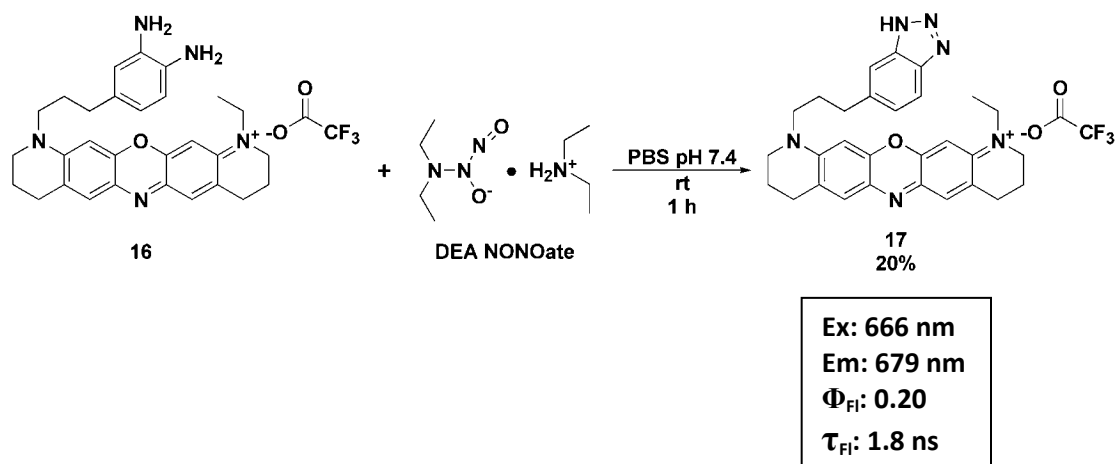
**Scheme 5.1: Synthesis of PET donor for oxazine-based nitric oxide sensor.**

Oxazine dyes are generally formed by condensation of an arylazo compound with an aminophenol (Hintersteiner et al., 2005). Previous work in our lab has found that TBS protection of the phenol increases the yield of amino alkylation for dye functionalization and does not interfere with oxazine dye synthesis (Pauff and Miller, 2011; Pauff and Miller 2013). We therefore employed this method for synthesis of the NO sensor (Scheme 5.2). 3,4-Dihydro-7-hydroxy-2(1*H*)-quinolinone was first reduced to 1,2,3,4-tetrahydroquinolin-7-ol **9** followed by TBS protection **10**. N-alkylation of **10** with the PET donor **8** produced the first half of the dye scaffold **11**. The arylazo portion of the dye **15** was synthesized from 3,4-dihydro-7-hydroxy-2(1*H*)-quinolinone via O-methylation, borane reduction, N-ethylation, and diazo coupling. Condensation of **11** and **15** in refluxing aqueous, acidic ethanol provided us with the PET-quenched NIR oxazine nitric oxide sensor **16**.



**Scheme 5.2: Synthesis of oxazine-based nitric oxide sensor.**

We next synthesized the benzotriazole form of our oxazine sensor **17** by treating **16** with the NO donor DEA NONOate (Scheme 5.3); formation of the product was confirmed via analytical HPLC and high-resolution mass spectrometry (Figure 5.8). Having obtained both the *o*-phenylenediamine **16** and benzotriazole **17** forms of the dye, we next sought to examine the photophysical properties of the compounds to determine whether the quenching strategy was successful.



**Scheme 5.3: Synthesis of unquenched (fluorescent) form of nitric oxide sensor.**



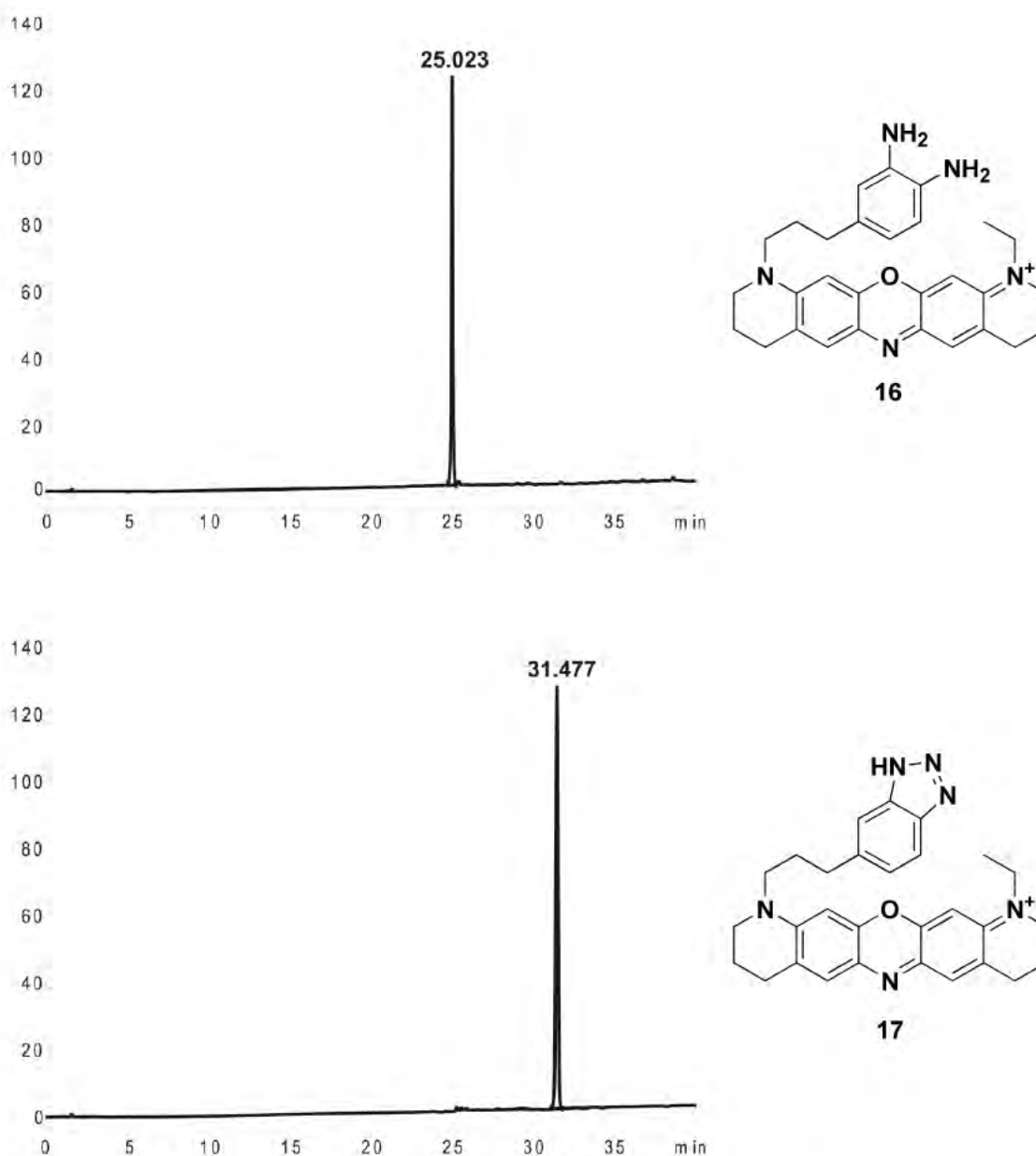


**Figure 5.8: Reaction of 16 with nitric oxide produces the benzotriazole functionalized NIR oxazine 17. Top: HPLC trace of compound 16. Bottom: HPLC trace of compound 16 treated with nitric oxide. Reaction produces a benzotriazole from *o*-phenylenediamine.**

Absorption and emission spectra of **16** and **17** were obtained in PBS (Figure 5.9 and 5.10). While there was little change in the emission wavelengths between the two dyes, the integrated fluorescence intensity of the unquenched dye **17** was 7-fold higher than that of the parent dye **16** (Figure 5.11). Although the fluorophore and PET donor are covalently connected, they are unconjugated; therefore, the ground state electronics of the oxazine dye in **16** and **17** are unchanged (Hall et al., 2006). This means that dyes **16** and **17** should absorb light with equal efficiency and thus, the low photon output of the NO sensor must be related to a decreased ability to relax radiatively (Figure 5.9). In other words, the fluorescence of **16** is quenched. This quenching was confirmed by comparing the fluorescence quantum yields of the two dyes. Fluorescence quantum yield ( $\Phi_{\text{F}}$ ) is a function of both the photons emitted and the photons absorbed by a compound (Equation 5.1).

$$5.1 \quad \Phi = \frac{\textit{photons emitted}}{\textit{photons absorbed}}$$

The quantum yield of NO sensor **16** was decreased to less than 6% of that of the unquenched benzotriazole dye **17** (Table 5.1). Thus, assuming equal efficiency in photon absorption, **16** does not efficiently fluoresce. As the only difference between NIR oxazines **16** and **17** is the presence of the PET donor on **16**, it can be concluded that the fluorescence of the oxazine dye is being quenched by PET.

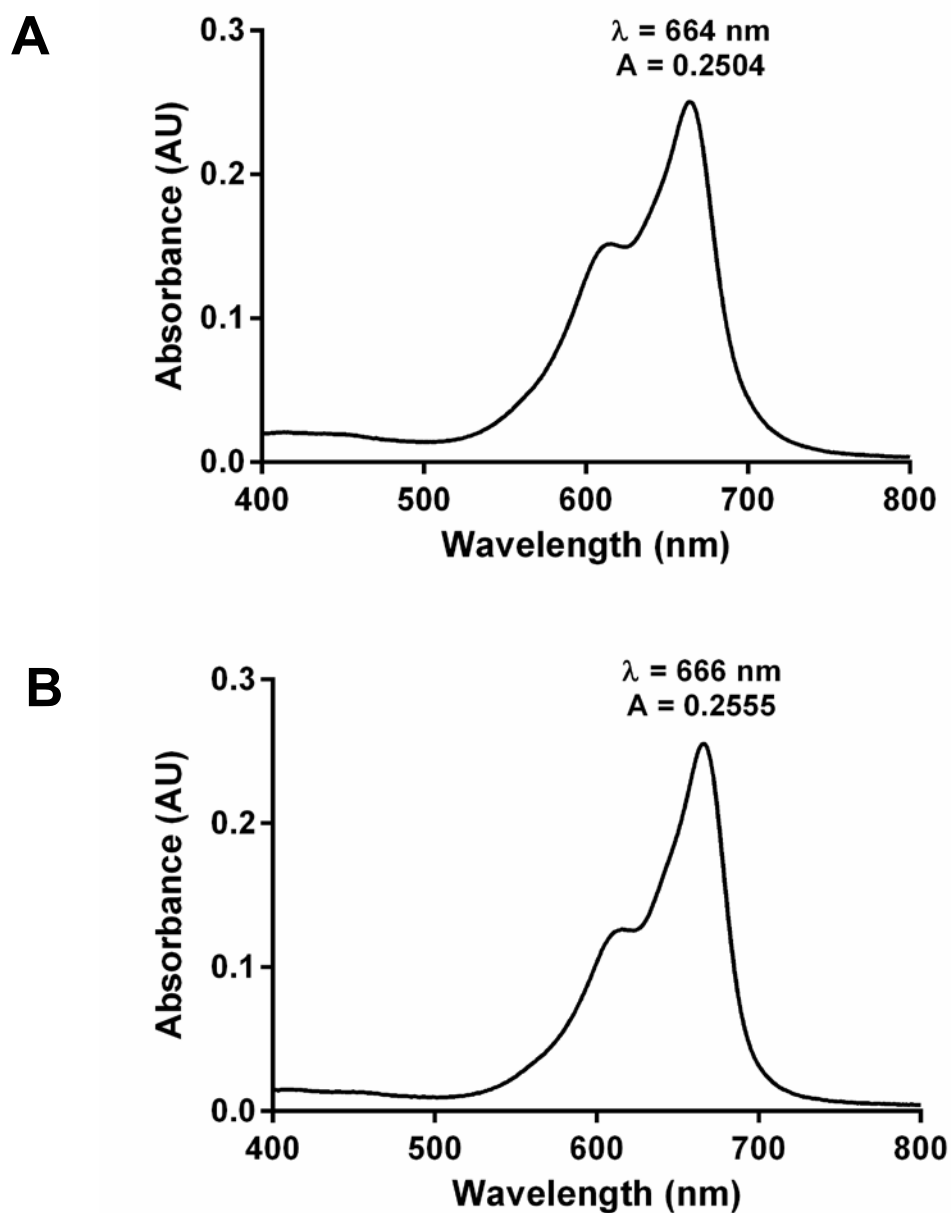


**Figure 5.9: Absorbance spectra of 16 and 17 in PBS, pH 7.4.** 10 mM DMSO stocks of **16** (A) and **17** (B) were dissolved in 1X PBS, pH 7.4 to give a final concentration of 10  $\mu\text{M}$ . AU: absorbance units.

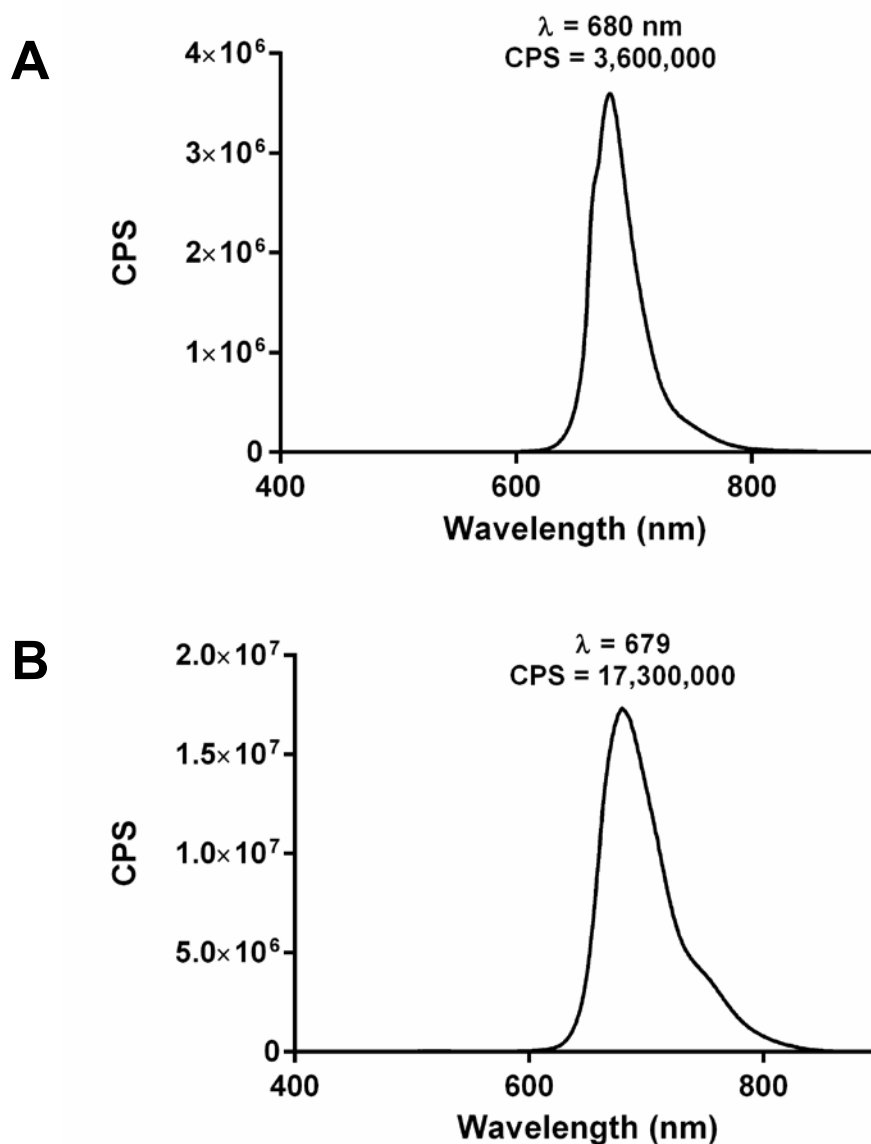


**Figure 5.10: Emission spectra of 16 and 17 in PBS, pH 7.4.** 10 mM DMSO stocks of **16** (A) and **17** (B) were dissolved in 1X PBS, pH 7.4 to give a final concentration of 10  $\mu\text{M}$ . Fluorescence intensity was measured using excitation at 665 nm for both **16** and **17**. Excitation/Emission slit width: 5 nm. CPS: counts per second.

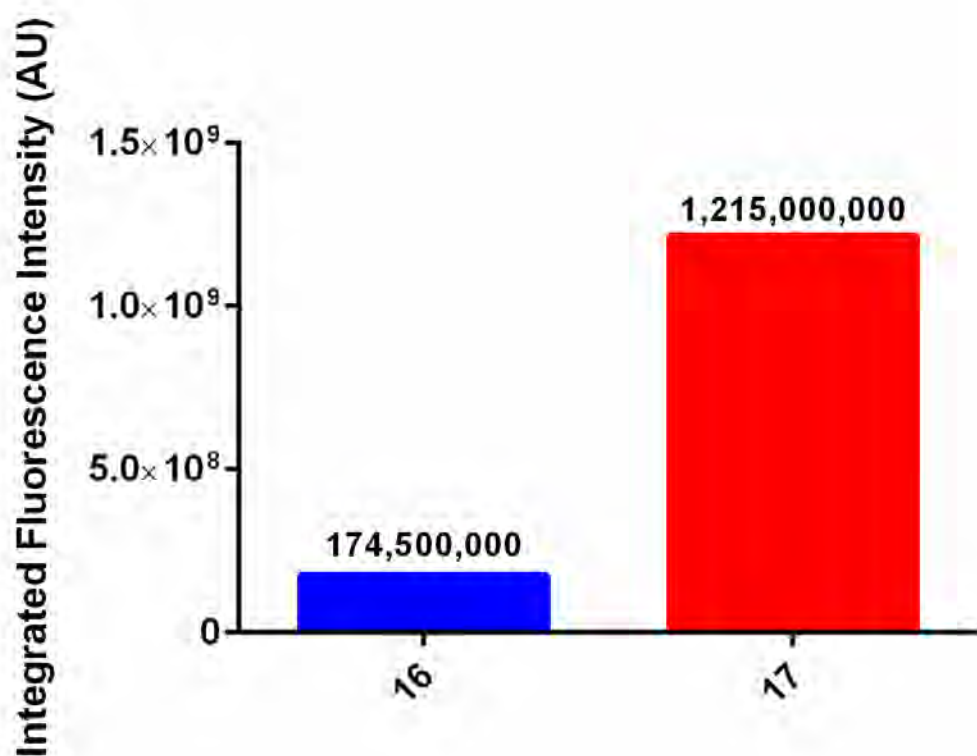


**Figure 5.11: Integrated fluorescence intensity of 10  $\mu$ M 16 and 17 in PBS, pH 7.4.** 10 mM DMSO stocks of quenched NO Sensor **16** and unquenched benzotriazole **17** were dissolved in 1X PBS, pH 7.4 to give a final concentration of 10  $\mu$ M. Fluorescence intensity was measured using excitation at 665 nm for both **16** and **17**. Excitation/Emission slit width: 5 nm. Integrated fluorescence intensity was obtained by integrating the area under the emission curves from 400-900 nm. AU: arbitrary units.

Compound	16	17
$\lambda_{\text{Ex}}$ (nm)	664	666
$\lambda_{\text{Em}}$ (nm)	680	679
$\Phi_{\text{Fl}}$	0.011	0.20
$\tau_{\text{Fl}}$ (ns)	1.5	1.8

**Table 5.1: Photophysical properties of 16 and 17 in PBS, pH 7.4.** Excitation and emission wavelengths and quantum yield were obtained using a 10  $\mu\text{M}$  final dye concentration. Fluorescence lifetime was measured using a 1  $\mu\text{M}$  final dye concentration.  $\lambda$ : wavelength.  $\Phi_{\text{Fl}}$ : fluorescence quantum yield.  $\tau_{\text{Fl}}$ : fluorescence lifetime.

Having confirmed that *o*-diaminobenzene can function as a PET donor for modulating NIR oxazine fluorescence, we wanted to determine the mechanism of quenching; i.e., static versus dynamic quenching. Static quenching is defined by formation of a ground state molecular complex that is non-fluorescent (Lakowicz, 2006; Marmé et al., 2003). Dynamic quenching results from any energetic process, electronic or kinetic, that depopulates the excited state of the fluorophore (Lakowicz, 2006). These two mechanisms are distinguished by comparing the fluorescence lifetimes of the quenched and unquenched fluorophore; in other words, how long the molecule stays in the excited state before relaxing via fluorescence. In static quenching, the lifetimes of the quenched and unquenched fluorophore will be similar, but fewer photons will be observed from the quenched fluorophore. Therefore, for equal concentrations of quenched and unquenched dye, the quenched compound will appear to be at a

lower concentration than the unquenched molecule. During dynamic quenching, the length of the lifetime itself is shortened.

Using time-correlated single-photon counting (TCSPC), we measured the fluorescence lifetime of 1  $\mu\text{M}$  **16** and **17** in PBS, pH 7.4 (Figure 5.12). The data was curve-fitted with a combination of two exponentials suggesting that the lifetime of both **16** and **17** consists of two components (Table 5.2). The narrowing of the exponential decay curve of **16** as compared to **17** in Figure 5.12 clearly indicates a decrease in the fluorescence lifetime of **16**. As shown in Table 5.2, the lifetime of **16** has decreased by approximately 0.33 ns. This indicates that the fluorescence of our NO sensor is being dynamically quenched, a mechanism which can be directly correlated to the activity of PET. However, our results also indicate a significant degree of static quenching. The pre-exponential amplitude (A) of the fitted curve describes the quantity of photons involved in a given fluorescence lifetime. Based on the curve-fitted value of the amplitudes shown in Table 5.2, more than 99% of the photons of **16** appear to be associated with a lifetime of 3 ps. This is beyond the instrument's measurement capacity and suggests the presence of a molecular species that relaxes almost instantaneously following photon absorption; i.e., a non-fluorescent complex. Thus, PET quenching of the NO sensor appears to involve both of the known quenching mechanisms.

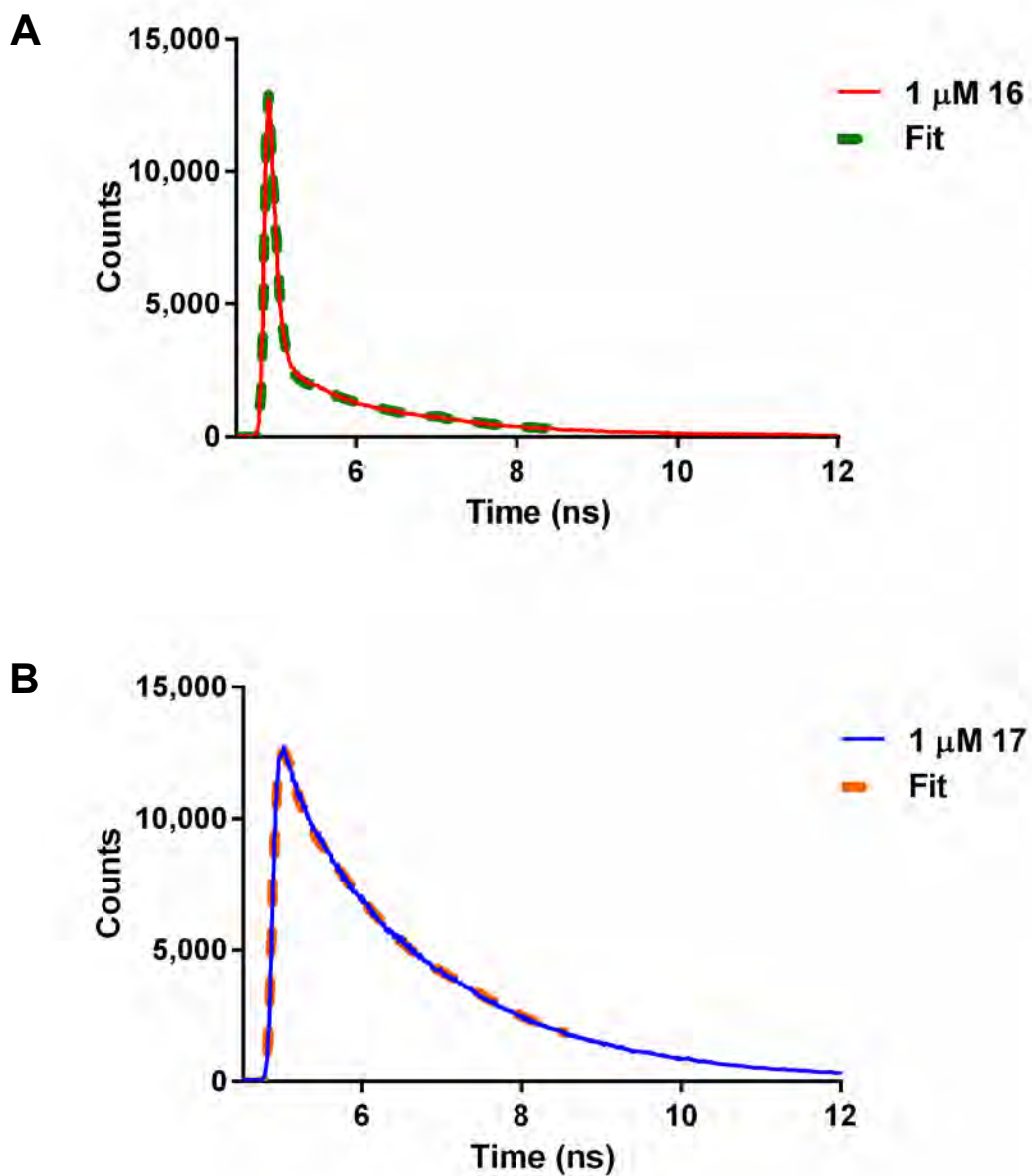


**Figure 5.12: Time correlated single photon counting (TCSPC) suggests a complex mechanism for quenching of NIR oxazine-derived NO sensor 16.** Fluorescence decay of 1  $\mu\text{M}$  **16** (A) and **17** (B) in 1X PBS, pH 7.4 was measured using TCSPC as described (see Methods). Data was fit using a sum of exponentials plus a constant.



Compound	16	17
$\tau_{FI(1)}$ (ns)	1.46 +/- 1.83E-3	1.79 +/- 1.12E-3
<b>A<sub>1</sub></b> (% total photons)	0.9%	53%
$\tau_{FI(2)}$ (ps)	3.54 +/- 0.281	76.2 +/- 9.49
<b>A<sub>2</sub></b> (% total photons)	99.1%	47%
$\chi^2_{red}$	3.8	1.86

**Table 5.2: Values for curve fitting of TCSPC data.**  $\tau_{FI}$ : Exponential time constant. A: Pre-exponential amplitude. Values were calculated from a global analysis of a dilution series of the dyes (100  $\mu$ M, 50  $\mu$ M, 25  $\mu$ M, 10  $\mu$ M, 1  $\mu$ M) using non-linear least squares fitting as described in methods (Dilution series not shown). The reduced chi squared values of the fits are slightly higher than ideal due to the excess number of photons employed in the analysis. While this prevented the residuals from achieving the desired randomness, it afforded an ideal fit that could be reproduced throughout the dilutions.

Upon observing that the fluorescence of **16** is indeed quenched via PET (Figure 5.12), and that this quenching can be relieved by treatment with nitric oxide (Figure 5.11), we needed to confirm that our sensor was actually specific for nitric oxide. Besides nitric oxide, living organisms contain a variety of other highly reactive molecules, including other nitrogen and oxygen species: nitrate ( $\text{NO}_3^-$ ), nitrite ( $\text{NO}_2^-$ ), superoxide anion ( $\text{O}_2^-$ ), hydrogen peroxide ( $\text{H}_2\text{O}_2$ ), and hydroxyl radical ( $\text{OH}^\cdot$ ), to name just a few (Ignarro et al., 1993; Novo and Parola, 2008; Ray et al., 2012; Stuehr and Marletta, 1987). Work in the Nagano lab has shown that BODIPY sensors functionalized with *o*-diaminobenzene are specific for nitric oxide over other RNS and ROS. Reaction with NO showed a 280-fold

increase in fluorescence intensity over the untreated compound, compared to only a 2 to 3-fold increase from reaction with the other reactive species (Gabe et al., 2004). To confirm that this feature also held for our oxazine-based NO sensor, 1  $\mu\text{M}$  **16** was treated with ROS ( $\cdot\text{OH}$  and  $\text{H}_2\text{O}_2$ ) and RNS ( $\text{NO}_2^-$  and  $\text{NO}_3^-$ ) in PBS, pH 7.4 (Figure 5.13). Similar to the BODIPY NO sensor, there was only a 1.3 to 1.7-fold increase in the fluorescence intensity of **16** upon treatment with the reactive nitrogen and oxygen species compared to the untreated compound. To ensure that the oxazine scaffold itself was not affected by these reactive species, the ROS/RNS-treated dye was incubated with nitric oxide (Figure 5.14). Treatment with nitric oxide resulted in a 4 to 6-fold increase in fluorescence intensity, and the fluorescence intensity was similar among the treatments. This suggests that the oxazine scaffold itself is unaffected by any ROS/RNS and that the limited fluxes in fluorescence intensity result from the limited reaction of the PET donor with species besides nitric oxide.

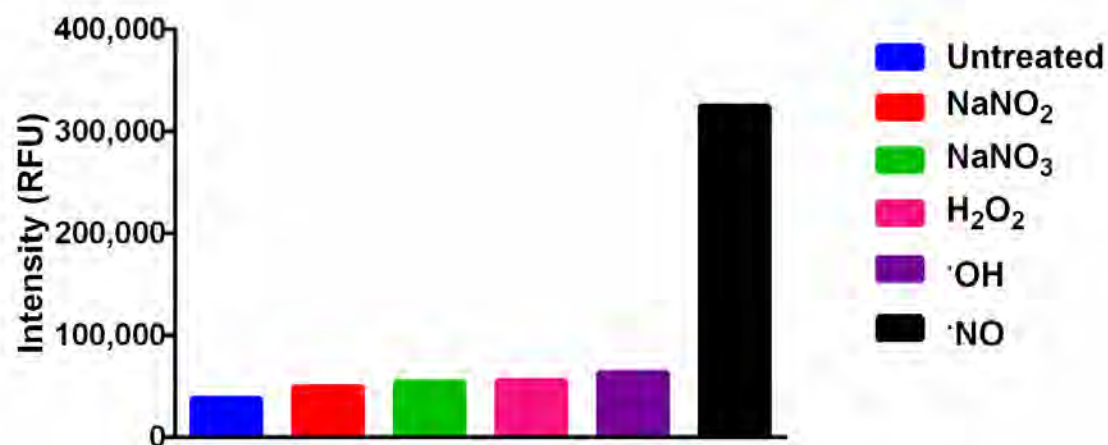


**Figure 5.13: Changes in the fluorescence intensity of 16 upon treatment with ROS and RNS.** Solutions of **16** (final concentration: 1  $\mu$ M, 0.1% DMSO) were prepared in 1X PBS, pH 7.4. ROS and RNS treatments are as follows: nitrate was added as NaNO<sub>3</sub> (100  $\mu$ M), nitrite was added as NaNO<sub>2</sub> (100  $\mu$ M), H<sub>2</sub>O<sub>2</sub> (1 mM), hydroxyl radical ( $\cdot$ OH) was prepared *in situ* via addition of ferrous sulfate heptahydrate (100  $\mu$ M) and H<sub>2</sub>O<sub>2</sub> (1 mM), nitric oxide was added with DEA NONOate (10  $\mu$ M). Upon treatment, the dye solutions were heated to 37  $^{\circ}$ C and stirred for 30 minutes. Fluorescence intensity was measured using excitation at 665 nm and emission at 679 nm. Excitation/Emission slit width: 2.5 nm.

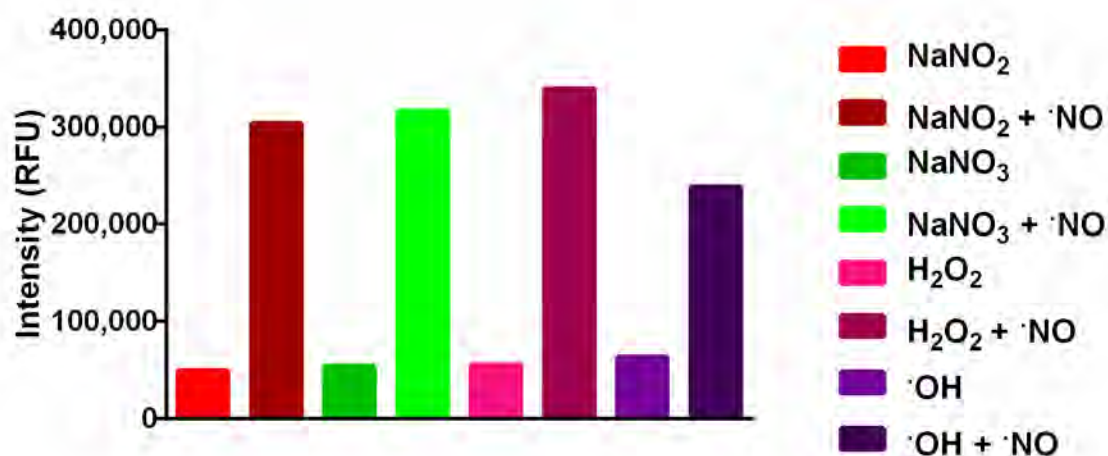


**Figure 5.14: Increase in the fluorescence intensity of ROS/RNS treated NO sensor upon treatment with nitric oxide.** ROS/RNS treated solutions of **16** were prepared as described in Figure 5.13 and heated with stirring at 37 °C for 30 minutes. DEA NONOate (10 μM) was then added and the solutions were stirred for another 30 minutes at 37 °C. Fluorescence intensity was then measured using excitation at 665 nm and emission at 679 nm. Excitation/Emission slit width: 2.5 nm.

As a final proof of principle, we wanted to illustrate the ability of our sensor to detect changes in NO concentration over time. We therefore treated **16** with increasing concentrations of nitric oxide and monitored changes in fluorescence intensity over 30 minutes (Figure 5.15). DEA NONOate was used as the NO donor for this work. Under the conditions employed, the NO donor DEA NONOate has a half-life of 16 minutes and dissociates to give 1.5 moles of nitric oxide for every mole of compound (Keefer et al., 1996). At supra-molar concentrations of NO, there is a rapid increase in fluorescence intensity that begins to plateau even before the half-life of the NO donor is reached. Both the rate of reaction and the half-time to peak signal increase with increasing NO

concentrations, confirming that our sensor could indeed be employed in the temporal and spatial detection of NO (Table 5.3).

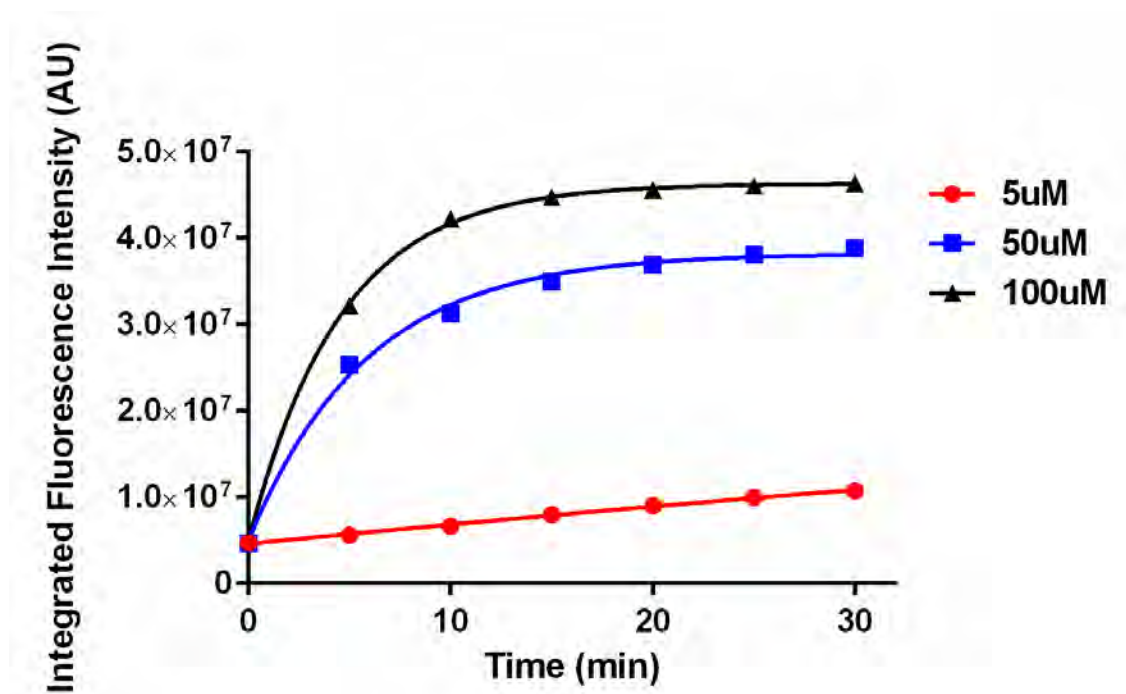


**Figure 5.15: NO sensor 16 can detect changes in nitric oxide concentration.** Solutions of **16** (final concentration: 10  $\mu$ M, 0.1% DMSO) were prepared in PBS, pH 7.4. Solutions of DEA NONOate in 1X PBS, pH 7.4 were prepared immediately before adding to dye solution. The reactions were incubated with stirring at room temperature and fluorescence intensity was measured every 5 minutes using excitation at 665 nm and emission at 679 nm. Excitation/Emission slit width: 2 nm. Integrated fluorescence intensity was obtained by integrating the area under the emission curves from 624-800 nm. Data points were fitted with a one-phase association model. AU: arbitrary units.

DEA NONOate Concentration ( $\mu\text{M}$ )	5	50	100
$I_0$ (RFU)	4.590E6	4.974E6	4.890E6
Plateau (RFU)	3.623E7	3.827E7	4.632E7
$k$ ( $\text{min}^{-1}$ )	0.007343	0.1716	0.2195
$\tau$ (min)	136.2	5.826	4.555
$\tau_{1/2}$ (min)	94.40	4.038	3.157
$R^2$ (%)	99.67	99.57	99.97

**Table 5.3: Non-linear regression parameters for the one-phase association model employed in Figure 5.15.**  $I_0$ : Initial intensity.  $k$ : rate constant.  $\tau$ : time constant.  $\tau_{1/2}$ : half-life. RFU: relative fluorescence units. Parameters calculated with GraphPad Prism.

To show that our NIR oxazine-based sensing strategy is not limited to the detection of small molecules, we sought to prepare sensors that could be used to detect other biologically-relevant environmental conditions. Changes in biological pH are involved in a diverse range of cellular functions including the cell cycle, endocytosis, and ion conductivity and are thus stringently controlled (Madhus, 1988). Due to the strict regulation of intracellular pH, detecting minor changes in pH requires a technique with high sensitivity, such as fluorescence imaging. Fluorescence-based sensors of pH have been prepared using both visible and NIR wavelength BODIPY-derivatives, but these suffer from the drawbacks previously described for BODIPY-type compounds (Jokic et al., 2012; Han et al., 2013; Ni and Wu, 2014). We can improve upon the known fluorescence-based pH sensors by incorporating NIR oxazine-derivatives into the tool kit.

During our work with NO Sensor **16**, we had been concerned that the presence of the two slightly basic amines on the PET-donor could result in our compound being pH sensitive. However, incubation of **16** in solutions of decreasing pH only resulted in a 1.8-fold change in fluorescence intensity (Figure 5.16). It is unlikely that both of the aromatic exocyclic amines would be protonated under the conditions we employed, which suggested to us that even a single aromatic exocyclic amine may have enough electron density to function as a PET donor.

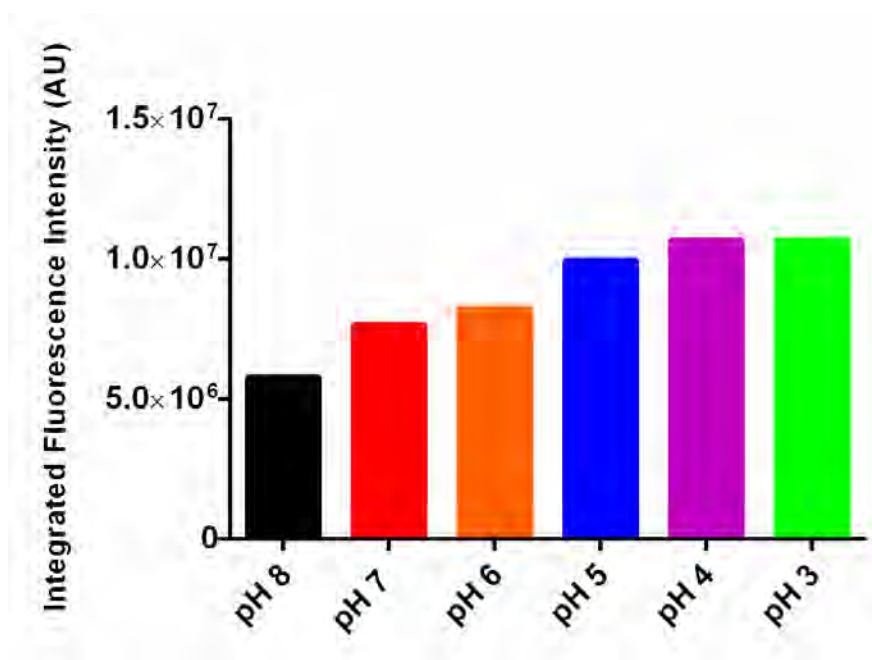


**Figure 5.16: Oxazine-derived NO sensor **16** is relatively insensitive to pH.** The fluorescence intensity of pH 3-8 buffered solutions of **16** (final concentration: 1  $\mu$ M, 0.1% DMSO) was measured using excitation at 665 nm and emission at 680 nm. Excitation/Emission slit width: 3 nm. Integrated fluorescence intensity was obtained by integrating the area under the emission curves from 600-850 nm. AU: arbitrary units.

One molecule that is both aromatic and bears a single exocyclic amine is aniline. Aniline is also slightly basic and can be protonated around pH 4-5. We hypothesized that the fluorescence of NIR oxazines could be quenched via an aniline-based PET donor and that this quenching could be relieved upon formation of the phenyl-ammonium cation (Figure 5.17). Furthermore, since our oxazine dyes are not particularly pH sensitive, we envisioned that our pH sensor would be specific for the pH range of the PET donor; i.e. pH 4-5.

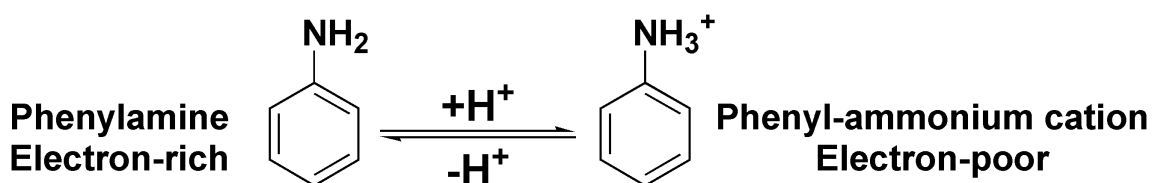
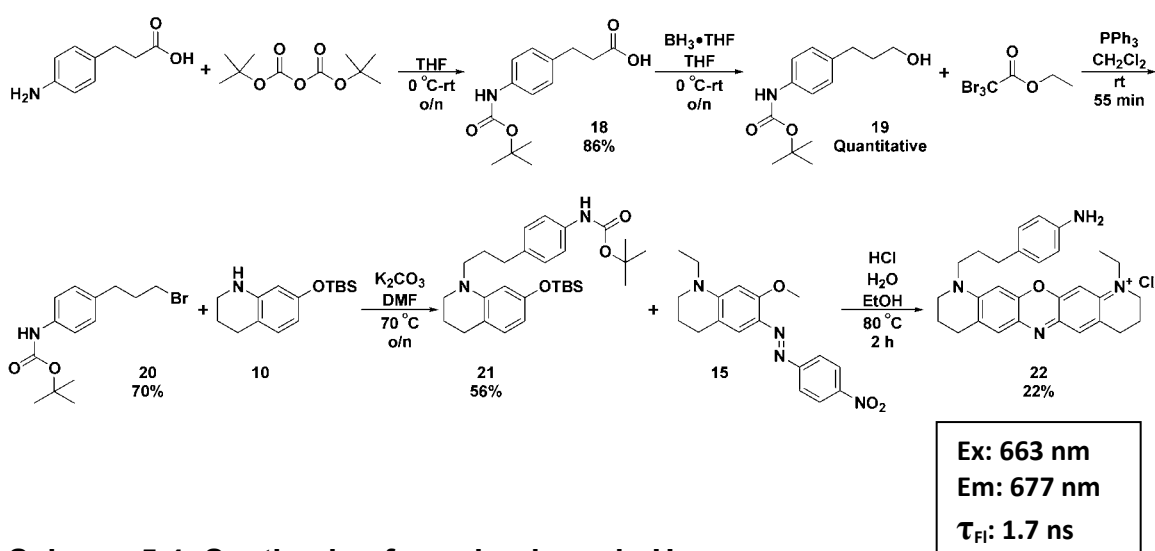


**Figure 5.17: The electron-rich phenylamine can be reversibly protonated to produce the electron poor phenyl ammonium cation.**

From work with our NO sensor, a propylene spacer allows van der Waals contact between an amino-substituted aromatic ring and the oxazine-dye scaffold. Building from this idea, we prepared a phenylamine-functionalized NIR oxazine (Scheme 5.4). Beginning with 3-(4-aminophenyl)propionic acid, the exocyclic aromatic amine was first Boc-protected to prevent the amino group from participating in subsequent reactions **18**. Borane reduction of the carboxylic acid of **18** followed by bromination of the resulting alcohol **19** provided the Boc-protected PET donor **20** in relatively high yield. N-alkylation of the TBS-protected



tetrahydroquinoline **10** with the PET donor **20** produced the first half of the dye scaffold **21**. Condensation of **21** with the arylazo functionalized tetrahydroquinoline **15** in refluxing aqueous, acidic ethanol provided us with the PET-quenched NIR oxazine pH sensor **22**.



**Scheme 5.4: Synthesis of oxazine-based pH sensor.**

As the pKa of the phenyl-ammonium cation is between 4.6 and 4.9, we predicted that pH sensor **22** would be highly fluorescent at pH 4 and quenched at pH 7. The absorption and emission of **22** were therefore taken in PBS, pH 7.4 and acetic acid/sodium acetate buffered solution, pH 4 (Figure 5.18). While the absorption and emission wavelengths were relatively unchanged in the different pH solutions, the acidic solution resulted in a 9-fold increase in the integrated fluorescence intensity compared to the PBS solution. This observation confirmed

that the phenylamine group can indeed function as a PET donor for modulating oxazine fluorescence (Figure 5.19).

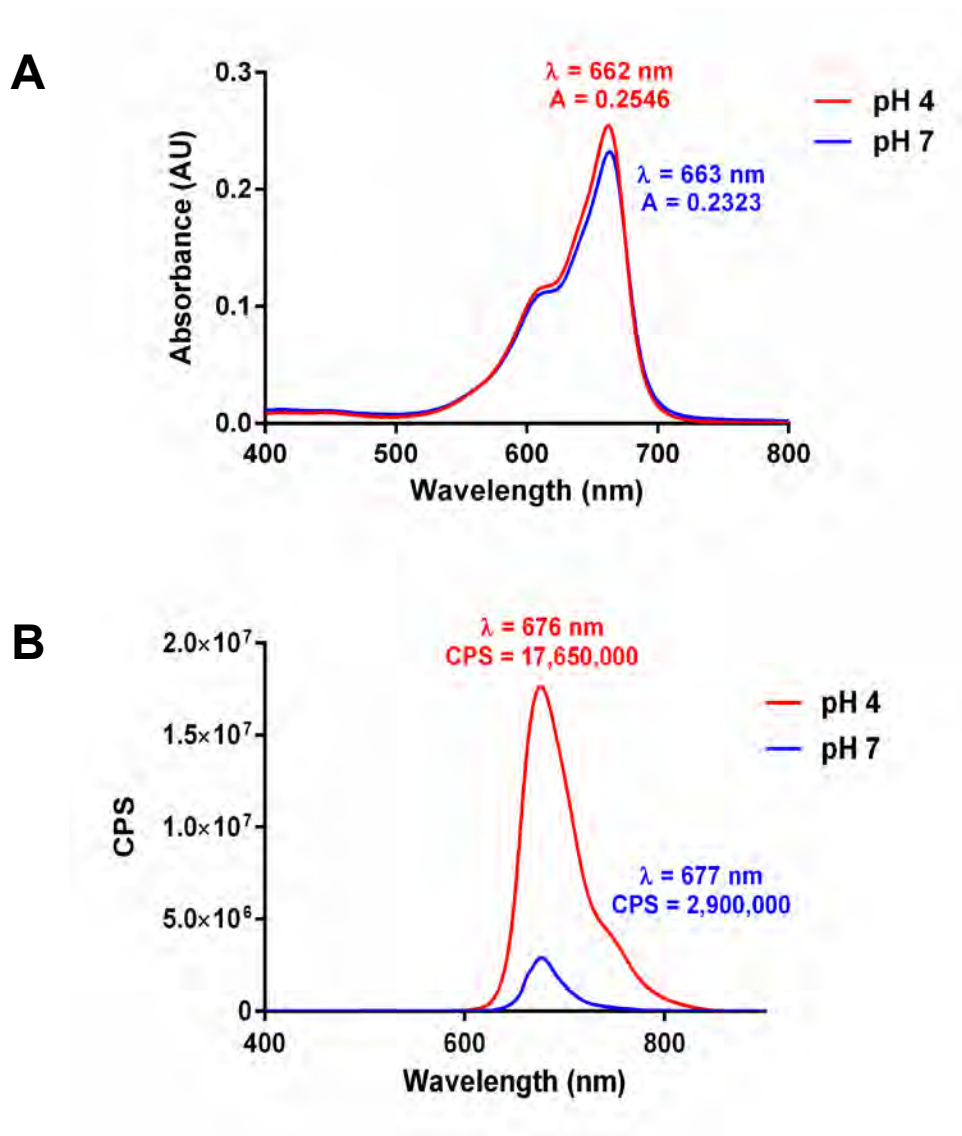


**Figure 5.18: Absorption (A) and emission (B) spectra for pH sensor 22 in pH 4 and pH 7 solutions.** A 10 mM DMSO stock of **22** was dissolved in 1X PBS, pH 7.4 or acetic acid/sodium acetate buffered solution, pH 4 to give a final concentration of 3.33  $\mu$ M. Fluorescence intensity was measured using excitation at 663 nm. Excitation/Emission slit width: 5 nm. AU: absorbance units. CPS: counts per second.

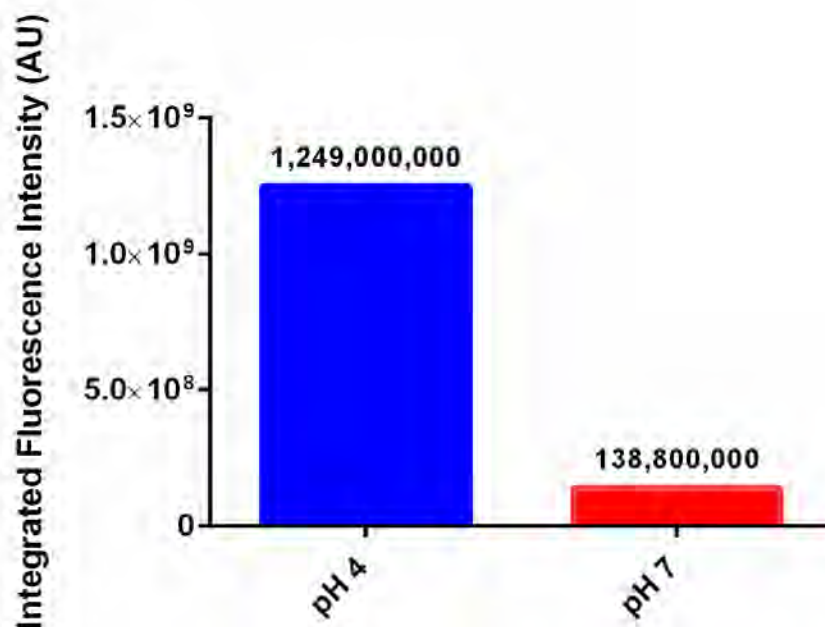


**Figure 5.19: Integrated fluorescence intensity of **22** in pH 4 and pH 7 solutions.** 10 mM DMSO stock of **22** was dissolved in 1X PBS, pH 7.4 or acetic acid/sodium acetate buffered solution, pH 4 to give a final concentration of 3.33  $\mu\text{M}$ . Fluorescence intensity was measured using excitation at 663 nm. Integrated fluorescence intensity was obtained by integrating the area under the emission curves from 400-900 nm. Excitation/Emission slit width: 5 nm. AU: arbitrary units.

To determine the range of the pH sensitivity of sensor **22**, we measured the fluorescence intensity of **22** in solutions with pHs varying from 2-8 (Figure 5.20). The integrated fluorescence intensity of the emission curves of **22** in the various pHs were then used to calculate the apparent pKa of our sensor (Figure 5.21 and 5.22). The apparent pKa of pH sensor **22** was found to be 4.8, close to the value of the protonated PET donor itself. This finding suggests that by simply altering the identity of the pH sensitive PET donor, we can design NIR fluorophores for the detection of specific pH ranges.

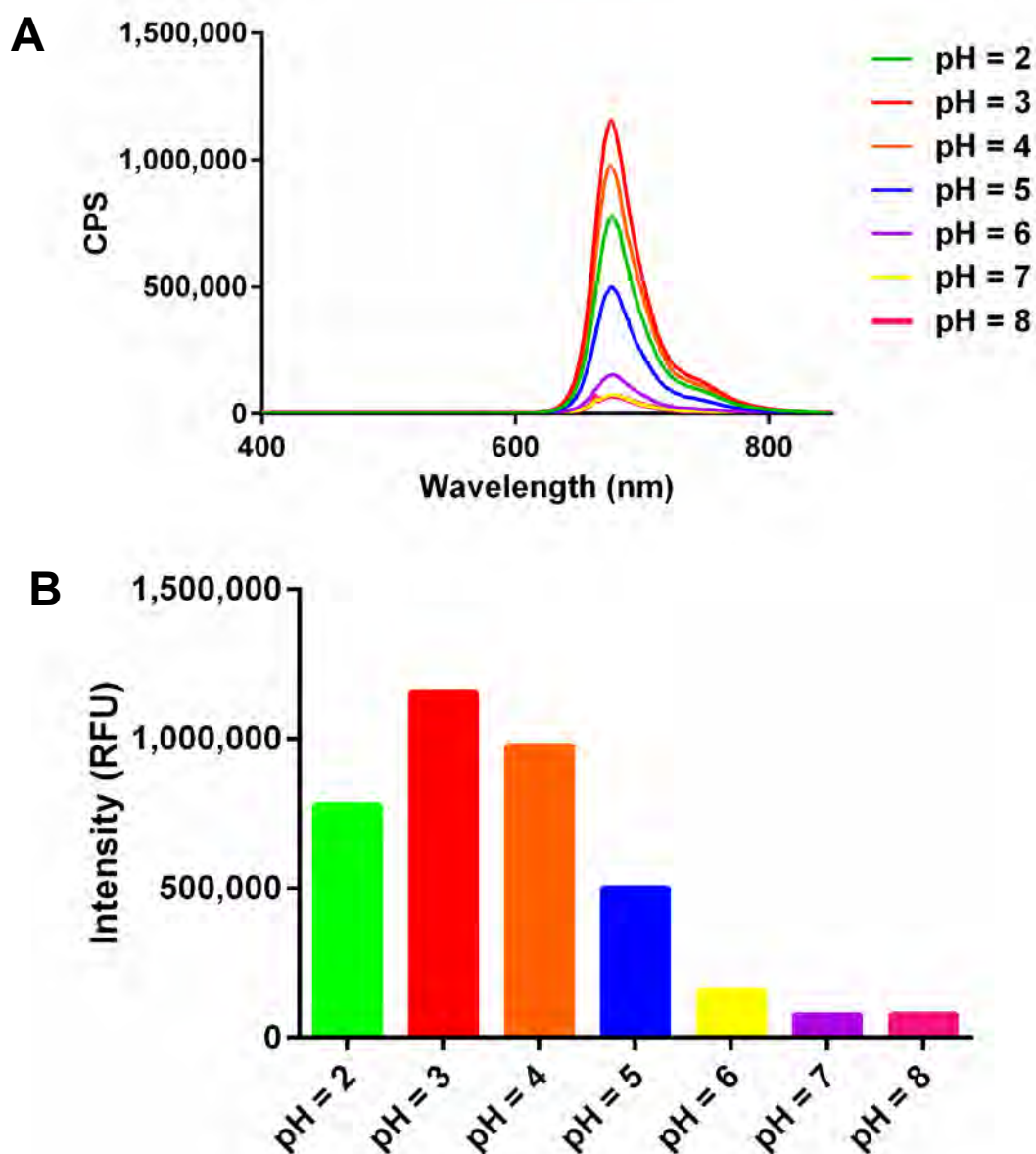


**Figure 5.20: Fluorescence intensity of 22 in pH 2-8 solutions.** Solutions of 22 (final concentration: 3.3  $\mu$ M, 0.1% DMSO) were prepared in buffered solution having pHs of 2-8. Fluorescence intensity measured using excitation at 663 nm and emission at 676 nm. Excitation/Emission slit width: 2 nm. A. Emission spectra. B. Comparison of fluorescence intensities. CPS: counts per second. RFU: relative fluorescence units.

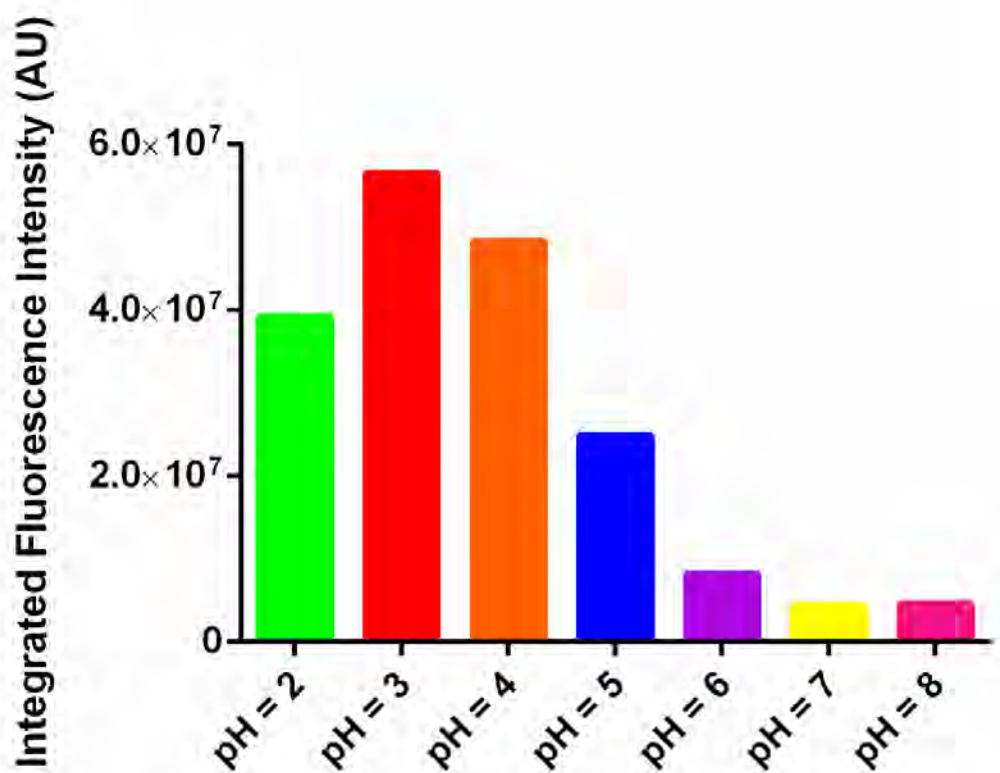


**Figure 5.21: Integrated fluorescence intensity of pH sensor 22 in solutions of pH 2-8.** Solutions of **22** (final concentration:  $3.3 \mu\text{M}$ , 0.1% DMSO) were prepared in buffered solution having pHs of 2-8. Fluorescence intensity measured using excitation at 663 nm and emission at 676 nm. Excitation/Emission slit width: 2 nm. The integrated fluorescence intensity was obtained by calculating the area under the emission curves from 600-850 nm. AU: arbitrary units.

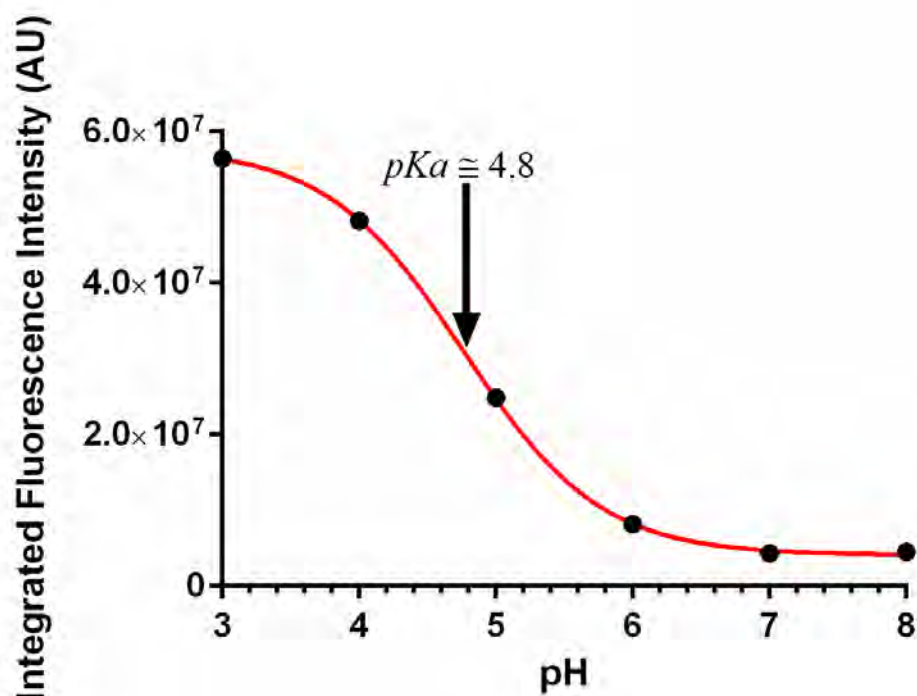


**Figure 5.22: The apparent pKa of pH sensor 22 is 4.8.** A plot of integrated fluorescence intensity (Figure 5.21) versus solution pH was fitted with a log versus response curve in GraphPad Prism to calculate the apparent pKa. AU: arbitrary units.  $R^2$  of fit: 99.99%

Figure 5.21 shows that there is more than a 13-fold increase in the integrated fluorescence intensity of **22** over the pH range of 8 to 3. At pH 2 though, there seems to be a 31% decrease in integrated fluorescence intensity from the peak fluorescence at pH 3. The protonated PET donor on **22** will not be protonated a second time; therefore, one possibility to explain the decrease in fluorescence of **22** may be that the phenyl ammonium cation is affecting the pKa of the dye scaffold itself. Perhaps one of the dye-scaffold nitrogen atoms is being protonated leading to a decrease in fluorescence. This was not investigated

further at this time but, as it is unlikely that this feature is due to the acidity/basicity of the PET donor, this data point was excluded from the pKa calculation (Figure 5.22).

As a final characterization of our pH sensor, we wanted to determine the effect of pH on the lifetime of **22**. Using TCSPC, we measured the fluorescence decay of 1  $\mu\text{M}$  **22** in pH 3 to 7 solutions (Figure 5.23). The results were analyzed using both a local and global analysis of the data and the local fit was chosen for this work as it illuminated molecular features not seen in the global analysis (Table 5.4). Most of the data could be well fitted with two or three exponentials, suggesting that there were multiple components to the fluorescence lifetime of pH Sensor **22**. This was extremely encouraging as we obtained a similar result when measuring the lifetime of NO Sensor **16** (Figure 5.12 and Table 5.2). The lifetime of one of our unquenched oxazines could be fit with a single exponential; i.e., it has a single component to its lifetime (Data not shown). The appearance of multiple lifetime components in our PET quenched dyes implies that the PET donor has an effect on the underlying electronic transitions of our NIR fluorophores.

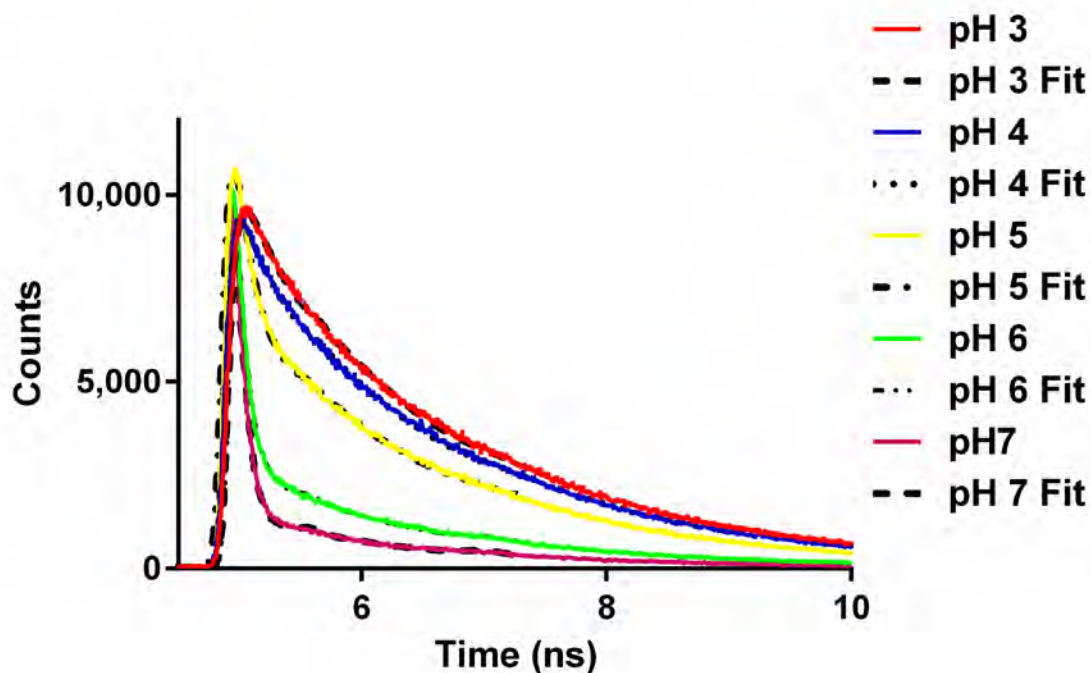


**Figure 5.23: Time correlated single photon counting (TCSPC) suggests that the pH-related PET-quenching of NIR oxazine-derived pH sensor 22 is complex.** The fluorescence decay of 1  $\mu\text{M}$  22 in buffered solutions having pHs of 3-7 was measured using TCSPC as described (see Methods). Data was fit using a sum of exponentials plus a constant as described in the methods. Solid lines indicate raw data. Dashed lines indicate fitted curve.



pH	3	4	5	6	7
$\tau_{FI(1)}$ (ns)	1.67 +/- 0.00499	1.65 +/- 0.00538	1.56 +/- 0.00375	1.56 +/- 0.00793	1.47 +/- 0.00872
<b>A<sub>1</sub></b> (% Total Photons)	10.4	10.3	32.2	4	3.1
$\tau_{FI(2)}$ (ps)	203 +/- 13.5	225 +/- 19.7	90.4 +/- 1.39	131 +/- 12.5	35.2 +/- 0.957
<b>A<sub>2</sub></b> (% Total Photons)	2.4	2.1	67.8	4.29	96.9
$\tau_{FI(3)}$ (ps)	1	5.63 +/- 2.77	N/A	21.0 +/- 1.77	N/A
<b>A<sub>3</sub></b> (% Total Photons)	87.2	87.6	N/A	91.7	N/A
$\chi^2_{red}$	1.43	1.34	1.36	1.48	1.79

**Table 5.4: Values for curve fitting of pH Sensor 22 TCSPC data.**  $\tau_{FI}$ : Exponential time constant. A: Pre-exponential amplitude. Values were calculated as described in methods using non-linear least squares fitting.

Like NO sensor **16**, the lifetime of pH sensor **22** seems to be modulated by both static and dynamic quenching mechanisms. At pH 3, when **22** has the highest fluorescence output, it also has the longest lifetime: 1.67 ns (Figure 5.21 and Table 5.4). With increasing pH, the lifetime decreases, reaching a minimum value of 1.47 ns at pH 7, when fluorescence output is at a minimum. This is a clear display of dynamic quenching, which is most certainly produced by photoinduced electron transfer. Furthermore, in general, the number of photons associated with the longer lifetime component decreases as pH increases. This indicates a decrease in the number of photons associated with this lifetime, and a decrease in concentration implies static quenching.

However, the fluorescence lifetime of pH sensor **22** cannot be described by a simple two-mechanism scenario. At pH 5, near the pKa of **22**, the concentration of photons associated with the long lifetime component actually increases. Additionally, while the lifetimes of **22** at pH 5 and 7 can be described by two components, at pH 3, 4, and 6, there is a 3<sup>rd</sup> lifetime component that is associated with the majority of emitted photons. The effects of PET-quenching on our pH sensor appear to be far more complex than observed with our NO sensor and will require a more detailed investigation before a valid explanation can be obtained. The primary conclusion obtainable from our current analysis is that changes in pH change the lifetime of our pH sensor.

### ***Conclusions***

Probes and sensors that absorb and emit NIR light are vital tools in the study of cellular biology. Yet, the current NIR palette is primarily limited to two dye scaffolds, indocyanines and BODIPYs, both which suffer from inherent drawbacks limiting their use in living systems. In an effort to expand and improve the toolkit of viable NIR scaffolds for use as biological probes, we have successfully developed sensors of nitric oxide and pH based on the scarcely employed NIR pentacyclic oxazine.

Both our nitric oxide sensor **16** and pH sensor **22** are easily prepared from commercially available starting materials using regularly employed synthetic techniques (Schemes 5.1, 5.2, and 5.4). Prior to reaction with the analyte of

interest, the fluorescence of **16** and **22** are quenched via PET, a commonly employed method in the development of fluorescent sensors (Figures 5.11 and 5.19). Furthermore, the only structural difference between **16** and **22** is the presence of a second amine on the electron-rich PET donor (Figure 5.5 and 5.17). These features reveal the modularity and functional ease with which NIR oxazine based sensors can be prepared, thus allowing for the customization of sensors for a variety of analytes.

Our NIR sensors have a 6 to 13-fold increase in fluorescence intensity upon analyte detection (Figures 5.11, 5.15, 5.19, and 5.21). This is noticeably lower than for some visible wavelength sensors derived from fluorescein and rhodamine (Kojima et al., 1998, Tian et al., 2012). However, the low background noise associated with NIR imaging means the signal to noise ratio of our NIR probes could actually exceed the signal obtained from their visible wavelength counterparts when applied to living systems.

One of the most exciting features discovered during this work was the targeted and modular nature of our pH sensor. pH sensor **22** has a pKa of 4.8 (Figure 5.22). This is within the pKa range of the protonated aniline PET donor, suggesting that the detection of pH is unaffected by our dye scaffold. Therefore, by simply choosing the right protonatable group that can also function as a PET donor, a NIR oxazine-based pH sensor can be developed for a wide range of pH values.

Much of the work performed when developing fluorescent probes focuses on their synthesis and reactivity with the target analyte. Unfortunately, very little work has been undertaken to investigate the actual mechanisms by which the fluorescence of these sensors are quenched. This limits our ability to understand the mechanics guiding the behavior of molecules frequently employed in biochemistry and biology. We sought to fill this gap by examining the effects of PET-quenching on the fluorescence lifetimes of our probes through time correlated single photon counting. We were quite gratified to find that the fluorescence of NO sensor **16** and pH sensor **22** was quenched by similar mechanisms. Both molecules undergo static and dynamic quenching, which is logical since these two compounds differ by only a single aromatic exocyclic amine (Table 5.2 and 5.4; Scheme 5.2 and 5.4). However, the aniline PET donor of **22** also appears to alter the lifetimes of the NIR fluorophore in ways that are distinct from NO sensor **16**. This suggests that there are minor modifications to the fluorophore structure that can drastically alter the underlying mechanics of quenching. This needs to be investigated in far greater detail as this would provide insight into the structural and/or chemical features that favor a given electronic relaxation pathway. Apart from a simply academic pursuit, this finding would be directly applicable to both chemistry and biology. Understanding how fluorescence-quenched probes actually relax from an excited state could aid in the intelligent design of molecules for probing biological environments.

## **Materials and Methods**

### **General Methods**

Chemicals were purchased from Aldrich, Acros, Matrix, Oakwood, and TCI and were used without further purification. Diethylammonium (Z)-1-(N,N-diethylamino)diazene-1,2-diolate (DEA NONOate) was purchased from Cayman Chemical. 10X phosphate buffered saline (PBS) was purchased from Aldrich and diluted to 1X with deionized water for all experiments. Organic solvents were ACS grade or Chromasolv<sup>®</sup> for HPLC grade and were purchased from Aldrich. Dry solvents were purchased from Acros. NMR solvents were purchased from Cambridge Isotope Laboratories. Unless otherwise stated, all reactions were performed under argon using dry organic solvents.

NMR spectra were recorded at 400 MHz for <sup>1</sup>H and 101 MHz <sup>13</sup>C using a Varian Mercury 400 MHz instrument. High-resolution electrospray ionization mass spectra were obtained on a Waters QToF Premier exact mass spectrometer. Absorbance measurements were obtained using an Agilent Cary Series 100 UV-Vis spectrophotometer. Fluorescence spectra were obtained using a Jobin Yvon Horiba SPEX FluoroMax-3. Data analysis was performed using GraphPad Prism.

### **Molecular Modeling**

Molecular models were generated using Schrödinger's Maestro (Schrödinger Release 2014-2: Maestro, version 9.8, Schrödinger, LLC, New York, NY, 2014)

Molecule conformations were minimized with the Schrödinger Semiempirical NDDO Module (Schrödinger, Suite 2012 Semiempirical NDDO Module, Schrödinger, LLC, New York, NY 2012). Other possible conformations were confirmed with Schrödinger Confgen constraining the distance between the diaminobenzene ring and center of the dye to 10 angstroms (Watts et al., 2010).

### **Reversed-phase High-performance Liquid Chromatography**

Analytical and semi-preparative HPLC were performed on a Hewlett Packard Agilent 1100 HPLC equipped with a G1315A DAD absorbance detector.

Absorbance detector was set at 800 nm for reference. All methods used aqueous 0.1% trifluoroacetic acid as Solvent A and acetonitrile/0.1% trifluoroacetic acid as Solvent B. Acetonitrile and trifluoroacetic acid were HPLC grade and were purchased from Aldrich. HPLC methods were as follows:

#### *Analytical*

Analytical HPLC was performed on a 4.6 x 250 mm C-18 column using a flow rate of 1.4 mL/min. Absorbance detector set at 280, 360, 615, 660 nm. 10% B for 5 minutes, 10-45% B over 35 minutes, 45-100% B over 5 minutes, 100% B for 10 minutes.

#### *Semi-preparative*

Compounds were purified on a 10 x 250 mm C-18 column using a flow rate of 5 mL/min.

**Compound 16:** Absorbance detector set at 211, 244, 299, 409, and 659 nm. 0% B for 5 minutes, 0-40% B over 40 minutes, 40-100% B over 5 minutes, 100% B for 5 minutes.

**Compound 17:** Absorbance detector set at 252, 610, 659, and 666 nm. 10% B for 5 minutes, 10-50% B over 45 minutes, 50-100% B over 5 minutes, 100% B for 10 minutes.

### **Absorbance Measurements**

Absorbance spectra were obtained from 400-800 nm using a 1 nm data interval and 0.1 s average time. The instrument was set for double beam mode with a spectral bandwidth of 2 nm and a scan of 600 nm/min. Samples were contained in Starna fluorometer cells having a path length of 10 mm and composed of optical glass. Absorbance of a blank sample was measured and subtracted from the samples to obtain the final spectra.

### **Fluorescence Measurements**

Emission spectra were obtained using 1 nm increments and an integration time of 0.1 s. Samples were contained in Starna fluorometer cells having a path length of 10 mm and composed of optical glass. Excitation wavelength, slit width, and wavelength span was adjusted for the experiments as needed.

### Reaction of Nitric Oxide Sensor with Reactive Nitrogen/Oxygen Species

Stock solutions of reactive nitrogen/oxygen species in 1X PBS were freshly prepared as follows: 40 mM DEA NONOate ( $\dot{\text{N}}\text{O}$  donor), 400 mM ferrous sulfate heptahydrate ( $\text{FeSO}_4 \cdot 7\text{H}_2\text{O}$ ), 4 M hydrogen peroxide ( $\text{H}_2\text{O}_2$ ), 400 mM sodium nitrate ( $\text{NaNO}_3$ ), 400 mM sodium nitrite ( $\text{NaNO}_2$ ). DEA NONOate solution was prepared immediately before adding to the reaction. Solutions of **16** (stock solution: 10 mM in DMSO; final concentration: 1  $\mu\text{M}$ , 0.1% DMSO) were prepared in 1X PBS, pH 7.4 (4 mL). Dye solutions were treated with stock solutions of ROS/RNS as follows:  $\dot{\text{N}}\text{O}$  (10  $\mu\text{M}$  DEA NONOate),  $\text{H}_2\text{O}_2$  (1 mM),  $\text{NaNO}_3$  (100  $\mu\text{M}$ ),  $\text{NaNO}_2$  (100  $\mu\text{M}$ ),  $\dot{\text{O}}\text{H}$  (hydroxyl radical was prepared *in situ* via addition of 100  $\mu\text{M}$   $\text{FeSO}_4 \cdot 7\text{H}_2\text{O}$  and 1 mM  $\text{H}_2\text{O}_2$ ). An untreated solution of **16** in 1X PBS, pH 7.4 was used as a control. Upon treatment, the dye solutions were heated to 37 °C and stirred for 30 minutes. Emission spectrum for each solution was then collected using excitation at 665 nm and emission at 679 nm. The excitation and emission slit widths were both set to 2.5 nm.

Solutions of **16** treated with RNS/ROS were subsequently treated with  $\dot{\text{N}}\text{O}$  through addition of 10  $\mu\text{M}$  DEA NONOate (freshly prepared as a 40 mM DEA NONOate stock solution in 1X PBS, pH 7.4). The  $\dot{\text{N}}\text{O}$ -treated solutions were heated to 37 °C and stirred for 30 minutes. Emission spectrum for each solution was then collected using excitation at 665 nm and emission at 679 nm. The excitation and emission slit widths were both set to 2.5 nm.



## **Reaction of Nitric Oxide Sensor with Increasing Concentrations of Nitric Oxide**

Solutions of **16** (stock solution: 10 mM in DMSO; final concentration: 10  $\mu$ M, 0.1% DMSO) were prepared in 1X PBS, pH 7.4 (3 mL). Emission spectrum for the untreated solutions were collected using excitation at 665 nm, emission at 679 nm, and excitation/emission slit widths of 2 nm. This was denoted as the zero time point.  $\cdot$ NO was introduced into the reaction via the  $\cdot$ NO donor, DEA NONOate. Stock solutions of DEA NONOate were prepared immediately before adding to the dye solution. The concentrations of the DEA NONOate stock solutions were: 5 mM, 50 mM, 100 mM; these concentrations were chosen to ensure that the total volume of the dye- $\cdot$ NO reaction would be relatively unchanged. The 10  $\mu$ M dye solutions were treated with either 5  $\mu$ M, 50  $\mu$ M, or 100  $\mu$ M DEA NONOate via dilution of the appropriate stock DEA NONOate concentration into the reaction. The reactions were then incubated with stirring at room temperature and emission spectra were collected every 5 minutes for 30 minutes using excitation at 665 nm and emission at 679 nm. The excitation and emission slit widths were both set to 2 nm.

## **Effects of pH on Fluorescence Intensity**

Dye solutions (stock concentration: 10 mM in DMSO) were prepared in buffered solutions (3 mL) having pHs of 2-8 to give a final DMSO volume of less than

0.1%). Aqueous pH buffered solutions were prepared as described in Table 5.5.

Emission spectrum for each solution was then collected as described below.

Compound **16**: Final concentration: 1  $\mu$ M. Excitation at 665 nm, emission measured at 680 nm, excitation/emission slit width: 3 nm.

Compound **22**: Final concentration: 3.33  $\mu$ M. Excitation at 663 nm, emission measured at 676 nm, excitation/emission slit width: 2 nm.

pH	Acid	Acid Volume (mL)	Base	Base Volume (mL)
2	0.2 M HCl	13	0.2 M KCl	50
3	0.1 M AcOH	982.3	0.1 M NaOAc	17.7
4	0.1 M AcOH	847	0.1 M NaOAc	153
5	0.1 M AcOH	357	0.1 M NaOAc	643
6	0.1 M AcOH	52.2	0.1 M NaOAc	947.8
7	1 X PBS			
8	0.1 M HCl	39	0.025 M Borax	100

**Table 5.5: Preparation of buffered solutions for pH sensitivity experiments.** 1X PBS was prepared from a 10X stock solution by diluting 100 mL into 900 mL deionized water. HCl: hydrochloric acid. AcOH: acetic acid. KCl: potassium chloride. NaOAc: sodium acetate. Borax: sodium tetraborate decahydrate ( $\text{Na}_2\text{B}_4\text{O}_7 \cdot 10\text{H}_2\text{O}$ ).

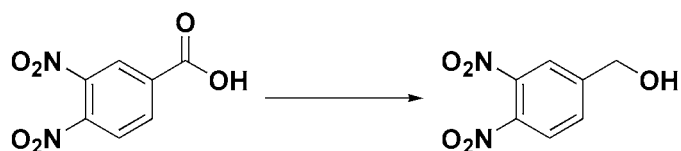
## Time-resolved Fluorescence

Excited-state decay lifetimes were measured using the time-correlated single photon counting (TCSPC) method as described previously (Lakowicz, 2006; O' Connor and Phillips, 1984). Excitation was provided by a mode-locked Titanium:sapphire laser emitting  $\sim 150$  fs pulses at  $685 \text{ nm} \pm 3 \text{ nm}$  with a 76 MHz repetition rate. The output of the laser was passed through a pair of Glan-Thompson polarizers, which act as an attenuator and flip the excitation polarization to vertical. Emission was collected by a 35 mm plano-convex lens, passed through a magic-angle ( $54.7^\circ$ ) Glan-Taylor polarizer, and then focused into a 0.25 m grating monochromator (CVI Laser). The monochromator was set to a detection wavelength of 715 nm, slit width of 3 mm, and spectral bandwidth of 11.31 nm (dispersion of 3.77 nm/mm). Detection utilized an id100 low-noise single-photon avalanche photodiode (idQuantique) and a Becker-Hickl SPC150 single-photon counting card. A 1 mm thick quartz slide was used to pick-off  $\sim 4\%$  of the excitation and focused onto a PHD400 fast photodiode to provide the TCSPC clock synchronization pulse. The sample was placed in a 1 cm x 1 cm S1UV fused silica cuvette and stirred during data collection. A buffer blank was collected for each sample. The blank count rate was typically less than 1% of that of the sample. An instrument response function was collected using a blank sample with identical configuration, with the exception that the monochromator was shifted near to the excitation wavelength to allow scattered light to enter the detector.

Dye samples were prepared from a 10 mM DMSO stock and diluted to a 1 mM stock in the appropriate buffer immediately before experiment. Experimental concentrations were then prepared by dilution of the 1 mM stock into the final working volume of 1 mL (final DMSO volume  $\leq$  0.007%). Buffers as described in Table 5.5.

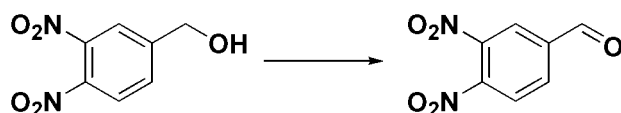
All data analysis utilized the normalized instrument response in an iterative reconvolution non-linear least squares fitting package (Kathuria et al., 2014). Data were fit using a sum of exponentials plus a constant. A number of exponentials were determined by examination of the residuals, reduced  $\chi^2$ , and an F-test on the inclusion of an additional exponential.

### Synthetic Procedures



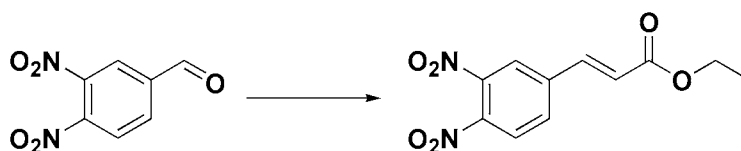
**(3,4-Dinitro-phenyl)-methanol (1).** 3,4-Dinitrobenzoic acid (2.2 g, 10 mmol) was dissolved in THF (10 mL) and cooled to 0°C. A 1 M solution of BH<sub>3</sub>·THF (52 mL) was added to the reaction dropwise via an addition funnel, resulting in the yellow solution becoming pink. The reaction was then brought to room temperature and stirred overnight, leading to a color change from pink to deep purple. The solution was then cooled to -15 °C and excess borane was quenched by the slow addition of methanol (24 mL), resulting in another color change from purple to bright

yellow. The solution was concentrated via rotary evaporation and the crude material was dissolved in 1 M HCl (200 mL). The aqueous phase was extracted with ethyl acetate (5 X 200 mL) and the combined organic phases were washed with water (150 mL), brine (150 mL), and dried over Na<sub>2</sub>SO<sub>4</sub>. Removal of the solvent via rotary evaporation provided the pure product as a yellow-orange solid (2 g, 95%). <sup>1</sup>H-NMR (DMSO-d<sub>6</sub>): δ 8.2 (d, 1H, *J* = 8.3 Hz), 8.084-8.076 (m, 1H), 7.87-7.84 (dm, 1H), 5.73 (t, 1H, *J* = 5.8 Hz), 4.67 (d, 2H, *J* = 5.7 Hz). <sup>13</sup>C-NMR (DMSO-d<sub>6</sub>): δ 151.6, 143, 140.9, 131.7, 126.3, 123.1, 62. HR-EIMS *m/z* calculated for C<sub>7</sub>H<sub>7</sub>N<sub>2</sub>O<sub>5</sub>: 199.0355, found: 199.0344.



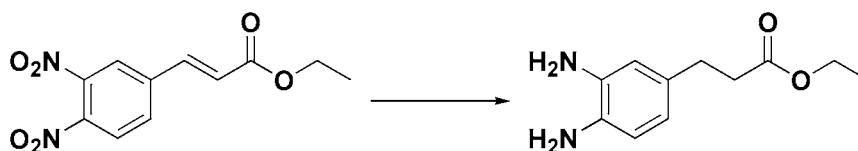
**3,4-Dinitro-benzaldehyde (2).** Dess-Martin periodinane (5 g, 12 mmol) was added to a solution of **1** (1.56 g, 7.87 mmol) in CH<sub>2</sub>Cl<sub>2</sub> (40 mL) and stirred for 2 hours. The reaction was diluted into ether (400 mL), added to a 5 % Na<sub>2</sub>S<sub>2</sub>O<sub>3</sub> solution in saturated NaHCO<sub>3</sub> (260 mL), and stirred for 10 minutes at ambient conditions. The organic phase was collected and the aqueous phase was extracted with ether (6 X 50 mL). The combined organic phases were washed with 5% NaHCO<sub>3</sub> (350 mL), water (350 mL), and brine (350 mL) and dried over Na<sub>2</sub>SO<sub>4</sub>. The organic phase was concentrated via rotary evaporation and the crude material was purified by flash column chromatography (0-50% ethyl

acetate/hexanes) to yield the pure product as a yellow-orange solid (1.41 g, 91%).  $^1\text{H-NMR}$  ( $\text{CDCl}_3$ ):  $\delta$  10.16 (s, 1H), 8.47 (d, 1H,  $J = 1.6$  Hz), 8.29 (dd, 1H,  $J = 1.6$  Hz, 8.2 Hz), 8.08 (d, 1H,  $J = 8.2$  Hz).  $^{13}\text{C-NMR}$  ( $\text{DMSO-d}_6$ ):  $\delta$  191.1, 145.3, 142.7, 140.0, 135.7, 127.3, 126.7. HR-EIMS  $m/z$  calculated for  $\text{C}_7\text{H}_3\text{N}_2\text{O}_5$ : 195.0042, found: 195.0134.



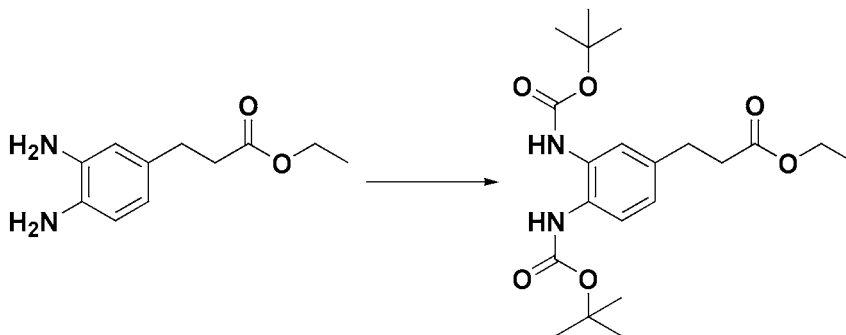
**3-(3,4-Dinitro-phenyl)-acrylic acid ethyl ester (3).** Triethyl phosphonoacetate (1.1 mL, 5.4 mmol) was added to a solution of LiBr (566 mg, 6.51 mmol) in THF (6 mL) and stirred for 5 minutes at room temperature.  $\text{Et}_3\text{N}$  (0.83 mL, 5.97 mmol) was then added to the reaction and stirring was continued for an additional 10 minutes, resulting in a white cloudy mixture. A solution of **2** (1.06 g, 5.40 mmol) in THF (6 mL) was added to the mixture dropwise over a period of 30 minutes resulting in a color change from white to brown. The reaction was stirred for an additional 3 hours and then diluted into 1 M HCl (120 mL) resulting in formation of a yellow precipitate. The product was extracted with diethyl ether (1 X 120 mL, 4 X 50 mL) and the combined organic phases were washed with brine (2 X 50 mL) and dried over  $\text{Na}_2\text{SO}_4$ . The solvent was evaporated under vacuum to yield the pure product as a lightweight yellow solid (1.28 g, 89%).  $^1\text{H-NMR}$  ( $\text{CDCl}_3$ ):

$\delta$  8.01 (d, 1H,  $J$  = 1.6 Hz), 7.98 (d, 1H,  $J$  = 8.4 Hz), 7.84 (dd, 1H,  $J$  = 1.7 Hz, 8.4 Hz), 7.68 (d, 1H,  $J$  = 16.1 Hz), 6.61 (d, 1H,  $J$  = 16.0 Hz), 4.3 (q, 2H,  $J$  = 7.1 Hz), 1.36 (t, 3H,  $J$  = 7.1 Hz).  $^{13}\text{C-NMR}$  ( $\text{CDCl}_3$ ):  $\delta$  165.5, 143.8, 142.7, 140.6, 139.4, 132.2, 126.2, 125.1, 123.9, 61.6, 14.4. HR-EIMS  $m/z$  calculated for  $\text{C}_{11}\text{H}_{10}\text{N}_2\text{O}_6\text{Na}$ : 289.0437, found: 289.0439.



**3-(3,4-Diamino-phenyl)-propionic acid ethyl ester (4).** 10% Pd/C (40 mg, 0.38 mmol) was added to a suspension of compound **3** (1 g, 4 mmol) in methanol (60 mL) and the black mixture was stirred at room temperature. The reaction was then treated with hydrogen (via a balloon connected to an inlet adapter) for 19 hours and filtered over a pad of AW Standard Super-Cel<sup>®</sup> NF Celite<sup>®</sup> to remove the catalyst. The Celite<sup>®</sup> was washed with methanol (400 mL) and the combined organic collections were concentrated under vacuum to yield the pure product as a viscous brown oil (765 mg, 98%).  $^1\text{H-NMR}$  ( $\text{DMSO-d}_6$ ):  $\delta$  6.37 (d, 1H,  $J$  = 7.7 Hz), 6.32 (d, 1H,  $J$  = 2 Hz), 6.19 (dd, 1H,  $J$  = 2.0 Hz, 7.8 Hz), 4.32 (br s, 4H), 4.01 (q, 2H,  $J$  = 7.1 Hz), 2.57 (t, 2H,  $J$  = 7.4 Hz), 2.45-2.41 (m, 2H), 1.14 (t, 3H,  $J$  = 7.1 Hz).  $^{13}\text{C-NMR}$  ( $\text{DMSO-d}_6$ ):  $\delta$  173.1, 135.6, 133.7, 129.7, 117.4, 115.2,

115.1, 60.3, 36.6, 30.7, 14.8. HR-EIMS  $m/z$  calculated for  $C_{11}H_{17}N_2O_2$ : 209.1290, found: 209.1305.



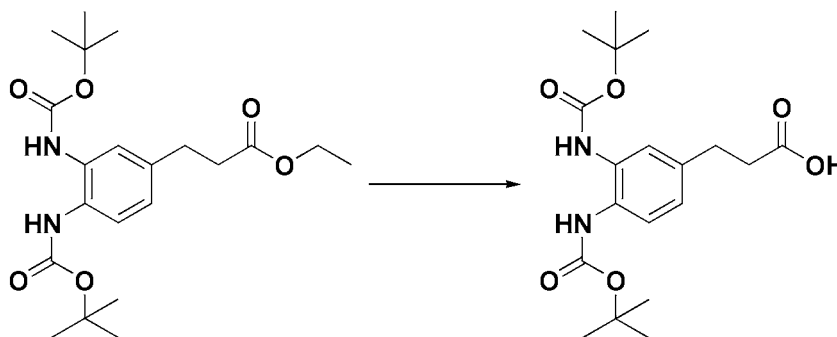
**3-(3,4-Bis-*tert*-butoxycarbonylamino-phenyl)-propionic acid ethyl ester (5).**

Compound **4** (765 mg, 3.67 mmol) was dissolved in THF (29 mL) and cooled to 0°C. A solution of Di-*tert*-butyl dicarbonate (3.21 g, 14.7 mmol) in THF (9 mL) was then added dropwise to the reaction. The reaction was then brought to room temperature and stirred overnight. The solution was poured into water (400 mL) and the product was extracted with dichloromethane (6 X 100 mL). The combined organic phases were washed with brine (300 mL) and dried over  $Na_2SO_4$ . The solvent was evaporated under vacuum and the crude material was purified by flash column chromatography (0-25% ethyl acetate/hexanes) to yield the pure product as a viscous purple oil (1.15 g, 77%).  $^1H$ -NMR (DMSO- $d_6$ ):  $\delta$  8.42-8.40 (m, 2H), 7.33-7.3 (m, 2H), 6.89 (dd, 1H,  $J$  = 2.0 Hz, 8.3 Hz), 4.02 (q, 2H,  $J$  = 7.1 Hz), 2.76 (t, 2H,  $J$  = 7.5 Hz), 2.54 (t, 2H,  $J$  = 7.5 Hz), 1.45 (s, 9H), 1.44 (s, 9H), 1.14 (t, 3H,  $J$  = 7.1 Hz).  $^{13}C$ -NMR (DMSO- $d_6$ ):  $\delta$  172.8, 154, 153.8,



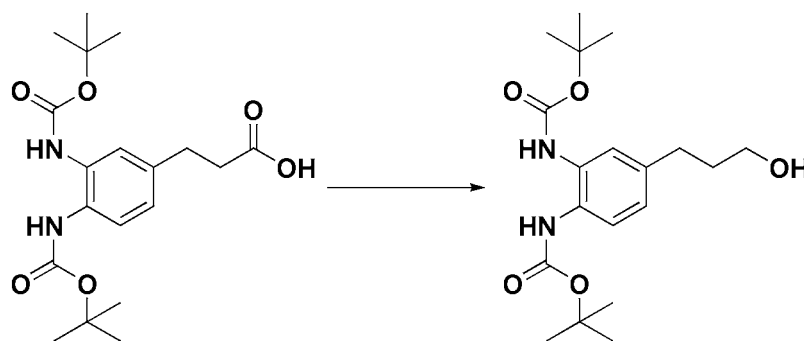
137.2, 130.8, 128.6, 124.7, 124.5, 124, 80.0, 79.9, 60.5, 35.9, 30.5, 28.7, 14.7.

HR-EIMS  $m/z$  calculated for  $C_{21}H_{33}N_2O_6$ : 409.2339, found: 409.2326.



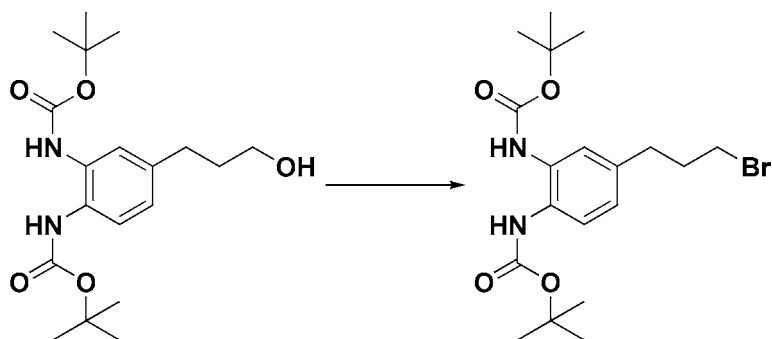
**3-(3,4-Bis-tert-butoxycarbonylamino-phenyl)-propionic acid (6).** Compound **5** (1.82 g, 4.44 mmol) was dissolved in a 9:1 v/v solution of dichloromethane/methanol (81 mL) and cooled to 0°C. 2 M methanolic NaOH (9 mL) was slowly added to the reaction to give a final NaOH concentration of 0.2 M (Theodorou et al., 2007). The reaction was then brought to room temperature and stirred overnight. The solution was concentrated under vacuum and the resulting residue was dissolved in water (200 mL). The aqueous phase was extracted with diethyl ether (3 X 70 mL), cooled in an ice bath, and acidified to pH 6 with 1 M HCl. The resulting precipitate was extracted with ethyl acetate (3 X 100 mL) and the combined organic phases were washed with brine (100 mL) and dried over  $Na_2SO_4$ . The solvent was evaporated under vacuum to yield the pure product as a pale, pink solid (1.29 g, 76%).  $^1H$ -NMR (DMSO- $d_6$ ):  $\delta$  12.12 (br s, 1H), 8.41 (br s, 2H), 7.32-7.29 (m, 2H), 6.90 (dd, 1H,  $J$  = 1.8 Hz, 8.3 Hz), 2.73 (t,

2H,  $J = 7.5$  Hz), 2.46 (t, 2H,  $J = 7.5$  Hz), 1.44 (s, 9H), 1.44 (s, 9H).  $^1\text{H-NMR}$  ( $\text{CD}_3\text{OD}$ ):  $\delta$  7.32-7.30 (m, 2H), 7 (dd, 1H,  $J = 2.0$  Hz, 8.2 Hz), 2.87 (t, 2H,  $J = 7.8$  Hz), 2.58 (t, 2H,  $J = 7.9$  Hz), 1.51 (s, 9H), 1.5 (s, 9H).  $^{13}\text{C-NMR}$  ( $\text{DMSO-d}_6$ ):  $\delta$  174.3, 154, 15, 137.6, 130.8, 128.6, 124.7, 124.5, 124.0, 80.0, 79.9, 36, 30.6, 28.7. HR-EIMS  $m/z$  calculated for  $\text{C}_{19}\text{H}_{29}\text{N}_2\text{O}_6$ : 381.2026, found: 381.2001.



**[2-tert-Butoxycarbonylamino-5-(3-hydroxy-propyl)-phenyl]-carbamic acid tert-butyl ester (7).** Compound **6** (1.19 g, 3.13 mmol) was dissolved in THF (33 mL) and cooled to  $0^\circ\text{C}$ . A 1 M solution of  $\text{BH}_3\cdot\text{THF}$  (33 mL) was added to the reaction dropwise via an addition funnel, resulting in the pale pink solution becoming pale yellow. The reaction was then brought to room temperature and stirred overnight leading to an almost complete loss of color. The solution was then cooled to  $-15^\circ\text{C}$  and excess borane was quenched by the slow addition of methanol (12 mL), resulting in the return of a pale pink hue. The solution was concentrated via rotary evaporation and the crude material was dissolved in 1 M HCl (100 mL). The aqueous phase was extracted with ethyl acetate (1 X 100 mL,

4 X 50 mL) and the combined organic phases were washed with 0.1 M HCl (100 mL), water (100 mL) and brine (100 mL) and dried over Na<sub>2</sub>SO<sub>4</sub>. The solvent was evaporated under vacuum and the crude material was purified by flash column chromatography (0-50% ethyl acetate/hexanes) to yield the pure product as a fluffy white solid (1.02 g, 89%). <sup>1</sup>H-NMR (DMSO-d<sub>6</sub>): δ 8.40-8.38 (m, 2H), 7.30-7.28 (m, 2H), 6.87 (dd, 1H, *J* = 2 Hz, 8.2 Hz), 4.44 (t, 1H, *J* = 5.2 Hz), 3.38 (q, 2H, *J* = 5.2 Hz), 2.52 (t, 2H, *J* = 7.5 Hz), 1.69-1.62 (m, 2H), 1.45 (s, 9H), 1.44 (s, 9H). <sup>13</sup>C-NMR (DMSO-d<sub>6</sub>): δ 154.0, 153.8, 138.9, 130.9, 128.1, 124.8, 124.6, 124.0, 80.0, 79.9, 60.7, 35.1, 31.9, 28.7. HR-EIMS *m/z* calculated for C<sub>19</sub>H<sub>30</sub>N<sub>2</sub>O<sub>5</sub>Na: 389.2047, found: 389.2034.



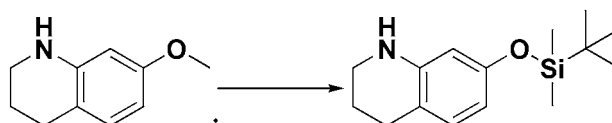
**[5-(3-Bromo-propyl)-2-tert-butoxycarbonylamino-phenyl]-carbamic acid tert-butyl ester (8).** Ethyl tribromoacetate (0.4 mL, 2.72 mmol) was added to a solution of **7** (996 mg, 2.72 mmol) and triphenylphosphine (1.07 g, 4.08 mmol) in dichloromethane (10 mL) (Tongkate et al., 2008). The reaction was stirred at room temperature and monitored by TLC (25% ethyl acetate/hexanes). After 40

minutes, no trace of **7** remained and the reaction was quenched with ice water (100 mL) and stirred at ambient conditions for 5 minutes. The aqueous phase was extracted with dichloromethane (1 X 100 mL, 2 X 50 mL) and the combined organic phases were washed with brine (100 mL) and dried over Na<sub>2</sub>SO<sub>4</sub>. The solvent was evaporated under vacuum and the crude material was purified by flash column chromatography (0-25% ethyl acetate/hexanes) to yield the pure product as a viscous, yellow oil. Upon washing with dichloromethane and drying under reduced pressure, the product becomes an airy white solid (1.05 g, 90%). <sup>1</sup>H-NMR (CDCl<sub>3</sub>): δ 7.29-7.24 (m, 2H), 7.07-6.97 (m, 2H), 6.81 (dd, 1H, *J* = 1.8 Hz, 8.2 Hz), 3.29 (t, 2H, *J* = 6.6 Hz), 2.61 (t, 2H, *J* = 7.1 Hz), 2.03 (p, 2H, *J* = 6.6 Hz, 7 Hz), 1.46 (s, 9H), 1.45 (s, 9H). <sup>13</sup>C-NMR (CDCl<sub>3</sub>): δ 154.3, 154.0, 138.0, 130.9, 128.0, 125.2, 124.8, 123.9, 80.8, 34.2, 33.6, 33.3, 28.5, 28.5. HR-EIMS *m/z* calculated for C<sub>19</sub>H<sub>29</sub>BrN<sub>2</sub>O<sub>4</sub>Na: 451.1203 and 453.1182, found: 451.1196 and 453.1175.



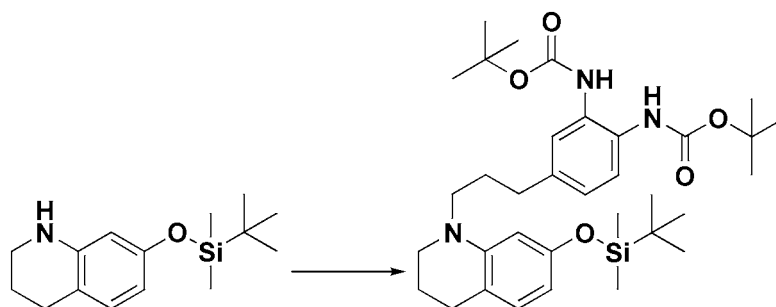
**1,2,3,4-tetrahydroquinolin-7-ol (9)**. 7-hydroxy-3,4-dihydro-1*H*-quinolin-2-one (2.19 g, 13.4 mmol) was dissolved in THF (20 mL) and cooled to 0 °C. 1 M BH<sub>3</sub>·THF (136 mL, 136 mmol) was added to the solution dropwise via an addition funnel over 85 minutes and the reaction was refluxed overnight. The reaction

was then cooled in a methanol/ice bath and quenched by the slow addition of methanol (24 mL). After quenching, the solution was acidified to pH 1 with concentrated hydrochloric acid (12 mL) and heated to 60 °C for 1 hour. The reaction was then cooled to 0 °C, neutralized with concentrated sodium hydroxide, and extracted with ethyl acetate (1X200 mL, 3X50 mL). The combined organic phases were washed with water (2X100 mL), brine (1X80 mL, 3X50 mL), and dried over sodium sulfate. Solvent was removed via rotary evaporation and the crude material was purified by flash column chromatography (0-25% ethyl acetate/hexanes) to yield the pure product as a white crystalline solid (1.91 g, 94 %). <sup>1</sup>H-NMR (CDCl<sub>3</sub>): δ 6.79 (d, 1H, *J* = 8.1 Hz), 6.09 (dd, 1H, *J* = 2.5 Hz, 8.1 Hz), 5.97 (d, 1H, *J* = 2.5 Hz), 4.19 (br s, 1H), 3.27 (t, 2H, *J* = 5.5 Hz), 2.68 (t, 2H, *J* = 6.4 Hz), 1.94-1.88 (m, 2H). <sup>13</sup>C-NMR (CDCl<sub>3</sub>): δ 155, 145.4, 130.6, 114.7, 105.7, 101.9, 42.2, 26.4, 22.6. HR-EIMS: *m/z* calculated for C<sub>9</sub>H<sub>12</sub>NO: 150.0919, found: 150.0938.



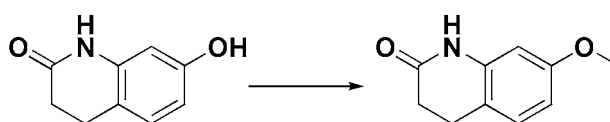
**7-(tert-Butyl-dimethyl-silyloxy)-1,2,3,4-tetrahydroquinoline (10).** Imidazole (1.14 g, 16.8 mmol) was added to a solution of **9** (1 g, 6.7 mmol) in DMF (13.4 mL) and stirred at room temperature for 10 minutes. *tert*-Butyldimethylchlorosilane (1.2 g, 8.04 mmol) was added to the reaction and the

solution was stirred at room temperature overnight. The reaction was diluted into 5% NaHCO<sub>3</sub> (140 mL) and extracted with ethyl acetate (6 X 50 mL). The combined organic phases were washed with 0.1 M HCl (100 mL), brine (100 mL), and dried over Na<sub>2</sub>SO<sub>4</sub>. The solvent was evaporated under vacuum and the crude material was purified by flash column chromatography (0-10% ethyl acetate/hexanes) to yield the pure product as a crystalline, white solid (1.61 g, 91%). <sup>1</sup>H-NMR (CDCl<sub>3</sub>): δ 6.76 (d, 1H, *J* = 8.1 Hz), 6.11 (dd, 1H, *J* = 2.4 Hz, 8.1 Hz), 5.98 (d, 1H, *J* = 2.4 Hz), 3.73 (br s, 1H), 3.26 (t, 2H, *J* = 5.5 Hz), 2.68 (t, 2H, *J* = 6.4 Hz), 1.94-1.88 (m, 2H), 0.96 (s, 9H), 0.17 (s, 6H). <sup>13</sup>C-NMR (CDCl<sub>3</sub>): δ 154.8, 145.9, 130.2, 114.8, 109.1, 105.8, 42.2, 26.8, 26.2, 22.8, 18.6, -4. HR-EIMS: *m/z* calculated for C<sub>15</sub>H<sub>26</sub>NOSi: 264.1784, found: 264.1752.



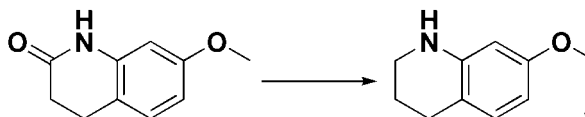
**(2-tert-Butoxycarbonylamino-5-{3-[7-(tert-butyl-dimethyl-silyloxy)-3,4-dihydro-2H-quinolin-1-yl]-propyl}-phenyl)-carbamic acid tert-butyl ester (11).** A reaction vial charged with compound **10** (250 mg, 0.949 mmol) and K<sub>2</sub>CO<sub>3</sub> (158 mg, 1.14 mmol) was evacuated and backfilled with argon.

Compound **8** (490 mg, 1.14 mmol) dissolved in DMF (2 mL) was added to the reaction vial and the mixture was heated to 65 °C and stirred for 2 days. The reaction was then cooled to room temperature, diluted into water (20 mL), and acidified to pH 1 with 1 M HCl. The aqueous phase was extracted with ethyl acetate (1 X 30 mL, 4 X 10 mL) and the combined organic phases were washed with 0.1 M HCl (30 mL) and brine (50 mL), and dried over Na<sub>2</sub>SO<sub>4</sub>. The solvent was evaporated under vacuum and the crude material was purified by flash column chromatography (0-5% ethyl acetate/hexanes) to yield the pure product as a viscous, gold oil (261 mg, 45%). <sup>1</sup>H-NMR (CDCl<sub>3</sub>): δ 7.35 (br s, 2H), 6.94 (d, 1H, *J* = 8.1 Hz), 6.75 (d, 2H, *J* = 8.0 Hz), 6.62 (br s, 1H), 6.04 (br s, 2H), 3.21 (t, 4H, *J* = 7.2 Hz), 2.66 (t, 2H, *J* = 6.3 Hz), 2.61 (t, 2H, *J* = 7.8 Hz), 1.93-1.84 (m, 4H), 1.51 (s, 9H), 1.51 (s, 9H), 0.97 (s, 9H), 0.18 (s, 6H). HR-EIMS: *m/z* calculated for C<sub>34</sub>H<sub>54</sub>N<sub>3</sub>O<sub>5</sub>Si: 612.3820, found: 612.3833.



**7-Methoxy-3,4-dihydro-1H-quinolin-2-one (12).** Potassium carbonate (3.8 g, 27.8 mmol) was suspended in a solution of 7-hydroxy-3,4-dihydro-1H-quinolin-2-one (3 g, 18.4 mmol) in DMF (37 mL). Methyl iodide (1.5 mL, 23.9 mmol) was added to the mixture, which resulted in the reaction becoming white and opaque. The reaction was then heated to 65 °C and stirred overnight. The mixture was

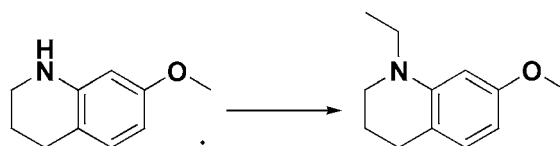
cooled to room temperature, poured into water (350 mL) and acidified to pH 5 with 1 M HCl (30 mL) with stirring. After 5 minutes, a frothy solid was suspended atop the aqueous solution which was then dissolved in ethyl acetate (150 mL). The organic phase was collected and the aqueous phase was further acidified to pH 1 with 1 M HCl (10 mL) and extracted with ethyl acetate (9 X 60 mL). The combined organic phases were washed with water (2 X 200 mL), brine (450 mL), and dried over Na<sub>2</sub>SO<sub>4</sub>. The solvent was evaporated under vacuum and the crude material was purified by flash column chromatography (0-50% ethyl acetate/hexanes) to yield the pure product as a white crystalline solid (2.84 g, 87 %). <sup>1</sup>H-NMR (CDCl<sub>3</sub>): δ 7.77 (br s, 1H), 7.06 (d, 1H, *J* = 8.3 Hz), 6.53 (dd, 1H, *J* = 2.5 Hz, 8.3 Hz), 6.30 (d, 1H, *J* = 2.4 Hz), 3.78 (s, 3H), 2.9 (t, 2H, *J* = 7.9 Hz), 2.62 (t, 2H, *J* = 7.8 Hz). <sup>13</sup>C-NMR (CDCl<sub>3</sub>): δ 172.8, 159.4, 138.5, 128.8, 115.9, 108.5, 101.9, 55.7, 31.3, 24.8. HR-EIMS *m/z* calculated for C<sub>10</sub>H<sub>12</sub>NO<sub>2</sub>: 178.0868, found: 178.0867.



**7-Methoxy-1,2,3,4-tetrahydroquinoline (13).** Compound **12** (2.77 g, 15.6 mmol) was dissolved in THF (60 mL) and cooled to 0 °C. 1 M BH<sub>3</sub>·THF (235 mL) was added to the solution dropwise through an addition funnel over 1.5 hours and the reaction was refluxed overnight. The reaction was then cooled in a methanol/ice

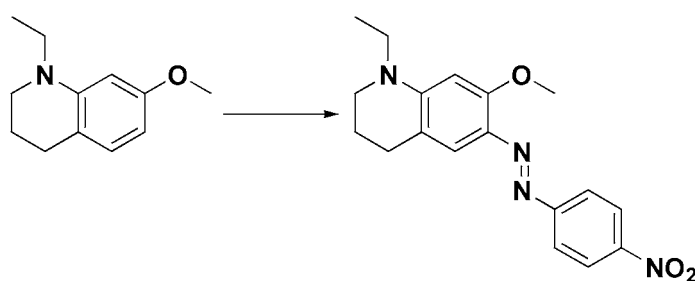


bath and quenched by the slow addition of methanol (40 mL). After quenching, the solution was acidified to pH 1 with concentrated hydrochloric acid (5 mL) resulting in formation of a white precipitate. The mixture was heated to 65 °C for 1 hour, cooled to 0 °C, and neutralized with 6.25 M NaOH (22 mL), resulting in the mixture obtaining a dull, yellow hue. The mixture was diluted into 50 % ethyl acetate/water (600 mL) and the organic phase was separated. The aqueous phase was further extracted with ethyl acetate (2 X 100 mL) and the combined organic phases were washed with brine (2 X 500 mL) and dried over sodium sulfate. Solvent was removed via rotary evaporation and the crude material was purified by flash column chromatography (0-25% ethyl acetate/hexanes) to yield the pure product as a non-viscous, yellow-orange oil (2.45, 96%). <sup>1</sup>H-NMR (CDCl<sub>3</sub>): δ 6.83 (d, 1H, *J* = 8.2 Hz), 6.2 (dd, 1H, *J* = 2.5 Hz, 8.2 Hz), 6.03 (d, 1H, *J* = 2.5 Hz), 3.8 (br s, 1H), 3.73 (s, 3H), 3.28 (t, 2H, *J* = 5.5 Hz), 2.69 (t, 2H, *J* = 6.4 Hz), 1.95-1.88 (m, 2H). <sup>13</sup>C-NMR (CDCl<sub>3</sub>): δ 159.2, 146.0, 130.4, 114.3, 103.0, 99.7, 55.4, 42.3, 26.7, 22.8. HR-EIMS *m/z* calculated for C<sub>10</sub>H<sub>14</sub>NO: 164.1075, found: 164.1075.



**1-Ethyl-7-methoxy-1,2,3,4-tetrahydroquinoline (14).** Potassium carbonate (1.16 g, 8.38 mmol) was suspended in a solution of compound **13** (912 mg, 5.59

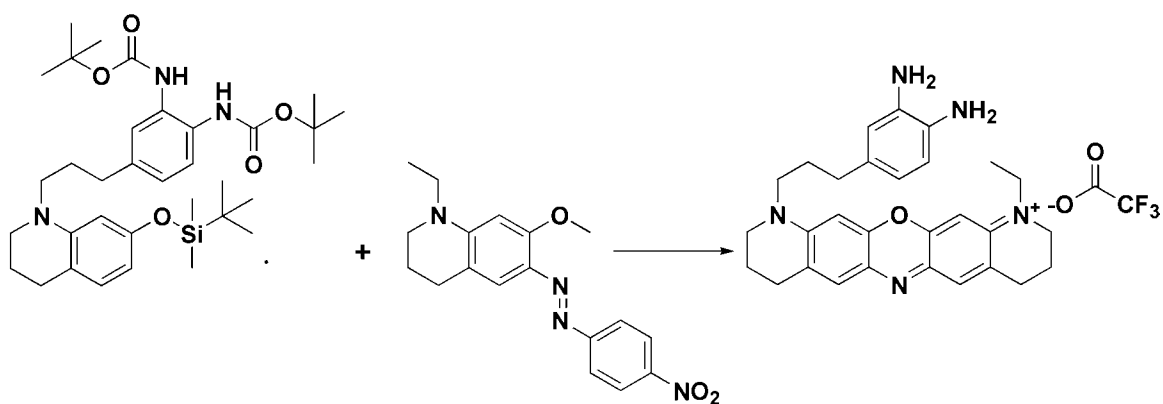
mmol) in DMF (5 mL). Ethyl iodide (0.54 mL, 6.75 mmol) was added to the mixture and the reaction was heated to 65 °C and stirred overnight. The mixture was cooled to room temperature, diluted into water (80 mL), and acidified to pH 3 with 1 M HCl. The aqueous phase was extracted with ethyl acetate (1 X 80 mL, 5 X 50 mL) and the combined organic phases were washed with water (3 X 60 mL) and brine (80 mL) and dried over Na<sub>2</sub>SO<sub>4</sub>. The solvent was evaporated under vacuum and the crude material was purified by flash column chromatography (0-5% acetone/hexanes) to yield the pure product as a pale yellow oil (907 mg, 85 %). <sup>1</sup>H-NMR (CDCl<sub>3</sub>): δ 6.84 (d, 1H, *J* = 8.1 Hz), 6.18 (d, 1H, *J* = 2.1 Hz), 6.13 (dd, 1H, *J* = 2.4 Hz, 8.1 Hz), 3.78 (s, 3H), 3.32 (q, 2H, *J* = 7.1 Hz), 3.24 (t, 2H, *J* = 5.6 Hz), 2.68 (t, 2H, *J* = 6.4 Hz), 1.96-1.9 (m, 2H), 1.14 (t, 3H, *J* = 7.1Hz). <sup>13</sup>C-NMR (CDCl<sub>3</sub>): δ 159.6, 146.1, 129.7, 115.6, 99.8, 97.6, 55.4, 48.6, 45.7, 27.8, 22.8, 11.1. HR-EIMS *m/z* calculated for C<sub>12</sub>H<sub>18</sub>NO<sub>2</sub>: 192.1388, found: 192.1379.



**(1-Ethyl-7-methoxy-1,2,3,4-tetrahydro-quinolin-6-yl)-(4-nitro-phenyl)-diazene**

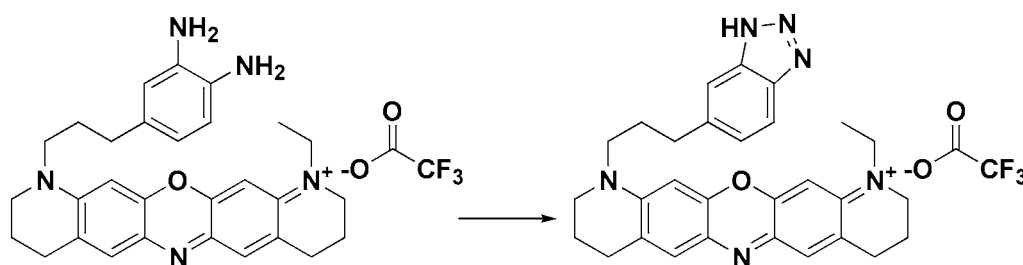
**(15).** 4-Nitrobenzenediazonium tetrafluoroborate (573 mg, 2.42 mmol) was suspended in 10% H<sub>2</sub>SO<sub>4</sub> (1.6 mL) and added dropwise to a solution of **14** (462

mg, 2.42 mmol) in methanol (2 mL) resulting in an opaque, deep red appearance. The solution was stirred at ambient conditions for 1 hour and then cooled in an ice bath. The reaction was neutralized with ammonium hydroxide solution (28-30%) and the crude product was isolated via filtration and washed with water (300 mL) to give a red-black solid. The crude material was then recrystallized in n-butanol/water to provide the pure compound as purple-black crystals (524 mg, 64%).  $^1\text{H-NMR}$  ( $\text{CDCl}_3$ ):  $\delta$  8.26 (d, 2H,  $J = 8.9$  Hz), 7.84 (d, 2H,  $J = 8.9$  Hz), 7.58 (s, 1H), 6.11 (s, 1H), 4.00 (s, 3H), 3.46 (q, 2H,  $J = 7.1$  Hz), 3.38 (t, 2H,  $J = 5.6$  Hz), 2.71 (t, 2H,  $J = 6.0$  Hz), 1.95 (p, 2H,  $J = 5.6$  Hz, 6.1 Hz), 1.26 (t, 3H,  $J = 7.1$  Hz).  $^{13}\text{C-NMR}$  ( $\text{CDCl}_3$ ):  $\delta$  160.3, 158, 151.4, 146.7, 133.6, 124.9, 122.5, 117.7, 116.5, 92.8, 56.5, 49.2, 46.3, 27.5, 22.2, 11.5. HR-EIMS  $m/z$  calculated for  $\text{C}_{18}\text{H}_{21}\text{N}_4\text{O}_3$ : 341.1614, found: 341.1625.



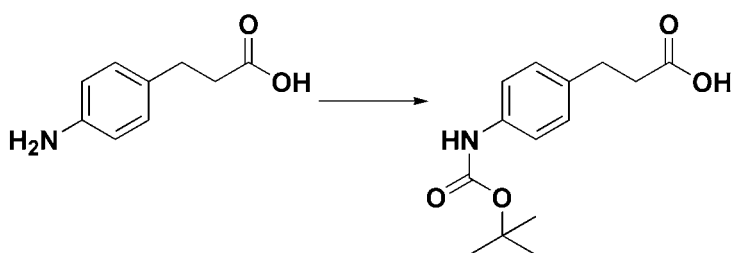
**11-[3-(3,4-diamino-phenyl)-propyl]-1-ethyl-3,4,8,9,10,11-hexahydro-2H-13-oxa-6,11-diaza-1-azonia-pentacene trifluoroacetate (16).** Compound 11 (80

mg, 131  $\mu\text{mol}$ ) and **15** (45 mg, 131  $\mu\text{mol}$ ) were dissolved in a 10:1 solution of EtOH/H<sub>2</sub>O (1 mL/100  $\mu\text{L}$ ). Concentrated HCl (70  $\mu\text{L}$ ) was added to the solution with stirring and the reaction was heated to 80 °C for 3 hours. The reaction was cooled to room temperature and concentrated under vacuum. The crude material was purified via RP-HPLC (0-40% 0.1% Trifluoroacetic acid in acetonitrile/0.1% Trifluoroacetic acid in water) to yield the pure product as a blue solid (16 mg, 21%). <sup>1</sup>H-NMR (CD<sub>3</sub>OD):  $\delta$  7.46 (s, 1H), 7.43 (s, 1H), 7.01 (s, 1H), 6.69 (d, 1H,  $J$  = 7.8 Hz), 6.62 (d, 1H,  $J$  = 1.9 Hz), 6.51 (dd, 1H,  $J$  = 2 Hz, 7.8 Hz), 6.47 (s, 1H), 3.75 (q, 2H,  $J$  = 7.2Hz), 3.7 (t, 2H,  $J$  = 5.6 Hz), 3.65-3.59 (m, 4H), 2.93 (t, 2H,  $J$  = 5.9 Hz), 2.89 (t, 2H,  $J$  = 5.9 Hz), 2.59 (t, 2H,  $J$  = 7 Hz), 2.08-1.97 (m, 6H), 1.37 (t, 3H,  $J$  = 7.2 Hz). HR-EIMS  $m/z$  calculated for C<sub>29</sub>H<sub>34</sub>N<sub>5</sub>O: 468.2763, found: 468.2775.



**11-[3-(3H-benzotriazol-5-yl)-propyl]-1-ethyl-3,4,8,9,10,11-hexahydro-2H-13-oxa-6,11-diaza-1-azonia-pentacene trifluoroacetate (17)**. Compound 16 (6.11 mg, 10.5  $\mu\text{M}$ ) was suspended in PBS, pH 7.4 (1 mL). A solution of Diethylammonium (Z)-1-(N,N-diethylamino)diazene-1-ium-1,2-diolate (DEA

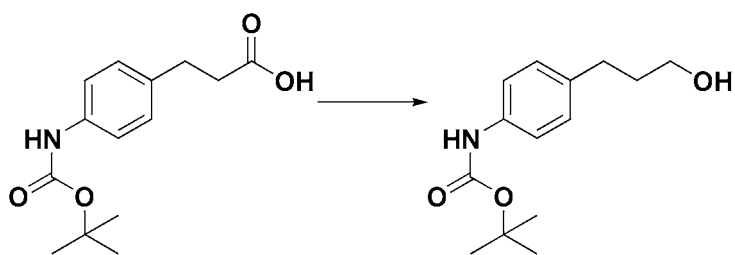
NONOate) (2.38 mg, 11.6  $\mu$ M) in PBS, pH 7.4 (1 mL) was added to the reaction and the mixture was stirred at ambient conditions for 1 hour. The reaction was dried under speed vacuum and purified via RP-HPLC (10-50% 0.1% Trifluoroacetic acid in acetonitrile/0.1% Trifluoroacetic acid in water) to yield the pure product as a blue solid (1.2 mg, 20%). HR-EIMS  $m/z$  calculated for  $C_{29}H_{31}N_6O$ : 479.2559, found: 479.2523.



**3-(4-tert-Butoxycarbonylamino-phenyl)-propionic acid (18).** 3-(4-

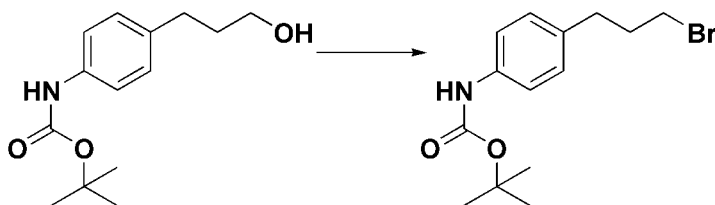
Aminophenyl)propionic acid (500 mg, 3.03 mmol) was dissolved in THF (15 mL) and cooled to 0°C. A solution of Di-tert-butyl dicarbonate (1.32 g, 6.05 mmol) in THF (15 mL) was then added dropwise to the reaction. The reaction was then brought to room temperature and stirred overnight. The solution was poured into water (300 mL) and acidified to pH 4 with 1 M HCl, resulting in precipitation of a yellow solid. The product was then extracted with dichloromethane (3 X 100 mL) and the combined organic phases were washed with brine (300 mL) and dried over  $Na_2SO_4$ . The solvent was evaporated under vacuum to yield a yellow solid that was identified by NMR to be the product and residual  $Boc_2O$ . The crude

material was dissolved in an 1:2 ethyl acetate/water mixture (300 mL), basified to pH 9 with 5 M NaOH and the organic phase was separated. The aqueous phase was further extracted with ethyl acetate (2 X 200 mL) and dichloromethane (100 mL) to remove any remaining impurity. The aqueous phase was then acidified to pH 1 with 1 M HCl, extracted with dichloromethane (3 X 100 mL), and the combined organic phases washed with brine (200 mL) and dried over Na<sub>2</sub>SO<sub>4</sub>. Evaporation of the solvent under vacuum gave the pure product as an off-white solid (689 mg, 86%). <sup>1</sup>H-NMR (DMSO-d<sub>6</sub>): δ 12.08 (s, 1H), 9.22 (s, 1H), 7.32 (d, 2H, *J* = 8.3 Hz), 7.07 (d, 2H, *J* = 8.5 Hz), 2.71 (t, 2H, *J* = 7.7 Hz), 2.45 (t, 2H, *J* = 7.7 Hz), 1.44 (s, 9H). <sup>1</sup>H-NMR (CD<sub>3</sub>OD): δ 7.28 (d, 2H, *J* = 8.4 Hz), 7.11 (d, 2H, *J* = 8.5 Hz), 2.84 (t, 2H, *J* = 7.8 Hz), 2.55 (t, 2H, *J* = 7.9 Hz), 1.50 (s, 9H). <sup>13</sup>C-NMR (DMSO-d<sub>6</sub>): δ 174.5, 153.5, 138.2, 135.0, 129.0, 118.8, 79.5, 36.1, 30.4, 28.8. HR-EIMS *m/z* calculated for C<sub>14</sub>H<sub>19</sub>NO<sub>4</sub>Na: 288.1212, found: 288.1225.



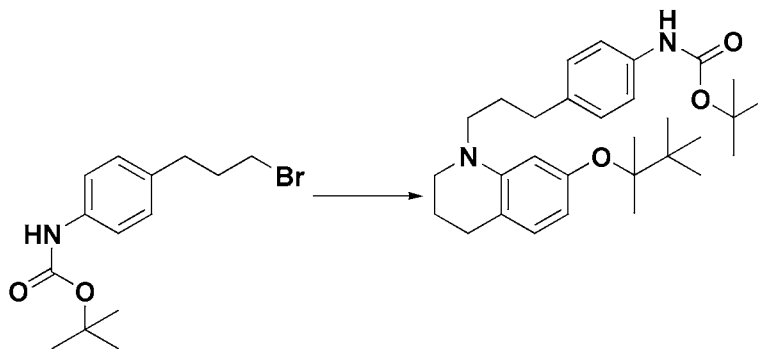
**[4-(3-Hydroxy-propyl)-phenyl]-carbamic acid tert-butyl ester (19).** Compound **18** (500 mg, 1.88 mmol) was dissolved in THF (19 mL) and cooled to 0°C. A 1 M solution of BH<sub>3</sub>·THF (19 mL) was added to the reaction dropwise over 35

minutes, resulting in the pale yellow solution becoming clear and colorless. The reaction was then brought to room temperature and stirred overnight. The solution was cooled to 0 °C and excess borane was quenched by the slow addition of methanol (10 mL). The solution was concentrated via rotary evaporation to give a clear oil which was dissolved in ethyl acetate (200 mL). The organic phase was washed with 1 M NaOH (2 X 50 mL), 1 M HCl (100 mL), and brine (100 mL) and dried over Na<sub>2</sub>SO<sub>4</sub>. The solvent was evaporated under vacuum and the crude material was purified by flash column chromatography (0-50% ethyl acetate/hexanes) to yield the pure product as a viscous, clear, colorless oil which becomes a white solid when cooled to 4 °C (473 mg, Quantitative). <sup>1</sup>H-NMR (CDCl<sub>3</sub>): δ 7.26 (d, 2H, *J* = 7.8 Hz), 7.11 (d, 2H, *J* = 8.4 Hz), 6.45 (br s, 1H), 3.65 (q, 2H, *J* = 5.3 Hz), 2.66 (t, 2H, *J* = 7.4 Hz), 1.89-1.82 (m, 2H), 1.51 (s, 9H), 1.36 (t, 1H, *J* = 5.1 Hz). <sup>1</sup>H-NMR (CD<sub>3</sub>OD): δ 7.27 (d, 2H, *J* = 8.3 Hz), 7.09 (d, 2H, *J* = 8.4 Hz), 3.55 (t, 2H, *J* = 6.5 Hz), 2.61 (t, 2H, *J* = 7.4 Hz), 1.83-1.76 (m, 2H), 1.50 (s, 9H). <sup>13</sup>C-NMR (CDCl<sub>3</sub>): δ 153.1, 136.7, 136.4, 129.1, 119.0, 80.6, 62.4, 34.5, 31.6, 28.6. HR-EIMS *m/z* calculated for C<sub>14</sub>H<sub>21</sub>NO<sub>3</sub>Na: 274.1419, found: 274.1433.



**[4-(3-Bromo-propyl)-phenyl]-carbamic acid tert-butyl ester (20)**. Ethyl tribromoacetate<sup>2</sup> (0.26 mL, 1.79 mmol) was added to a solution of **19** (451 mg, 1.79 mmol) and triphenylphosphine (717 mg, 2.69 mmol) in dichloromethane (3.6 mL) (Tongkate et al., 2008). The reaction was stirred at room temperature and monitored by TLC (25% ethyl acetate/hexanes). After 55 minutes, no trace of **19** remained and the reaction was quenched with ice water (80 mL) and stirred at ambient conditions for 5 minutes. The aqueous phase was extracted with dichloromethane (1 X 20 mL, 2 X 30 mL) and the combined organic phases were washed with brine (30 mL) and dried over Na<sub>2</sub>SO<sub>4</sub>. The solvent was evaporated under vacuum and the crude material was purified by flash column chromatography (0-10% ethyl acetate/hexanes) to yield the pure product as a white, crystalline solid (395 mg, 70%). <sup>1</sup>H-NMR (DMSO-d<sub>6</sub>): δ 9.23 (s, 1H), 7.34 (d, 2H, *J* = 8.4 Hz), 7.06 (d, 2H, *J* = 8.5 Hz), 3.46 (t, 2H, *J* = 6.6 Hz), 2.61 (t, 2H, *J* = 7.1 Hz), 2.03 (p, 2H, *J* = 6.4 Hz, 7.2 Hz), 1.44 (s, 9H). <sup>13</sup>C-NMR (DMSO-d<sub>6</sub>): δ 153.5, 138.2, 134.7, 129.2, 118.9, 79.5, 35.1, 34.7, 33.4, 28.8. HR-EIMS *m/z* calculated for C<sub>14</sub>H<sub>20</sub>BrNO<sub>2</sub>Na: 336.0575 and 338.0556, found: 336.0535 and 338.0516.





**(4-{3-[7-(tert-Butyl-dimethyl-silyloxy)-3,4-dihydro-2H-quinolin-1-yl]-**

**propyl}-phenyl)-carbamic acid tert-butyl ester (21).** Potassium carbonate (81

mg, 0.59 mmol) was suspended in a solution of compound **10** (129 mg, 0.49

mmol) in DMF (2 mL). Compound **20** (200 mg, 0.636 mmol) was added to the

mixture and the reaction was heated to 70 °C and stirred overnight. The reaction

was then cooled to room temperature, diluted into water (50 mL), and acidified to

pH 1 with 1 M HCl. The aqueous phase was extracted with ethyl acetate (1 X 60

mL, 4 X 20 mL) and the combined organic phases were washed with 0.1 M HCl

(80 mL), water (80 mL), and brine (80 mL), and dried over Na<sub>2</sub>SO<sub>4</sub>. The solvent

was evaporated under vacuum and the crude material was purified by flash

column chromatography (0-5% ethyl acetate/hexanes) to yield the pure product

as an orange oil (136 mg, 56%). <sup>1</sup>H-NMR (CDCl<sub>3</sub>): δ 7.29 (d, 2H, *J* = 8.2 Hz),

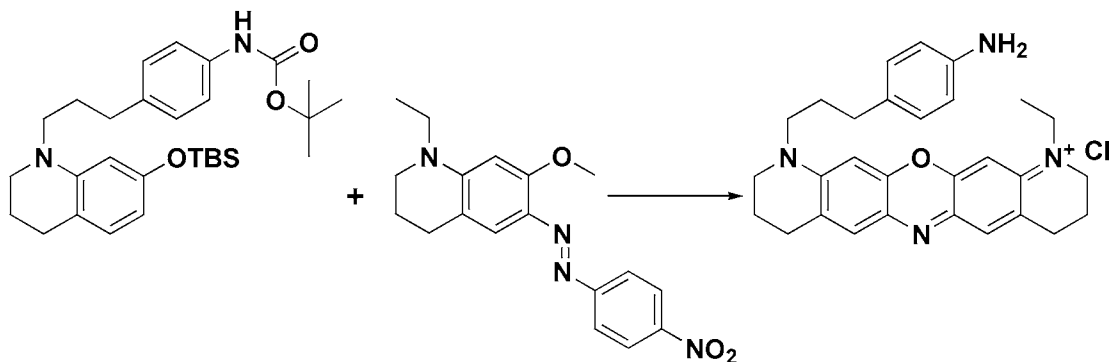
7.12 (d, 2H, *J* = 8.5 Hz), 6.76 (d, 1H, *J* = 7.9 Hz), 6.51 (s, 1H), 6.06 (dd, 1H, *J* =

2.3 Hz, 7.9 Hz), 6.03 (d, 1H, *J* = 2.3 Hz), 3.23-3.2 (m, 4H), 2.67 (t, 2H, *J* = 6.3

Hz), 2.62 (t, 2H, *J* = 7.6 Hz), 1.94-1.85 (m, 4H), 1.53 (s, 9H), 0.99 (s, 9H), 0.19

(s, 6H). <sup>13</sup>C-NMR (CDCl<sub>3</sub>): δ 155.1, 146.2, 136.7, 136.4, 129.6, 129, 118.9,

115.6, 107.1, 102.8, 51.3, 49.4, 33.0, 28.6, 28, 27.7, 26.1, 22.7, 18.5, -4.0. HR-EIMS:  $m/z$  calculated for  $C_{29}H_{44}N_2O_3SiNa$ : 519.3019, found: 519.2989.



**11-[3-(4-Amino-phenyl)-propyl]-1-ethyl-3,4,8,9,10,11-hexahydro-2H-13-oxa-6,11-diaza-1-azonia-pentacene chloride (22).** Compound **15** (93 mg, 274  $\mu\text{mol}$ ) and **21** (136 mg, 274  $\mu\text{mol}$ ) were dissolved in a 10:1 solution of EtOH/H<sub>2</sub>O (1.5 mL/150  $\mu\text{L}$ ). Concentrated HCl (105  $\mu\text{L}$ ) was added to the solution with stirring and the reaction was heated to 80 °C for 2 hours. The reaction was cooled to room temperature and the crude dye was isolated via flash chromatography (0-50% methanol/dichloromethane). The pure product was isolated with a 2<sup>nd</sup> round of flash chromatography (0-10% methanol/dichloromethane) to yield a blue solid (29.55 mg, 22%). <sup>1</sup>H-NMR (CD<sub>3</sub>OD):  $\delta$  7.36 (s, 1H), 7.32 (s, 1H), 7 (d, 2H,  $J = 8.3$  Hz), 6.92 (s, 1H), 6.72 (d, 2H,  $J = 8.3$  Hz), 6.37 (s, 1H), 3.74-3.51 (m, 9H), 3.6 (t, 2H,  $J = 5.8$  Hz), 3.53 (t, 2H,  $J = 8$  Hz), 2.89 (t, 2H,  $J = 6.3$  Hz), 2.84 (t, 2H,  $J = 6.4$  Hz), 2.61 (t, 2H,  $J = 7.0$  Hz), 2.05-1.94 (m, 7H), 1.35 (t, 3H,  $J = 7.1$  Hz). <sup>13</sup>C-NMR

(CD<sub>3</sub>OD):  $\delta$  154.2, 154.1, 148.7, 148.4, 146, 134.1, 133.9, 130.5, 130.4, 130.3, 129.1, 129.0, 128.9, 115.8, 95.0, 94.9, 52.0, 50.7, 50, 47.8, 31.8, 28.2, 27.3, 27.2, 20.8, 20.7, 10.6. HR-EIMS  $m/z$  calculated for C<sub>29</sub>H<sub>33</sub>N<sub>4</sub>O: 453.2654, found: 453.2647.

## CHAPTER VI: Discussion

Live cell and *in vivo* fluorescence imaging have led to innumerable and unquestioningly vital discoveries in biology. Since the inclusion of the Green Fluorescent Protein and its derivatives in basic research, we have been able to study protein localization, kinetics, and intracellular interactions in real time (Tavaré et al., 2001; Zimmer, 2002). Organic fluorophores like rhodamine and fluorescein have also been extensively exploited in the biological field. Rhodamine 123 has been utilized in studies of mitochondrial function and ABC transporter activity (Johnson et al., 1980; Twentyman et al., 1994). FITC has long been used in flow cytometry but has also been employed in the study of the extracellular matrix (Hsieh et al., 1980). The list of achievements attributable to the use of fluorescence is vast and the work we have presented is by no means an attempt to discount even the smallest of contributions. Nevertheless, like most advances in science, more can always be done.

While fluorescent proteins and organic fluorophores have aided the life sciences, most of these molecules absorb and emit visible light (400-650 nm), a feature which limits their use for the very purposes in which they are employed. Cellular autofluorescence of visible light means low signal to noise ratio for these fluorophores during cell imaging (Escobedo et al., 2010; Rao et al., 2007). Absorption of visible light by hemoglobin and other biological molecules results in limited uses of visible light absorbing fluorophores when imaging live animals

(Hilderbrand and Weissleder, 2010; Rao et al., 2007). Fortunately, the solution to these problems is simple: NIR light. NIR light (650-900 nm) is optimal for imaging live cells and organisms; therefore, NIR fluorophores are the ideal imaging reagents (Escobedo et al., 2010; Frangioni, 2003; Guo et al., 2014; Hilderbrand and Weissleder, 2010; Shcherbakova and Verkhusha, 2013; Weissleder, 2001).

Unfortunately, as discussed in Chapter I, NIR fluorophores themselves are not optimal imaging reagents. There are very few NIR absorbing fluorescent proteins, and NIR organic fluorophores have inherent flaws (Bunting et al., 1989; Cunningham et al., 2010; Johnson, 1998; Keppler et al., 2006; Shcherbakova and Verkhusha, 2013). The planarity and high degree of conjugation required for absorption of NIR light means that NIR fluorophores are hydrophobic and cationic. The hydrophobicity of these compounds often leads to dye aggregation in water, which for some of these dyes, in particular the polymethine family of NIR dyes, results in fluorescence quenching (Mishra et al., 2000; Mujumdar et al., 1993; Peng and Draney, 2004; Zhegalova et al., 2014). Hydrophobic dyes also tend to accumulate in hydrophobic environments, such as membranes (Cunningham et al., 2010; Johnson, 1998). Furthermore, the cationic nature of NIR dyes produces mitochondrial staining due to accumulation in the negatively charged mitochondrial membrane (Bunting et al., 1989). Therefore, unless mitochondrial and membrane staining are desired, NIR dyes are not the ideal choice for imaging within biological environments like the cytoplasm and blood.

To prevent dye aggregation and eliminate the cationic charge on NIR dyes, these molecules are often functionalized with highly polar sulfonate groups (Li et al., 2008; Morgan et al., 2011; Mujumdar et al., 1993; Niu et al., 2009; Panchuk-Voloshina et al., 1999). As discussed in Chapters II and III, sulfonation imparts a high level of water-solubility to molecules. However, addition of the sulfonate group often affects synthetic tractability. This functionality can limit the ease of purification, often necessitating semi-preparative HPLC purification, a procedure associated with a decrease in product yields. Furthermore, due to the high polarity of the sulfonate group, reactions in non-polar organic solvents can be problematic owing to the insolubility of the sulfonate-functionalized compound. This problem has been addressed for other functionalities using protecting groups (Green and Wuts, 1999). Unfortunately, the palette of sulfonate protecting groups is not as vast as for amines, hydroxyls, carbonyls, etc. In particular, sulfonate protecting groups tend to be either too difficult to remove or too labile to be employed (Miller, 2010).

We sought to overcome this problem, particularly since my work necessitates the use of sulfonated dyes. In Chapter II, I presented a new sulfonate protecting group which has features desirable for synthetic organic chemistry. Our TFMT group is easily prepared from commercially available materials (two steps from *p*-Tolualdehyde), readily attached to sulfonates ( $\geq 85\%$  yields), stable to a variety of synthetic conditions, and importantly, cleanly cleaved by trifluoroacetic acid to give the pure sulfonated compound ( $>98\%$

purity) in high yield (99% yield of dye) without the need for column or HPLC purification. AlexaFluor dyes (Molecular Probes, Inc.) are simply the sulfonated counterparts of other dyes and tend to be quite costly due to the difficulty associated with their production. Through implementation of our TFMT group, these same dyes can be produced in any lab without requiring the difficult sulfonate purification that may necessitate their purchase. Furthermore, the use of TFA as the TFMT-deprotection reagent has implications apart from dye chemistry. TFA is commonly employed in the deprotection of acid-labile protecting groups, such as Boc (Green and Wuts, 1999). The TFMT sulfonate protecting group is thus not only a viable tool for the chemistry of sulfonated dyes and other molecules in solution phase chemistry, but could potentially be employed in the preparation of sulfonated peptides during Fmoc solid-phase peptide synthesis. TFMT could therefore aid in the synthesis of non-natural amino acids and peptides and could thus find use in biochemical studies or even contribute to the development of novel pharmaceuticals.

Although the development of our TFMT sulfonate protecting group was a great advance in the preparation of sulfonated dyes, in Chapters III and IV we discussed the impediments brought about by sulfonation with regard to live cell imaging. In particular, although sulfonation imparts water-solubility, it also prevents the dye from diffusing through cells. As this defeats the purpose of developing water-soluble NIR imaging reagents, we set our sights on rapidly overcoming this hurdle.

In Chapter III, I described the synthesis and *in vitro* evaluation of NIR oxazine dyes functionalized with AcOTFMB-sulfonate esters. AcOTFMB was developed in our lab as an esterase-labile sulfonate protecting group and was successfully used to deliver the small fluorophore dansyl sulfonate into live cells (Rusha and Miller, 2011). However, the synthesis of the AcOTFMB-functionalized dansyl sulfonate was simple, requiring only a single step from the commercially available dansyl chloride to product. Unfortunately, attempts to prepare our oxazine dyes as sulfonyl chlorides directly from the sulfonates failed to deliver consistent, significant yields of product, a problem which will be discussed shortly. This meant that the AcOTFMB group would have to be prepared as a sulfonate ester, attached to dye precursor, and undergo the relatively harsh conditions of dye formation. Fortunately, no major difficulties arose during the preparation of our dyes and we successfully developed both mono-sulfonate and bis-sulfonate AcOTFMB ester-functionalized NIR oxazine dyes. Our AcOTFMB sulfonate ester NIR oxazines are chemically stable but are rapidly converted to the hydrophilic, free sulfonates upon treatment with pig liver esterase *in vitro*. This confirms that AcOTFMB can be utilized in NIR dyes and, like its dansyl sulfonate counterpart, will aid in the delivery of sulfonated NIR fluorophores; a result that was decisively confirmed by our work discussed in Chapter IV.

We are highly encouraged by the ability to apply AcOTFMB to our NIR oxazines and have no question that this can be applied to other NIR scaffolds



such as BODIPY dyes and the heptamethine indocyanines. Like Tsien's use of carboxylate esters to deliver visible wavelength fluorophores bearing carboxylic acids into cells, we believe application of AcOTFMB could expand the intracellular use of NIR dyes to levels seen for fluorescein and rhodamine (Minta and Tsien, 1989; Minta et al., 1989; Tsien, 1981; Tsien, 1989). However, this work is far from complete. As alluded to above, the ideal synthetic route would be to prepare the dye itself as a sulfonyl chloride and then directly attach the ACOTFMB group to the dye. This would prevent any loss of the AcOTFMB-sulfonate ester during dye synthesis. In particular, while we found that this group could survive reaction in hot acetic acid or refluxing ethanol and hydrochloric acid, the synthesis of rhodamines usually requires refluxing acetic acid, a relatively harsh condition which could result in ester deprotection. We explored several routes for developing activated sulfonates including sulfonyl chlorides (phosphorous oxychloride, phosphorous pentachloride, thionyl chloride) and fluorides (DAST), but none were greatly promising. By addressing this issue, one can imagine an assembly line scenario where NIR sulfonated dyes are easily prepared via TFMT-assisted synthesis, activated by chlorination/fluorination, and functionalized with AcOTFMB or other biologically relevant functionality to rapidly produce the desired imaging reagent in high yield without the cost associated with outsourcing.

Whereas our work with TFMT and AcOTFMB seeks to aid in the development of NIR dyes for live cell and whole animal imaging, we also sought

to increase the palette of NIR reagents used during imaging. As discussed in Chapters I and V, the majority of NIR imaging is performed with derivatives of heptamethine indocyanine dyes (Escobedo et al., 2010; Frangioni, 2003; Rao et al., 2007). However, as outlined throughout this work, NIR oxazines are an excellent alternative to NIR indocyanine dyes having such favorable characteristics as high photostability and decreased hydrophobicity (Anzalone et al., 2013; Vogelsang et al., 2009). By applying our AcOTFMB strategy to the pentacyclic NIR oxazine scaffold, I developed sulfonated oxazine dyes that could be used for live cell and *in vivo* imaging (Chapter III).

In Chapter IV, I showed that, not only can AcOTFMB-sulfonate esters be used to deliver sulfonated NIR dyes into live cells, but that NIR oxazine dyes can be used to image both live cells and mice. One of our dyes, the bis-sulfonated **Sulf-Ox2**, delivered as **AcOTFMB-Ox2**, displays truly cytoplasmic fluorescence, indicating that **Sulf-Ox2** can access the entire cell. Most organic dyes, NIR and otherwise, do not have this ability (Cunningham et al., 2010; Thorp-Greenwood et al., 2012) which reinforces the advantage of utilizing sulfonated fluorophores. This is of particular interest in the field for two reasons: our NIR fluorophore was one of the first to display true cytoplasmic fluorescence, and it was derived from an oxazine dye. This clearly confirms that, despite the popularity of indocyanine dyes for NIR imaging, NIR oxazines are strong candidates for potential imaging reagents. Our NIR **AcOTFMB-Ox2** dye rapidly diffuses into cells, is quickly converted into **Sulf-Ox2**, and can be exported from cells via drug efflux

transporters. With the appropriate protein-labeling functionalization, use of **AcOTFMB-Ox2** would allow for bright, diffuse intracellular fluorescence with low background since unbound dye would be easily cleared from the cell by transporter activity. Our attempts at functionalizing our dyes for protein labeling were unsuccessful, but work on this front should be continued. The ability to fluorescently label both nuclear and cytoplasmic proteins with NIR fluorophores would be an essential tool when studying protein function and localization in cells and animals.

Achieving diffuse, NIR intracellular fluorescence from live cells was a hallmark of our work and our imaging results in live mice, while preliminary, were very promising. However, we wanted to demonstrate that NIR oxazines were a multi-purpose reagent, and in Chapter V, I describe the synthesis and *in vitro* characterization of nitric oxide and pH sensors derived from the pentacyclic oxazine scaffold. Our NIR oxazine-derived nitric oxide and pH sensors rapidly report on their target via an increase in fluorescence intensity. While the off/on signal change is not as extreme as that observed for similar visible wavelength fluorescent sensors, the higher signal to noise ratio achievable by NIR dyes when used in live cells and organisms may favor the use of our molecules. More importantly, we have shown that NIR oxazines can indeed function as sensors of biologically relevant environmental conditions. Whereas BODIPYs, indocyanines, oxazines, and silicon-rhodamines have been employed for NIR imaging, small molecule NIR sensors, with a few exceptions, are primarily heptamethine

indocyanine derivatives (Han et al., 2013; Han et al., 2013; Karton-Lifshin et al., 2011; Li et al., 2011; Sasaki et al., 2005). Our work indicates that this limitation is unwarranted.

While we are excited about the ability of our NIR oxazines to function as fluorescent sensors, the results from my work would benefit from optimization. We obtained a maximum 12-fold increase in fluorescence intensity between the off/on states of our sensors. The quantum yield of the visible wavelength diaminofluorescein nitric oxide sensor developed in the Nagano lab was reported to increase by 100 times upon reaction with nitric oxide (Kojima et al., 1998). To improve the sensitivity of our sensors for use in live cells, we should likewise focus on maximizing the difference in off/on fluorescence intensity. The key optimization will be modulation of the quenched form of our dyes. Organic fluorophores utilized as sensors often employ PET as the mechanism of modulating fluorescence (Kobayashi et al., 2010; Ni and Wu, 2014; Song et al., 2005). Work by Sauer has shown that the fluorescence of NIR oxazines is well modulated by PET and this finding held in our work (Doose et al., 2009; Marmé et al., 2003; Valana et al., 2003). Yet, the fact that we still obtained a measurable amount of fluorescence with our quenched molecules indicates that the PET donor we employed was less than ideal. By focusing efforts on increasing the electron donating ability of our PET quencher, potentially via addition of another electron-rich functionality, the off-state fluorescence output of our dye could be

minimized which would result in a net increase in on-state fluorescence worthy of a commercial, biological sensor.

Overall, this work aimed to increase the palette of NIR imaging reagents for use in live cells and animals. This was achieved specifically for oxazine dyes by showing they had the same potential uses as the more commonly employed NIR BODIPYs and indocyanines. NIR oxazines are fairly underrepresented as sensors and intracellular fluorophores, but they need not be. Our NIR oxazines can sense small molecules, sense environmental changes, label mitochondria, illuminate the cytoplasm, and even fluoresce within living animals. More generally though, we sought to increase the utility of all NIR dyes. Due to their hydrophobicity, the use of NIR fluorophores in live cells is often limited, and the sulfonation, which neutralizes this problem, hinders their intracellular delivery. However, we shall overcome. Sulfonated NIR dyes can be successfully delivered into cells, and these molecules can be employed for any level of imaging which has been the purview of visible light emitting fluorophores. We can achieve biological imaging that is unimpeded by background and unattenuated by off-target light absorption. The key, as always, is chemistry.

## BIBLIOGRAPHY

Akaike, T. et. al. *Nitric Oxide: Biology and Pathophysiology*. Ignarro, L. J., Ed.; Academic Press: Florida, 2000.

Ali, A. M.; Hill, B.; Taylor, S. D. *J. Org. Chem.* **2009**, *74*, 3583-3586.

Allen, A. D.; Fujio, M.; Tee, O. S.; Tidwell, T. T.; Tsuji, Y.; Tsuno, Y.; Yatsugi, K. *J. Am. Chem. Soc.* **1995**, *117*, 8974-8981.

Allen, A. D.; Ambidge, I. C.; Che, C.; Micheal, H.; Muir, R. J.; Tidwell, T. *J. Am. Chem. Soc.* **1983**, *105*, 2343-2350.

Allen, C. M.; Sharman, W. M.; Van Lier, J. E. *J. Porphyrins Phthalocyanines* **2001**, *5*, 161-169.

Allen, J. D.; van Loevezijn, A.; Lakhai, J. M.; van der Valk, M.; van Tellingen, O.; Reid, G.; Schellens, J. H. M.; Koomen, G.; Schinkel, A. H. *Mol. Cancer Ther.* **2002**, *1*, 417-425.

Andersson-Engels, S.; Klinteberg, C.; Svanberg, K.; Svanberg, S. *Phys. Med. Biol.* **1997**, *42* (5), 815-824.

Anzalone, A. V.; Wang, T. Y.; Chen, Z.; Cornish, V. W. *Angew. Chem. Int. Ed. Engl.* **2013**, *52* (2), 650-654.

Aubin, J. E. *J. Histochem. Cytochem.* **1979**, *27* (1), 36-43.

Barta, C.; Kálai, T.; Vass, I.; Hideg, K.; Hideg, É. *Acta Biol. Szeged.* **2002**, *46* (3-4), 149-150.

Berridge, M. V.; Herst, P. M.; Tan, A. S. *Biotechnol. Annu. Rev.* **2005**, *11*, 127-152.

Borst, P. and Elferink, R. O. *Annu. Rev. Biochem.* **2002**, *71*, 537-592.

Botta, C.; Di Giorgio, C.; Sabatier, A.; De Méo, M. *Environ. Toxicol.* **2009**, *24* (5), 492-505.

Bryan, A. J.; de Silva, A. P.; de Silva, S. A.; Rupasinghe, R. A. D. D.; Sandanayake, K. R. A. S. *Biosensors* **1989**, *4*, 169-179.

Bunting, J. R.; Phan, T. V.; Kamali, E.; Dowben, R. M. *Biophys. J.* **1989**, *56*, 979-993.

Chen, P. B.; Hung, J.; Hickman, T. L.; Coles, A. H. Carey, J. F.; Weng, Z.; Chu, F.; Fazio, T. G. *eLife* **2013**, *2*, e01557.

- Cheong, W. -F. Prael, S. A.; Welch, A. J. *IEEE J. Quantum Electron.* **1990**, *26*, 2166-2185.
- Cole, S. P. C.; Sparks, K. E.; Fraser, K.; Loe, D. W.; Grant, C. E.; Wilson, G. M.; Deeley, R. G. *Cancer Res.* **1994**, *54*, 5902-5910.
- Coskun, A.; Yilmaz, M. D.; Akkaya, E. U. *Org. Lett.* **2007**, *9* (4), 607-609.
- Cunningham, C. W.; Mukhopadhyay, A.; Lushington, G. H.; Blagg, B. S. J.; Prisinzano, T. E.; Krise, J. P.; *Molecular Pharm.* **2010**, *7*, 1301-1310.
- Doose, S.; Neuweiler, H.; Sauer, M. *ChemPhysChem* **2009**, *10*, 1389-1398.
- Dobrucki, J. W.; Feret, D.; Noatynska, A. *Biophys. J.* **2007**, *93* (5), 1778-1786.
- Egawa, T.; Hanaoka, K.; Koide, Y.; Ujita, S.; Takahashi, N.; Ikegaya, Y.; Matsuki, N.; Terai, T.; Ueno, T.; Komatsu, T.; Nagano, T. *J. Am. Chem. Soc.* **2011**, *133*, 14157-14159.
- Eggeling, C.; Widengren, J.; Brand, L.; Schaffer, J.; Felekyan, S.; Seidel, C. A. *M. J. Phys. Chem. A* **2006**, *110*, 2979-2995.
- Escobedo, J. O.; Rusin, O.; Lim, S.; Strongin, R.M. *Curr. Opin. Chem. Biol.* **2010**, *14* (1), 64-70.
- Falcone, R. D.; Baruah, B; Gaidamauskas, E.; Rithner, C. D.; Correa, N. M.; Silber, J. J.; Crans, D. C.; Levinger, N. E. *Chem. Eur. J.* **2011**, *17* (24), 6837-6846.
- Fei, X. and Gu, Y. *Prog. Nat. Sci.* **2009**, *19*, 1-7.
- Fernández-Suárez, M. and Ting, A. Y. *Nat. Rev. Mol. Cell Biol.* **2008**, *9* (12), 929-943.
- Fox, M. E. *Photochem. Photobiol.* **1990**, *52* (3), 617-627.
- Franca, L. T. C.; Carrhlo, E.; Kist, T. B. L. *Q. Rev. Biophys.* **2002**, *35* (2), 169-200.
- Frangioni, J. V. *Curr. Opin. Chem. Biol.* **2003**, *7* (5), 626-634.
- Gabe, Y.; Ueno, T.; Urano, Y.; Kojima, H.; Nagano, T. *Anal. Bioanal. Chem.* **2006**, *386*, 621-626.
- Gabe, Y.; Urano, Y.; Kikuchi, K.; Kojima, H.; Nagano, T. *J. Am. Chem. Soc.* **2004**, *126* (10), 3357- 3367.
- Genina, E. A.; Bashkatov, A. N.; Tuchin, V. V. *Advances in Optical Technologies* **2008**, *2008*, 8 pages.

- Ghoroghchian P. P.; Therien, M. J.; Hammer, D. A. *Wiley Interdiscip. Rev. Nanomed. Nanobiotechnol.* **2009**, 1 (2), 156-167.
- Glavinas, H.; Krajcsi, P.; Cserepes, J.; Sarkadi, B. *Curr. Drug Deliv.* **2004**, 1 (1), 27-42.
- Grabolle, M.; Pauli, J.; Brehm, R.; Resch-Genger, U. *Dyes Pigments* **2014**, 103, 118-126.
- Greene, T. W.; Wuts, P. G. M. *Protective Groups in Organic Synthesis*. Third ed.; John Wiley & Sons: New York, 1999.
- Guichard, S.; Chatelut, E.; Lochon, I.; Bugat, R.; Mahjoubi, M.; Canal, P. *Cancer Chemother. Pharmacol.* **1998**, 42 (2), 165-170.
- Guo, Z.; Park, S.; Yoon, J.; Shin, I. *Chem. Soc. Rev.* **2014**, 43, 16-29.
- Hall, C. N. and Garthwaite, J. *Nitric Oxide* **2009**, 21 (2), 92-103.
- Hall, M. J.; Allen, L. T.; O'Shea, D. F. *Org. Biomol. Chem.* **2006**, 4, 776-780.
- Han, F.; Xu, Y.; Jiang, D.; Qin, Y.; Chen, H. *Anal. Biochem.* **2013**, 435 (2), 106-113.
- Han, J.; Han, M. S.; Tung, C. *Mol. Biosyst.* **2013**, 9 (12), 10.1039/c3mb70269c.
- Han, Z.; Yang, Q.; Liang, L.; Zhang, X. *AMPC* **2013**, 3, 314-319.
- Heiskanen, J. P.; Hormi, O. E. O. *Tetrahedron* **2009**, 65, 518-524.
- Herrmann, R.; Josel, H.; Drexhage, K.; Marx, N.; *EP 757447*, 1996.
- Hilderbrand, S. A.; Weissleder, R. *Curr. Opin. Chem. Biol.* **2010**, 14 (1), 71-79.
- Hintersteiner, M.; Enz, A.; Frey, P.; Jatton, A.; Kinzy, W.; Kneuer, R.; Neumann, U.; Rudin, M.; Staufienbiel, M.; Stoeckli, M.; Wiederhold, K.; Gremlich, H. *Nat. Biotech.* **2005**, 23 (5), 577-583.
- Hirotsu, M.; Urano, Y.; Kikuchi, K.; Higuchi T.; Nagano, T. *Tetrahedron Lett.* **2000**, 41, 69-72.
- Hou, J.; Wu, M.; Li, K.; Yang, J.; Yu, K.; Xie, Y.; Yu, X. *Chem. Commun.* **2014**, 50, 8640-8643.
- Hsieh, P.; Segal, R.; Chen, L. B. *J. Cell Biol.* **1980**, 87 (1), 14-22.
- Hush, N. S.; Paddon-Row, M. N.; Cotsaris, E.; Oevering, H.; Verhoeven, J. W.; Heppener, M. *Chem. Phys. Lett.* **1985**, 117 (1), 8-11.



- Ignarro, L. J.; Fukuto, J. M.; Griscavage, J. M.; Rogers, N. E.; Byrns, R. E. *Proc. Natl. Acad. Sci. USA* **1993**, *90*, 8103-8107.
- Jansen, E. D.; Pickett, P. M.; Mackanos, M. A.; Virostko, J. *J. Biomed. Opt.* **2006**, *11* (4), 041119.
- Jiang, N.; Fan, J.; Liu, T.; Cao, J.; Qiao, B.; Wang, J.; Gao, P.; Peng, X. *Chem. Commun.* **2013**, *49*, 10620.
- Johnson, I. *Histochem. J.* **1998**, *30*, 123-140.
- Johnson, L. V.; Walsh, M. L.; Chen, L. B. *Proc. Natl. Acad. Sci. USA* **1980**, *77* (2), 990-994.
- Jokic, T.; Borisov, S. M.; Saf, R.; Nielsen, D. A.; Kuhl, M.; Klimant, I. *Anal. Chem.* **2012**, *84*, 6723-6730.
- Kanitz, A.; Hartmann, H. *Eur. J. Org. Chem.* **1999**, *4*, 923-930.
- Karolin, J.; Johansson, L. B. A.; Strandberg, L.; Ny, T. *J. Am. Chem. Soc.* **1994**, *116* (17), 7801-7806.
- Karton-Lifshin, N.; Segal, E.; Omer, L.; Portnoy, M.; Satchi-Fainaro, R.; Shabat, D. *J. Am. Chem. Soc.* **2011**, *133* (28), 10960-10965.
- Kathuria, S. V.; Kayatekin, C.; Barrea, R.; Kondrashkina, E.; Graceffa, R.; Guo, L.; Nobrega, R. P.; Chakravarthy, S.; Matthews, C. R.; Irving, T. C.; Bilsel, O. *J. Mol. Biol.* **2014**, *426* (9), 1980-1994.
- Keefer, L. K.; Nims, R. W.; Davies, K. M.; Wink, D. A. *Methods Enzymol.* **1996**, *268*, 281-293.
- Keppler, A.; Arrivoli, C.; Sironi, L.; Ellenberg, J. *BioTechniques* **2006**, *41* (2), 167-175.
- Keppler, A.; Gendreizig, S.; Gronemeyer, T.; Pick, H.; Vogel, H.; Johnsson. *Nat. Biotechnol.* **2003**, *21* (1), 86-89.
- Kikuchi, K.; Komatsu, K.; Nagano, T. *Curr. Opin. Chem. Biol.* **2004**, *8*, 182-191.
- Kobayashi, H.; Ogawa, M.; Alford, R.; Choyke, P. L.; Urano, Y. *Chem. Rev.* **2010**, *110* (5), 2620-2640.
- Koide, Y.; Urano, Y.; Hanaoka, K.; Terai, T.; Nagano, T. *ACS Chem. Biol.* **2011**, *6*, 600-608.
- Koide, Y.; Urano, Y.; Hanaoka, K.; Terai, T.; Nagano, T. *J. Am. Chem. Soc.* **2011**, *133*, 5680-5682.

- Koide, Y.; Urano, Y.; Hanaoka, K.; Piao, W.; Kusakabe, M.; Saito, N.; Terai, T.; Okabe, T.; Nagano, T. *J. Am. Chem. Soc.* **2012**, *134*, 5029-5031.
- Koide, Y.; Urano, Y.; Kenmoku, S.; Kojima, H.; Nagano, T. *J. Am. Chem. Soc.* **2007**, *129*, 10324-10325.
- Kojima, H.; Hirotsu, M.; Nakatsubo, N.; Kikuchi, K.; Urano, Y.; Higuchi, T.; Hirata, Y.; Nagano, T. *Anal. Chem.* **2001**, *73*, 1967-1973.
- Kojima, H.; Nakatsubo, N.; Kikuchi, K.; Kawahara, S.; Kirino, Y.; Nagoshi, H.; Hirata, Y.; Nagano, T. *Anal. Chem.* **1998**, *70*, 2446-2453.
- Kolmanov, K.; Belov, V. N.; Bierwagen, J.; Ringemann, C.; Muller, V.; Eggeling, C.; Hell, S. W. *Chem. Eur. J.* **2010**, *16*, 158-166.
- König, K. *J. Microsc.* **2000**, *200* (2) 83-104.
- Krishnamurti, R.; Bellew, D. R.; Prakash, G. K. S. *J. Org. Chem.* **1991**, *56*, 984-989.
- Lakowicz, J. R. *Principles of Fluorescence Spectroscopy*. 2<sup>nd</sup> ed.; Springer: New York, 2006.
- Lebedeva, I. V.; Pande, P.; Patton, W. F. *PLoS ONE* **2011**, *6* (7), e22429.
- Lee, C. *Focal Points* **2008**, *129*, 1-4.
- Lemke, E. A.; Schultz, C. *Nat. Chem. Biol.* **2011**, *36*, 993-1017.
- Li, L.; Han, J.; Nguyen, B.; Burgess, K. *J. Org. Chem.* **2008**, *73*, 1963-1970.
- Li, P.; Duan, X.; Chen, Z.; Lin, Y.; Xie, T.; Fang, L.; Li, X.; Yin, M.; Tang, B. *Chem. Commun.* **2011**, *47* (26), 7755-7757.
- Lieberwirth, U.; Arden-Jacob, J.; Drexhage, K. H.; Herten, D. P.; Müller, R.; Neumann, M.; Schulz, A.; Siebert, S.; Sagner, G.; Klingel, S.; Sauer, M.; Wolfrum, J. *Anal. Chem.* **1998**, *70* (2), 4771-4779.
- Loe, D. W.; Deeley, R. G.; Cole, S. P. C. *J. Pharmacol. Exp. Ther.* **2000**, *293*, 530-538.
- Luo, S.; Zhang, E.; Su, Y.; Cheng, T.; Shi, C. *Biomaterials* **2011**, *32*, 7127-7138.
- Ma, J. D.; Nafziger, A. N.; Mylott, W.; Haughey, D. B.; Rocci M. L. Jr.; Bertino, J. S. Jr. *Eur. J. Clin. Pharmacol.* **2008**, *64* (11), 1133-1134.
- Madshus, I. H. *Biochem. J.* **1988**, *250*, 1-8.

- Marmé, N.; Knemeyer, J.; Sauer, M.; Wolfrum, J. *Bioconjugate Chem.* **2003**, *14* (6), 1133-1139.
- Marshall, M. V.; Rasmussen, J. C.; Tan, I.; Aldrich, M. B.; Adams, K. E.; Wang, X.; Fife, C. E.; Maus, E. A. Smith, L. A.; Sevick-Muraca, E. M. *Open. Surg. Oncol. J.* **2010**, *2* (2), 12-25.
- Martin, V. V.; Rothe, A.; Diwu, Z.; Gee, K. R. *Bioorg. Med. Chem. Lett.* **2004**, *14*, 5315-5316.
- Martin, V. V.; Rothe, A.; Gee, K. R. *Bioorg. Med. Chem. Lett.* **2005**, *15*, 1851-1855.
- Matsui, A.; Umezawa, K.; Shindo, Y.; Fujii, T.; Citterio, D.; Oka, K.; Suzuki, K. *Chem. Commun.* **2011**, *47*, 10407.
- Miller, S. C. *J. Org. Chem.* **2010**, *75*, 4632-4635.
- Miller, S. C. *WO 2009036351 (A2)*, 2009.
- Minta, A.; Kao, J. P.; Tsien, R. Y. *J. Biol. Chem.* **1989**, *264* (14), 8171-8178.
- Minta, A.; Tsien, R. Y. *J. Biol. Chem.* **1989**, *264* (32), 19449-19457.
- Mishra, A.; Behera, R. K.; Behera, P. K.; Mishra, B. K.; Behera, G. B. *Chem. Rev.* **2000**, *100* (6), 1973-2011.
- Monici, M. *Biotechnol. Annu. Rev.* **2005**, *11*, 227-256.
- Moody, E. D.; Viskari, P. J.; Colyer, C. J. *J. Chromatogr. B Biomed. Sci. App.* **1999**, *729* (1-2), 55-64.
- Morgan, M. T.; Bagchi, P.; Fahrni, C. J. *J. Am. Chem. Soc.* **2011**, *133*, 15906-15909.
- Muckle, T. J. *Biochem. Med.* **1976**, *15* (1), 17-21.
- Mujumdar, R. B.; Ernst, L. A.; Mujumdar, S. R.; Lewis, C. J.; Waggoner, A. S. *Bioconjugate Chem.* **1993**, *4*, 105-111.
- Munoz, M.; Henderson, M.; Haber, M.; Norris, M. *IUBMB Life* **2007**, *59* (12), 752-757.
- Musicki, B.; Widlanski, T. S. *J. Org. Chem.* **1990**, *55*, 4231-4233.
- Ni, Y.; Wu, J. *Org. Biomol. Chem.* **2014**, *12*, 3774-3791.
- Nijegorodov, N. I. and Downey, W. S. *J. Phys. Chem.* **1994**, *98*, 5639-5643.

- Nijegorodov, N.; Luhanga, P. V. C.; Nikoma, J. S.; Winkoun, D. P. *Spectrochim. Acta A* **2006**, *64* (1), 1-5.
- Niu, S. L.; Ulrich, G.; Ziessel, R.; Kiss, A.; Renard, P.; Romieu, A. *Org. Lett.* **2009**, *11*, 2049-2052.
- Ntziachristos, V. *Annu. Rev. Biomed. Eng.* **2006**, *8*, 1-33.
- Novo, E. and Parola, M. *Fibrogenesis Tissue Repair* **2008**, *1* (5).
- O' Connor, D. V. and Phillips, D. *Time Correlated Single Photon Counting*. Academic Press: New York, 1984.
- Ohba, S. Yokoyama, J. Fujimaki, M. Ito, S.; Kojima, M. Shimoji, K.; Ikeda, K. *Oral. Oncol.* **2012**, *48* (11), 1101-1105.
- Ozmen, B.; Akkaya, E. U. *Tetrahedron Lett.* **2000**, *41*, 9185-9188.
- Panchuk-Voloshina, N.; Haugland, R. P.; Bishop-Stewart, J.; Bhalgat, M. K.; Millard, P. J.; Mao, F.; Leung, W. Y.; Haugland, R. P. *J. Histochem. Cytochem.* **1999**, *47*, 1179-1188.
- Pansare, V.; Hejazi, S.; Faenza, W.; Prud'homme, R. K. *Chem. Mater.* **2012**, *24* (5), 812-827.
- Park, M. H.; Hyun, H.; Ashitate, Y.; Wada, H.; Park, G.; Lee, J. H.; Njiojob, C.; Henary, M.; Frangioni, J. V.; Choi, H. S.; *Theranostics* **2014**, *4* (8), 823-833.
- Pauff, S. M. and Miller, S. C. *J. Org. Chem.* **2013**, *78* (2), 711-716.
- Pauff, S. M. and Miller, S. C. *Org. Lett.* **2011**, *13* (23), 6196-6199.
- Pauli-Magnus, C.; von Richter, O.; Burk, O.; Ziegler, A.; Mettang, T.; Eichelbaum, M.; Fromm, M. F. *J. Pharmacol. Exp. Ther.* **2000**, *293*, 376-382.
- Peng, X.; Draney, D. R. *LPI* **2004**.
- Perlasamy, A., ed. *Methods in Cellular Imaging*. Oxford University Press: New York, 2001.
- Perry, S. W.; Norman, J. P.; Barbieri, J.; Brown, E. B.; Gelbard, H. A. *Biotechniques* **2011**, *50* (2), 98-115.
- Pflaum, M.; Kielbassa, C.; Garmyn, M.; Epe, B. *Mutat. Res.* **1998**, *408* (2), 137-146.
- Pflaum, M.; Boiteux, S.; Epe, B. *Carcinogenesis* **1994**, *15* (2), 297-300.

- Piatkevich, K. D.; Subach, F. V.; Verkhusha, V. V. *Chem. Soc. Rev.* **2013**, *42* (8), 3441-3452.
- Pick, A.; Klinkhammer, W.; Wiese, M. *ChemMedChem* **2010**, *5* (9), 1498-1505.
- Pluth, M. D.; Tomat, E.; Lippard, S. J. *Annu. Rev. Biochem.* **2011**, *80*, 333-335.
- Prendergast, F. G. *Curr. Opin. Struc. Biol.* **1991**, *1* (6), 1054-1059.
- Rao, J.; Dragulescu-Andrasi, A.; Yao, H. *Curr. Opin. Biotech.* **2007**, *18*, 17-25.
- Ray, P. D.; Huang, B.; Tsuji, Y. *Cell Signal.* **2012**, *24* (5), 981-990.
- Reid, G.; Wielinga, P.; Zelcer, N.; van der Heijden, I.; Kuil, A.; de Haas, M.; Wijnholds, J.; Borst, P. *PNAS* **2003**, *100* (16), 9244-9249.
- Roberts, J. C.; Gao, H.; Gopalsamy, A.; Kongsjahju, A.; Patch, R. J. *Tetrahedron Lett.* **1997**, *38*, 355-358.
- Rusha, L. and Miller, S. C. *Chem. Commun.* **2011**, *47*, 2038-2040.
- Russel, F. G.; Koenderink, J. B.; Masereeuw, R. *Trends Pharmacol. Sci.* **2008**, *29* (4), 200-207.
- Sasaki, E.; Kojima, H.; Nishimatsu, H.; Urano, Y.; Kikuchi, K.; Hirata, Y.; Nagano, T. *J. Am. Chem. Soc.* **2005**, *127* (11), 3684-3685.
- Sauer, M.; Han, K.-T.; Müller, R.; Nord, S.; Schulz, A.; Seeger, S.; Wolfrum, J.; Arden-Jacob, J.; Deltau, G.; Marx, N. J.; Zander, C.; Drexhage, K. H. *J. Fluoresc.* **1995**, *5* (3), 247-261.
- Sauer, M.; Hofkens, J.; Enderlein, J. *Handbook of Fluorescence Spectroscopy and Imaging: From Single Molecules to Ensembles*. Wiley-VCH Verlag GmbH & Co. KGaA: Germany, 2011.
- Schäferling, M. *Angew. Chem. Int. Ed.* **2012**, *51* (15), 3532-3554.
- Seeberger, S.; Griffin, R. J.; Hardcastle, I. R.; Golding, B. T. *Org. Biomol. Chem.* **2007**, *5*, 132-138.
- Sharom, F. J. *Front. Oncol.* **2014**, *4* (41).
- Sharom, F. J. *Pharmacogenomics* **2008**, *9* (1), 105-127.
- Shcherbakova, D. M. and Verkhusha, V. V. *Nat. Methods* **2013**, *10* (8), 751-754.
- Sim, K.; Bibee, K.; Wickline, S.; Sept, D. *Cancer Res.* **2011**, *71* (3), 686-692.
- Simpson, L. S.; Widlanski, T. S. *J. Am. Chem. Soc.* **2006**, *128*, 1605-1610.

- Song, F.; Peng, X.; Lu, E.; Wang, Y.; Zhou, W.; Fan, J. *Tetrahedron Lett.* **2005**, *46*, 4817-4820.
- Song, J. J.; Tan, Z.; Reeves, J. T.; Gallou, F.; Yee, N. K.; Senanayake, C. H. *Org. Lett.* **2005**, *7*, 2193-2196.
- Soons, P. A.; de Boer, A.; Cohen, A. F.; Breimer, D. D. *Br. J. Clin. Pharmacol.* **1991**, *32*, 697-704.
- Stöhr, K.; Sieberg, D.; Ehrhard, T.; Lymperopoulos, K.; Öz, S.; Schulmeister, S.; Pfeifer, A. C.; Bachmann, J.; Klingmüller, U.; Sourjik, V.; Herten, D. *Anal. Chem.* **2010**, *82* (19), 8186-8193.
- Stolz, A. *Appl. Microbiol. Biotechnol.* **2001**, *56*, 69-80.
- Stuehr, D. J.; Marletta, M. A. *Cancer Res.* **1987**, *47*, 5590-5594.
- Sullivan, K. F., ed. *Fluorescent Proteins*. 2<sup>nd</sup> ed.; Academic Press: USA, 2007.
- Tasler, R.; Moises, T.; Frankenberg-Dinkel, N. *FEBS J.* **2005**, *272*, 1927-1936.
- Tavaré, J. M.; Fletcher, L. M.; Welsh, G. I. *J. Endocrinol.* **2001**, *170*, 297-306.
- Theoclitou, M.; Robinson, L. A. *Tetrahedron Lett.* **2002**, *43*, 3907-3910.
- Theodorou, V.; Skobridis, K.; Tzakos, A. G.; Ragoussis, V. *Tetrahedron Lett.* **2007**, *48*, 8230-8233.
- Thorp-Greenwood, F. L.; Coogan, M. P.; Mishra, L.; Kumari, N.; Rai, G.; Saripella, S. *New J. Chem.* **2012**, *36*, 64-72.
- Tian, J.; Chen, H.; Zhuo, L.; Xie, Y.; Li, N.; Tang, B. *Chem.-Eur. J.* **2011**, *17* (24), 6626-6634.
- Tian, M.; Peng, X.; Fan, J.; Wang, J.; Sun, S. *Dyes Pigments* **2012**, *95* (1), 112-115.
- Tongkate, P.; Pluempanupat, W.; Chavasiri, W. *Tetrahedron Lett.* **2008**, *49*, 1146-1148.
- Toutchkine, A. *WO 2009/152024 A1*, 2009.
- Tromberg, B. J.; Shah, N.; Lanning, R.; Cerussi, A. Espinoza, J.; Pham, T.; Svaasand, L.; Butler, J. *Neoplasia* **2000**, *2* (1-2), 26-40.
- Tsai, C.; Chen, J.; Wang, W. *J. Med. Biol. Eng.* **2001**, *21* (1), 7-14.
- Tsien, R. Y. *Annu. Rev. Biochem.* **1998**, *67*, 509-544.

- Tsien, R. Y. *Methods Cell Biol.* **1989**, 30, 127-156.
- Tsien, R. Y. *Nature* **1981**, 290, 527-528.
- Tsuritani, T.; Yamamoto, Y.; Kawasaki, M.; Mase, T. *Org. Lett.* **2009**, 11 (5), 1043-1045.
- Twentyman, P. R.; Rhodes, T.; Rayner, S. *Eur. J. Cancer.* **1994**, 30A (9), 1360-1369.
- Valana, A. C.; Neuweiler, H.; Schulz, A.; Wolfrum, J.; Sauer, M.; Smith, J. C. *J. Am. Chem. Soc.* **2003**, 125 (47), 14564-14572.
- Van de Linde, S.; Heilemann, M.; Sauer, M. *Annu. Rev. Phys. Chem.* **2012**, 63, 519-540.
- Vogelsang, J.; Cordes, T.; Forthmann, C.; Steinhauer, C.; Tinnefeld, P. *PNAS* **2009**, 106 (20), 8107-8112.
- Wakata, A.; Lee, H.; Rommel, P.; Touthkine, A.; Schmidt, M.; Lawrence, D. S. *J. Am. Chem. Soc.* **2010**, 132, 1578-1582.
- Watts, K. S.; Dalal, P.; Murphy, R. B.; Sherman, W.; Friesner, R. A.; Shelly, J. C. *J. Chem. Inf. Model.* **2010**, 50, 534-546.
- Weissleder, R. *Nat. Biotechnol.* **2001**, 19, 316-317.
- Whitacre, C. M.; Feyes, D. K.; Satoh, T.; Grossman, J.; Mulvihill, J. W.; Mukhtar, H.; Oleinick, N. L. *Clin. Cancer. Res.* **2000**, 6, 2021-2027.
- Williams, G. C.; Liu, A.; Knipp, G.; Sinko, P. J. *Antimicrob. Agents Chemother.* **2002**, 46 (11), 3456-3462.
- Wu, B.; Piatkevich, K. D.; Lionnet, T.; Singer, R. H.; Verkhusha, V. V. *Curr. Opin. Cell Biol.* **2011**, 23, 310-317.
- Wuhrmann, K.; Mechsner, K.; Kappeler, T. *European J. Appl. Microbiol. Biotechnol.* **1980**, 9, 325-338.
- Xie, M.; Widlanski, T. S. *Tetrahedron Lett.* **1996**, 37, 4443-4446.
- Xu, K.; Sun, S.; Li, J.; Li, L.; Qiang, M.; Tang, B. *Chem. Commun.* **2012**, 48, 684-686.
- Yang, X.; Shi, C.; Tong, R.; Qian, W.; Zhau, H. E.; Wang, R.; Zhu, G.; Cheng, J.; Yang, V. W.; Cheng, T.; Henary, M.; Strekowski, L.; Chung, L. W. K. *Clin. Cancer Res.* **2010**, 16 (10), 2833-2844.

Zehri, A. H.; Ramey, W. Georges, J. F.; Mooney, M. A.; Martirosyan, N. L.; Preul, M. C.; Nakaji, P. *Surg. Neurol. Int.* **2014**, *5*, 60.

Zhang, C.; Liu, T.; Su, Y.; Luo, S.; Zhu, Y.; Tan, X.; Fan, S.; Zhang, L.; Zhou, Y.; Cheng, T.; Shi, C. *Biomaterials* **2010**, *31* (25), 6612-6617.

Zhang, X.; Bloch, S.; Akers, W.; Achilefu, S. *Curr. Protoc. Cytom.* **2012**, CHAPTER:Unit 12.27.

Zhang, X.; Kim, W.; Hatcher, N.; Potgieter, K.; Moroz, L. L.; Gillette, R.; Sweedler, J. V. *J. Biol. Chem.* **2002**, *277*, 48472-48478.

Zhao, L.; Yin, R.; Wei, B.; Li, Q.; Jiang, Z.; Chen, X.; Bi, K. *Acta Pharmacol. Sinica* **2012**, *33*, 1348-1352.

Zhegalova, N. G.; He, S.; Zhou, H.; Kim, D. M.; Berezin, M. Y. *Contrast Media Mol. Imaging* **2014**, *9*, 355-362.

Zilles, A.; Arden-Jacob, J.; Drexhage, K.; Kemnitzer, N. U.; Hamers-Schneider, M. *US 2006/0179585 A1*, 2006.

Zimmer, M. *Chem. Rev.* **2002**, *102*, 759-781.



## APPENDIX 1

### Multimedia Legend

**Movies 4.1-4.8: Real-time monitoring of AcOTFMB-Ox1 and 2 and TFMB-Ox 1 and 2 diffusion into U2-OS cells.** Cells were pretreated with OPTI-MEM 1 and monitored via spinning disc confocal microscopy as described (see Chapter IV Methods). After a brief interval, dye was added and the cells were again monitored via spinning disc confocal microscopy. **AcOTFMB-Ox1** (4.1 and 4.2): Cells imaged 3 minutes before dye addition, 33 minutes after dye addition. **TFMB-Ox1** (4.3 and 4.4): Cells imaged 3 minutes before dye addition, 33 minutes after dye addition. **AcOTFMB-Ox2** (4.5 and 4.6): Cells imaged 5 minutes before dye addition, 31 minutes after dye addition. **TFMB-Ox2** (4.7 and 4.8): Cells imaged 2 minutes before dye addition, 34 minutes after dye addition. Cell movies were prepared using the Universal Imaging Metamorph software and show both DIC and NIR imaging with playback at 1.5 frames/second.

Note: Movies available on the electronic copy of this thesis or by contacting Dr. Stephen Miller at the University of Massachusetts Medical School.